Distribution of Nitrifying Bacteria Under Fluctuating Environmental Conditions

Joseph M. Battistelli
Stratford, Connecticut

B.S., Rutgers, the State University of New Jersey, New Brunswick Campus, 2002

A Dissertation presented to the Graduate Faculty
of the University of Virginia in Candidacy for the Degree of
Doctor of Philosophy

Department of Environmental Sciences

University of Virginia
December, 2012
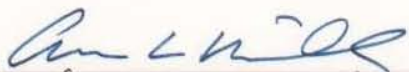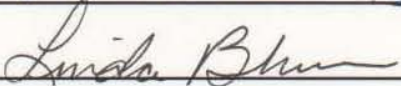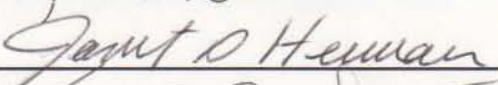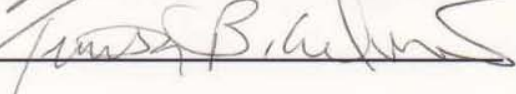
Abstract

Engineered systems that mimic tidal wetlands are ideal for point-of-source treatment of wastewater due to their low energy requirements and small physical footprint. In this study, vertical columns were constructed to mimic the flood-and-drain cycles of tidal wetland treatment systems (TWTS) in order to study how variations in the frequency and duration of flooding affect the efficiency of microbially-mediated nitrogen removal from synthetic wastewater (containing whey protein and NH_4^+). Altering the frequency of flooding, which determines the temporal juxtaposition of aerobic and anaerobic conditions in the reactor, had a significant effect on overall nitrogen removal; columns more frequent cycling were very efficient at converting the NH_4^+ in the feed to NO_3^-. At a flooding frequency of 8-cycles per day, NO_3^- began to disappear from the systems in both High- and Low - N treatments. The longer flooding duration appeared to increased anaerobiosis and allowed denitrification to proceed more effectively, while allowing nitrification to proceed when oxygen was available.

Analysis of depth profiles of abundance revealed distinct differences between the tidal and trickling systems abundance profiles. Overall, these results demonstrate a tight coupling of environmental conditions with the abundance of ammonium oxidizing bacteria and suggest several experimental modifications, such variable tidal cycles, could be implemented to enhance the functioning of TWTS.

Field work conducted at Cobb Mill Creek showed similar distribution patterns in denitrifying bacteria. Denitrifiers were enumerated using an MPN-PCR approach utilizing the *nosZ* gene as a presence-absence indicator. Vertical profiles of creek sediments showed a relationship between denitrifier abundance and organic matter

content. Like the treatment columns, there was a zone where abundance showed a significant increase. Increases in abundance represent a Golidlocks zone, a region where conditions are optimized for microbial growth and metabolism. Potential denitrification rates confirmed increased metabolic activity concurrent with increases in denitrifier abundance. Both TWTS and sediment profiles offer a unique look at the distribution of microorganisms often treated as a black box, summarized as a reaction rate constant by engineers or modelers.

Table of Contents

List of Figures

List of Tables

List of Boxes

Acknowledgement

Within a single page, I could not hope to individually thank the many people that have helped me along the way to the completion of my dissertation. My advisor, Aaron L. Mills, and my committee, Linda K. Blum, Janet S. Herman, and Teresa B. Culver, have always been there, even when my needs were remedial. More impressively, they never lost faith in my abilities. For that, I cannot thank them enough.

Members of the Laboratory of Microbial Ecology (LMECOL) past and present have contributed significantly to the development of my skills and knowledge. Of the many students, two stand out in my mind as needing special acknowledgement. Dr. Rima Franklin (LMECOL 2003) has made considerable contribution starting in 2002 when she taught me how to trouble shoot PCR and has adopted me in her lab at VCU saving me from countless miles of commuting to the Mills lab at UVA. Also needing special acknowledgement, is Amanda Floyd Beaty (LMECOL 2006), who even after graduating still responded kindly to my e-mails when I needed a little support— with science and emotions! Abigail Wise Porter, has also participated in many discussions about molecular microbiology since our time in Lily Young's laboratory. Jess Wenger, Katie McKee, and Christine Malash have also dutifully served in the role of e-mail confidant and I am eternally grateful for their patience with me.

At VCU, Dr. Bonnie Brown welcomed me into her lab, where I conducted most of the hybridizations for the nitrification study. Also, Ember Morrisey and Jaimie Gillespie have made significant contributions to my understanding of multivariate statistics and molecular genetics.

I would like to thank Worrell Water for allowing me access to their systems to conduct a microbial ecology study. Special thanks to Eric Lohan (LMECOL) for column design and project initiative; Kristina Reid Black (LMECOL) for column maintenance and processing IC samples; Nate Nickerson for aiding in sample collection; and Rachel Turley (LMECOL) for helping with sample collection and toiling away in lab weighing 1 g of LESA repeatedly with unfounded precision and then continuing with cell extractions from said LESA.

I would like to thank my parents, Katherine M. and Joseph L. Battistelli for putting me through college, encouraging me to do my best and to pursue my education, so I could have this opportunity. My sister, Victoria K. Battistelli's determination and success at her own trials are a constant tribute to the value of perseverance.

Lastly I would like to thank my loving partner Leland R. Deeds. I'm not sure where I would be without him, but I know it would be a lackluster imitation of where I am now.

1   Introduction

1.1   Statement of the problem

Water is an increasingly limited resource and technologies that reduce the demand for potable water are sorely needed. Since the development of the Haber-Bosch process in 1913, nitrogenous fertilizers have been readily available, which has lead to a drastic alteration of human population dynamics and agricultural practices (Galloway et al. 2004). Agriculture has expanded dramatically, thereby augmenting the planet's human carrying capacity. As of 2002, the nutritional needs of 40% of the human population were being met by N-based fertilizers (Fixen and West 2002). Since 2002, the dependence on N fertilizer has only increased. Concomitant with increased fertilizer usage is increased nitrogen pollution, both as unabsorbed, excess agricultural fertilizer, and as nitrogenous human and animal waste that results from the larger population size of humans and the animals used to help feed them (Galloway and Cowling 2002). The Haber-Bosh process has made the fixation of N_2 gas into NH_4^+ or NO_3^- cheap and available thereby greatly increasing the amount of N waste reaching our water systems.

Nitrogenous waste is a major contaminant of surface water and the ultimate removal of fixed nitrogen (either biologically or from anthropogenic sources) by conversion to N_2 gas falls to bacteria. In our current age water is a limiting resource with less than 3% of our resources available for research and industry and an even smaller amount available as potable water. In the interest of preserving our potable water resources a local research and development company Worrell Water has designed tidal water treatment systems (TWTS) for onsite water treatment and reuse to reduce the demand for potable water. The treated water, or reclaimed water, is utilized as flush

water, water features, or irrigation. Potable water is expensive to produce and meets health standards not required to accomplish any of these tasks, while reclaimed water has a lower price tag and often residual N is of benefit as a fertilizer. The TWTS are dependent on microbial communities to oxidize NH_4^+ and then reduce NO_3^- to N_2 to generate a reclaimed water source. Experimentation on the parameters that control the distribution and activity of the bacteria responsible for these oxidation-reduction reactions in both a natural setting and in the TWTS provides important ecological information about nitrification, which oxidizes NH_4^+ to NO_3^- and denitrification which reduces NO_3^- to N_2.

Research in engineered and natural systems often treats microbial processes as a black box summarized as a net biogeochemical process despite the benefits of understanding organism level interactions (Gutknecht et al. 2006, Prosser 2012). Results from this study support the idea that there is a structure-function link in microbial communities. Vertical abundance profiles from Cobb Mill Creek sediments, a riparian buffer, and tidal and trickling treatment systems showed distinct changes in functional group abundances. Understanding the environmental parameters responsible for controlling shifts in abundance and function are critical for making informed decisions regarding land use or water treatment design. Particularly for engineered systems, management of environmental parameters can lead to energy and space efficiency. The intimate linkages between hydrology, nutrient cycling and microbial communities are represented by observed changes in community abundance profiles in both systems.

1.2   Background

1.2.1   Organization of Microbial Communities

Bacteria seldom exist as a single cell, or in populations of a single species. While in the lab, *in vitro* studies of an individual species may occur, microorganisms in the environment exist in complex communities. An individual bacterial cell can produce a 5% change in the solute concentration in its surroundings at a range of 20 times the radius of an average spherical bacterium (Franklin and Mills 2007). This represents an interaction distance of approximately 10 micrometers. Although, a distance of 10 micrometers may seem insignificant, each organism exists as part of a larger interactive community able to extend the interaction distance, utilize available substrates, and produce new substrates, effectively altering landscape scale processes and structures. To truly understand the ecology of these tiny organisms we must study them on the scale of the microorganism – a feat that is not easy to achieve (Brock 1987, Mills and Bell 1986). Despite the many obstacles associated with understanding the interactions of individual microorganisms, much can be learned from studying ecosystem level distributions and net ecosystem processes of microorganisms due to the intrinsic relationship between microbial community structure and function (Forney et al. 2004).

Ecosystem scale studies have revealed much about the activity and organization of populations of microbial functional groups. There are many instances where microorganisms are oriented along gradients in the environment on a large scale. In the soil subsurface, studied by Kang, et al. (2005) in meadow at Blandy Experimental Farm, vertical profiles of microbial communities showed significant changes in abundance, as determined by acridine orange direct counts, and in community structure as determined

by community finger printing and subsequent discriminant function analysis to

produce n ordination plot. In the Santa Ynez Valley, CA, soils inhabited by annual

grasses also exhibited changes in microbial abundance and community composition along

a 200 cm vertical profile. Abundance was greatest at approximately 5 cm depth.

Variation in abundance and community structure was attributed to variation in

environmental parameters, such as labile carbon availability (Fierer et al. 2003).

Similarly, results from vertical profiles of tidal flat subsurface sediments also showed

changes in community composition and in nutrient availability along a vertical profile.

Phylogentic clustering demonstrated increased similarity between microbial communities

from within the same region of the sediment than with communities found at different

depths (Wilms et al. 2006). The phylogentic stratification observed in tidal sediments is

akin to the functional group stratification seen in Winogradsky columns. Microbes in

these columns are strongly stratified based on resource availability (Fig. 1.1). Algae,

cyanobacteria, and aerobic heterotrophs grow in the water and at the surface of the

sediment column. Below the sediment surface, microaerophilic sulfide oxidizers such as

Beggiatoa grow. The upper-most portion of the sand, below the microaerophilic region

takes on a reddish brown hue from the growth of purple, non-sulfur phototrophic

bacteria, such as the Rhodospirillaceae. Purple sulfur bacteria create a red-violet region

below the purple non-sulfur bacteria. As the entire column is transparent, and therefore

exposed to light, beneath purple sulfur bacteria, a greenish region composed of

phototrophic green sulfur bacteria forms. At the bottom of the column a black zone forms

due to the formation of iron sulfides from the products of sulfidogenic microorganisms

(Atlas and Bartha 1998). Winogradsky columns demonstrate the ability of

microorganisms to recycle; the waste products of one functional group are the energy

source or electron acceptor of a different group. The ability to recycle nutrients is a

common trait of microbial communities. The recycling of nutrients within a large scale

system is seen in Lake Pluss. Although thermally stratified there are multiple instances of

changes in microbial abundance and recycling of nutrients between functional groups,

such as sulfur oxidation and reduction along in benthic sediments (Rheinheimer 1991).

Within microbial communities, or across landscapes, one organism will often utilize the

waste product of another as an energy source, electron source, or electron acceptor.

Because of this, microorganisms can be categorized by the function(s) they fulfill or their

particular strategy for sustenance (Ehrlich and Newman 2009, Gottschalk 1979, Madigan

et al. 2000).
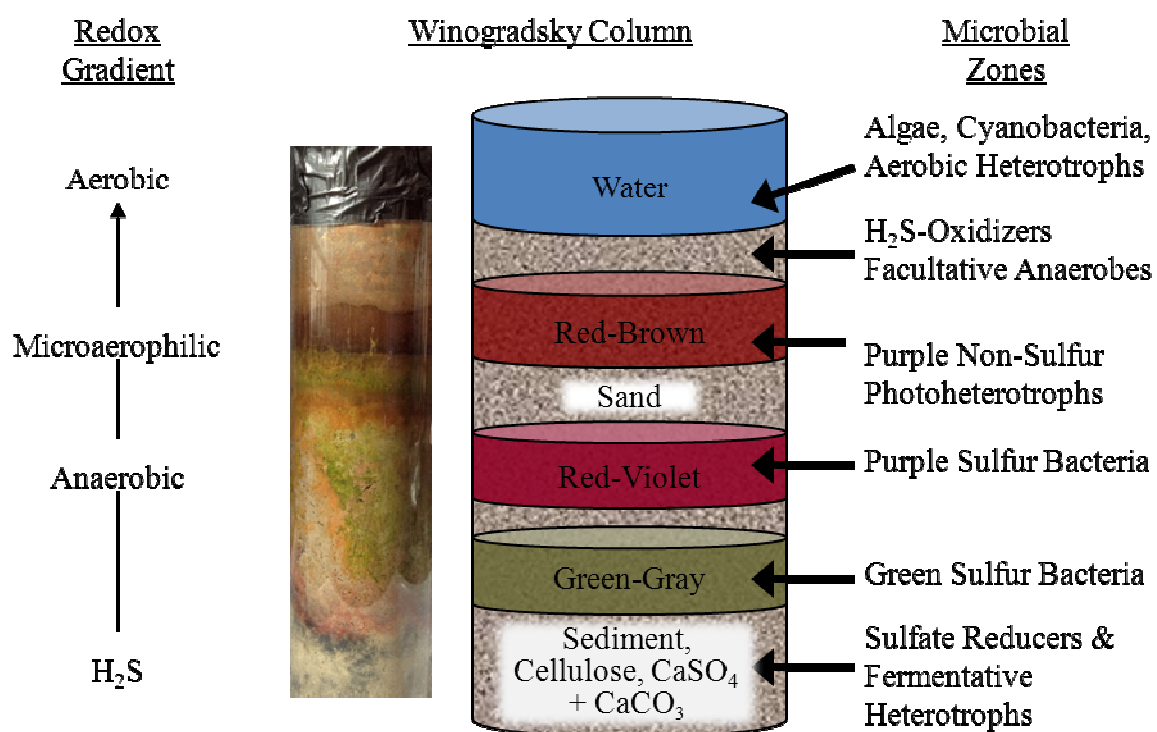
Fig. 1.1 – A depiction of the stratification of bacterial functional groups within a Winogradsky column adapted from Atlas and Bartha (1998) and a photograph of a Winogradsky column inoculated with sediment from the James River at the Virginia Commonwealth University Rice Center. Photo Credit: Jaimie Gillespi

For example, an aerobic heterotroph utilizes organic matter as an energy and electron source and oxygen as an electron acceptor, or a facultative anaerobe is capable of anaerobic respiration based on electron acceptors other than oxygen, but prefers aerobic respiration. Denitrifiers which use NO_3^- as an electron acceptor are a common example of facultative anaerobes (Atlas and Bartha 1998). In this way, much of life is organized around thermodynamic principles of oxidation and reduction reactions. As a result, the organisms conducting these reactions are organized in space and time by resource availability

In the experiments studying the Winogradsky columns the relationship between distribution and redox gradients was based on different terminal electron acceptors used by heterotrophs or electron sources in the case of phototrophs. The depth profiling studies in sediments, soils and Winogradsky columns are all examples of the Goldilocks Principle. The Goldilocks Principle is used by a variety of disciplines from astronomy to psychology, to business, to foreign affairs. While the specifics can vary among disciplines, the basis of the principle in all applications is that given a wide range of possible conditions, only a narrow range of those will be "just right" for optimal behavior (or in some cases even the existence) of the system of interest. The Goldilocks Principle is very similar to the niche theory which states a species fills a specific role in an ecosystem defined by multiple variables such as temperature, time, pH and function. The activity of microorganisms can be particularly difficult to define due to their small size and many subtle functions such as soil structure maintenance and pathogen control (Prosser 2012, Ritz et al. 2009). Astronomers take a very literal view of the Goldilocks story in understanding what conditions could lead to a planet that might be capable of

supporting life similar to that on earth. The Goldilocks Zone refers to a narrow range of distance from a star in which a planet can orbit that is neither too hot nor too cold, but is "just right" for the existence of liquid water, and an atmosphere comprising a gas mix similar to that of earth (Franck et al. 2007, von Bloh et al. 2011). In psychology, attention span can be influenced by the Goldilocks Principle. Visual stimuli that are too simple fail to captivate people, but overly complex stimuli will likewise not maintain peoples' interest. However, moderately captivating visual stimuli result in maintaining a person's interest for the longest time period (Kidd et al. 2012). Oncologists have also found that oncogenes that successfully convert a cell to a cancer cell have a Goldilocks activity spectrum. An oncogene that over stimulates a cell will trigger autophagocytosis, while a moderate oncogene will not do so. Further, cell death can help alleviate ischemic stress in tumors allowing them to persist, while rapid cell death, in general, is detrimental to tumor cells. In this way oncogene expression also adheres to the Goldilocks Principle (Martin 2011).

To further the study of microorganisms in the context of the Goldilocks Principle, we will study different functional groups of nitrogen-processing bacteria at both a landscape and mesocosm scale. Bacteria that can utilize nitrogen as a terminal electron acceptor, an energy and electron source, or all three, are ideal for studying energetic flow through a microbial ecosystem. Additionally, there are multiple applications for ecological information about nitrogen processing bacteria.

1.2.2   Nitrogen Reduction, Oxidation and Bacteria

Understanding how bacterial functional groups organize, based on abundance, along environmental gradients of different spatial scales is critical for the research,

development, and utilization of natural and engineered systems for technological

advancement and environmental protection. Microorganisms are not all created equal;

among the abilities of the various microbes involved with nitrogen cycling are the

capabilities to oxidize NH_3 into NO_3^-, known as nitrification, and the ability to reduce

nitrate into N_2, known as denitrification. However, these two capabilities are carried out

by different functional groups of bacteria that require mutually exclusive conditions in

which to oxidize or reduce N. Furthering the complexity of nitrification, the complete

oxidation of NH_4^+ to NO_3^- is carried out by two different and distinct functional groups.

Ammonia-oxidizing bacteria (AOB) convert NH_4^+ to NO_2^- and nitrite-oxidizing bacteria

(NOB) oxidize NO_2^- to NO_3^-. The nitrifying bacteria are obligate aerobes and

autotrophic. The energy obtained through nitrification is very small compared with that

obtained from heterotrophic metabolism. Energy yield is represented by the Gibbs free

energy of reaction (ΔG). Changes in free energy represent a change in the capacity of a

system to do work. Microbial metabolism harnesses this work potential through the

production of ATP associated with changes in free energy as the energy source is

oxidized (Madigan et al. 2000, Smith 1993). Compounds such as acetate yield a large

amount of energy when oxidized using compounds such as NO_3^-, compared to the

oxidation of NH_4^+; thus denitrification has a substantially more negative ΔG (per mole of

N transformed) than nitrification (See Box 1.1 for microbially mediated N reactions and

associated ΔG values).

In addition to aerobic ammonium oxidation, some AOB are also capable of

"nitrifier denitrification," in which the NO_2^- resultant from NH_4^+ oxidation is reduced to

N_2 gas through the same biochemical enzyme system as denitrification, using NH_4^+ as an

energy and electron source (Philips et al. 2002, Poth and Focht 1985, Verstraete and Philips 1998). Denitrification is usually a heterotrophic reaction conducted largely by facultative anaerobes that use NO_3^- as the electron acceptor in place of oxygen. In the case of nitrifier denitrification (also called OLAND for Oxygen Limited Autotrophic Nitrification Denitrification), the reaction is lithotrophic, as NH_4^+ is used as an energy and electron source. The denitrification reaction reduces NO_3^- to N_2 and is responsible for a large portion of Nr conversion to N_2 globally.

Box 1.1 – Biologically Mediated Nitrogen Oxidation-Reduction Reactions.

AEROBIC REACTIONS

Reaction	Eq. #	ΔG ** $(kJ\ (mol\ N)^{-1})$	Functional Group†	Reference
Nitrification				
Ammonium Oxidation $NH_4^+ + 1.5O_2 \rightarrow NO_2^- + H_2O + 2H^+$	*1.1*	-275	AOB	(Prosser 1989)
Nitrite Oxidation $NO_2^- + O_2 \rightarrow NO_3^- + H_2O$	*1.2*	-74	NOB	(Prosser 1989)

ANAEROBIC REACTIONS

Reaction	Eq. #	ΔG ** $(kJ\ (mol\ N)^{-1})$	Functional Group†	Reference
Denitrification $NO_3^- + 1.25CH_2O + H^+ \rightarrow 1.25CO_2 + 0.5N_2 + 1.75H_2O$	*1.3*	-595	DNF	(Hedin et al. 1998)
Nitrifier denitrification (OLAND*) $NH_4^+ + NO_2^- \rightarrow N_2 + 2H_2O$	*1.4*	-360	AOB	(Poth and Focht 1985)
Anaerobic Ammonium Oxidation (anammox) $NH_4^+ + NO_2^- \rightarrow N_2 + 2H_2O$	*1.5*	-358	AXB	(Jetten et al. 1998)

*OLAND, or oxygen limited autotrophic nitrification is lithotrophic denitrification conducted by some AOB.

** Free energy calculations were determined at standard conditions, 25°C, atmospheric pressure, and pH = 7.

† Ammonia oxidizing bacteria (AOB); Nitrite oxidizing bacteria (NOB); Denitrifiers (DNF); Anaerobic ammonia oxidizing (anammox) bacteria (AXB).

Since the widespread utilization of the Haber-Bosch process to fix N from the atmosphere for fertilizer application and other uses there has been an imbalance in the nitrogen cycle. In some instances the denitrifiers (DNF) have effectively converted fixed N to N_2 gas thereby removing excess N from terrestrial and aquatic ecosystems; however, more frequently there is a need to adjust land use practices or remediate waste water to effectively remove Nr (Galloway and Cowling 2002, Zumft 1997). Unused fertilizer enters ground water aquifers or is carried by rain water runoff to adjacent aquatic ecosystems. Mass-balance techniques to quantify the amount of fertilizer not taken up by crops, but denitrified before entering aquatic systems can be difficult to achieve, but estimates range from a global average of 8% of fertilizers being mineralized to N_2 within the agricultural ecosystem to numbers as high as 48% of fertilizer N ultimately being denitrified after exportation from agricultural systems (Galloway and Cowling 2002, Van Breemen et al. 2002). At Cobb Mill Creek, on the Eastern Shore of Virginia at least 70% of the nitrogenous fertilizer is removed from groundwater and subsurface flow prior to entering the stream water (Gu et al. 2007, Mills et al. 2008).

It is also important to note that N applied as fertilizer and taken up by plants remains a biologically active compound and even though it is not initially exported to adjacent aquatic systems, ultimately the N in crops is consumed by animals and humans and only a small percentage of the consumed N is retained in the body. The remainder is excreted, usually as NH_4^+, and commonly into a public water treatment system, which attenuates, but does not completely remove N pollution before ultimately discharging to local rivers and streams. Therefore, most N applied as fertilizer ultimately ends up in aquatic ecosystems if not converted to N_2 gas through denitrification. One of the

difficulties of assessing the fate of N compounds is the multitude of reactions that N can participate in and the many forms of N that can result. While N_2 is a reasonably stable compound that requires a significant energy input to transform, compounds such as NH_4^+, NO_3^- NO_2^-, NO, and N_2O are reactive compounds that are utilized biologically and participate in abiotic reactions in the atmosphere. As the five compounds mentioned are so reactive compared to N_2, they are often termed Nr, for reactive N compounds (Galloway and Cowling 2002, Galloway et al. 2002). Denitrification does not always run to completion. For example, N_2O is an intermediate step in the reduction of NO_3^- to N_2 gas and as a gas, N_2O is often lost from sediments, soils, or water treatment systems before complete denitrification can utilize the N_2O as an electron acceptor (Zumft 1997). Release of N_2O from a denitrifying system is problematic as it is a greenhouse gas that is approximately 300 times more effective at trapping heat than CO_2 (IPCC 2001).

The discovery of the anaerobic oxidation of ammonium, known as anammox, creates further ambiguity because N_2 is also the final N product of that process, and anammox can masquerade as denitrification or nitrification followed by denitrification. Despite the similarity of the end products of both nitrifier denitrification, and combined nitrification and denitrification, anammox is a different biochemical reaction pathway. The bacteria that conduct anammox are highly specialized and phylogenetically distinct. Anaerobic ammonium oxidizing bacteria (AXB), such as *candidatus brocadia anamoxidans*, have yet to be grown in pure culture; therefore, AXB are resigned to candidate species status (Jetten et al. 2001, Schmidt et al. 2002). While anammox appears to play a large role in the deep ocean, its role in fresh water systems and in wastewater treatment is less well understood, even though anammox has been effectively

incorporated as a component of N removal in water treatment. In the early 1980s, scientists hypothesized that a reaction coupling the reduction of NO_3^- with the oxidation of NH_4^+ was responsible for N removal in deep sea sediments. Conjectures were based on disproportionate losses of N compared to observed C mineralization losses (Emerson et al. 1980, Thamdrup and Dalsgaard 2002). In 1995, van de Graaf et al. (1995) identified anaerobic ammonium oxidation (anammox) as a biological process, and Mulder et al. (1995) confirmed the existence of anammox in wastewater treatment systems. Although bacteria capable of anammox have never been isolated, microbial consortia have been developed that contain a high percentage of anammox-capable organisms. The consortia have been used to identify the organisms as members of the phylum planctomycetes and to develop phylogentic probes for *in situ* identification (Jetten et al. 1997, Schmid et al. 2000, Schmid et al. 2005, Strous et al. 1999a, Strous et al. 1999b).

Since its discovery, and identification, anammox has been found in multiple locations, and it appears to account for large percentages of fixed N (i.e., Nr) losses. Marine sediments in the deeper parts of the ocean are where anaerobic ammonium oxidation is responsible for the largest percentage of N loss. In sediments taken from the North Sea, anammox contributed from 2 to 67% of N conversion to N_2. Offshore sediment samples were collected in the Skagerrak Straights at 200 m and 700 m depths, while coastal samples were collected from Aarhus Bay. The percentage of N loss in the Skagerrak samples attributed to anammox ranged from 24–67%. At the 700m-depth location, anammox consistently contributed to Nr conversion to N_2. The high anammox rates were likely due to environmental limitations on denitrification. At that depth, Skagerrak sediments have a high concentration of manganese in the sediments and low

organic matter content. The high manganese oxide content may enrich for Mn-reducing

bacteria which then compete with denitrifiers for the already scarce organic matter. Such

a limitation on denitrification may be responsible for NO_2^- and NO_3^- availability for

utilization by AXB. Mineralization rates of carbon suggest that organic matter was more

readily available at the shallower (200m depth) location and even more available in the

Aarhus Bay location (Canfield et al. 1993, Haese 2006, Thamdrup and Dalsgaard 2002).

Similar research was later conducted in the Black Sea to assess the abundance of

anammox-capable bacteria (AXB), anammox activity, and observed concentrations of N_r

compounds. Along a vertical profile of the Western Basin of the Black Sea, near the

bottom of the suboxic zone (approximately 90 m below the ocean surface), the maximum

abundance of AXB occurred at the same depth as the peak in NO_2^- concentration, and a

decline in NH_4^+ to below detection limit. The detection of ladderane lipids in extracted

organic matter also peaked at the same depth, as did anammox activity based on cultures

spiked with ^{15}N. Ladderane lipids are a biologically produced molecules specific to

anammox bacteria and a few archaea (Damste et al. 2005, Damste et al. 2002, Jaeschke et

al. 2009). Further, the cell activity determined by FISH direct counts and the ^{15}N tracer

study were congruent with flux rates calculated from chemical data. The congruency

between two techniques for assessing activity suggests a high likelihood that the

laboratory estimates of anammox activity were a good approximation of *in situ* activity,

and that the distribution profile accurately reflects the organisms spatial organization

along the Black Sea depth gradient (Kuypers et al. 2003). Results similar to those

observed in the North Sea were seen in the open waters of Benguela upwelling, a 150,000

km^2 area in the Atlantic Ocean off the coast of southern Africa. The upwelling is a region

of deep ocean water mixing with warmer surface water, and it encourages a highly

productive ecosystem in the intermixing zone of the Benguela upwelling. In addition, the

upwelling causes elevated water exchange rates, and therefore more variability in

dissolved oxygen, N inputs, and organic matter (Boyer et al. 2000). Despite the increased

variability, the slow-growing anammox bacteria were still identifiable in the open water.

In the oxygen minimum zone, NO_3^- concentration declined to near 0 ppm, while the

concentration of ladderane lipids increased, as did the production of N_2 by AXB in

cultures incubated with ^{15}N, and the abundance of cells identified as AXB through

fluorescent *in situ* hybridization (FISH, explained in detail in section 2.1.6). Findings,

from the Benguela upwelling, are important because they suggest that anammox is a

functional process not only in sediments and pore water, but also in the open ocean.

Calculations from ^{15}N incubations indicate that up to one teragram of N may be lost from

the Benguela system alone. In comparison, the oxygen minimum zone of the entire global

ocean system is expected to lose 80–150 Tg year^{-1} (Kuypers et al. 2005). The open ocean

represents a 3.6 x 10^8 km^2 surface area, so the Benguella upwelling represents 0.04% of

the ocean's surface, yet it represents 0.6–1.2% of the ocean's N mineralization to N_2 gas

and this disproportionately large component of ocean N conversion to N_2 is conducted

by anammox bacteria.

In terrestrial and freshwater ecosystems anammox has been shown to play a

substantially smaller role. Paddy soils in Southern China were found to be the greatest

terrestrial source of anammox activity in literature reviews (Hu et al. 2011, Zhu et al.

2011). In freshwater locations, the highest reported contribution of anammox to N_2

production is 40% in some Canadian groundwater systems; however, this finding is a

deviation from the more common failure to detect any anammox at all (Hu et al. 2011).

Although anammox appears to make only a small contribution to N_2 production in

terrestrial and freshwater ecosystems, the organisms can be enriched and utilized in

wastewater treatment systems. As an anaerobic, autotrophic organism, anammox

bacteria do not require aeration to oxidize NH_4^+. Furthermore, they produce thin biofilms,

thereby reducing sloughing of biofilm material which inevitably clogs or otherwise

reduces efficiency of biological water treatment systems. Unlike denitrifiers, AXB do

not require organic matter, which can be a costly additive required to enhance

denitrification. The ability to treat wastewater without aeration or organic matter

amendments significantly reduces treatment costs (Daims and Wagner 2010).

Engineers are currently designing systems that take advantage of anammox known as

SHARON and CANNON. The SHARON process is a Single reactor system for High-

rate Ammonium Removal Over Nitrite, whereas the CANON process is Completely

Autotrophic Nitrogen-removal Over Nitrite. In a SHARON system a single chamber is

used to generate partial nitrification, converting NH_4^+ to NO_2^-. To prevent complete

nitrification, the system takes advantage of the increased activity of ammonia oxidizing

bacteria (AOB) at higher temperatures and the slower growth rate of nitrite oxidizing

bacteria (NOB). A SHARON system operates at an elevated temperature, (above 26°C)

and has a 1-day retention time which prevents NOB from reaching a meaningful

abundance in the reactor system. The system is periodically aerated to provide O_2 for

nitrification to occur. Aeration also strips CO_2 from the liquid preventing acidification.

The SHARON reactor also has an anaerobic phase where the reactor is not aerated, and

during which methanol is added to act as an electron donor and energy source for

denitrification that utilizes the NO_2^- produced by AOB. Effluent from SHARON systems

is often treated with a second batch reactor enriched for AXB. The combined two stage

process is often colloquially referred to as "SHanammox." The CANON process, also a

single stage reactor system, utilizes a combination of nitrification and anammox. The

first step is ammonia oxidation by AOB, which produce NO_2^- and consume O_2, thereby

creating an anaerobic environment with plentiful NO_2^- for anammox to occur. In

CANON systems, oxygen availability must be closely monitored to prevent NO_2^-

accumulation (Schmidt et al. 2003).

Nitrifying biofilms from wastewater treatment systems have been studied using a

combination of microscale electrodes and FISH. Schramm et al. (2003), found distinct

regions of nitrifier biofilm activity and composition based on dissolved O_2. The observed

relationship between nitrifier distribution and dissolved oxygen profiles is a good

example of a Goldilocks effect of optimal conditions on microscale bacterial

distributions. In addition to these microscale structural relationships to dissolved O_2,

some nitrifying bacteria, such as *Nitrosomonas eutropha,* are capable not only of aerobic

ammonium oxidation, but are also capable of OLAND nitrification, the lithotrophic

oxidation of NH_4^+ using NO_2^-. (Zart and Bock 1998). This additional trait may create

niches for some species of AOB thereby increasing their abundance and distribution

range. Vertical profile studies of biofilms at the microscale have shown structural

organization based on dissolved O_2 availability. Schramm et al. (2003) demonstrated that

nitrifying biofilms orient themselves along dissolved O_2 gradients (Fig. 1.2). The fully

oxygenated surface layers of the biofilm are predominantly AOB (red), and as oxygen is

consumed, the AOB abundance declines and NOB (green) abundance increases. Similar

results were found by Aoi et al. (2004) on biofilms grown on cement balls in aerated

batch reactors. The vertical profile of AOB and heterotroph abundance was
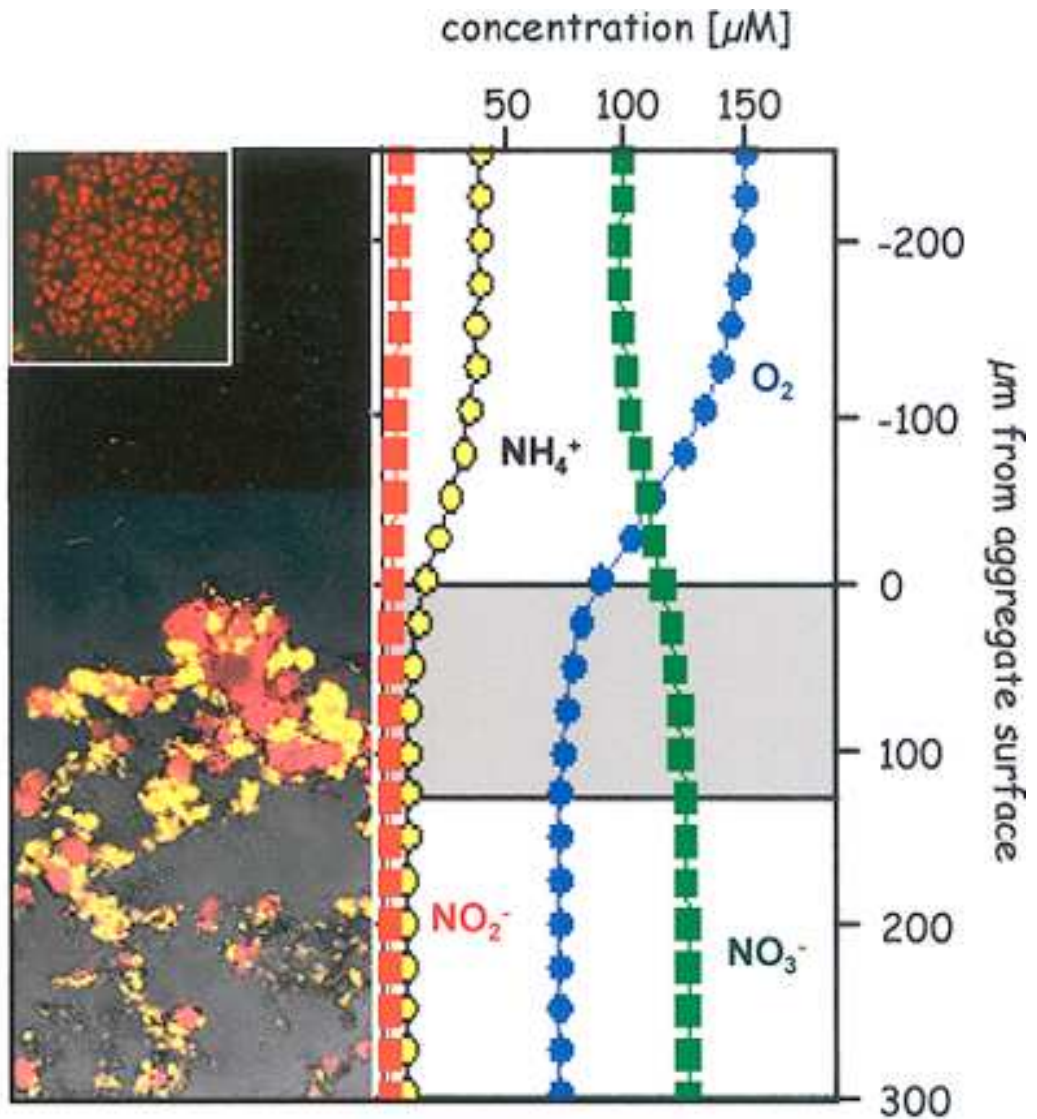
1.2 – Distribution of nitrifiers within a mixed biofilm, taken from Schramm, et al., 2003. Dissolved oxygen, NH_4^+, NO_2^- and NO_3^- concentration form within a biofilm are displayed on the left and a digitally edited micrograph taken using confocal scanning microscope of the biofilm is displayed on the left.

found to change in response to dissolved oxygen stress. Heterotrophs were able to out

compete nitrifiers for biofilm surface space. Heterotroph dominance in the surface layers

of the biofilm was likely due to the energetic advantage aerobic respiration gives

heterotrophic bacteria over lithotrophihc bacteria, such as nitrifiers, due to the larger

energy yield of organic matter oxidation compared to NH_4^+ or NO_2^- oxidation.

Studies on continuously mixed systems focus on planktonic cells suspended in the

bulk fluid, or on organization within cell aggregates. Daims, et al. (2001), studied

nitrifiers in sequencing batch reactors and although AOB and NOB colonies exhibited

heterogeneous distribution, the AOB composed 55% of the total microbial community

while NOB were a mere 8%. Carvalho et al. (2006), found inconsistent abundances of

AOB and NOB in cell aggregates from nitrifying/denitrifying sequencing batch reactors.

High-density aggregates comprised more NOB than AOB, but there were also low-

density cell aggregates containing greater numbers of AOB than NOB. One potential

explanation for this is that NO_2^- availability in the bulk fluid may have made it possible

for NOB to flourish in some aggregates. Microscale biofilm studies (e.g., (Gieseke et al.

2003)) have also reported hollow spheres of cells that are potentially indicative of biofilm

succession based on dissolved O_2 availability, an observation which may alter

interpretation of Carvalho et al.'s (2006) findings by suggesting there was unnoticed

temporal variation within individual cellular aggregates. Therefore, understanding the

both the spatial and temporal distribution of microbes is important if we are to understand

their ecological impacts on net system processes.

As the microbes responsible for oxidation and reduction of N compounds are

diverse and require very different environmental conditions, understanding the

parameters affecting distribution and net community activity of these functional groups is imperative for improved water regeneration. Water-treatment systems are the ideal location to study factors that control the distribution of nitrogen – processing bacteria. The primary species of N in the municipal waste stream is NH_4^+, thereby requiring both nitrification and denitrification, or anammox for effective removal. Water is a diminishing resource and using technology based on microbiological processes is one of the most energy efficient ways to attenuate nitrogen waste. Domestic wastewater is usually collected and treated by wastewater treatment plants (WWTP) prior to release into local rivers. Agricultural runoff, however, most often contains nitrogen as NO_3^-, and the runoff enters adjacent aquatic ecosystems without treatment, unless an adequate vegetated riparian buffer zone is in place. Riparian buffers and wastewater treatment plants are just two examples of management strategies for reducing N_r inputs into the environment (Rabalais 2002). Microorganisms play large role in the removal of N_r in both riparian buffer zones and in waste water treatment plants. Consequently, both natural and engineered water treatment systems are ideal places to study the ecology of N-processing organisms because the findings will have direct applications to the efficacy of those systems as well as shedding light on how microbial communities organize themselves spatially in the environment.

1.2.3 Utilizing Bacteria for Water Remediation

In contrast to centralized WWTPs, conventional on-site treatment systems include septic systems or treatment wetlands. A septic system is, in essence, a static batch reactor which will leach Nr into the surrounding groundwater. Constructed treatment wetlands have similar issues. Horizontal wetlands are dominated by horizontal flow through the

treatment system while vertical flow wetlands apply wastewater to the surface of the

wetland and it trickles downward through the wetland bed material. Horizontal wetlands,

like septic systems, offer little opportunity for aerobic processes to occur. Because of the

large amount of organic matter in the physical wetland matrix, there is often very little O_2

in the discharging water. Vertical wetlands attempt to remedy this, but often, they do not

provide an anaerobic phase for extended time periods, a condition necessary for

denitrification to occur. In addition, both types of treatment wetlands require extensive

energy inputs and space to treat wastewater. Neither treatment wetlands nor septic

systems are easily adapted to allow water reclamation.

Wastewater treatment plants are commonly designed in multiple stages to support

both nitrification and denitrification. An aerobic stage supports nitrifying microbes,

through constant bubbling aeration, and nitrification converts NH_4^+ to NO_3^-. Following

aeration, the nitrified wastewater is allowed to stagnate in a second treatment stage in

which heterotrophs quickly consume the available oxygen resulting in an anoxic

environment. In this treatment stage, denitrifiers readily consume organic matter while

reducing NO_3^- to N_2 (Austin and Nivala 2009, Wallace and Austin 2008). Wastewater

treatment plants that use a two-stage design are large and require a tremendous amount of

energy for aeration and fluid transport. For these reasons they are ill suited to treat

smaller waste streams that cannot be adapted to connect to local waste water treatment

plants.

Sewage is approximately 95% water and only 5% contaminants such as BOD,

TSS and grease oils and fats (Benefield 2002), so that much or all of the water contained

in the waste stream should be able to be reclaimed for purposes that do not require

potable H_2O, for example, irrigation, flush water, and water features (fountains, etc.). While it is expensive to purify water to drinking-quality standards, use of reclaimed water where potable water is not needed can be an effective way to reduce the demand for potable water, thereby making a limited resource more available.

Worrell Water Technologies, Inc., a local company in Charlottesville, VA, has attempted to fill this market niche while addressing water resource availability issues by constructing on-site, tidal-flow wastewater treatment systems to produce water for irrigation, flush water, cooling water, or groundwater recharge, i.e., uses that do not require the high purity level of potable water. Water treatment systems used by Worrell Water have the benefit of small footprint, low energy consumption, and on-site water reuse (Austin and Nivala 2009).

In many cases, at least half the demand for water can be met with reclaimed water thereby reducing the demand for potable water. Diminishing water availability over the next 40 years will only increase the need to reclaim wastewater (Hinrichsen et al. 1998). Standards for reclaimed water in the United States are highly variable based on the intended fate of the reclaimed water. In general, secondary treatment and disinfection are required and fecal coliforms and total suspended solids need to be monitored (EPA 2004). Guidelines for water reuse established by the WHO have a high degree of variability depending on the intended application. Guidelines set in place by the WHO largely focus on controlling exposure to pathogens, not chemical exposure such as NO_2^- and NO_3^- exposure (WHO 2006). For more information on wastewater reuse please see (http://www.who.int/water_sanitation_health/wastewater/gsuww/en/index.html). Water re-use usually

does require Nr attenuation to prevent rapid eutrophication in receiving bodies of water, or in on-site re-use applications.

While water re-use standards are nuanced based on variation in intended use, the drinking water standards for N are very clear. Drinking water standards for NO_3^- and NO_2^- are established to prevent methaemoglobinaemia. Potable water in the US is subject to EPA drinking water standards which set acceptable concentration maxima for nitrate at 10 ppm NO_3^-–N, and for nitrite at 1 ppm NO_2^-–N. There is not a drinking water regulation for NH_4^+. For more information on EPA established drinking water guidelines please see (http://water.epa.gov/drink/contaminants/basicinformation/#nlink). The World Health Organization (WHO) has set the nitrate drinking water standard at 50 ppm NO_3^- or 11 ppm NO_3^- –N and the nitrite drinking water standard at 3 ppm NO_2^- or 0.9 ppm NO_2^- –N. WHO does not set a drinking water standard for NH_4^+ because it occurs in most water supplies at levels far below cause for concern (WHO 2006). Additional information, regarding water quality standards established by WHO, can be found at

http://www.who.int/water_sanitation_health/publications/2011/dwq_guidelines/en/index.html.   Meeting the full criteria for drinking water quality is considerably more energy and time intensive, in most instances, than meeting the requirements for water re-use, which can have substantial appeal, especially for on-site treatment of small wastewater streams that still require treatment.

While engineered systems treat water that was primarily used by direct human consumption, natural systems treat water that has been discharged from non-point sources or as agricultural run off. Riparian buffers, natural systems, are forested areas along side water bodies such as creeks and rivers. In the western United States, oligotrophic water

systems with hyporheic exchange experience large amounts of denitrification along a large portion of the riparian zone (Jordan et al. 1993). However, on the East Coast, stream systems often have fine clay sediments interlaced with lenses of organic matter. These systems often have little to no hyporheic exchange, but denitrification is still possible in the subsurface stream sediments where anoxic microsites encourage denitrification. Microsites where denitrification can occur generally have high organic matter content and low permeability. Sediments with low permeability increase the hydraulic retention time thereby increasing the contact time of Nr contaminated waters with bacteria capable of denitrification. Organic matter, such as decaying leaves, creates an impermeable layer rich in organic matter thus increasing residence time and providing the necessary organic matter. Low permeability itself does not ensure denitrification because organic matter is still required as an energy and electron source (Cooke and White 1987, Hill 1983, McClain et al. 2003). This creates a great deal of spatial heterogeneity in sediments resulting in a likely patchy distribution of denitrifiers. Despite spatial heterogeneity, Gu et al.(2007) have noted that variation in residence time in intact sediment cores collected from Cobb Mill Creek can impact NO_3^- removal and that substantial NO_3^- is removed from groundwater as it passes through the subsurface sediments of Cobb Mill Creek (for more details about Cobb Mill Creek see Methods 2.2.1 Site Description). While ideal for removing excess nitrate present in fertilizer, riparian buffers cannot remove large loads of NH_4^+ associated with the high organic matter content of municipal waste. Riparian buffer zones are ill suited to treat municipal wastewater because the high organic matter load would drive the system anoxic, thus preventing nitrification, the first step of Nr removal (Rabalais 2002).

1.3   **Objectives and Hypothesis**

To expand our understanding of distributions of nitrogen-cycling organisms under various scenarios my dissertation research uses a bench-scale engineered wastewater treatment system to study the distribution and activity of autotrophic nitrifiers along with a study of the spatial distribution of denitrifying bacteria sediments of a low-relief coastal stream on the Eastern Shore of VA. This work utilizes techniques in molecular microbiology and analytical chemistry to quantitatively analyze the structure-function relationship of microbial communities in two distinct systems: an engineered tidal wetland treatment system and the Cobb Mill Creek experimental hill slope on the Eastern Shore of Virginia. Specific applications of my research findings have included alterations to tidal cycling regimes in tidal treatment systems to better utilize the available space for nitrification and subsequent denitrification and a better understanding of environmental factors resulting in 70% of agricultural N runoff removal in less than 1 m of subsurface creek sediment.

Inside tidal wastewater treatment systems microbial distributions were manipulated by adjusting tidal cycling frequency which likely governed dissolved oxygen availability. It is likely the limiting reagent in nitrification and an inhibitor of denitrification. Competition for dissolved oxygen between AOB and NOB likely regulates the abundance of NOB and organisms capable of anaerobic ammonia oxidation (anammox). While AXB require an anaerobic environment, NH_4^+ and NO_2^-, the NOB require NO_2^- and oxygen. As NOB generate a mere 22 kcal mol^{-1} NO_2^- oxidized, they are

not capable of competing with AOB under oxygen limited conditions. Therefore AXB are likely to proliferate when NOB are unable to garner sufficient oxygen for growth.

The major findings of this study are that functional group abundances follow the Goldilocks Principle— the bacteria proliferate at a depth within the column where conditions are just right to allow optimal growth. This optimal location is usually around 60 cm below the top of the Tidal column, or at the top of the Trickling-flow column, though magnitude of abundance appears related to N loading. Functional group abundances almost always reflected a short redox tower where the total abundance of bacteria was always greatest, followed by the abundance of AOB. The smallest component of the microbial community was most frequently AXB, however there were instance were AXB outnumbered the NOB.   Also of interest is the low energy input required to run the tidal treatments compared to the Trickling-flow treatments (Austin and Nivala 2009). While both Tidal- and Trickling-flow treatments often had the same abundance values there was substantially more energy used in the Trickling-flow treatments. Abundance of the various bacteria was largely controlled by N availability if the columns were given extended time period to reach steady state. The four-week incubations after changing flow volumes likely did not allow microbial communities to equilibrate to their new environment

Both riparian buffer systems and wastewater treatment plants depend on microbial activity to transform reactive nitrogen (N_r) to N_2 gas, which composes over 70% of the atmosphere. However, transforming reactive N to N_2 gas requires several different functional groups of bacteria that need distinct environments. Nitrification is an aerobic process that oxidizes NH_4^+ to NO_3^- that is subsequently reduced to N_2 gas through

denitrification which is an anaerobic process inhibited by the presence of O_2. Denitrification in wastewater treatment is a heterotrophic process in which oxidized forms of N are used as a terminal electron acceptor for the oxidation of reduced organic carbon. In contrast, nitrification is an autotrophic process in which oxygen is used as a terminal electron acceptor for the oxidation of reduced N species. The organisms that carry out these complementary but opposing processes have very different requirements in order to carry out their functions. Differences in environmental conditions such as resource availability, or organic matter gradients can have a profound effect on the distribution and activity of these two functional groups.

Denitrification was studied in the Cobb Mill Creek experimental hill slope. The denitrifiers studied were primarily heterotrophic and as such the abundance of denitrifiers was found to be largely controlled by the presence of organic matter which served not only as an energy source, but to remove O_2 from the environment through aerobic respiration. As a result of this finding, denitrification is thought to occur through the entire TWTS system because organic matter is plentiful and distributed throughout the system. Nitrification however was expected to be less uniformly distributed due to the limited diffusion-based replenishment of oxygen during long inundation periods and abundance data confirm this finding. Nitrifiers were shown to exhibit a peak in abundance at some region within the TWTS which has we have termed the "Goldilocks Zone." At this location, usually at ~60 cm depth, conditions are just right to encourage proliferation of nitrifying bacteria. Experimentation found that altering the frequency of tidal cycles could disrupt the microbial distributions, but returning tidal cycling to the initial state appeared to restore the community activity, if not the original distribution

pattern. There is potential concern scaling these results to full size reactors because the TWTS studies were mesocosm scale systems that had a high degree of "edge". The small system had a high degree of surface area compared to a normal system therefore oxygen diffusion in larger systems may not be as uniform, especially in the deeper regions of actual TWTS where the mesocosm study found the greatest abundance of nitrifiers.

2.   Materials and Methods

2.1   Nitrification Study

2.1.1   Experimental Approach

To assess the variation and response of nitrifying bacteria, and AXB to changing

environments, four bench-scale biological reactors were constructed and housed at

Worrell Water. The four reactors each represented a different treatment based on

nitrogen loading and flow type. Tidal treatment reactors filled from the bottom and

remained saturated until they drain completely. To simulate standard vertical flow

wetlands two of the columns were intermittent trickling-flow columns. Approximately

every 15 minutes the columns were pulsed with water that immediately trickled through

the column and drained back to the reservoir. One tidal column and one intermittent

trickling-flow column each receive a high nitrogen load (202 g N m^{-3}) and the remaining

two columns received a Low-nitrogen load (51 g N m^{-3}). Each month, the volume of

water passing through the columns was altered, thereby simulating a type of

environmental disturbance on the system.

2.1.2   Biological Reactor Design

In order to assess the effects of N loading and hydraulic regime on the ecology of

bacteria relevant to wastewater treatment, four mesocosm-scale column reactors were

constructed from PVC. Two of the columns were established as Tidal-flow columns, one

receiving a High-N feed and the other receiving a Low-N feed. Two of the columns were

established as trickling-flow columns and one received the High-N feed while the other

received Low-N feed. All four columns underwent sequential hydraulic regime

treatments. The columns were packed with a light weight expanded shale aggregate

(LESA), and fitted with sampling portals approximately every 20 cm (Fig. 2.1). LESA

served as structural support for biofilm development.

A. 3 g LESA

B. Completed Columns

D. Trickling Flow Column

C. Tidal Flow Column

20 cm

122 cm

280 cm

61 cm

20 cm

122 cm

280 cm

61 cm

Sampling
Port

Multidirectional
Valve

Reservoir
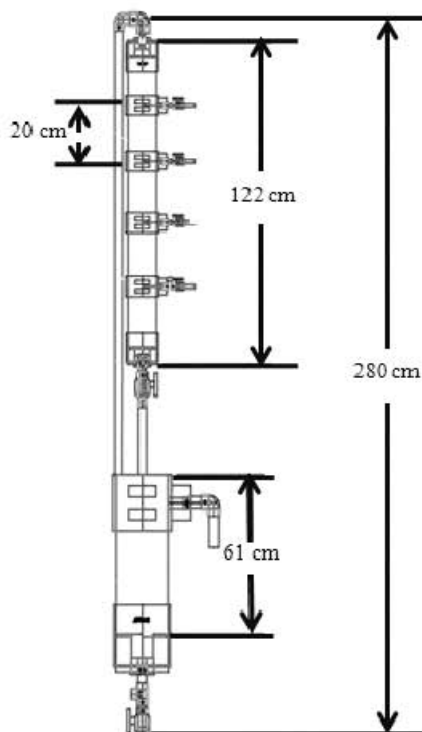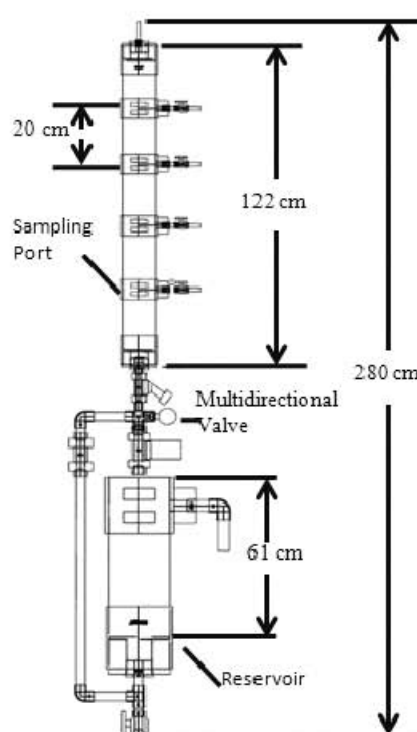
Fig. 2.1– A.) a photo of LESA, B.) a photograph of all four completed columns, C.) Schematic diagram of the Tidal-flow column and D.) a diagram of the Trickling-flow column.

The shale aggregate was a processed material giving it unique properties that make it ideal for biofilm support in wastewater treatment.   Shale was baked at high temperatures, in excess of 1000° C, causing the sedimentary layers to expand, resulting in a porous, highly fractured, light-weight fill that provided microbial biofilms ample surface area for colonization. Further, compared to other fill options such as pebbles or crushed bricks, the aggregate had a high cation exchange capacity (1.2 meq 100 g^{-1} LESA) allowing it to retain NH_4^+ during drained phases. Therefore the LESA could serve as a source of NH_4^+ to aerobic nitrifiers with while the columns were drained, and saturated with air (Austin 2006). Other common uses of LESA include backfill at construction sites for increased soil stability, inclusion in rooftop garden soils, and integration with cement to form lightweight high-performance concrete (For additional information please see http://www.escsi.org).

All four column reactors were connected to, and their operation controlled by, a computer (Siemens TD-200 Programmable Logic Controller) and associated I/O modules. The computer was programmed by an engineer at Worrell Water using Ladders, a computer code designed for operating Programmable Logic Controllers. The column reactors were constructed and programmed to be either Tidal-flow columns or Trickling-flow columns. To make comparisons possible, tidal and trickling processes were standardized by the total volume of water re-circulated within the reactors.

2.1.3   Tidal-Flow Column Specifications

The High- and Low-N tidal columns were each fitted with a multidirectional valve (Fig. 2.1) that enabled the tidal columns to fill and drain from the bottom of the column. Each tidal cycle consisted of a dry phase and a wet phase of equivalent time periods. Tidal columns flooded from the bottom and remained filled for the saturated phase, and then emptied and remained unsaturated for the drained phase. For example, during the initial hydraulic treatment the tidal columns remained saturated with water for a 30 minute saturated phase, after which the tidal columns drained immediately through the bottom and remained unsaturated for 30 minutes and then the tidal process repeated itself. This initial hydraulic treatment results in 24 cycles day^{-1}. There were then four sequential hydraulic treatment periods, each lasting 4 weeks (Table 2.1). In order to distinguish the initial and final treatments, both of which were 24 cycles day^{-1}, the letters i and f are included in the cycling treatment name (e.g. see Cycles day^{-1} column in Table 2.1).

Table 2-1. Tidal-flow and intermittent trickle flow frequencies throughout the course of the experiment. Trickling-flow columns always have 96 cycles per day.

Tidal-Flow Columns			Water Pumped (L Day^{-1})	Intermittent-Trickling-Flow Columns	
Cycles day^{-1}	*Saturated Phase* (min phase^{-1})	*Drained Phase* (min phase^{-1})		*Trickling Phase* (min phase^{-1})	*Draining Phase* (min phase^{-1})
24i	30	30	73i	0.8i	14.2
16	45	45	49	0.5	14.5
8	90	90	24	0.3	14.7
4	180	180	12	0.2	14.8
24f	30	30	73f	0.8f	14.2

2.1.4   Intermittent Trickling-Flow Column Specifications

Trickling-flow columns were pulse fed, continuously draining reactors. These

columns were fitted with a Lifeguard Quiet One Model 4000 pump to circulate water.

Synthetic wastewater was pumped from the reservoir to the top of the column through an

external conduit and allowed to trickle through the LESA and return directly to the

reservoir. The water was applied at uniform time increments throughout the course of the

day, resulting in trickling minutes per quarter hour. For example, during the initial

treatment, the pumps on the non-tidal columns circulated water for 0.8 minutes. For the

following 14.2 minutes, the Trickling-flow columns drained into the reservoir resulting in

a 0.8 min (0.25 hr)$^{-1}$ trickling treatment. The re-circulation pattern repeated itself

throughout the day. There were 4 sequential trickling treatments, each lasting for four

weeks, with trickling duration adjusted to produce re-circulated water volumes equivalent

to the volume of water re-circulated in the tidal columns (Table 2.1). Similar to the tidal

columns, the initial and final treatments had identical hydraulic parameters and to

distinguish these two temporally distinct treatments the letters i and f were added to the

treatment name.

2.1.5   Reactor Feed

To examine the effect of nitrogen loading on microbial assemblages two N-loading schema were used: a High-nitrogen feed and a Low-nitrogen feed (Table 2.2). There was a Tidal-flow and there was a Trickling-flow column receiving each type of feed. The columns that received high nitrogen feed had 3.7 g d^{-1} of urea, equivalent to 2.33 g d^{-1} of NH_4^+–N added. The Low-Nitrogen columns received 0.9 g d^{-1} of urea, equivalent to 0.47 g d^{-1} of NH_4^+–N added.

Table 2-2. Synthetic sewage deposited in the reservoir each day.

Compound	Dose (g d^{-1})		C and N Load (g d^{-1})	
	High-N Feed	Low-N Feed	High-N Feed	Low-N Feed
Whey	1.5	1.5	1.71 g COD§	1.71 g COD§
Urea	3.7	0.9	2.33 g NH_4^+ -N	0.47 g NH_4^+ -N
Sodium Bicarbonate	8.9	2.2		

§Chemical oxygen demand (COD) is expressed in g of O_2 consumed for complete oxidation of organic matter

The amount of sodium bicarbonate required to buffer acid production from nitrification was also added to each column daily. The required amount of sodium bicarbonate was calculated based on complete nitrification of one day's N addition.

Organic carbon loading, expressed as chemical oxygen demand (COD) loading, was consistent among all columns and was made up of whey protein and NH_4^+. The COD load was 300 g O_2 m^{-3} d^{-1} and included the NH_4^+ in urea combined with 2.61 g d^{-1} whey protein. As chemical oxygen demand represented the mass of oxygen capable of being consumed by the chemicals dissolved in a liter of water, COD included both the oxygen required to convert NH_4^+ to NO_3^- and the whey to CO_2. Whey protein also contributes a small amount of organic N to the system: 0.0145 g N g^{-1} whey. The columns received their COD and N loads as a dry mix each day along with approximately

2 L of fresh water. After the fresh water and whey-urea powder mixed with the liquid in the reactor, approximately 2 L of liquid exited the system through the overflow portal. On Fridays two bags of feed were deposited in the reservoir to account for the inability to feed on weekends. Double doses of feed were not used on Mondays to prevent overloading the system with feed.

2.1.6   Sampling

At the end of each hydraulic treatment, 3-g samples of LESA were collected from each sampling portal (Fig. 2.2). Collected samples represented both the effect of the prior hydraulic treatment and the starting conditions for the following treatment. Liquid samples were also collected from each sampling portal and immediately filtered through 0.2 μm filters and frozen for later ion chromatograph analysis (Dionex) to determine NO_2^-, NO_3^- and NH_4^+ concentrations. The filters were collected in 2-mL centrifuge tubes and archived at -80 °C for future molecular analysis of the suspended cells.
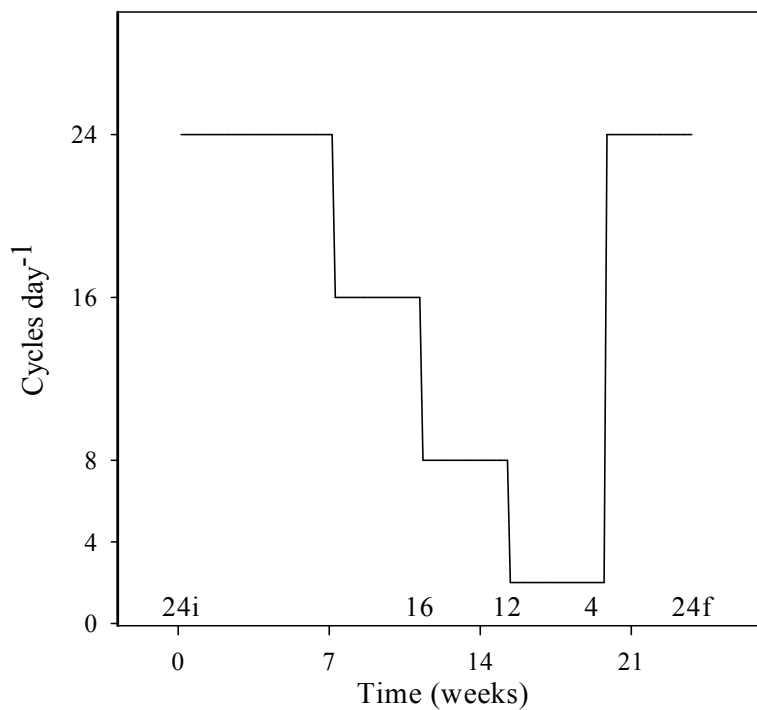
Fig. 2.2 – Diagram of sampling events and sequential hydraulic treatments. The number of tidal cycles per day is reflected on the y-axis and the time since the initial sampling is represented on the x-axis. Sampling events are demarcated by the tidal cycling regime the samples represent. The trickling durations equivalent to the given tidal cycling regimes, given in chronological order, are 0.8i min (0.25 hr)$^{-1}$; 0.5 min (0.25 hr)$^{-1}$; 0.3 min (0.25 hr)$^{-1}$; 0.2 min (0.25 hr)$^{-1}$; 0.8f min (0.25 hr)^{1}.

Triplicate samples of approximately 3 g of LESA were collected in 50-mL tubes. Then, 1 g of each sample was placed in a 15-mL centrifuge tube, with 3 mL of phosphate buffer solution (PBS, prepared as in Wright (1994)). To preserve sample integrity, PBS was filtered through a 0.2-μm supore filter and autoclaved prior to use, to produce shelf-stable, sterile, cell-free PBS.

The tubes were then placed horizontally on a vortex unit and agitated for 10 minutes to remove cells from the LESA surface. After dispersal, 1 mL of sample was transferred to a 2-mL centrifuge tube and archived at -80 °C for community structure analysis, and 1 mL was transferred to a 2-mL centrifuge tube, centrifuged at 10,000 x g for 10 minutes to separate cells from the liquid. The cell pellet was then re-suspended in a 50% methanol-50% PBS for 24 hours at 4 °C to cause protein precipitation, thereby preserving the sample for FISH. After 24 hours the sample was centrifuged again, at 10,000 x g for 10 minutes to separate cells from the methanol and PBS, and re-suspended in a 50% PBS-50% ethanol solution for long term storage at -20 °C.

2.1.7   Fluorescent *in situ* Hybridization (FISH)

Prior to hybridization samples were re-suspended by gentle horizontal agitation on a vortex mixer for 10 minutes. Fluorescent *in situ* hybridization of AOB, NOB and total abundance of bacteria (TAB) was conducted using the probes and reagents provided in Nitri-VIT kits (Vermicon) with a modified protocol for reagent application. The Nitri-Vit kit is sold as a semi-quantitative analysis for nitrifier abundance and enumeration of bacteria. Protocols were significantly altered and tested to utilize the Nitri-Vit kit as a quantitative assay for nitrifiers and microbial abundance, and to process a larger number

of samples than the kits intend. Slides printed with hydrophobic wells

(ThermoScientific) were used in place of the slides included in the Nitri-Vit kit. The

surface area of the wells on the Nitri-Vit slides was 3 times larger than the surface area of

the wells on the purchased slides, making it possible to use 1/3 the volume of reagents to

conduct hybridizations. Reduced reagent volume still provided ample coverage of

sample. Methanol preserved samples were appropriately diluted and 10 µL of sample

were dried in each well of the slide. Solutions for preparing samples for hybridization

and hybridization buffers were used as described in the Nitri-Vit Kit instructions, except

in place of the provided reagent dispensers a 10-µL pipetman was used to dispense 10 µL

of reagents to the slide wells. Slides were incubated for 2 hours at 46° C and then washed

in rinse buffer, also at 46 ° C. Slides were then rinsed in ice-cold, cell-free DI water for 1

second to remove residual salts, allowed to dry and stored under vacuum at -20° C until

analysis with epifluorescent microscopy.

Anammox identification was conducted using probe S-*-Amx-0368-a-A-18

(Amx368) sequence 5'- CCTTTCGGGCATTGCGAA (Schmid et al. 2003), which

targets all anammox-capable bacteria, in conjunction with the planctomycetes probe S-P-

Planc-0046-a-A-18 (Pla046) sequence 5'- GACTTGCATGCCTAATCC (Neef et al.

1998), to confirm correct hybridization. Probe Amx368 was labeled with FAM and probe

Pla046 was labeled with Cy3 (IDT). The Amx368 probe was hybridized at 15%

formamide and the Play046 probe was hybridized as 25% formamide. Both

hybridizations occurred at 46°C and were followed by a rinse step at 48°C, and a 1

second rinse in cell-free DI water to remove residual salts. Slides were then dried and

stored under vacuum at -20°C until enumeration under epifluorescence microscopy.

Further details concerning probe specificity reaction conditions and other available probes are also available in ProbeBase (Loy et al. 2007).

After hybridization, functional group abundances were determined by manual counting using either a Zeis Axioscope or an Olympus BX41 epifluorescence microscope at 1000x magnification, both fitted with filter sets for Cy3 and FAM. Total abundance of bacteria was determined following standard counting procedures outlined in Hobbie et al., (1977). The functional groups represented a small fraction of the total biomass so ten fields were counted for each sample irrespective of the functional group cell count. This approach is consistent with the findings of Kepner et al., (1994) which found that 51% of researchers studying bacterial abundances set a minimum number of fields to count. Although reaching cell counts of at least 200 would be ideal, it was not possible because concentrating samples to the required level increased sample auto-fluorescence effectively obscuring the target cells.

To assess counting efficiency and adhesion of cells to the purchased slides three replicate samples from sampling portal 4 of the Low-N tidal column were collected and cells were extracted from the LESA as described. Appropriate dilutions of cells extracted from the LESA were filtered onto a black, 0.22-μM nuclepore filter and stained with Live-dead stain as described by Floyd (2007). Hybridization slides were also prepared with appropriate dilutions of cells extracted from LESA, and hybridized with Eub338-I and –II (Daims et al. 1999). After hybridization cells were counterstained with DAPI as per the manufacturer's directions (Amann et al. 1990). In theory hybridization detects only cells that are metabolically active because it requires 50 copies of rRNA to be present for detectable fluorescence. In contrast to FISH probes, DAPI is a nucleic acid

stain and will stain both live and dead cells indiscriminately. Live-dead stain determines live cells as cells with intact cell membranes. Propidium iodine is a red stain which cannot pass intact cell membranes thereby staining dead cells red. The live stain is Syto-9 which stains intact nucleic acids green. The summation of live and dead cells should be equivalent to cells stained by DAPI. The live cell counts should be equivalent to EUB 338 counts. As seen in Fig. 2.3, abundance values determined by filtration were approximately twice the abundance values determined by hybridization on slides. However, a paired t-test between the ratio of live to dead cells did not detect a difference between live-dead stain, and Eub338 and DAPI stain, suggesting that hybridizations were behaving as expected and any difference between filter based counts and slide based counts can be attributed to cell loss during rinsing steps. A biomass loss of 50% when using centrifugation and glass slides compared to nuclepore filters is consistent with what is observed in the literature (Lemke et al. 1997).
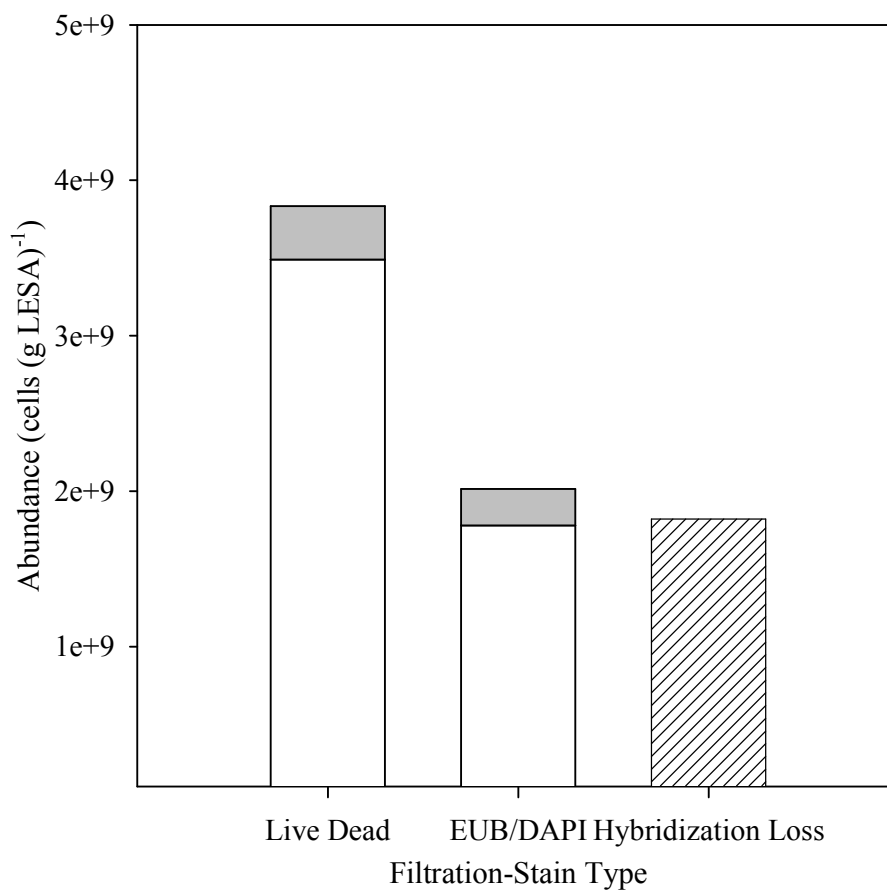
Fig. 2.3 − Results from live-dead cell stains on nuclepore filters and hybridizations with EUB338 and DAPI from three replicate samples are presented. Cells determined as live by Syto 9 or EUB338 stain are white. Cells determined to be dead by propidium iodine or the difference between DAPI and EUB338 abundance are in grey. The number of cells lost during hybridization, compared to total abundance determined by filter concentration is hashed. The standard errors for each cell count were 1.3 x 10^8 for Syto 9, 4.7 x 10^7 for propidium iodine, 2.5 x 10^8 for EUB338, and 1.0 x 10^8 for DAPI. For all measurements n = 3.

2.1.8   Abundance Integration

Abundances of microorganisms were calculated per gram of LESA taken from each sampling portal. The values for each point were then multiplied over the region of the column represented by that sampling portal in order to calculate total column abundances. For example, the first sampling portal represented the abundance of bacteria from the top of the column to halfway between sampling portal 1 and sampling portal 2. The density of LESA is 1.13 g cm^{-3} and each column has a radius of 4.9 cm. The column was subdivided into four segments corresponding to the four sampling portals. Segment lengths from portal 1 to portal 4 were 27.5, 25, 24 and 45.5 cm. Abundance values were multiplied by the density of LESA, the volume of the associated column segment, and then summed to produce integrated abundance values.

2.2   **Denitrification Study**

2.2.1   **Experimental Approach**

To assess sediment based denitrification 9 replicate sediment cores were collected from Cobb Mill Creek. Each core was representative of an assumed vertical flow path of groundwater entering the creek. Groundwater samples, taken along horizontal transects of the adjacent hill slope, demonstrated that no denitrification was occurring prior to entering the streambed. Pore water and sediment subsamples from the collected cores allowed assessment of potential denitrification rates, NO_3^- concentration, denitrifier abundance and factors controlling distribution and activity of denitrifiers. A new technique *nosZ* MPN-PCR was developed to quantify denitrifiers and the technique was successfully used to gain insight on the environmental controls on denitrifier abundance.

2.2.2   **Field Site**

The positioning of microbes responsible for denitrification was examined in a field setting in the sediment of a low-relief coastal stream. The site examined in this report (75.93W 37.29N) is in the Cobb Mill Creek watershed located at the Anheuser Busch Coastal Research Center on Virginia's Eastern Shore. General site characteristics have been previously reported (Gu et al. 2008b, a, Gu et al. 2007). Cobb Mill Creek drains into the seaside lagoon through the harbor at Oyster, VA which is about 1 km downstream from the study site (Fig. 2.4). Fields adjacent to the stream are intensively cropped and receive substantial nitrogenous fertilizer during the growing season. Concentrations of NO_3^- in the groundwater under those fields range from 8-30 mg NO_3^--N L^{-1}.

2.2.3   Sampling

Sediment cores were collected from the Cobb Mill Creek study site in three transects

perpendicular to stream flow (Fig. 2.3). Cores were driven to approximately 80 cm

below the sediment water interface. Cores were transported to the Laboratory of

Microbial Ecology at the University of Virginia, and incubated at 4.0˚C until the

following day. Portals were drilled into the sediment cores for collection of subcores with

1-mL syringes (Fig. 2.3). Subcore samples were then taken 3 cm below the sediment

water interface and at 10 cm intervals below that. Subcore samples for DNA extraction

and MPN analysis were stored at -80˚C. Samples for potential denitrification rate were

briefly stored at 4˚C until being set in incubations for potential denitrification rate

analysis (see (Galavotti 2004)for further details on potential denitrification rate details).

63
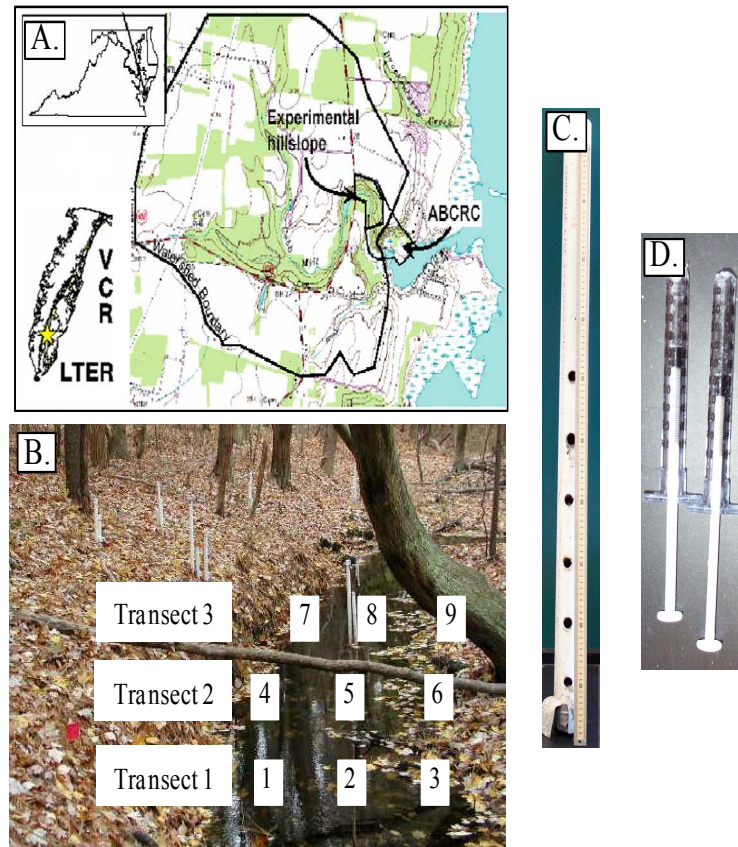
Fig. 2.4 – A. Map of field site location, B. Photograph of Cobb Mill Creek with sediment core collection sites demarcated, C. Photograph of an intact sediment core after sampling portals have been drilled, and D. Photograph of 1-mL syringes used to collect subcores for molecular work.

Denitrifying organisms were enumerated using a PCR-MPN technique testing for the presence or absence of the nitrous oxide reductase (*nosZ*) gene. DNA was extracted from sub core samples using MoBio Soil DNA Isolation Kits. Approximately 0.3g of wet sediment was used in the extraction. The concentration of extracted DNA was determined by Picogreen dye (Invitrogen) analyzed on a SpectraMax Gemini EM spectrofluorometer. For MPN analysis a DNA dilution series was constructed with final DNA concentrations of 5 ng $(50 \ \mu L)^{-1}$; 0.5 ng $(50 \ \mu L)^{-1}$; and 0.05 ng $(50 \ \mu L)^{-1}$. The 50-μL aliquots of DNA were then divided equally between 5 PCR reactions. Amplification of a fragment of approximately 1,000 base pairs (bp) was accomplished using primers nos661F and nos1773R, developed by Scala and Kerkhof (1998).

2.2.4   Polymerase Chain Reaction (PCR)

PCR was conducted using AmpliTaq and accompanying reagents from Sigma Genosys. A 2.0 mM concentration of $MgCl_2$ was used in a 5x solution of PCR Buffer II. The nos661F (5'CGGCTGGGGGCTGACCAA) and nos1773R (5'ATRTCGATCARCTGBTCGTT) primers, developed by Scala and Kerkoff (1998), were used to amplify a gene fragment of approximately 1000 base pairs. Primer concentrations were each 20 μMolar. The dNTP concentration was 0.125 mM. Bovine serum albumin (New England Biolabs) was added to the reaction mixture at a final concentration of 2 mg L^{-1}. The final PCR reaction volume was 50 μL. The reaction was carried out in an MJ Scientific PTC 200 DNA engine under the reaction conditions used by Scala and Kerkoff (1998). PCR product analysis was performed by gel electrophoresis in a 1% agarose gel and ethidium bromide staining. Resultant bands were visualized on a UV transilluminator. Samples were scored for the presence or absence of the 1 kbp band

against the amplification product of a control organism isolated from Cobb Mill Creek

sediments. The control organism was demonstrated to denitrify in culture and produced

consistent amplification of the target DNA fragment. Results were then compared to an

MPN table to generate the most probable number of copies of *nosZ* present in the aliquot

of DNA added to the second dilution. The number is then multiplied by the dilution

factor of the DNA and then the dilution of sediment to generate the most probable

number of copies of the *nosZ* gene per gram wet weight of sediment. It was then

assumed that each cell contained only 1 copy of the *nosZ* gene in its genome so that the

most probable number of organisms capable of denitrification can be inferred.

3   Results

3.1   Reactor Study Results

3.1.1   Tidal Columns

There were several instances where some region within a column had a peak in abundance, suggesting enhanced microbial growth. These peaks likely occurred in places with idealized niche conditions, a situation referred to as a Goldilocks Zone. Further, changes in hydraulic regime were associated with microbial activity based on concentration of the microbial reactants and products NH_4^+, NO_2^-, and NO_3^- in the reactors. To explore the relationship of functional group abundances and activities, i.e., the Goldilocks Principle, concentrations of N species and vertical profiles of bacterial abundances were monitored in high and Low-N treatments subjected to sequential tidal-cycling frequency.

3.1.1.1   Abundance Profiles

In the Low-N treatment, there were multiple instances where a peak in abundance was observed. At the end of the 24i-cycles day^{-1} treatment, the only observed peak in abundance occurred in the NOB. At the third and fourth sampling portals, a broad peak in NOB abundance was observed (Fig. 3.1). The average NOB abundance was 2.9×10^8 cells (g LESA)$^{-1}$ while at portals three and four the average abundance was 5.2×10^8, a 1.8-fold increase in abundance. No peaks in abundance were seen in the vertical profiles resulting from the 16-cycles day^{-1} treatment (Fig. 3.2). Vertical profiles observed at the close of the 8-cycles day^{-1} treatment had a peak in TAB at the fourth sampling portal. The average abundance of TAB during the 8-cycles day^{-1} treatment was 2.8×10^9 cells (g LESA)$^{-1}$, while the abundance at the fourth portal was 4.2×10^9 cells (g LESA)$^{-1}$, a 1.5-

fold increase in abundance. There was also a peak in AXB abundance at the second

sampling portal during the 8-cycles day^{-1} treatment (Fig. 3.3). The average AXB

abundance was 3.3 x 10^6, while AXB abundance at sampling portal 2 was
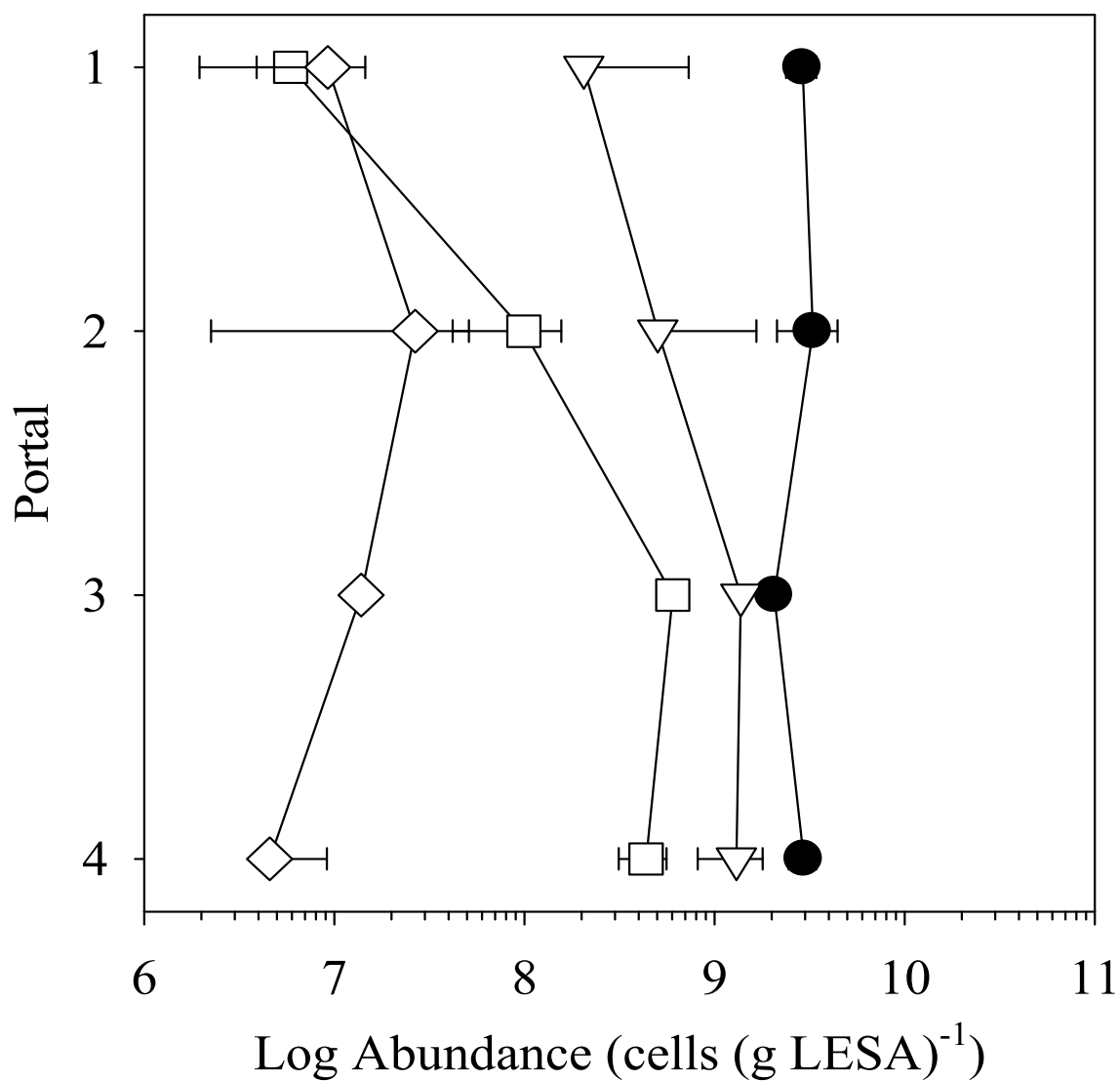
Fig. 3.1 – Abundance profiles for the 24i-cycles day^{-1} treatment for the total abundance of bacteria (TAB, circles), ammonia oxidizing bacteria (AOB, triangles), nitrite oxidizing bacteria (NOB, squares) and anaerobic ammonium oxidizing (anammox) bacteria (AXB, diamonds) in the Low-N treatment.
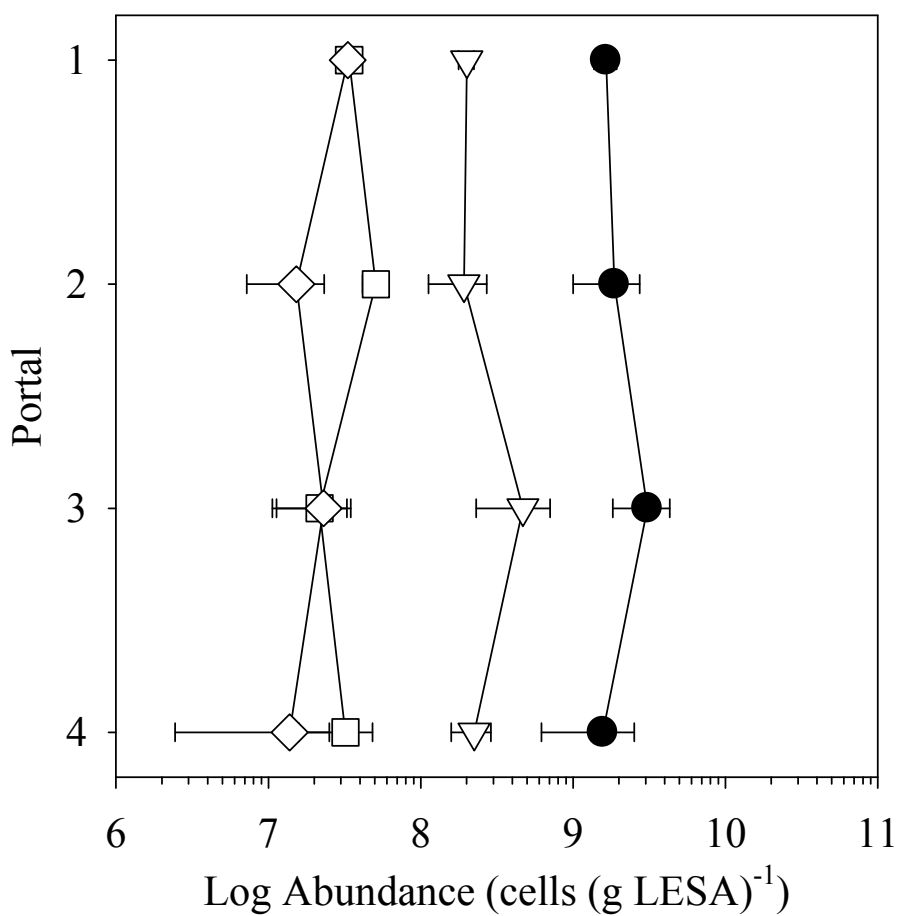
Fig. 3.2 – Abundance profiles at the conclusion of the 16-cycles day^{-1} treatment for the total abundance of bacteria (TAB, circles), ammonia oxidizing bacteria (AOB, triangles), nitrite oxidizing bacteria (NOB, squares) and anaerobic ammonium oxidizing (anammox) bacteria (AXB, diamonds) in the Low-N treatment.
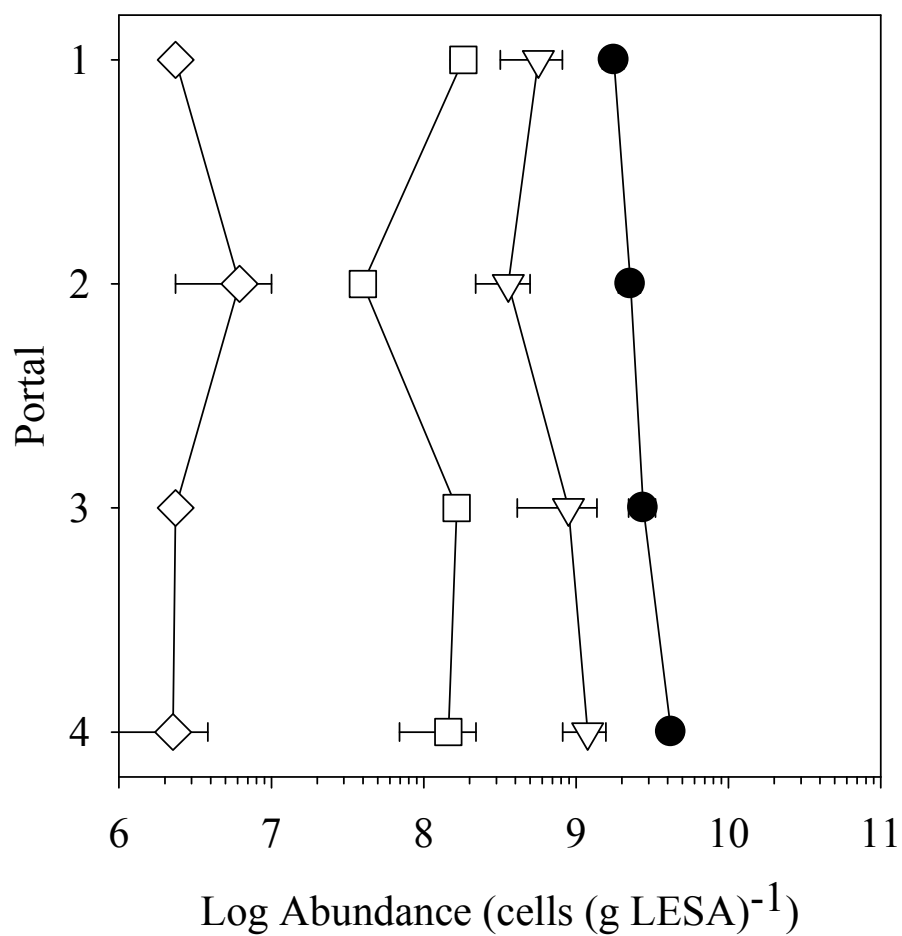
Fig. 3.3 – Abundance profiles of the total abundance of bacteria (TAB, circles), ammonia oxidizing bacteria (AOB, triangles), nitrite oxidizing bacteria (NOB, squares) and anaerobic ammonium oxidizing (anammox) bacteria (AXB, diamonds) in the Low-N treatment at the conclusion of the 8 cycles day[-1].

6.2×10^6 cells (g LESA)$^{-1}$, which was 1.9 times the average AXB abundance. There were no observable peaks in abundance at the end of the 4-cycles day^{-1} treatment (Fig. 3.4). After the 24f-cycles day^{-1} treatment, there was elevated AOB abundance at the third and fourth sampling portals (Fig. 3.5). The average abundance of these two portals was 1.3×10^9 cells (g LESA)$^{-1}$, while the average abundance of all four portals was 8.5×10^8 cells (g LESA)$^{-1}$. The average abundance of portals 3 and 4 was 1.6 fold greater than the average abundance of AOB within the column. The presence or absence of abundance peaks appeared to be related to changes in tidal cycling, possibly related to the availability of O_2.

Although the general ranking of abundance of the several guilds had NOB exceeding AXB (see section 3.1.1.2 Integrated Abundance Values, and discussion section Y.Y for elaboration), in the Low-N treatment, AXB were occasionally of greater abundance than NOB. This phenomenon occurred at the first sampling portal during the 24i-cycles day^{-1} treatment in which the AXB abundance was 1.6 fold greater than the NOB abundance (Fig. 3.1). During the 16-cycles day^{-1} treatment, AXB abundance was 110% of the NOB at the third sampling portal (Fig. 3.2). During the 8-cycles day^{-1} treatment, NOB were more abundant than AXB at all four sampling portals (Fig. 3.3). However, at the end of the 4-cycles day^{-1} regimen, at the second sampling portal, the AXB abundance was 3.5 fold greater than the NOB abundance (Fig. 3.4).

In the High-N treatment, abundance peaks occurred more frequently. During the 24i-cycles day^{-1} treatment, there was a peak in TAB, AOB, and NOB. The TAB peaked at 4.0×10^{10} cells (g LESA)$^{-1}$ ($2.1 \times$ the average) at the fourth sampling portal (Fig. 3.6). The peak in AOB abundance occurred at the third sampling portal and was 1.1×10^{10}

cells (g LESA)$^{-1}$, which was a 2.4 fold increase in abundance compared to the average

AOB abundance for the High-N
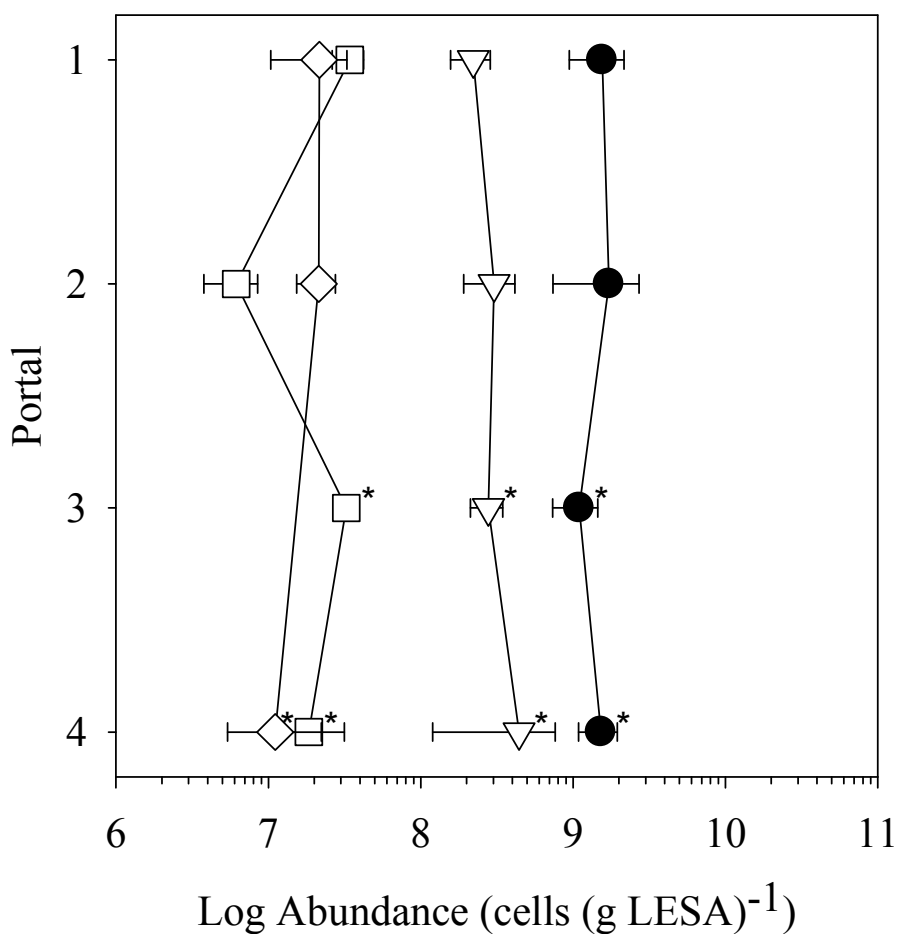
Fig. 3.4 – Abundance profiles in the Low-N treatment for total abundance of bacteria (TAB, circles), ammonia oxidizing bacteria (AOB, triangles), nitrite oxidizing bacteria (NOB, squares) and anaerobic ammonia oxidizing (anammox) bacteria (AXB, diamonds) at the conclusion of the 4-cycles day^{-1} tidal treatment. For all sampling portals n = 3 except where noted. At the third sampling portal AXB were not detected in any replicate samples so the point was omitted from the graph.

* Denotes locations where only two samples were processed.
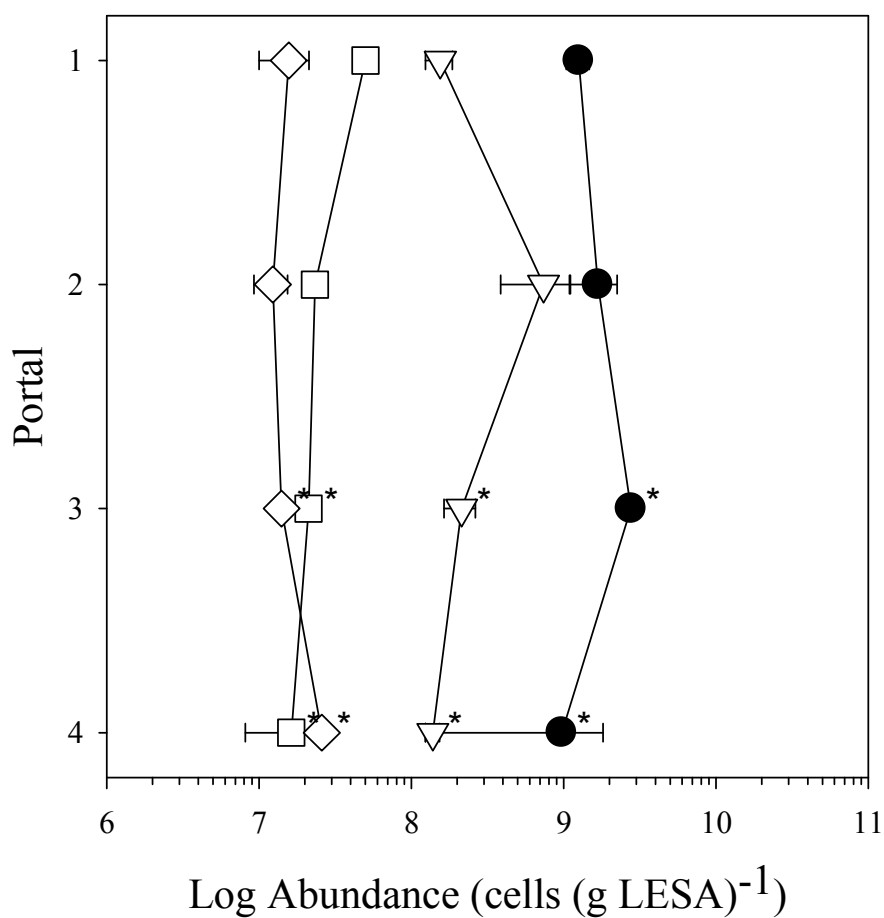
Fig. 3.5 – Abundance profiles of the total abundance of bacteria (TAB, circles), ammonia oxidizing bacteria (AOB, triangles), nitrite oxidizing bacteria (NOB, squares) and anaerobic ammonia oxidizing (anammox) bacteria (AXB, diamonds) at the conclusion of the 24f-cycles day-1 for the Low-N tidal treatment.

* Denotes locations where only two samples were processed.
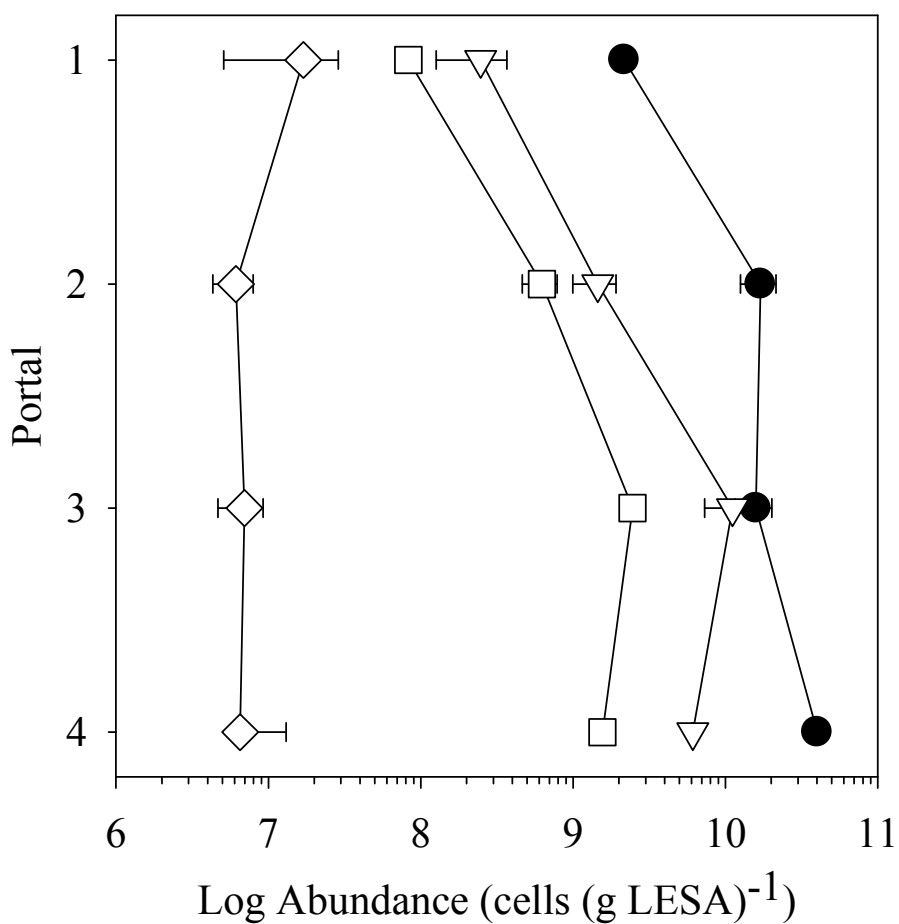
Fig. 3.6 – Profiles of abundance in the High-N treatment of the total abundance of bacteria (TAB, circles), ammonia oxidizing bacteria (AOB, triangles), nitrite oxidizing bacteria (NOB, squares) and anaerobic ammonia oxidizing (anammox) bacteria (AXB, diamonds) at the conclusion of the 24i-cycles day^{-1}.

column under the 24i-cycles day^{-1} hydraulic regime (Fig. 3.6). An NOB abundance peak of 2.5 x 10^9 cells (g LESA)$^{-1}$ also occurred at the third sampling portal. This abundance peak was 2.1 fold greater than the average abundance of NOB in the High-N tidal column during the 24i-cycling treatment (Fig. 3.6).

During the 16-cycles day^{-1} treatment, there was a subtle peak in AXB abundance at the second sampling portal. That peak was 5.0 x 10^7 cells (g LESA)$^{-1}$, or approximately twice the average AXB abundance of 2.6 x 10^7 cells (g LESA)$^{-1}$ seen at the close of this sampling period (Fig. 3.7). No distinct peaks were observed in the 8-cycles day^{-1} regimen (Fig. 3.8).

At the conclusion of the 4-cycles day^{-1} treatment there was a peak in AOB abundance at the second sampling portal. The abundance value of AOB at this peak was 7.4 x 10^8 cells (g LESA)$^{-1}$, which represented a 2.4-fold increase in abundance compared to the average AOB abundance of 3.1 x 10^8 cells (g LESA)$^{-1}$ (Fig. 3.9). The 4-cycles day^{-1} treatment was also the only hydraulic regimen where the abundance of AXB was greater than NOB the High-N tidal treatment. At the fourth sampling portal AXB abundance was 1.6 fold greater than NOB. The AXB abundance was 2.6 x 10^7 cells (g LESA)$^{-1}$, while the NOB abundance was 1.6 x 10^7 cells (g LESA)$^{-1}$.

There was also a peak in NOB abundance measured at the conclusion of the 24f-cycles day^{-1} regimen. Under this cycling regime, NOB abundance was maximal at the first sampling portal at 3.0 x 10^8 cells (g LESA)$^{-1}$. This abundance value was 2.4 fold greater than the average abundance of NOB in the column under this tidal regime (Fig. 3.10)
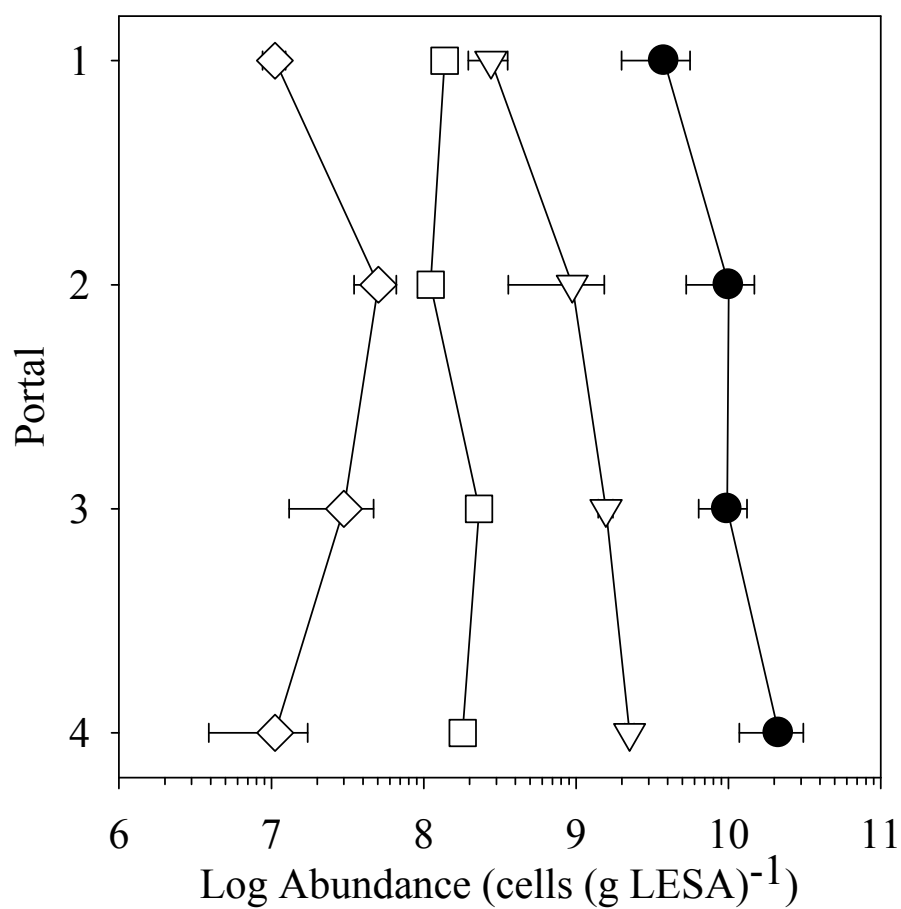
Fig. 3.7 – Abundance profiles of the total abundance of bacteria (TAB, circles), ammonia oxidizing bacteria (AOB, triangles), nitrite oxidizing bacteria (NOB, squares) and anaerobic ammonia oxidizing (anammox) bacteria (AXB, diamonds) for the High-N tidal treatment at the conclusion of the 16- cycles day[-1] treatment.
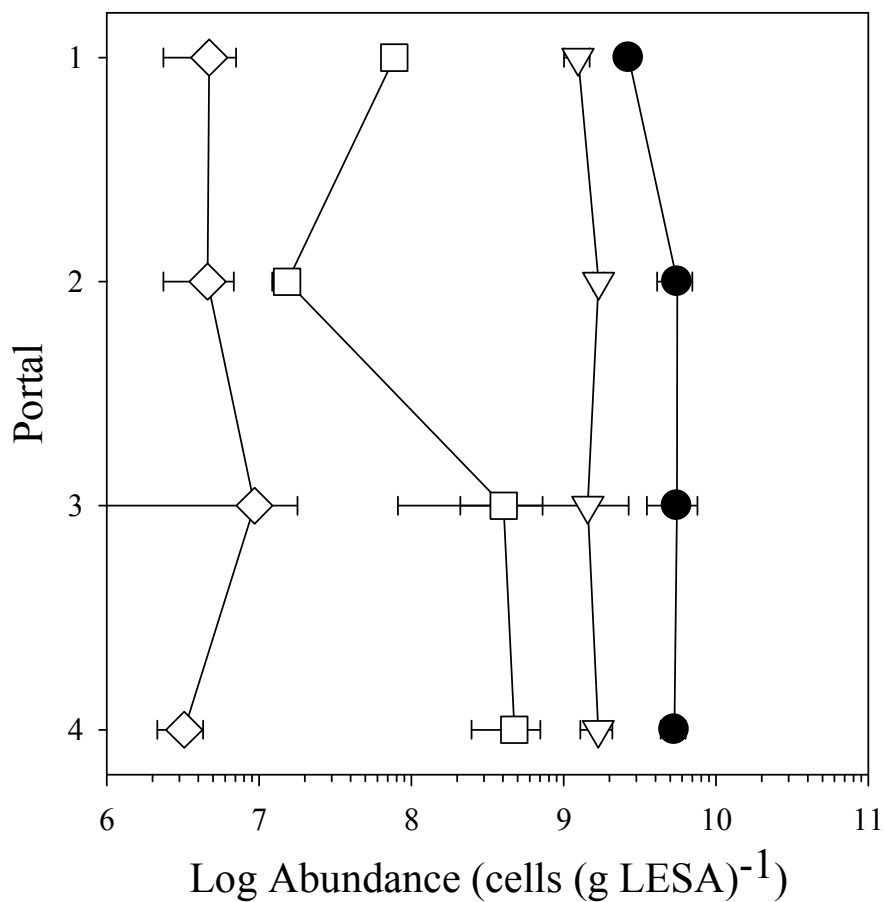
Fig. 3.8 –The total abundance of bacteria (TAB, circles), ammonia oxidizing bacteria (AOB, triangles), nitrite oxidizing bacteria (NOB, squares), and anaerobic ammonia oxidizing (anammox) bacteria (AXB, diamonds) abundance profiles at the conclusion of the 8-cycles day-1 regimen in the High-N tidal treatment.
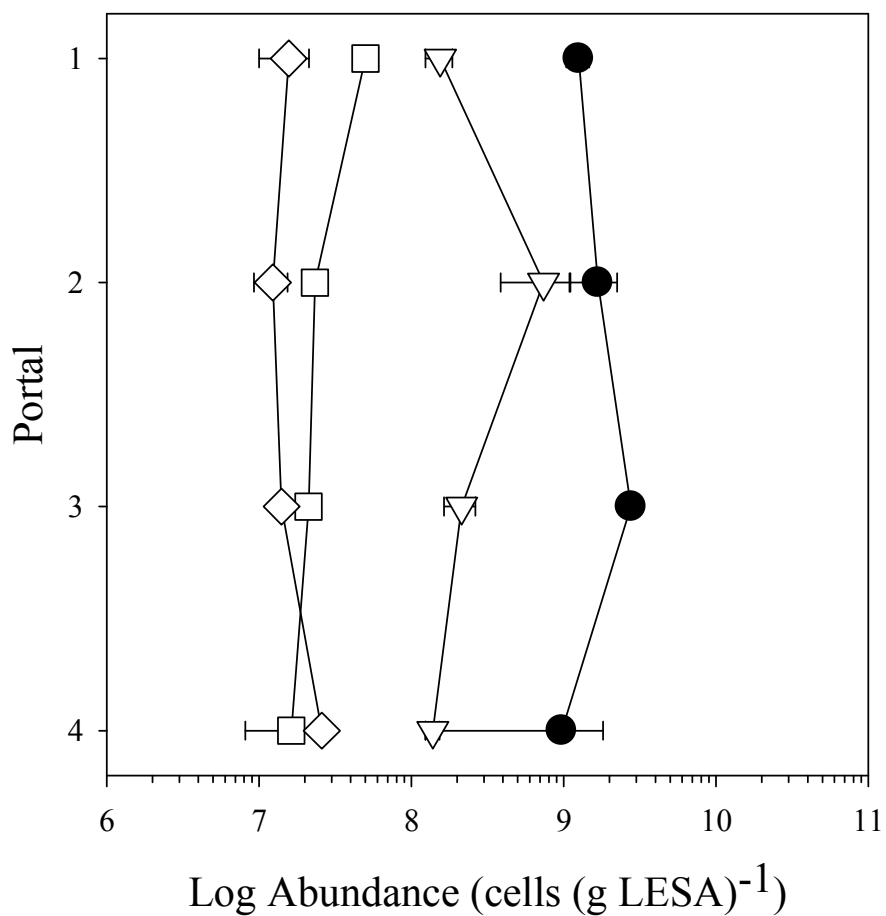
Fig. 3.9 – Abundance profiles in the High-N treatment, at the conclusion of the 4-cycles day[-1] regimen, of the total abundance of bacteria (TAB, circles), ammonia oxidizing bacteria (AOB, triangles), nitrite oxidizing bacteria (NOB, squares), and anaerobic ammonia oxidizing (anammox) bacteria (AXB, diamonds).
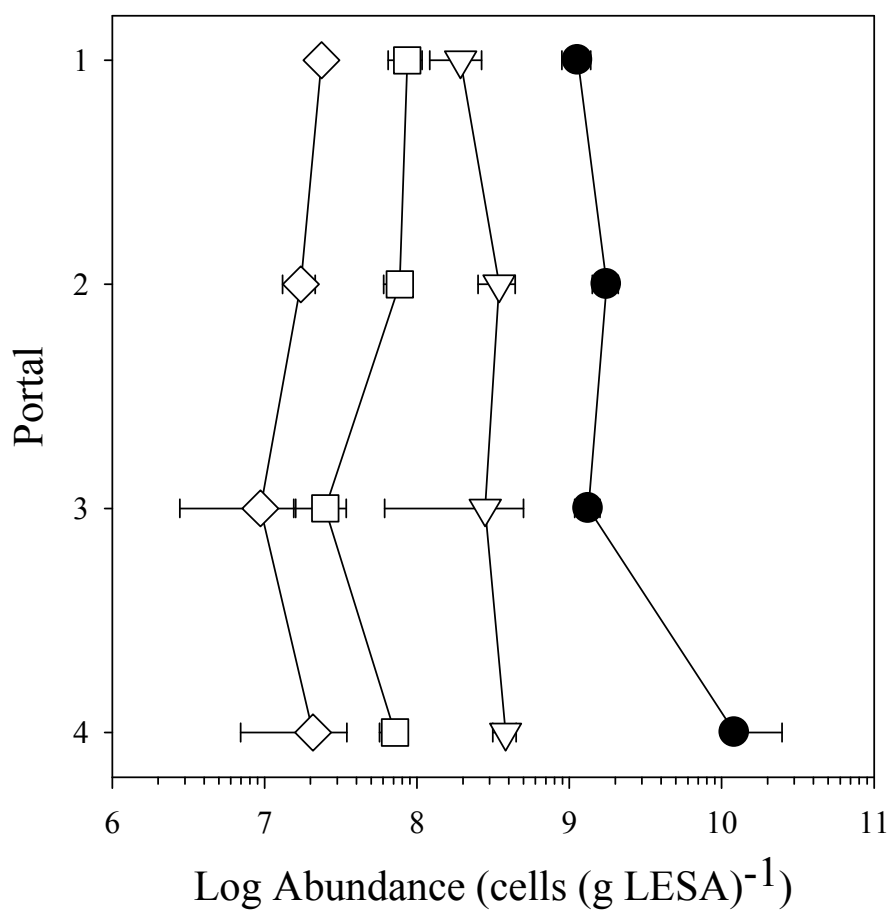
Fig. 3.10 – Profiles of the total abundance of bacteria (TAB, circles), ammonia oxidizing bacteria (AOB, triangles), nitrite oxidizing bacteria (NOB, squares) and anaerobic ammonia oxidizing (anammox) bacteria (AXB, diamonds) abundance at the conclusion of the 24f-cycles day[-1] regimen in the High-N treatment. The 24f-cycles day[-1] treatment was the final tidal treatment.

3.1.1.2 Integrated Abundances

Total abundances for TAB, AOB, NOB and AXB in each column, at the end of each tidal-regime were calculated by integrating the abundance values from each sampling portal. The abundance values in the High-N treatment were consistently greater, usually by at least a factor of 3, than the abundance values in the Low-N treatment (Fig. 3.11). The average TAB from all tidal regimes in the High-N treatment was 1.0×10^{14} cells, whereas the average abundance in the Low-N treatment was 2.6×10^{13} cells, a 3.9-fold increase in abundance in the High-N column. The AOB abundance in the High-N treatment was 3 fold greater than the abundance observed in the Low-N treatment: 2.0×10^{13} cells and 6.4×10^{12} cells for the High-N and Low-N treatments, respectively. Similarly, the NOB were 3.2 fold greater in the High-N treatment with an average abundance of 3.8×10^{12} cells, while the Low-N had an average NOB abundance of 1.2×10^{12} cells. The integrated abundance values for AXB were the lowest among the guilds enumerated, and there was little difference between the columns. AXB in the Low-N column numbered 1.8×10^{11} cells and 1.6×10^{11} cells were present in the High-N column.

The Low-N treatment showed a decline in abundance of TAB, AOB, and NOB values integrated for the whole column that was associated with reduction in tidal cycling frequency (Fig. 3.11). TAB during the 24i-cycling regime numbered 3.0×10^{13} cells (g LESA)$^{-1}$ while at the end of the 4-cycles day^{-1} treatment, the abundance was only 1.5×10^{13} cells, a 47% decrease in abundance. By the end of the 24f-cycles day^{-1} treatment, TAB had increased to 3.1×10^{13} cells, approximately equaling the abundance at the initial sampling.   The AOB abundance in the Low-N tidal column exhibited a similar pattern

to that of the total bacteria; AOB abundance decreased from 9.5 x 10^{12} cells to 3.5 x 10^{12}

cells: abundance equaled 37% of the initially determined AOB abundance.
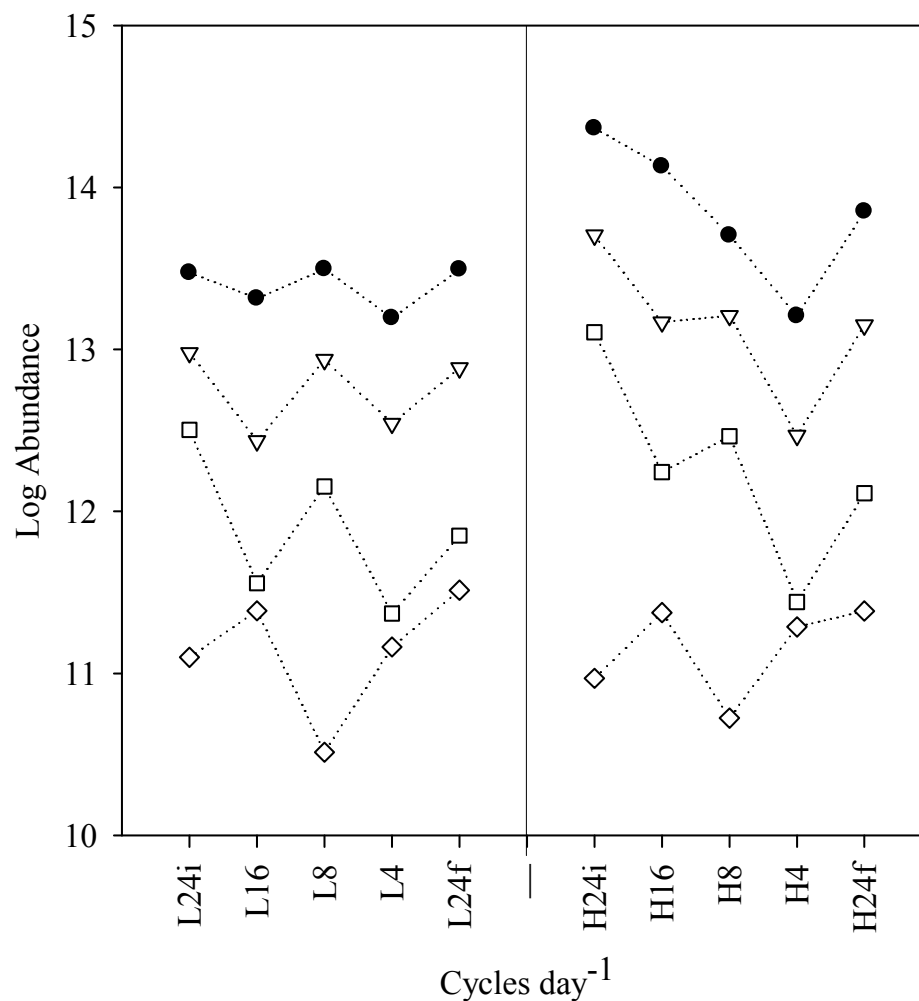
Fig. 3.11 – Integrated abundances values, grouped by Low- or High-N treatment (L or H) and tidal regime, for total abundance of bacteria (TAB, filled circles), ammonia oxidizing bacteria (AOB, triangles), nitrite oxidizing bacteria (NOB, squares) and anaerobic ammonia oxidizing (anammox) capable bacteria (AXB, diamonds) in the tidal systems are displayed. The initial and final tidal treatments were 24 cycles day^{-1} and are distinguished by the letters i and f respectively. The dotted lines are visual aids only and do not denote linear regressions.

The abundance of AOB then increased by a factor of 2.2 to 7.7×10^{12} cells when the cycle rate was returned to 24-cycles day^{-1} treatment. The NOB abundance in the Low-N treatment also appeared to decline in association with the reduction in tidal cycling frequency: going from 32 to 2.3×10^{11} cells. The decline in NOB abundance was a 93% decrease in abundance. By the end of the 24f-cycles day^{-1} treatment, the abundance had risen to 7.1×10^{11} cells, a 3.0 fold increase in abundance. The AXB abundance within the Low-N treatment remained reasonably constant over the entire length of the experiment, and the abundance averaged 1.8×10^{11} cells.

In the High-N column, the patterns of change in abundance associated with changes in cycling frequency were similar to those observed in the Low-N treatment, but the differences among the hydraulic treatments were more pronounced (Fig. 3.11). The TAB experienced a 93% reduction in abundance, declining from 2.4×10^{14} cells at the end of the 24i-cycles day^{-1} treatment, to 1.6×10^{13} cells at the close of the 4-cycles day^{-1} treatment. The abundance then increased by a factor of 4.4 during the 24f-cycles day^{-1} treatment, resulting in an integrated abundance of TAB of 7.1×10^{13} cells. The AOB exhibited a similar pattern, with abundance declining by a 63% between the 24i- and the 4-cycles day^{-1} treatment: going from 5.1×10^{13} to 3.0×10^{12} cells. The AOB abundance then rebounded during the 24f-cycles day^{-1} regime and increased by 4.8 to 1.4×10^{13} cells. The NOB-abundance values also followed a similar pattern. The abundance of NOB was 1.3×10^{13} cells at the close of the 24i-cycles day^{-1} treatment, and it declined to 2.8×10^{11} cells at the close of the 4-cycles day^{-1} treatment. The NOB population then increased again, but only to 1.3×10^{12} cells by the end of the 24f-cycles day^{-1} treatment. The AXB population exhibited an inconsistent response to changes in tidal cycling

frequency. The average abundance over the duration of the experiment was 1.7×10^{11} cells, and abundance tended to vary between 5.3 and 24×10^{10} cells. The undulating pattern of AXB abundance made it difficult to discern any possible treatment affect from the noise in the abundance values.

Microbial abundances were consistently separated by group (Fig. 3.11). The TAB was always greatest and comprised AOB, NOB and AXB as well as other unidentified organisms including heterotrophs. Of the three functional groups enumerated, AOB were always the most abundant, in both the High- and Low-N treatments, and across all hydraulic regimes (Fig. 3.11). The average level of TAB in the Low-N treatment was 2.6 $\times 10^{13}$ cells while the average AOB abundance was 6.4×10^{12} cells. The average TAB abundance was approximately 4 times larger than the abundance of AOB. The NOB were commonly the next most abundant organism with an average abundance of 1.2 $\times 10^{12}$ cells. The average NOB population was less than one fifth the size of the average AOB population. The average AXB abundance was 1.8×10^{11} cells, less than 15% of the size of the average NOB population and less than 1% of the total microbial population. However, there were multiple instances in which AXB were more abundant than NOB, as reported earlier (section 3.1.1.1).

In the High-N treatment, a similar abundance cascade was observed. The average TAB, 1.0×10^{14}, cells was 5 times larger than the average AOB abundance of 2.0×10^{13} cells. The average abundance of AOB was 5.2 fold larger than the average NOB abundance of 3.8×10^{12} cells, which was, in turn, 23 times larger than the average abundance of AXB (1.6×10^{11} cells). The average AXB abundance in the High-N treatment was also less than 1% of the total microbial population.

3.1.1.3 Water Chemistry

Chemical data from weekly samples supported the theory that changes in abundance of the functional groups were connected to both changes in cycling frequency and changes in the level of metabolic activity. Vertical profiles of water chemistry from samples collected with LESA samples showed that N compounds were uniformly distributed within minutes of the column filling and reflected concentrations of N compounds in the reservoir samples, therefore the nutrient data are from the reservoir only. Data from vertical profiles are presented in Appendix II. As seen in Fig. 3.12 and 3.13, in the Low-N treatment there was minimal variation in NH_4^+, or NO_2^- concentration for the duration of the experiment in the Low-N column. The average NH_4^+ concentration was 9.3 ppm NH_4^+ –N (S.E. = 2.0, n = 29) for samples collected over all tidal treatments. There was a slight increase in NH_4^+ during the 4 and 8-cycles day^{-1} regimen. During these two cycling regimes, the average NH_4^+ concentration was 24 ppm NH_4^+ –N (S.E. = 1.4, n = 8). During the 24f-cycles day^{-1}, treatment the average NH_4^+ concentration was 4 ppm NH_4^+ –N. The average NO_2^- concentration in the Low-N column was 3.5 ppm NO_2^- –N (S.E. = 0.7, n = 29), with an increase to about 7.0 ppm NO_2^- –N during the 4-cycles day^{-1} regimen followed by a decline to 1.3 ppm NO_2^- –N when the cycling frequency returned to 24-cycles day^{-1} at the end of the experiment.

The NO_3^- concentration in the Low-N column was considerably more variable than either NH_4^+ or NO_2^- throughout the experiment (Fig. 3.14), and it averaged 155.8 ppm NO_3^-–N (S.E. = 13.7, n = 29). NO_3^- concentrations exhibited sharp peaks in concentration. For example, there was a peak of 342.5 ppm NO_3^-–N during the 24i-cycles

day^{-1}. There was also a sharp decline to 45.2 ppm NO_3^-–N immediately prior to the

transition to 16-cycles day^{-1}. After the decline to 45.2 ppm NO_3^- –N, the NO_3^-

concentration rose 239 ppm NO_3^- –N, and slowly declined to 52 ppm NO_3^- –N at the end

of the 4-cycles day^{-1} treatment. During the 24f-cycles day^{-1} treatment the NO_3^-

concentration slowly rose to 126.1 ppm NO_3^- –N. The concentration appeared to

continue rising. Had the 24f regime been extended we may have seen a dramatic rise in

NO_3^- concentration.
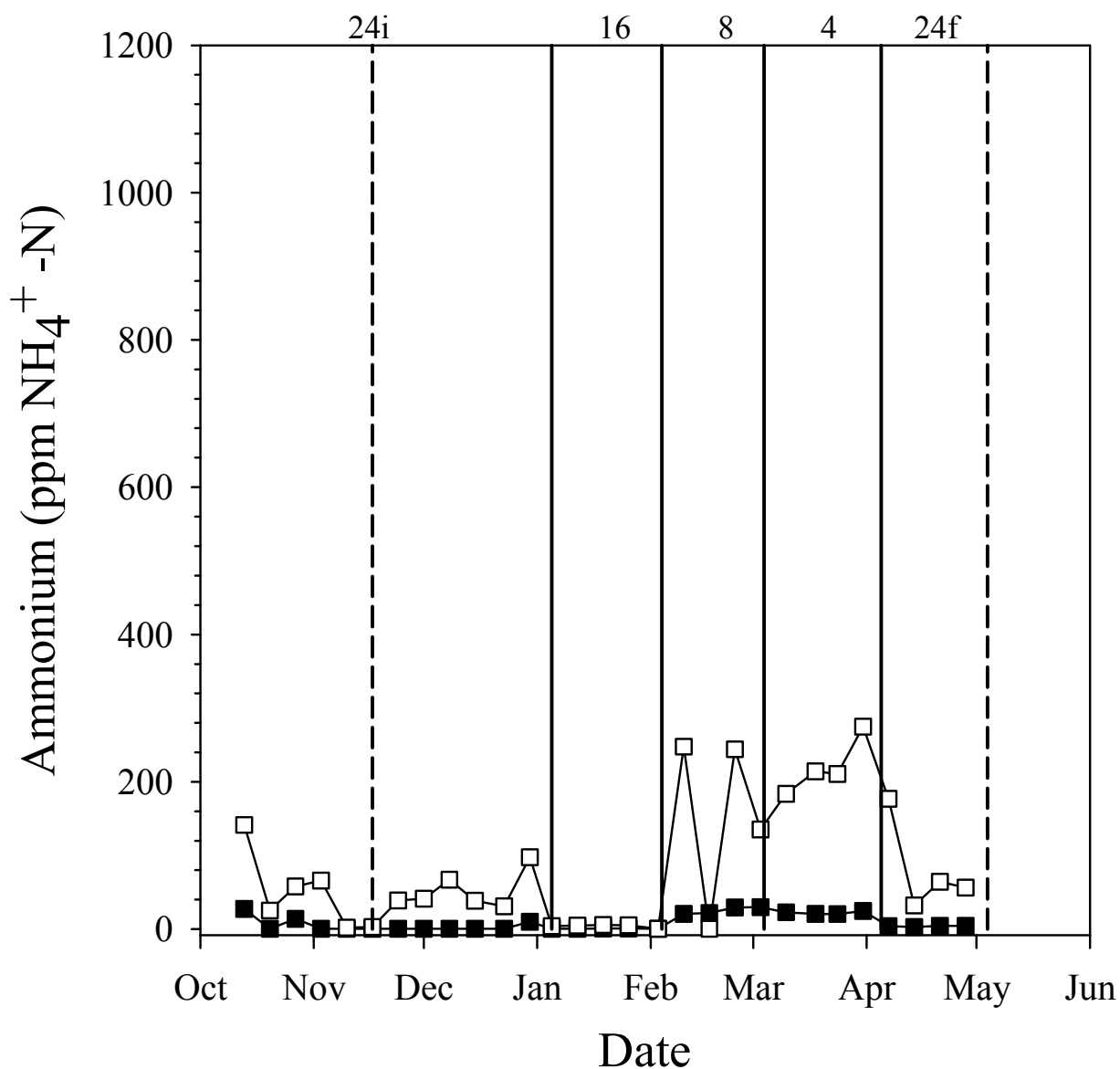
Fig. 3.12 – Concentration of NH$_4^+$ in high- (open circles) and Low-N (closed circle) tidal columns measured weekly throughout the duration of the test period. The dashed vertical lines represent the first and final sampling events. Solid vertical lines depict the end of a cycling regime. Cycles per day are depicted along the top of the graph. The letters i and f distinguish the initial and final 24 cycles day^{-1} treatment.
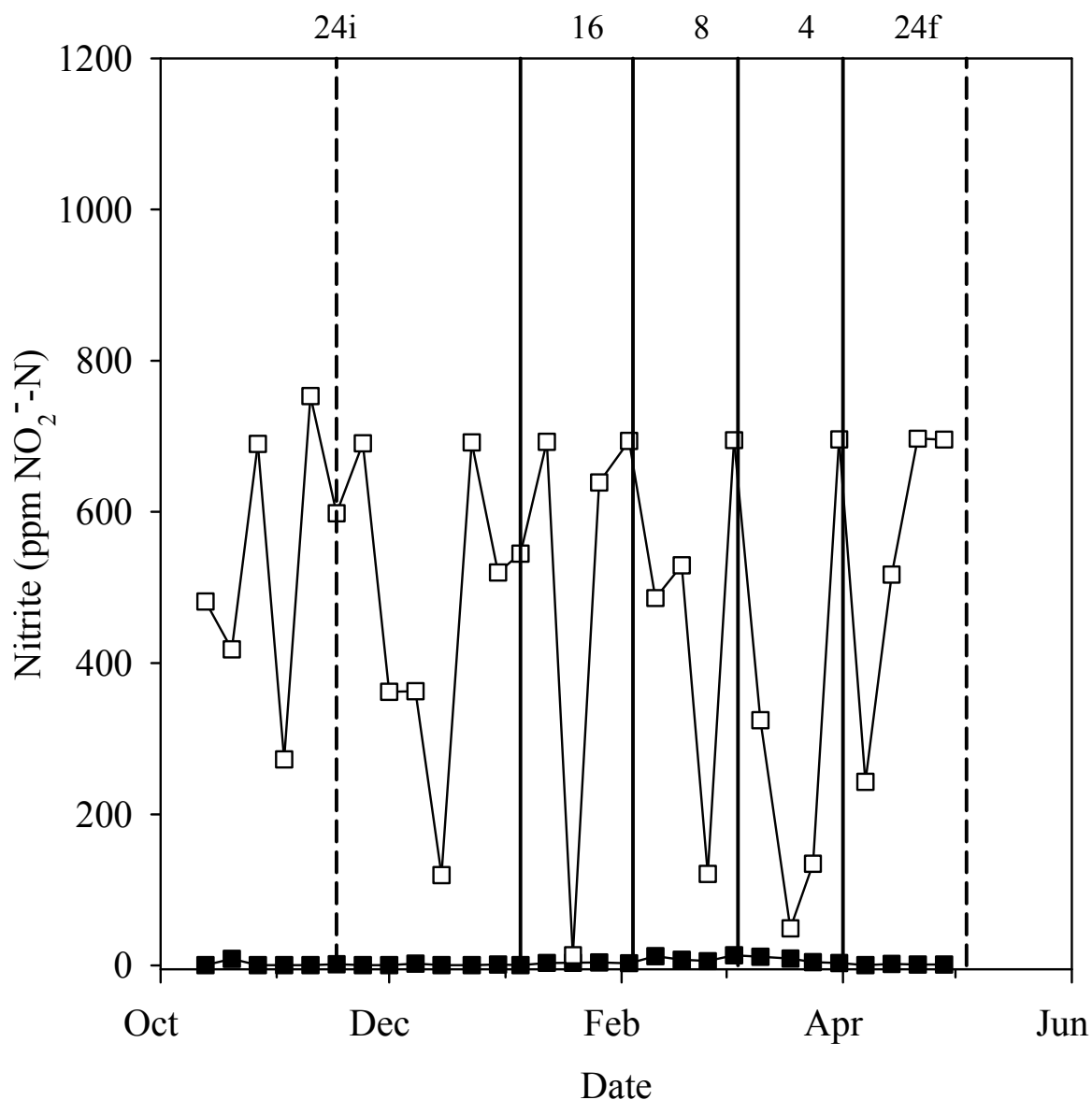
Fig. 3.13 – Concentration of NO$_2^-$ in high- (open circles) and Low-N (closed circle) tidal columns measured weekly throughout the duration of the test period. The dashed vertical lines represent the first and final sampling events. Solid vertical lines depict the end of a cycling regime. Cycles per day are depicted along the top of the graph. The letters i and f distinguish the initial and final 24 cycles day^{-1} treatment.
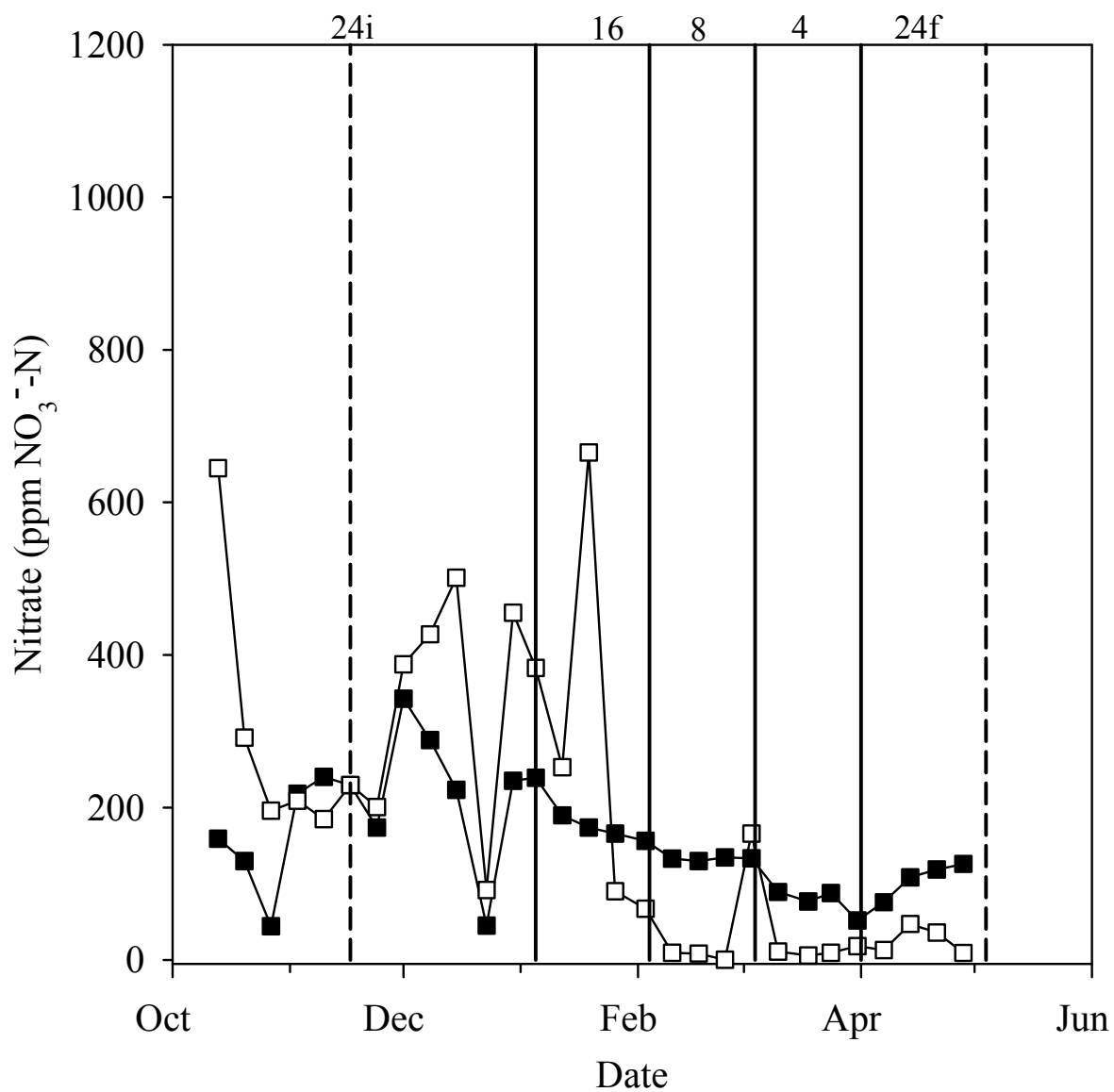
Fig. 3.14 – Concentration of NO₃⁻ in high- (open circles) and Low-N (closed circle) tidal columns measured weekly throughout the duration of the test period. The dashed vertical lines represent the first and final sampling events. Solid vertical lines depict the end of a cycling regime. Cycles per day are depicted along the top of the graph. The letters i and f distinguish the initial and final 24 cycles day^{-1} treatment.

In the High-N treatment, there was substantially more variation in the concentration of

the measured N compounds (Fig. 3.12) when compared to the Low-N treatment. The

average NH_4^+ concentration over the duration of the experiment was 514.9 ppm NH_4^+ –N

(S.E. = 104.7, n = 29).   The NH_4^+ concentrations were low during the 24i- and 16-cycles

day^{-1} treatment. During the 8-cycles day^{-1} treatment there was considerable variation.

The concentration of NH_4^+ went from 247.8 to 0.4 and back to 244.2 ppm NH_4^+ –N in a 3

week period. The 4-cycles day^{-1} treatment yielded considerable different NH_4^+

concentrations. The average NH_4^+ concentration during this treatment was 220.8 ppm

NH_4^+ –N, while the concentration during the preceding three hydraulic treatments was

60.4 ppm NH_4^+ –N. During the 24f-cycles day^{-1} regime the concentration of NH_4^+

returned to 82.6 ppm NH_4^+–N (S.E = 32.2, n = 4).

Concentrations of NO_2^- were highly variable over the course of the experiment

(Fig. 3.13).   The average NO_2^- concentration over the course of the entire experiment

was 473.5 ppm NO_2^- –N (S.E. = 42.5, n = 29). An example of the high variability can be

seen during the 4-cycles day^{-1} treatment. The concentration of NO_2^- is 324.4 ppm NO_2^- –

N at the beginning of the 4-cycles day^{-1} treatment and the concentration then plummets to

49.2 ppm NO_2^- –N. The concentration then climbs to 695.8 ppm NO_2^- –N by the end of

the 4-cycles day^{-1} treatment. This rapid fluctuation in NO_2^- concentration can be

observed throughout all tidal treatments in the High-N treatment. Despite this variation

the 4-cycles day^{-1} treatment has a distinctly different concentration than the preceding

three tidal treatments. The average concentration during the first 3 tidal regiments was

485.0 ppm NO_2^- –N, whereas during the 4-cycles day^{-1} treatment the average

concentration was 301 ppm NO_2^- –N. During the 24f-cycles day^{-1} treatment the average concentration escalated to 538 ppm NO_2^- –N.

The concentration of NO_3^- was also highly variable in all tidal regimes. The average concentration of NO_3^- of all tidal regimes was 193.5 ppm NO_3^- –N (S.E. = 37.2, n = 29). However, the concentration was not stable. For example, during the 24i-cycles day^{-1} treatment, the NO_3^- concentration went from over 500 ppm NO_3^- –N to 92 ppm NO_3^- –N, and back to 455 ppm NO_3^- –N in a 3 week period. Like NO_2^- and NH_4^+ concentrations, NO_3^- concentrations during the 4-cycles day^{-1} treatment were substantially different from concentrations found in other tidal regimes. During the first three tidal regimes, the average NO_3^- concentration was 246 ppm NO_3^- –N, while during the 4-cycles day^{-1} regiment the average concentration was 11.3 ppm NO_3^- –N. During the 24f-cycles day^{-1} regiment the concentration of NO_3^- increased to 26.5 ppm NO_3^- –N suggesting an increasing concentration of NO_3^- under highly aerobic conditions.

Removal of N from the reactors was determined based on weekly N inputs and calculation of total inorganic dissolved N present in the reactor. This calculation assumes organic and precipitated N is not a significant reservoir of N. Biomass calculations, based on the average N content of a cell (Vrede et al. 2002), confirm that at most microbial biomass only stored 1–5 g of N. Based on percent N removal, the Low-N tidal treatment performed consistently after the 8-cycles day^{-1} treatment (Fig. 3.15) Based on percent N removal, the High-N treatment does not perform consistently. However, there were large changes in percent removal coincident with changes in cycling rate between the 8- and 4-cycles day^{-1} and the 4- and 24f-cycles day^{-1} treatments (Fig. 3.16)
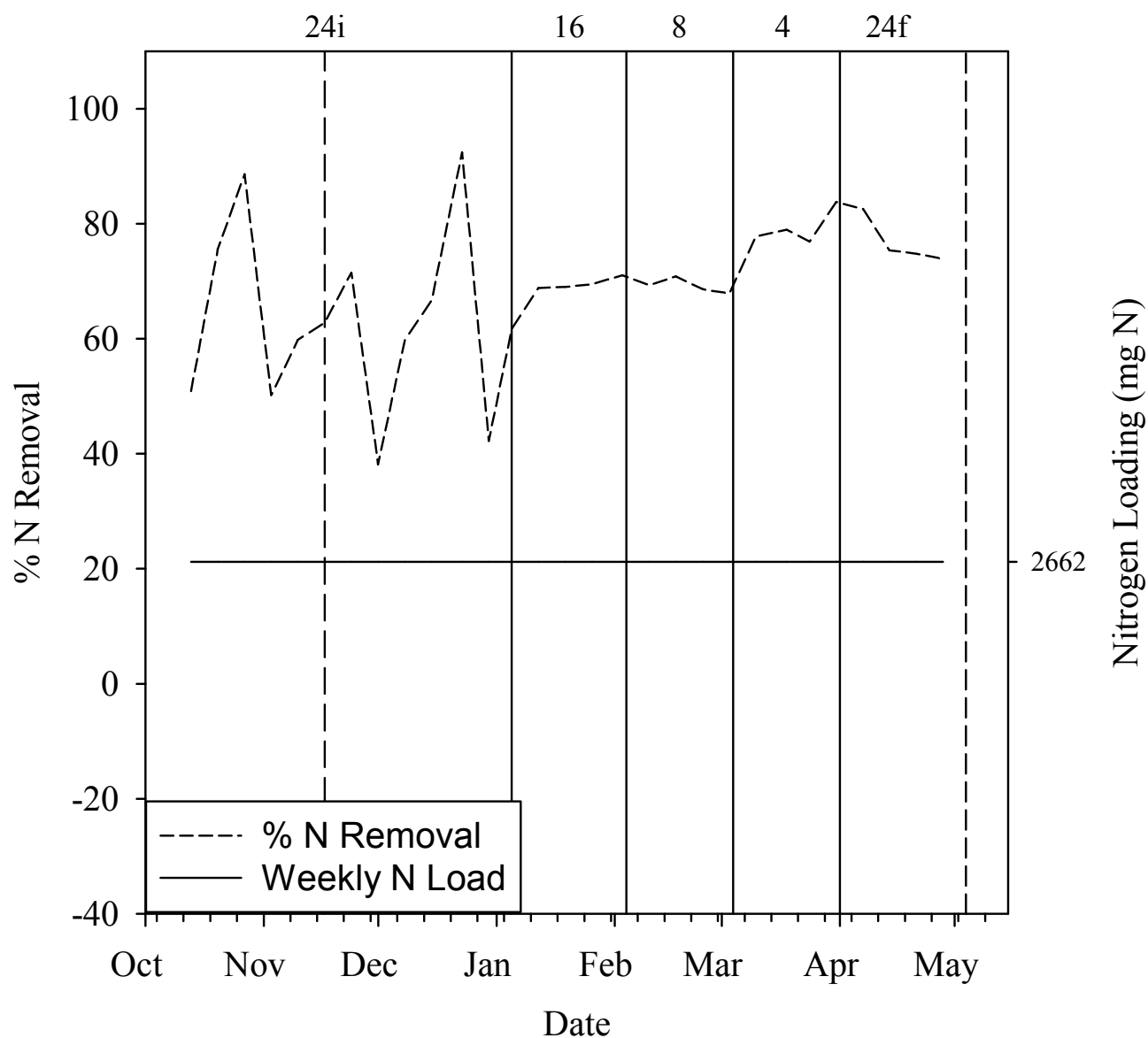
Fig. 3.15 – The percent N removal observed in the Low-N, tidal treatment, based on microbial mediated, and effluent N losses. The dashed vertical lines represent the first and final sampling events. Solid vertical lines depict the end of a cycling regime. Cycles per day are depicted along the top of the graph. The letters i and f distinguish the initial and final 24 cycles day^{-1} treatment.
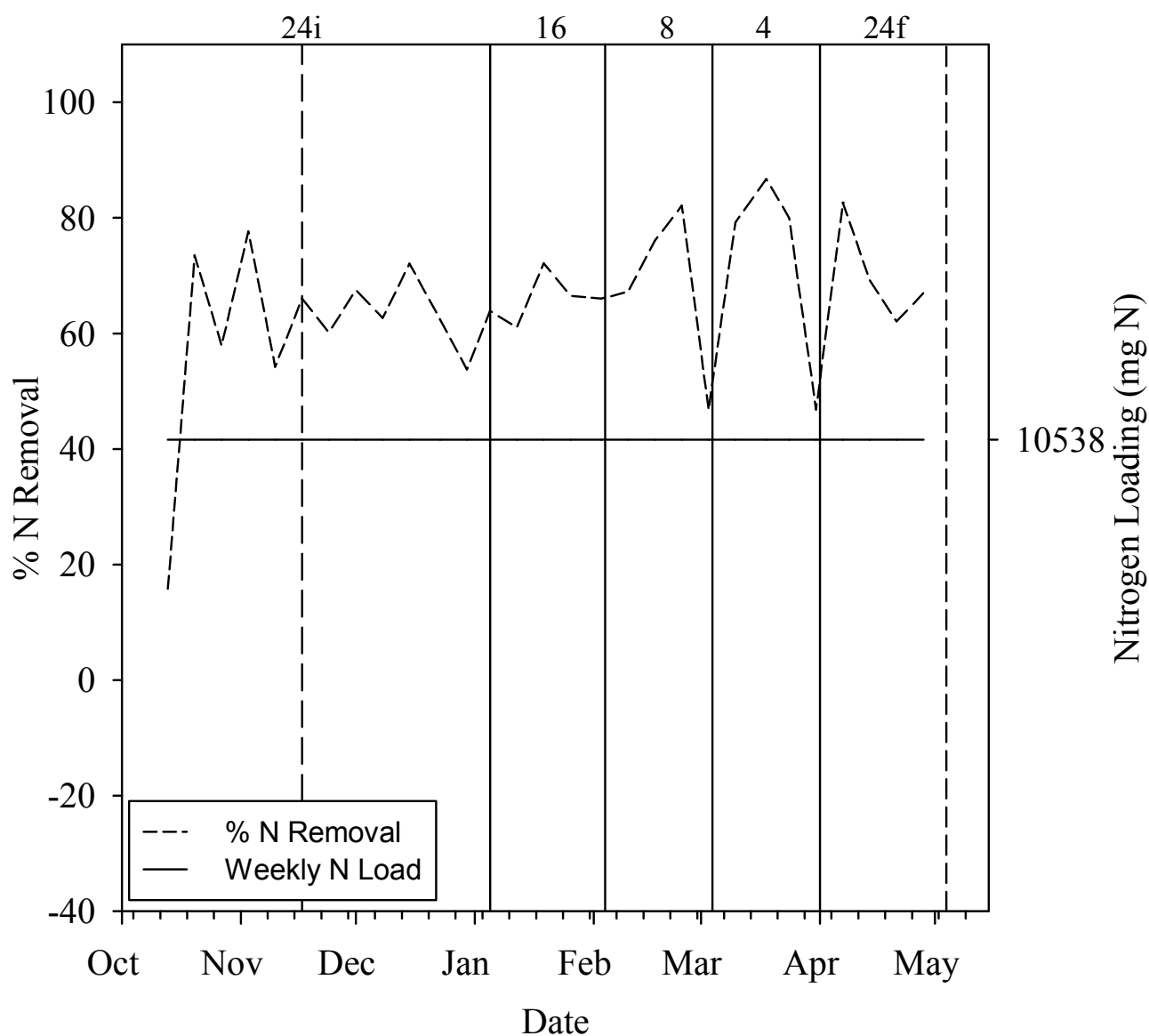
Fig. 3.16 – Percent N removed in the High-N Tidal Treatment. The dashed vertical lines represent the first and final sampling events. Solid vertical lines depict the end of a cycling regime. Cycles per day are depicted along the top of the graph. Removal of N is based on both microbially mediated processes and on effluent losses. The letters i and f distinguish the initial and final 24 cycles day^{-1} treatment.

3.1.2   Trickling-Flow Columns

Trickling-flow columns exhibited similar abundance and distribution trends as the Tidal-flow columns. The overall relationship of total abundance being greatest, followed by AOB, then by NOB, and then AXB was maintained. In these columns, however, numbers of AXB never exceeded those of NOB. Additionally, the general trend appeared to be a decline in abundance associated with depth within the column.

3.1.2.1   Abundance Profiles

Under the initial conditions, 0.8i-min $(0.25 \text{ hr})^{-1}$, there were no observable peaks in abundance along the vertical profile of the Low-N column (Fig. 3.17). In the 0.5-min (0.25 hr^{-1}) treatment, however, there was a decline in abundance associated with change in depth within the Low-N column (Fig. 3.18). The TAB peaked at the first sampling port. The TAB was 2.7×10^9 cells $(\text{g LESA})^{-1}$ at the first sampling portal, which was 1.4 fold greater than the average abundance during this treatment. At the fourth sampling portal, the abundance was 1.2×10^9 cells.
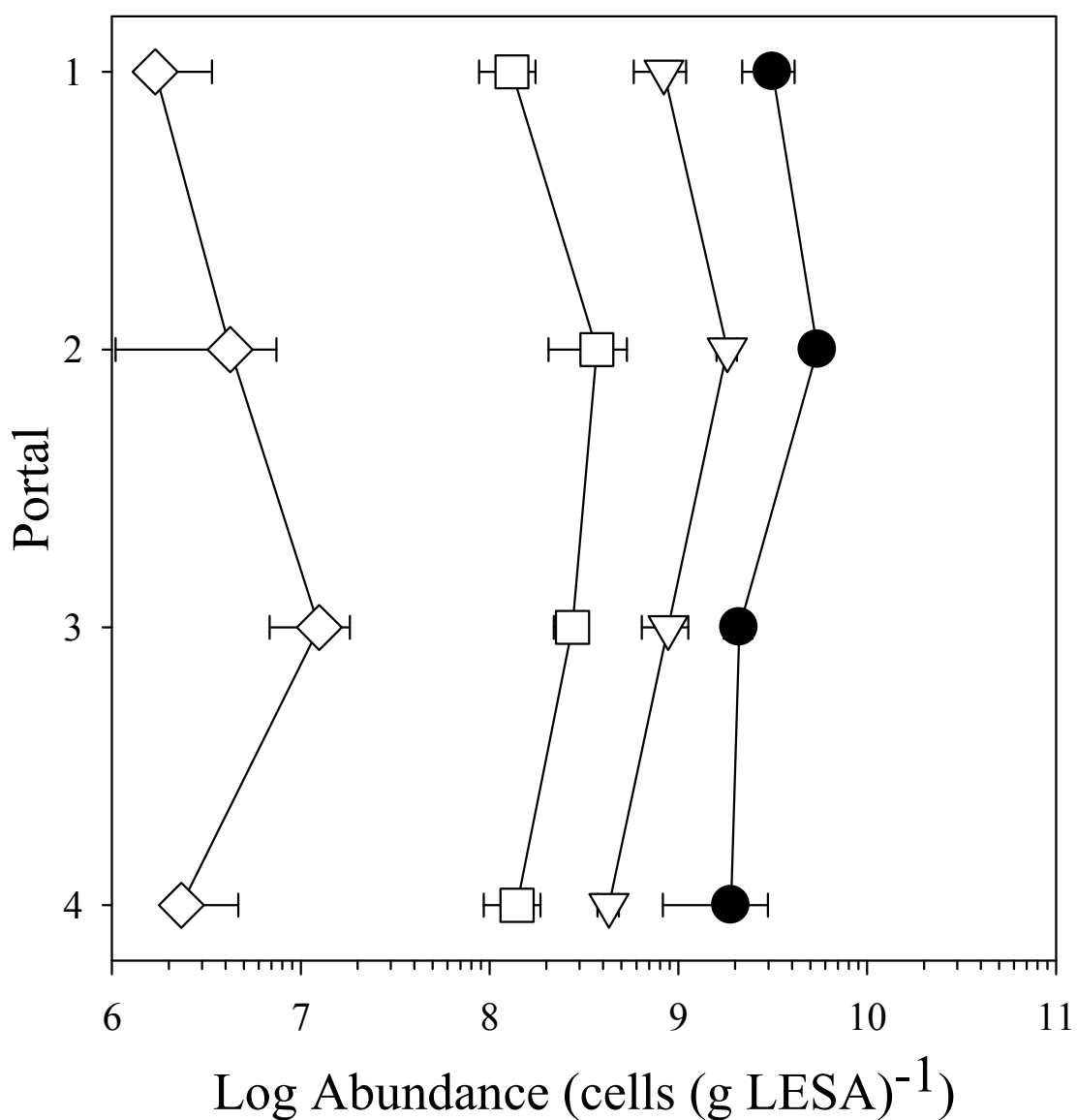
Fig. 3.17 – Abundance profiles of the total abundance of bacteria (TAB, circles), ammonia oxidizing bacteria (AOB, triangles), nitrite oxidizing bacteria (NOB, squares), and anaerobic ammonia oxidizing (anammox) bacteria (AXB, diamonds), for the Low-N treatment, at the conclusion of the 0.8i-min (0.25 hr)$^{-1}$ treatment.
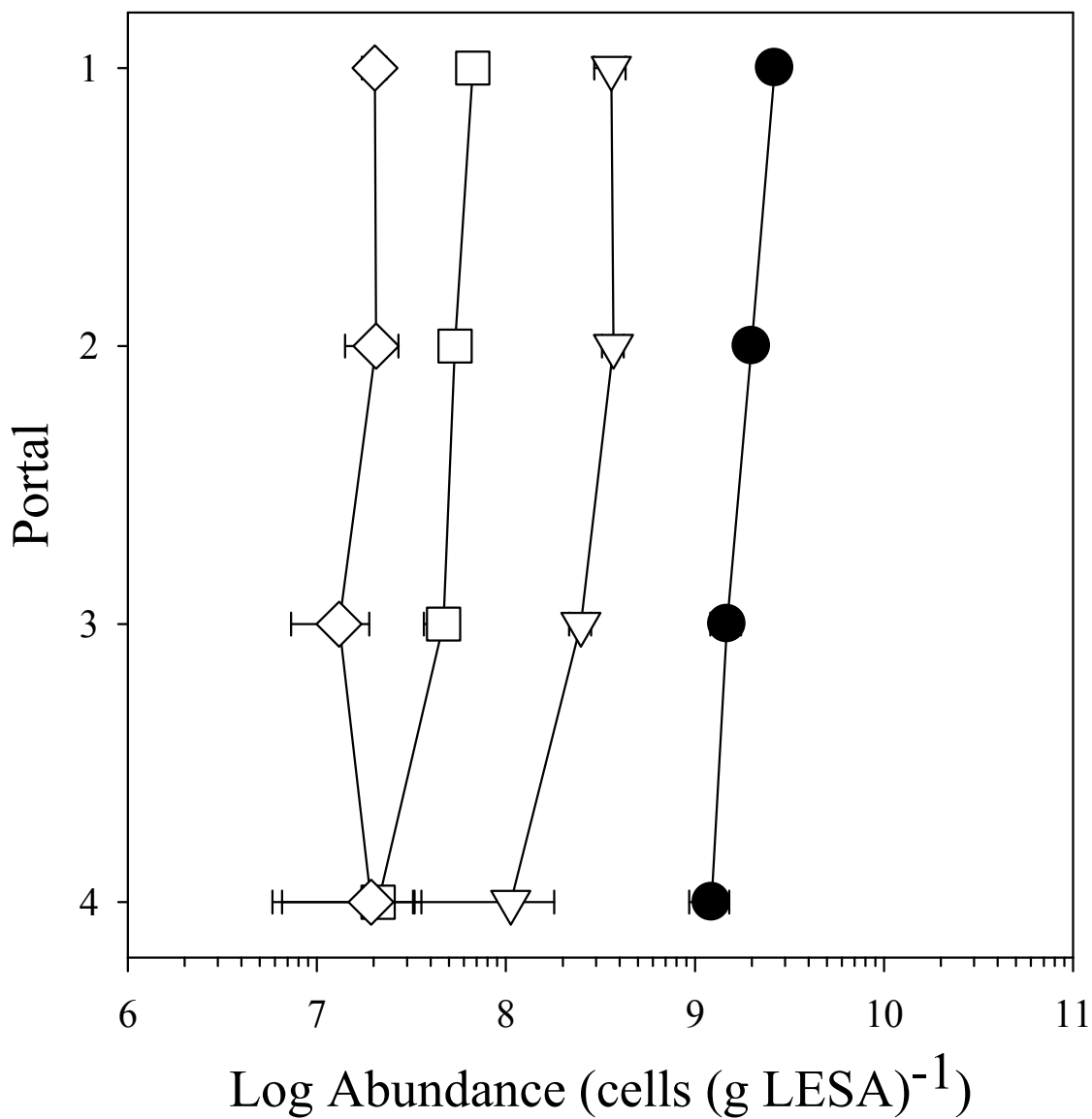
Fig. 3.18 – Profiles of the total abundance of bacteria (TAB, circles), ammonia oxidizing bacteria (AOB, triangles) nitrite oxidizing bacteria (NOB, squares) and anaerobic ammonia oxidizing (anammox) bacteria (AXB, diamond) abundance at the conclusion of the 0.5 min (0.25 hr)$^{-1}$ treatment in the Low-N treatment.
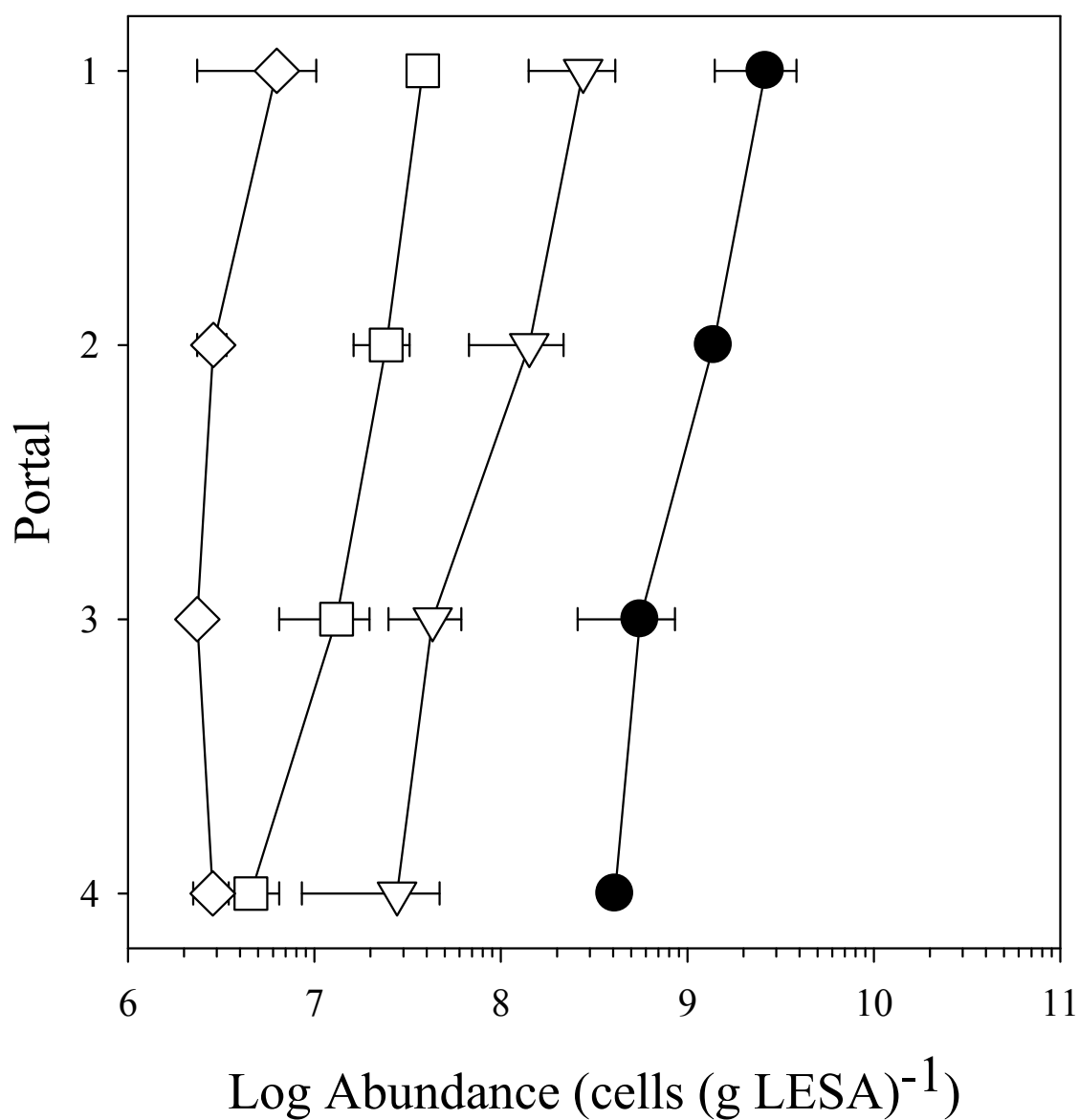
Fig. 3.19 – Abundance profiles in the Low-N treatment of total abundance of bacteria (TAB, circles), ammonia oxidizing bacteria (AOB, triangles), nitrite oxidizing bacteria (NOB, squares) and anaerobic ammonia oxidizing (anammox) bacteria (AXB, diamonds) at the conclusion of the 0.3 min (0.25 hr)$^{-1}$ treatment.

(g LESA)$^{-1}$, which marked the end of the slow decline of microbial abundance in the

Trickling-flow column. The AOB abundance exhibited a similar decline, going from 3.6

to 1.1 x 10^8 cells (g LESA)$^{-1}$ over the length of the column. The peak abundance at the

first sampling portal was 1.3 times greater than the average AOB abundance of 2.7 x 10^8

cells (g LESA)$^{-1}$.

In the Low-N trickling column, the 0.3-min (0.25 hr^{-1}) trickling treatment had the

most pronounced examples of abundance changes associated with depth (Fig. 3.19). For

example, there was a decline in TAB from 26×10^8 to 4.1 x 10^8 cells (g LESA)$^{-1}$ between

the first and fourth sampling portals. The peak in abundance observed at the first portal

was 2.1 fold greater than the average abundance of 1.3 x 10^9 cells (g LESA)$^{-1}$. A similar

decline was also seen in the AOB abundance, which declined from 28×10^7 to 2.8×10^7

cells (g LESA)$^{-1}$ (Fig. 3.19). The peak AOB abundance was 2.3 fold greater than the

average AOB abundance of 12 x 10^7 cells (g LESA)$^{-1}$. The NOB also exhibited a decline,

going from 38×10^6 to 4.6 x 10^6 cells (g LESA)$^{-1}$ (Fig. 3.19). The peak NOB abundance

was nearly twice the average NOB abundance of 2.0 x 10^7 cells (g LESA)$^{-1}$.

The abundance profile that resulted at the end of the 0.2-min (0.25 hr)$^{-1}$ treatment

did not show trends with depth (Fig. 3.20). Although averages and measured values were

not identical along the vertical profile, there was significant variation as shown by the

error bars. The lack of precision in the measurements here precluded analysis of

abundance along the vertical profile for this trickling treatment.

During the 0.8f-min (0.25 hr)$^{-1}$ there were no discernible peaks in TAB, AOB or

NOB abundances (Fig. 3.21). However, the AXB abundance peaked at the first sampling

portal with an abundance of 8.2 x 10^7 cells (g LESA)$^{-1}$. The abundance at the first

sampling portal was 2.1 fold greater than the average AXB abundance of 3.9×10^7 cells

(g LESA)$^{-1}$ (Fig. 3.21).
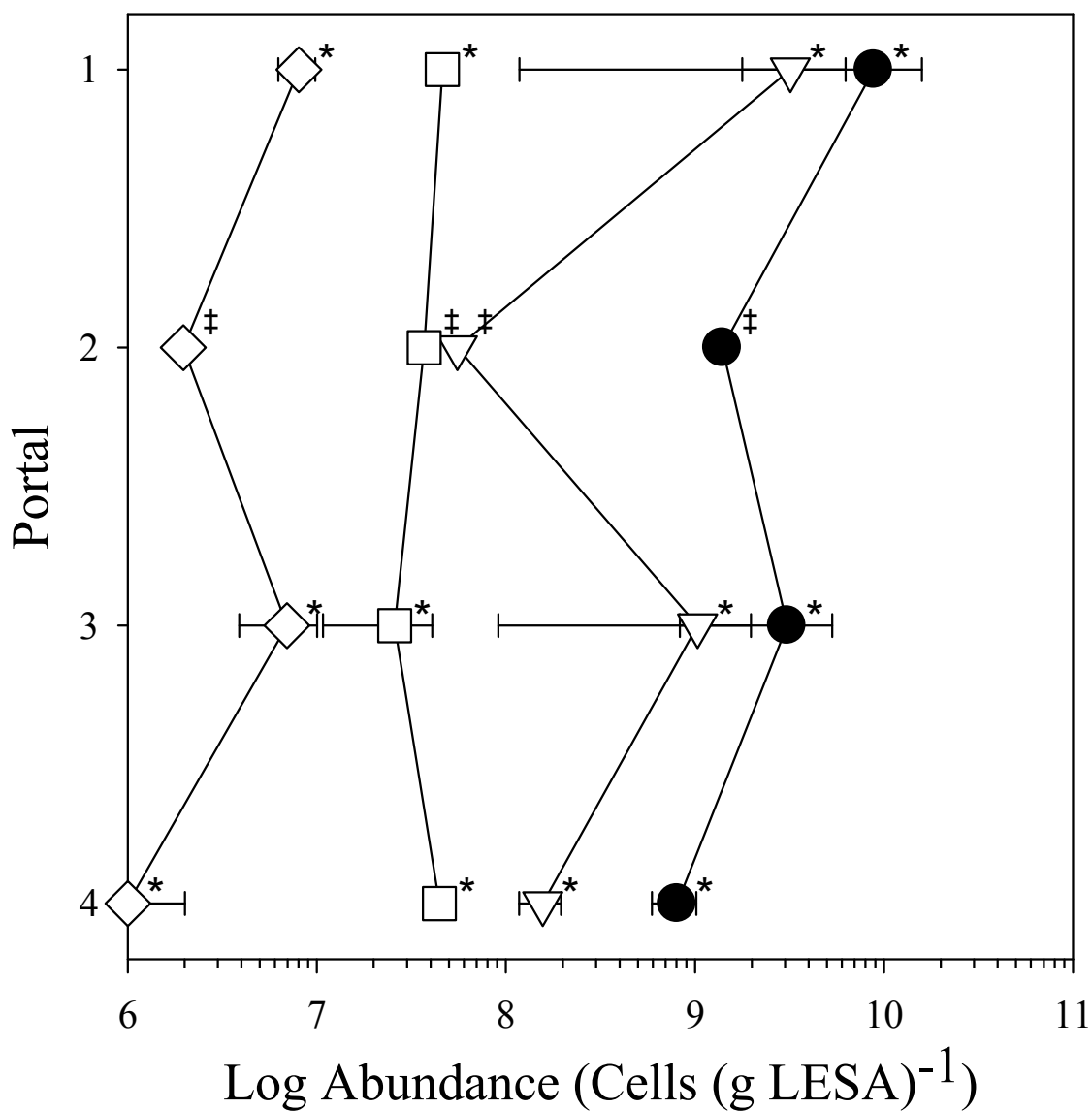
Fig. 3.20 – Profiles at the conclusion of the 0.2 min (0.25 hr)⁻¹ treatment of total abundance of bacteria (TAB, circles), ammonia oxidizing bacteria (AOB, triangles), nitrite oxidizing bacteria (NOB, squares) and anaerobic ammonia oxidizing (anammox) bacteria (AXB, diamonds) for the Low-N treatment.

* Denotes locations where only two samples were processed.
‡ Denotes locations where only one sample was processed
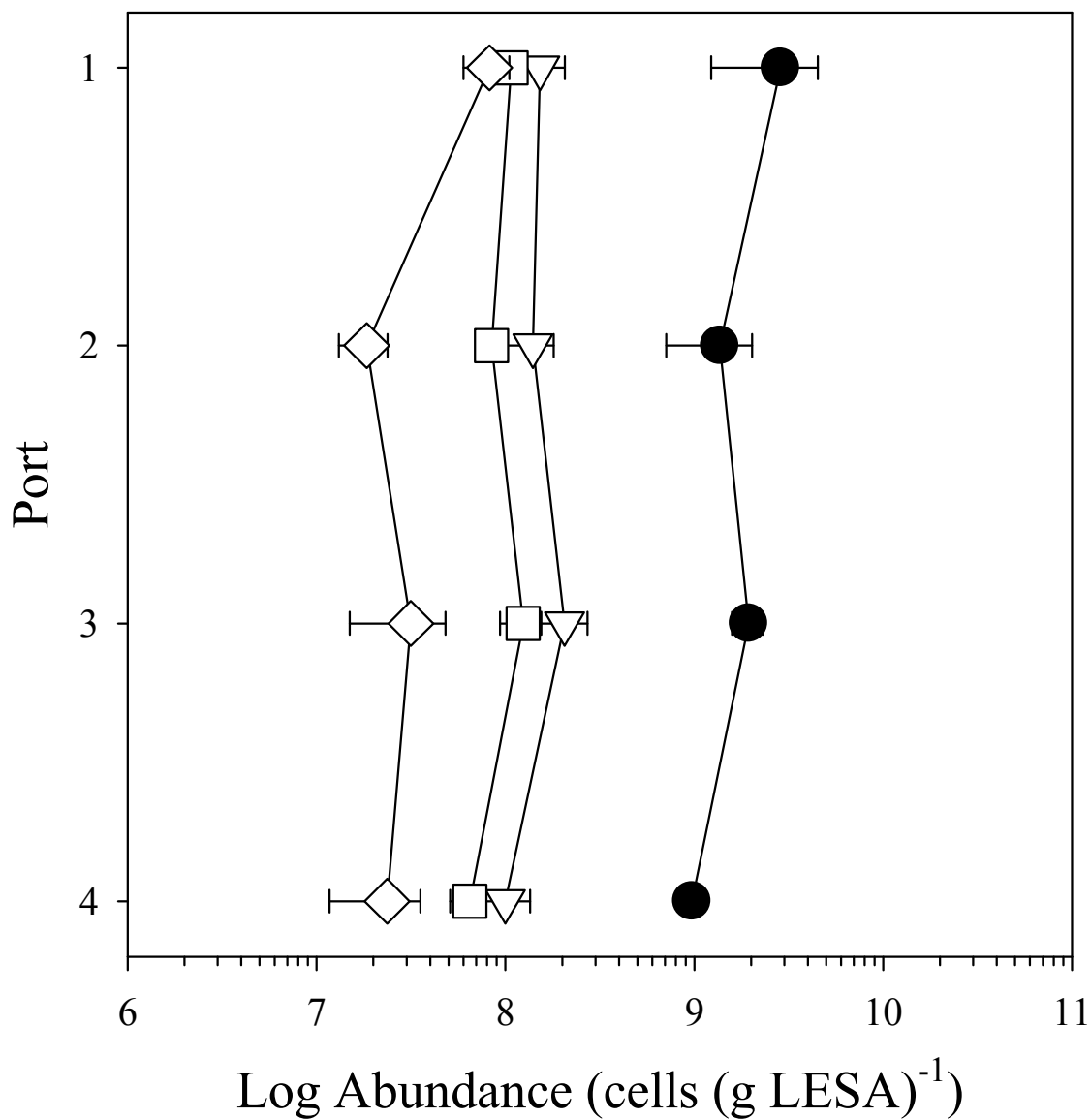
Fig. 3.21 – Abundance profiles of total abundance of bacteria (TAB, circles), ammonia oxidizing bacteria (AOB, triangles), nitrite oxidizing bacteria (NOB, squares) and anaerobic ammonia oxidizing (anammox) bacteria (AXB, diamonds) for the Low-N treatment at the conclusion of the 0.8f-min (0.25 hr)$^{-1}$ treatment.
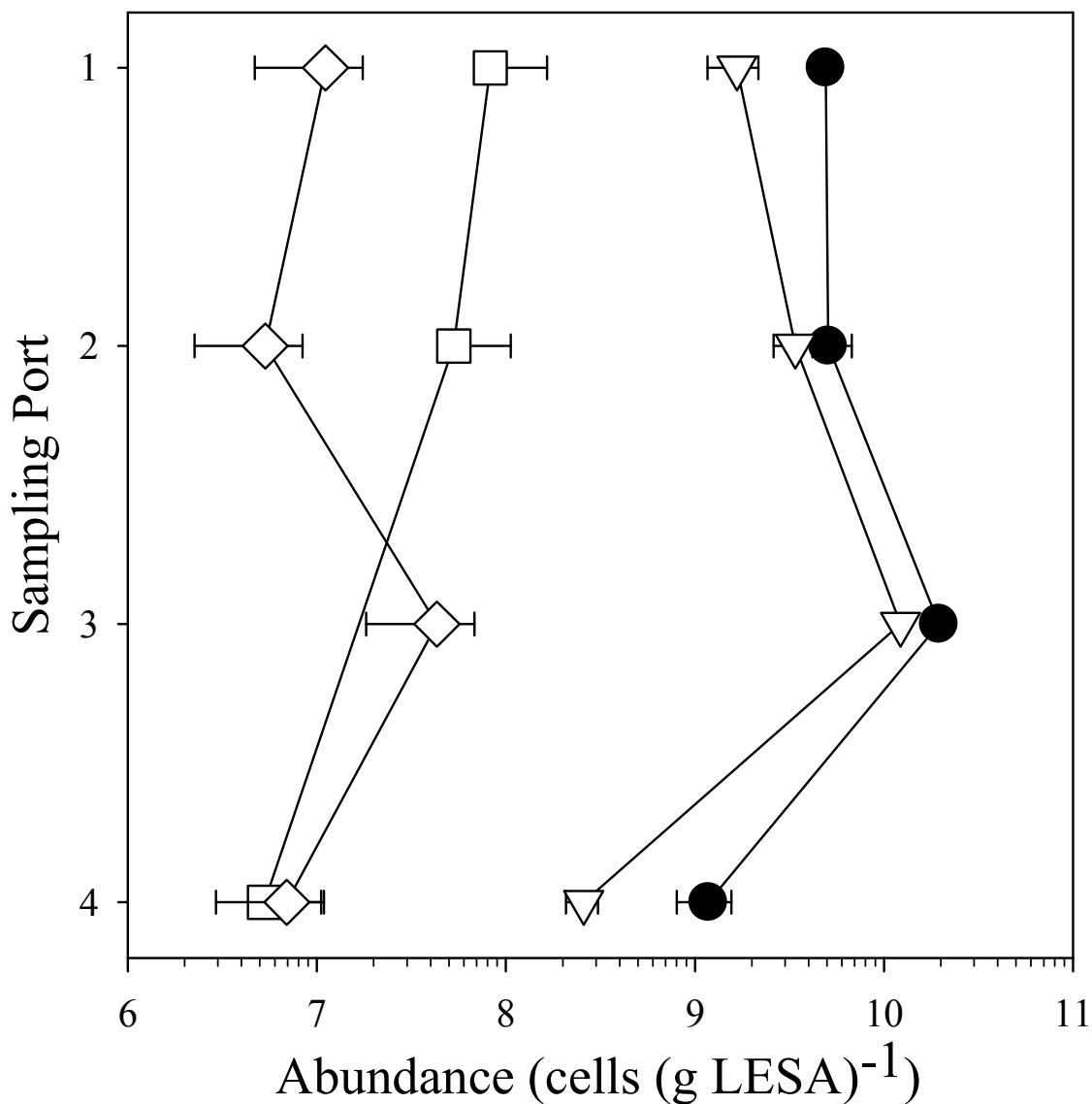
Fig. 3.22 – Profiles from the High-N treatment total abundance of bacteria (TAB, circles), ammonia oxidizing bacteria (AOB, triangles), nitrite oxidizing bacteria (NOB, squares) and anaerobic ammonia oxidizing (anammox) bacteria (AXB, diamonds) at the conclusion of the 0.8i-min (0.25 hr)$^{-1}$ treatment.
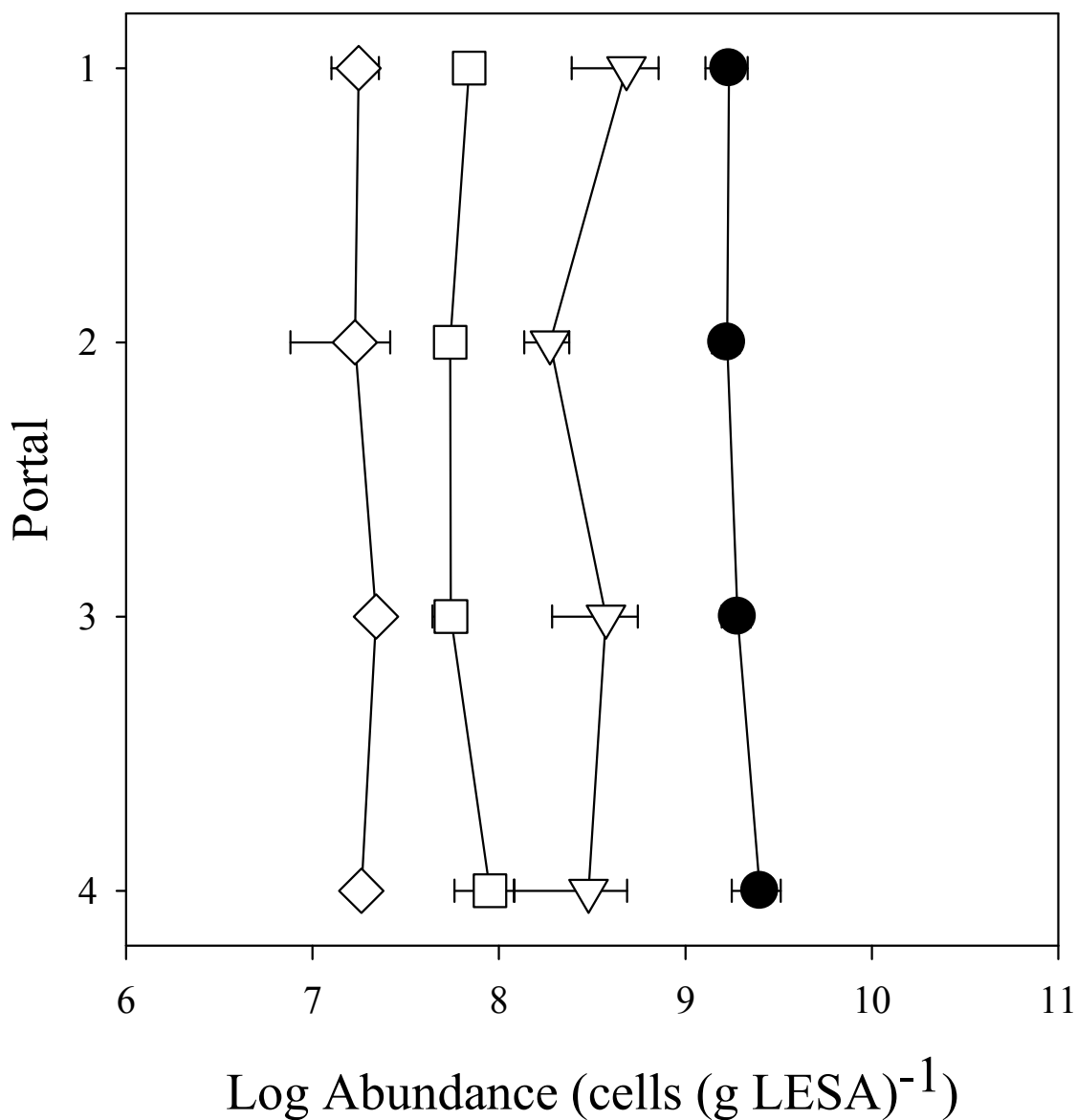
Fig. 3.23 – Abundance profiles at the conclusion of the 0.5-min (0.25 hr)[-1] treatment of total abundance of bacteria (TAB, circles), ammonia oxidizing bacteria (AOB, triangles), nitrite oxidizing bacteria (NOB, squares) and anaerobic ammonia oxidizing (anammox) bacteria (AXB, diamonds) for the High-N treatment.
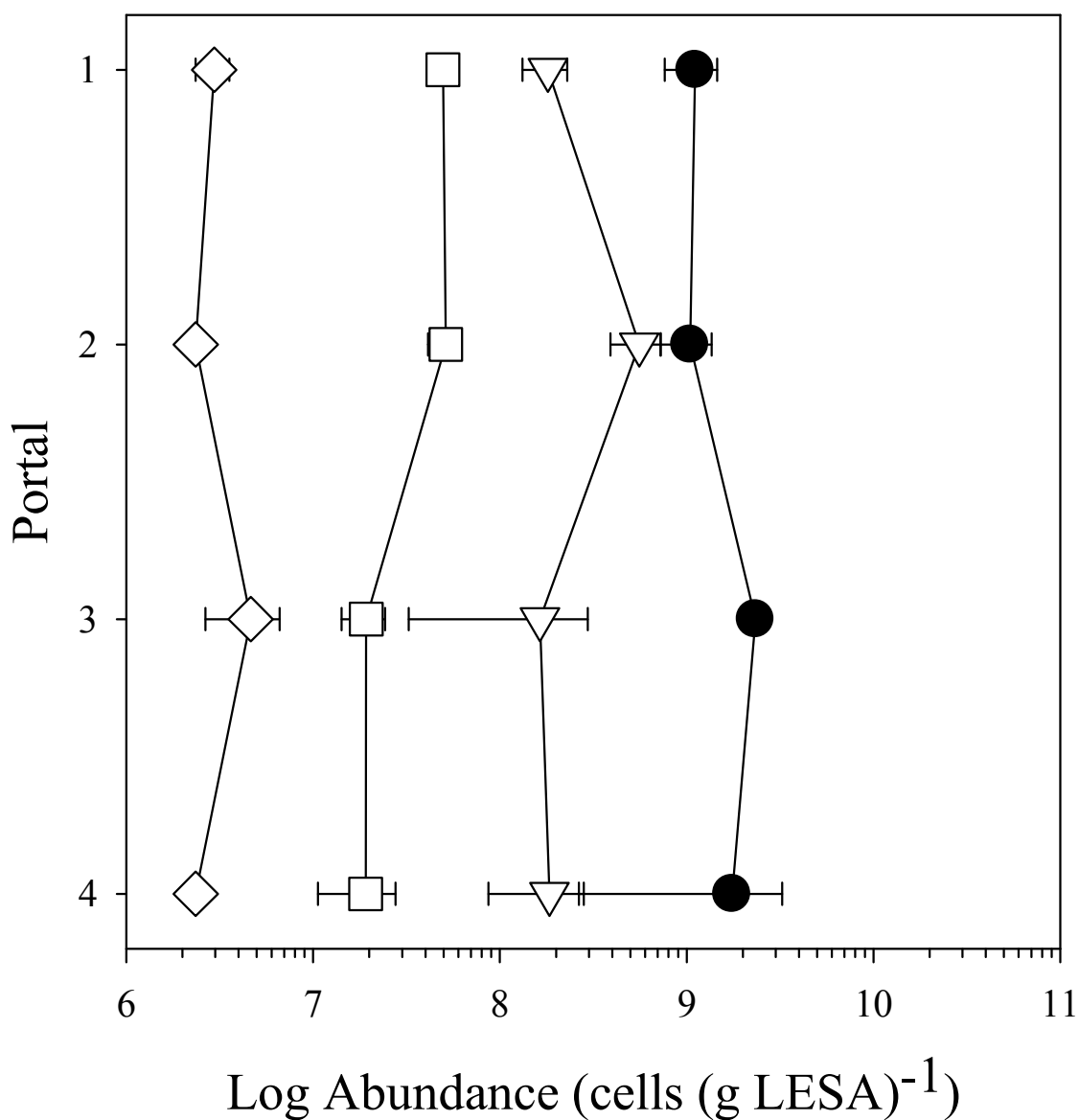
Fig. 3.24 – Abundance profiles of total abundance of bacteria (TAB, circles), ammonia oxidizing bacteria (AOB, triangles), nitrite oxidizing bacteria (NOB, squares) and anaerobic ammonia oxidizing (anammox) bacteria (AXB, diamonds) for the High-N treatment at the conclusion of the 0.3-min (0.25 hr)[-1] treatment.
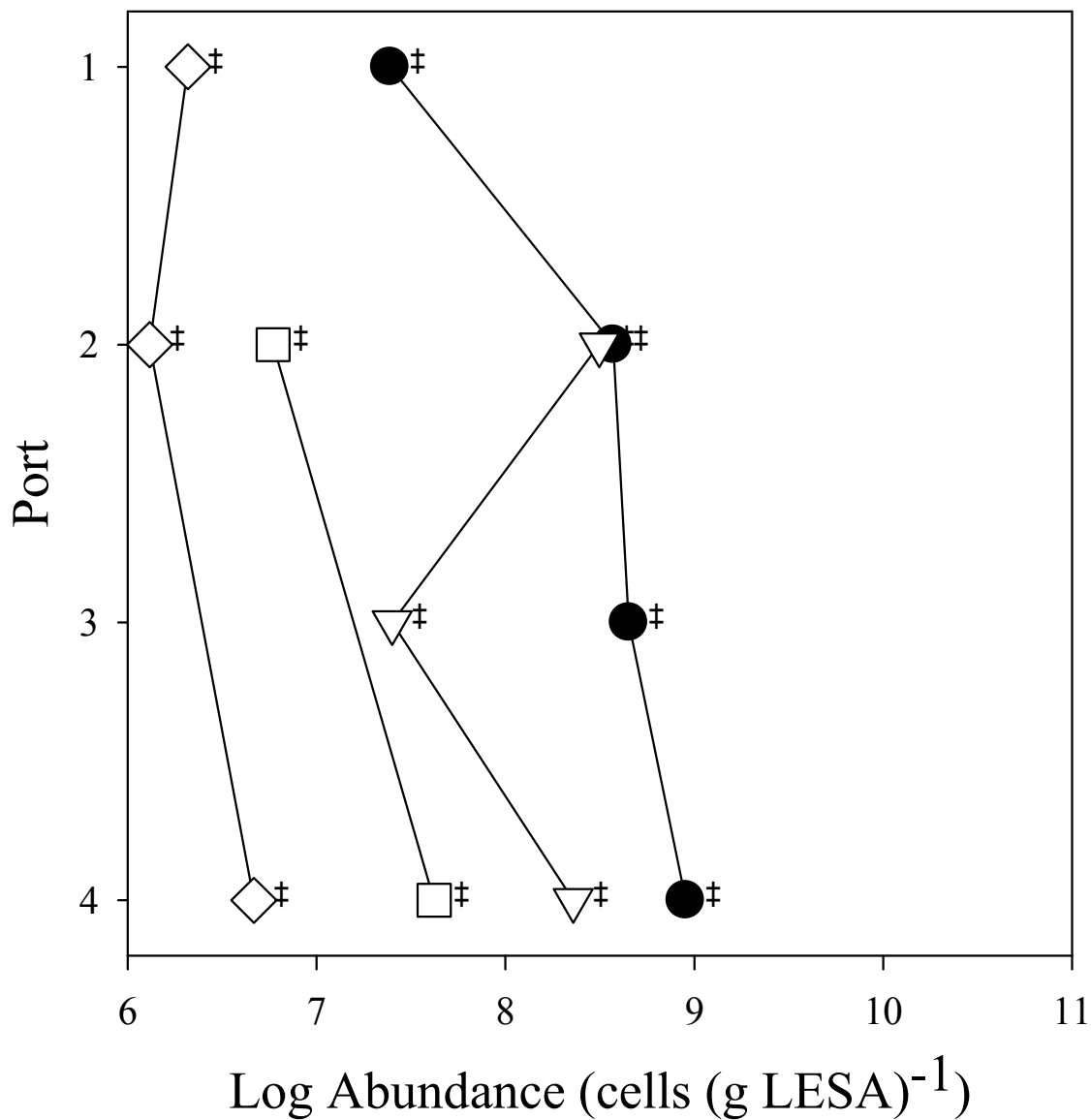
Fig. 3.25 – Total abundance of bacteria (TAB, circles), ammonia oxidizing bacteria (AOB, triangles), nitrite oxidizing bacteria (NOB, squares) and anaerobic ammonia oxidizing (anammox) bacteria (AXB, diamonds) abundance profiles for the High-N treatment at the conclusion of the 0.2-min (0.25 hr)$^{-1}$ treatment.

‡ Denotes locations where only one sample was processed.
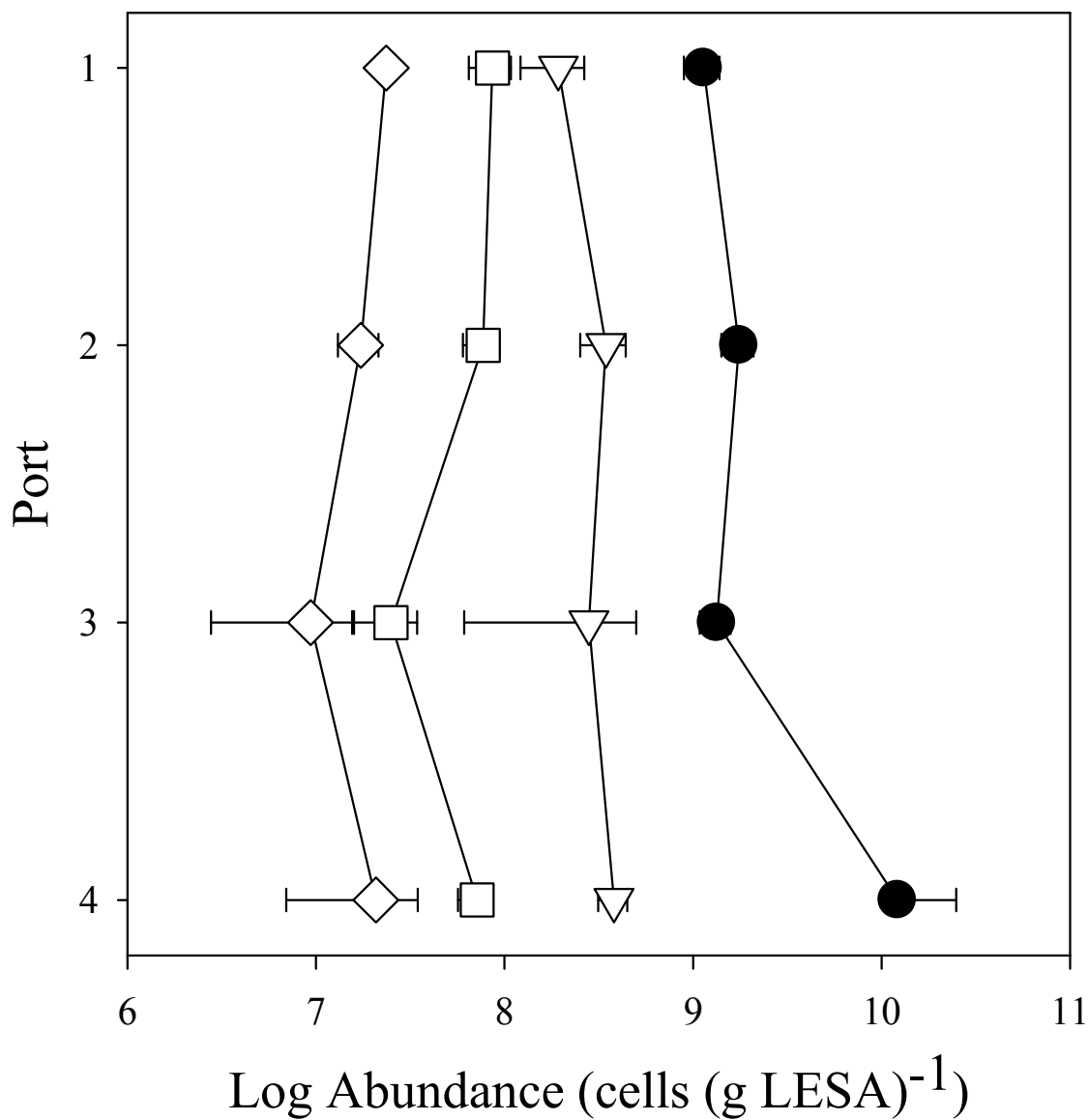
Fig. 3.26 – Profiles of the total abundance of bacteria (TAB, circles), ammonia oxidizing bacteria (AOB, triangles), nitrite oxidizing bacteria (NOB, squares), and anaerobic ammonia oxidizing (anammox) bacteria (AXB, diamonds) abundance at the conclusion of the 0.8f-min (0.25 hr)$^{-1}$ treatment in the High-N treatment.

The High-N, Trickling-flow column had multiple peaks in microbial abundances. During the 0.8i-min (0.25 hr)$^{-1}$ trickling treatment, the TAB and AOB abundance exhibited a peak at the third sampling portal (Fig. 3.22). The TAB had an abundance of 2.0 x 10^{10} cells (g LESA)$^{-1}$, compared to an average abundance of 7.7 x 10^9 cells (g LESA)$^{-1}$, which was a 2.5-fold increase in abundance. The AOB abundance at the third portal, 1.2 x 10^{10} cells (g LESA)$^{-1}$, was 2.8 fold larger than the average AOB abundance of 4.4 x 10^9 cells (g LESA)$^{-1}$during this trickling treatment. No abundance peaks were observed at the end of the 0.5-min (0.25 hr)$^{-1}$ treatment (Fig. 3.23). However, there were peaks after the 0.3-min (0.25 hr^{-1}) treatment (Fig. 3.24). The AOB abundance was 5.6 x 10^8 cells (g LESA)$^{-1}$ at the second sampling port, a 2-fold increase in abundance compared to an average abundance of 2.7 x 10^8 cells (g LESA)$^{-1}$. No peaks in abundance were observed at the close of the 0.2-min (0.25 hr)$^{-1}$ treatment (Fig. 3.25). There was a peak in TAB at the fourth sampling portal after the 0.8f-min (0.25 hr^{-1}) treatment, at which point the TAB was 1.2 x 10^{10} cells (g LESA)$^{-1}$ (Fig. 3.26), compared to an average abundance of 4.1 x 10^9 cells (g LESA)$^{-1}$.

3.1.2.2   Integrated Abundances

In most cases, the High-N trickling treatment had greater abundance than the Low-N trickling treatment (Fig. 3.27). The average TAB across all hydraulic treatments in the Low-N treatment was 2.3 x 10^{13} cells and was 3.4 x 10^{13} cells in the High-N treatment. The average AOB abundance across all hydraulic treatments in the Low-N treatment was 5.0 x 10^{12} cells, and was 9.7 x 10^{12} cells in the High-N treatment, a 1.9 fold increase in abundance compared to the Low-N trickling column (Fig. 3.27). The nitrite-oxidizing functional group represented an exception to the generalization that the High-N

treatment supported greater abundance of each group of bacteria. In the Low-N treatment,

average NOB abundance was 8.5 x 10^{11} cells and it was 4.6 x 10^{11} cells in the High-N

treatment: a 1.8 fold increase favoring the Low-N treatment.
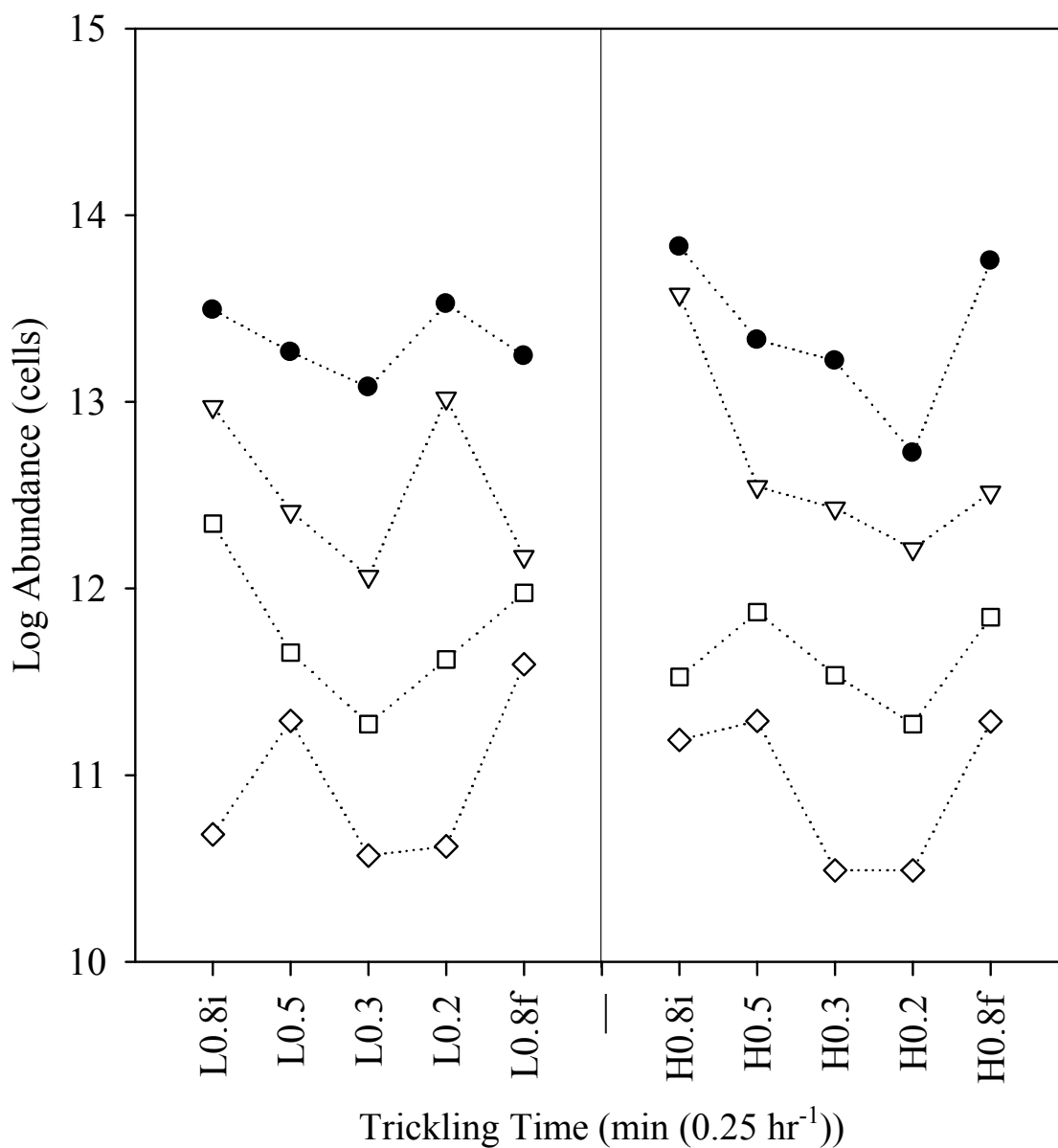
Fig. 3.27 – Integrated abundances for the Trickling-flow columns grouped by Low- and High-N treatment (L and H) and by trickling time per quarter hour for the total abundance of bacteria (TAB, filled circles), ammonia oxidizing bacteria (AOB, triangles), nitrite oxidizing bacteria (NOB, squares), and anaerobic ammonia oxidizing (anammox) bacteria (AXB, diamonds). The initial and final trickling treatments of the columns were 0.8 min (0.25 hr)$^{-1}$ and are distinguished by the letters i and f. Dotted lines are only a visual aid and do not denote regression analysis.

The 0.3-min $(0.25\ hr)^{-1}$ trickling treatment however, was consistent with the trend that the High-N treatment supported a greater number of organisms. At the end of the 0.3-min $(0.25\ hr)^{-1}$ treatment, NOB were more abundant in the High-N treatment than in the Low-N treatment. The average NOB abundance in the High-N treatment, $3.4\ x\ 10^{11}$ cells, was nearly twice the average NOB abundance, $1.9\ x\ 10^{11}$ cells, in the Low-N treatment.

The overall AXB abundance exhibited little difference between High- and Low-N treatments; however, similar to the NOB, average AXB abundance was greater in Low-N treatment. The AXB abundance in the Low-N treatment was $1.4\ x\ 10^{11}$ cells, whereas the average AXB abundance in the High-N treatment was $1.2\ x\ 10^{11}$ cells. The exception was the 0.8i-min $(0.25\ hr)^{-1}$ trickling treatment which had greater abundance in the High-N treatment. The AXB abundance in the High-N treatment was $1.5\ x\ 10^{11}$ cells, compared to that in the Low-N treatment, $4.8\ x\ 10^{10}$ cells. During the 0.8i-min $(0.25\ hr)^{-1}$ treatment, abundance in the High-N treatment was 3.2 fold greater than in the Low-N treatment.

Integrated abundance values for the trickling-flow columns revealed that they behaved similarly to the tidal columns, and there was a decline in most abundance values that was associated with the decline in Trickling-flow time. During the 0.2-min $(0.25\ hr)^{-1}$ treatment, the TAB value increased to $3.3\ x\ 10^{13}$ cells. The observed increase was likely the result of experimental error. Samples collected at the end of the 0.2-min $(0.25\ hr)^{-1}$ trickling time period were processed hastily to meet a deadline imposed by Worrell Water and as such, multiple people counted hybridized bacteria and introduced additional inconsistency. Samples processed from this treatment had multiple instances of AOB

values greater than TAB values. As this could not be possible, such cell counts were removed from analysis and were not presented in the graph. However, that action reduced the accuracy of abundance measurements, which were already suspect due to human error. This occlusion in the data was also observed in the AOB and NOB abundance data. In addition to the increased human error, the data from this time point were not consistent with the chemical data which showed an increase in NH_4^+ and NO_2^-, which generally coincided with a decline in abundance of nitrifiers.

Abundance values in the Low-N column declined from 3.1 x 10^{13} cells to 1.2 x 10^{13} cells during the 0.3-min (0.25 hr)$^{-1}$ treatment (Fig. 3.27). By omitting the 0.2-min (0.25 hr)$^{-1}$ time point, the overall trend in abundance seen in the tidal columns, and the High-N, Trickling-flow column was observed in the Low-N treatment as well. The TAB declined by 61% between the 0.8i- and 0.3-min (0.25 hr)$^{-1}$ treatments, and then abundance increased by 30% by the end of the 0.8f-min (0.25 hr)$^{-1}$ treatment. For the AOB, there was an 87% decline in abundance between the 0.8i-min (0.25 hr)$^{-1}$, and the 0.3-min (0.25 hr)$^{-1}$ treatment. In the Low-N treatment, the AOB abundance went from 9.4 × 10^{12} to 1.2 x 10^{12} cells (Fig. 3.27). At the close of the 0.8f-min (0.25 hr)$^{-1}$ treatment, the AOB abundance had increased by a factor of 1.3, to 1.5 x 10^{12} cells. The NOB exhibited similar behavior. During the time span between the endings of the 0.8i- and 0.3-min (0.25 hr)$^{-1}$ treatments, the abundance of NOB declined by 92%, going from 22 to 1.9 x 10^{11} cells. During the 0.8f-min (0.25 hr)$^{-1}$ treatment the NOB abundance increased to 9.5 x 10^{11} cells: a 5-fold increase in abundance from the 0.3-min (0.25 hr)$^{-1}$ regiment. The AXB bacteria followed a similar trend (Fig. 3.27). There was a 23% decrease in AXB abundance between the 0.8i- and 0.3-min (0.25 hr)$^{-1}$ treatments,

followed by an 11-fold increase in AXB abundance between the 0.3- and 0.8f-min (0.25 hr)$^{-1}$ treatments.

The High-N treatment followed the same observed trend. The abundance of bacteria declined in association with reduction in trickling times. The TAB declined from 68 to 5.3 x 10^{12} cells, a 92% decline in abundance between the 0.8i-and 0.2-min (0.25 hr)$^{-1}$ treatments (Fig. 3.27). The TAB then increased by a factor of 11 to 5.7 x 10^{13} cells. The AOB followed a similar pattern. The abundance of AOB declined by 53% between the 0.8i- and 0.2-min (0.25 hr)$^{-1}$ treatments, and then increased by a factor of 2 during the 0.8f-min (0.25 hr)$^{-1}$ treatment. The AOB abundance began at 3.8 x 10^{13} cells, declined to 1.6 x 10^{12} cells at the end of the 0.2-min (0.25 hr)$^{-1}$ treatment, and then rose to 3.3 x 10^{12} cells (Fig. 3.27). The NOB abundance values followed the same trend declining by a factor of 1.8 between the 0.8i-and 0.2-min (0.25 hr)$^{-1}$ treatments. Abundance of NOB at the end of the 0.8i-min (0.25 hr)$^{-1}$ treatment was 3.4 x 10^{11} cells, and it subsequently declined to 1.9 x 10^{11} cells by the close of the 0.2-min (0.25 hr)$^{-1}$ treatment. The abundance then increased by a factor of 3.8, to a final abundance measurement of 7.0 x 10^{11} cells at the end of the 8f-min (0.25 hr)$^{-1}$ period (Fig. 3.27). The maximal value of NOB abundance in the High-N trickling column of 7.5 x 10^{11} was seen under the 0.5-min (0.25 hr)$^{-1}$ treatment.

The AXB abundance values behaved less consistently. There was little change between the 0.8i- and 0.5-min (0.25 hr)$^{-1}$ treatment periods (Fig. 3.27). Abundance of AXB went from 1.5 to 1.9 x 10^{11} cells. Then, there was an 84% decline in abundance to 3.1 x 10^{10} cells at the end of the 0.3-min (0.25 hr)$^{-1}$ treatment. There was no detectable change between the 0.3- and 0.2-min (0.25 hr)$^{-1}$ treatments. Finally, there was a 6.3-fold

increase between the 0.2- and 0.8f-min $(0.25 \text{ hr})^{-1}$ treatments, consistent with the

increases seen in other functional groups and treatments.

Overall, the general trend was that abundance declined with reduction in trickling

time. While increased trickling time at the end of the experiment was associated with an

increase in the abundance of bacteria in a short time, whether or not steady state was

reached cannot be determined in these short experimental periods.

3.1.2.3   Water Chemistry

Chemical data for the duration of the experiment suggested there was a

relationship between the trickling duration and the N transformations occurring in the

trickling-flow treatments (Fig. 3.28–3.30). In the Low-N, trickling-flow treatment, there

was minimal variation in NH_4^+ for the duration of the experiment. The average NH_4^+

concentration was 4.0 ppm NH_4^+–N (S.E. = 5.9, n = 29). The concentration of NH_4^+ was

briefly elevated to 17 ppm NH_4^+ –N for two weeks during the 0.2-min $(0.25 \text{ hr})^{-1}$

treatment period. In the Low-N trickling treatment, the concentration of NO_2^- showed a

similar trend (Fig. 3.29). The average NO_2^- concentration was 17.2 ppm NO_2^- –N (S.E. =

61.9, n = 29). Two peaks in NO_2^- were observed. Prior to the initial sampling, the NO_2^-

concentration peaked at 287 ppm NO_2^- –N. The second peak occurred during the 0.3-min

$(0.25 \text{ hr})^{-1}$ treatment during which NO_2^- reached 181.3 ppm NO_2^- –N.

In the Low-N treatment, the concentration of NO_3^- was elevated and considerably

more variable compared to the concentrations of NO_2^- or NH_4^+ (Fig. 3.30). The average

NO_3^- concentration was 216.7 ppm NO_3^- –N (S.E. = 62.9, n= 29). During the 0.8i (0.25

$\text{hr})^{-1}$ treatment, there was a peak of 396 ppm NO_3^- –N. The NO_3^- concentration remained

fairly constant during the 0.5- and 0.3- min $(0.25 \text{ hr})^{-1}$ treatments, but declined during the

0.2-min $(0.25 \text{ hr})^{-1}$ treatment. During the 0.2-min $(0.25 \text{ hr})^{-1}$ treatment the average NO_3^-

concentration was 164.6 ppm $NO_3^- - N$ (S.E. $= 18.5$, n $= 4$). The NO_3^- concentration then

increased during the 0.8f $(0.25 \text{ hr})^{-1}$ treatment. The average concentration was 237.4 ppm

$NO_3^- - N$ (S.E. $= 11.7$, n $= 4$).

In the High-N trickling column, the average NH_4^+ concentration was 68.1 ppm

$NH_4^+ - N$ (S.E. $= 20.1$, n $= 29$) (Fig. 3.28). During the 0.5-min $(0.25 \text{ hr})^{-1}$ trickling

treatment, the NH_4^+ concentration was less than 10 ppm. After this treatment, the NH_4^+

concentration remained near the average of 68.1 ppm $NH_4^+ - N$ consistently (Fig. 3.28).
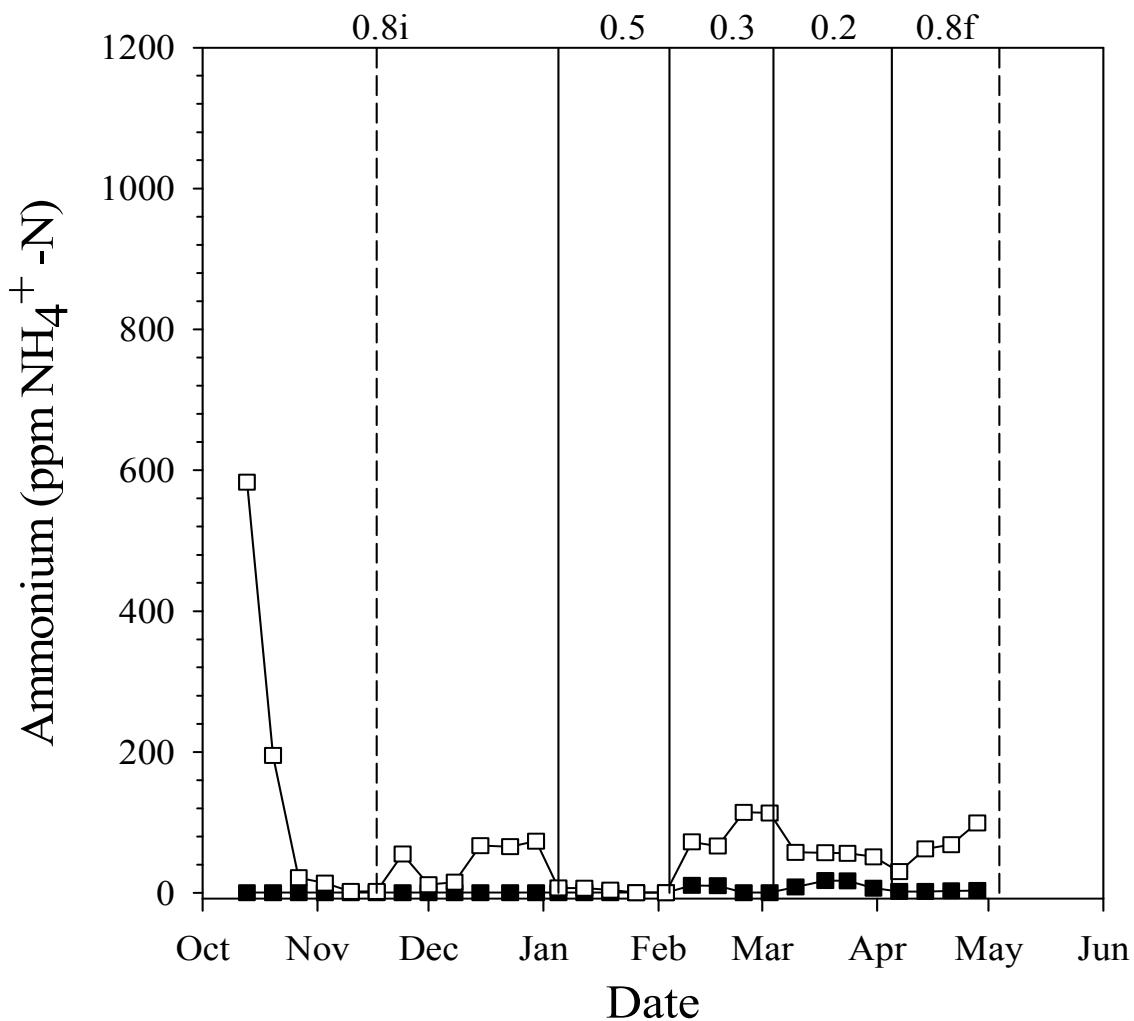
Fig. 3.28 – Concentration data for NH$_4^+$ in the high- (open circles) and Low-N (closed circle) trickling-flow columns measured weekly through the entire duration of the test period. The dashed vertical lines represent the initial and final sampling events. The solid vertical lines represent changes in trickling time per quarter hour. Trickling duration is given along the top of the graph as trickling min (0.25 hr)$^{-1}$. The letters i and f distinguish the initial and final 0.8 min (0.25 hr)$^{-1}$ treatments.
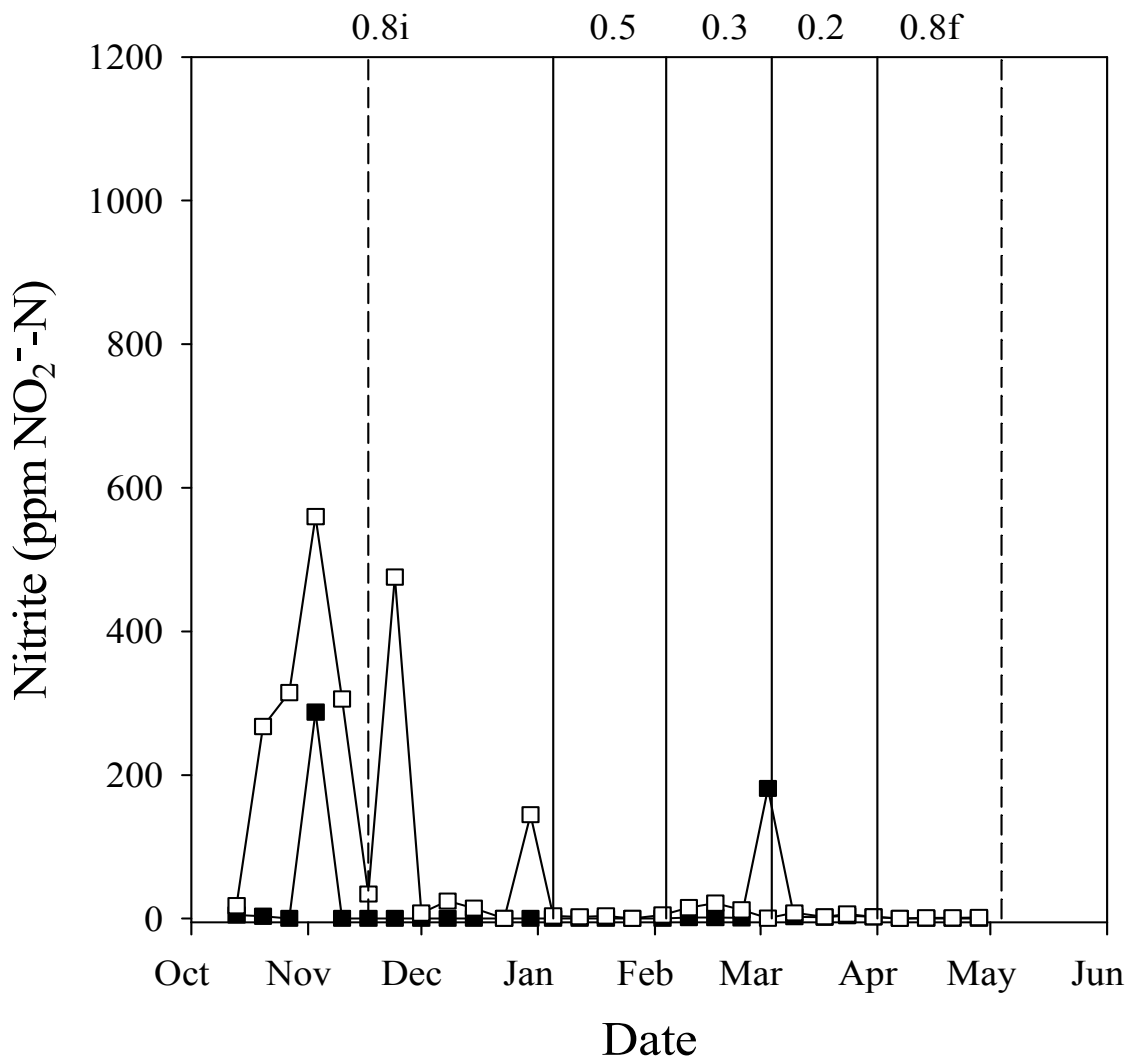
Fig. 3.29 – Concentration data for NO$_2^-$ in the high- (open circles) and Low-N (closed circle) trickling-flow columns measured weekly through the entire duration of the test period. The dashed vertical lines represent the initial and final sampling events. The solid vertical lines represent changes in trickling time per quarter hour. Trickling duration are depicted along the top of the graph. Trickling duration is given along the top of the graph as trickling min (0.25 hr)$^{-1}$. The letters i and f distinguish the initial and final 0.8 min (0.25 hr)$^{-1}$ treatments.
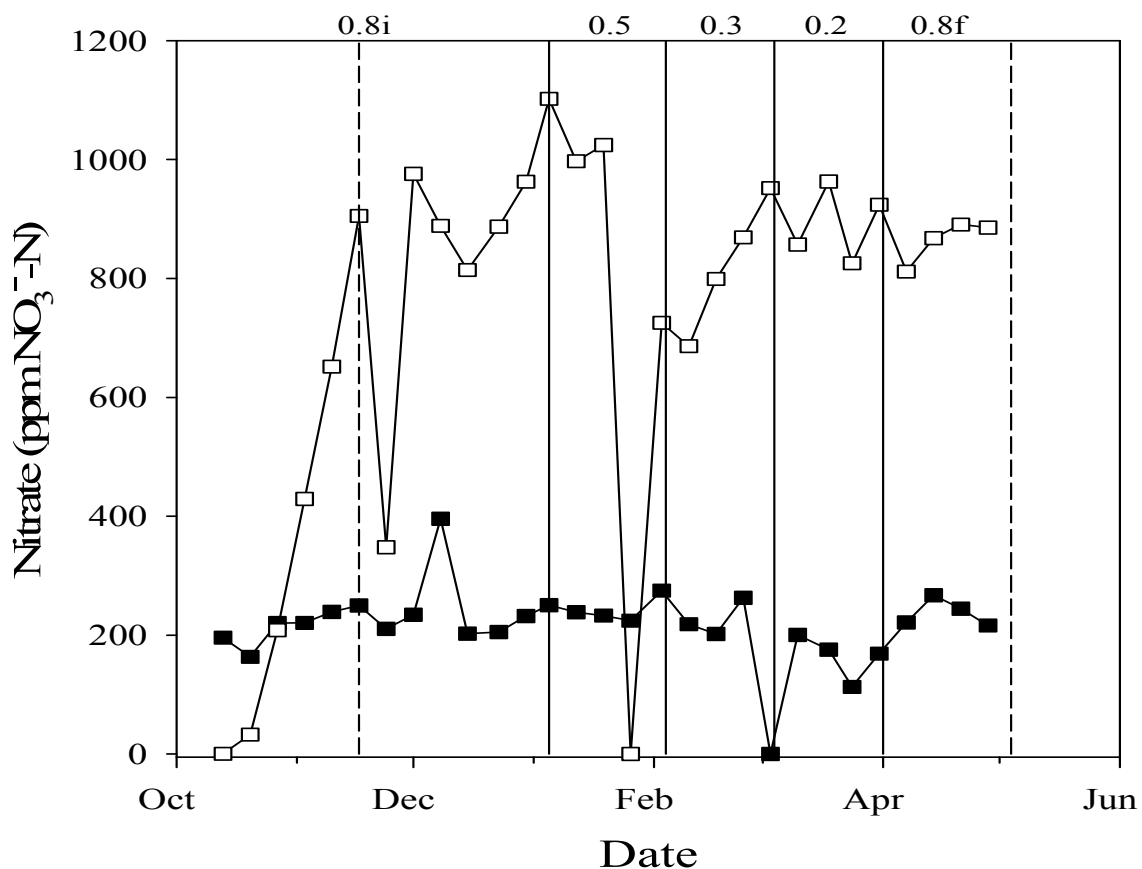
Fig. 3.30 – Concentration data for NO$_3^-$ in the high- (open circles) and Low-N (closed circle) trickling-flow columns measured weekly through the entire duration of the test period. The dashed vertical lines represent the initial and final sampling events. The solid vertical lines represent changes in trickling time per quarter hour. Trickling duration is given along the top of the graph. Trickling duration is given along the top of the graph as trickling min (0.25 hr)$^{-1}$. The letters i and f distinguish the initial and final 0.8 min (0.25 hr)$^{-1}$ treatments.

The NO_2^- concentration was also consistent throughout the course of this study (Fig 3.29). The average NO_2^- concentration was 77.8 ppm NO_2^- –N (S.E. = 28.4, n = 29). Prior to the initial sampling there was a peak in NO_2^- of 560 ppm NO_2^- –N. A smaller peak of 475 ppm NO_2^- –N was observed during the 0.8i-min $(0.25 \text{ hr})^{-1}$ treatment. During the transition from 0.8i- to 0.5-min $(0.25 \text{ hr})^{-1}$, there was a peak of 144.8 ppm NO_2^- –N.

Although NO_3^- concentration exhibited more variation than NO_2^- or NH_4^+, the fluctuation in concentration remained near the average concentration of 734 ppm NO_3^- – N (S.E. = 59.1, n = 29) (Fig. 3.30). Prior to initial sampling, there was a steady climb in NO_3^- concentration over a 6 week period, from below detection limit to over 900 ppm NO_3^- –N at the time of initial sampling. During the 0.5-min $(0.25 \text{ hr})^{-1}$ treatment, the concentration of NO_3^- dropped from 1,024 ppm NO_3^- –N to below detection limit, and then returned to725 ppm NO_3^- –N within a three week period. The percentage of N removed was calculated for the Trickling-flow columns based on effluent and microbially mediated N losses (Fig. 3.31 and 3.32). Additional graphs depicting the summation of NO_2^- and NO_3^- are also included for comparison with other studies where a combined value was reported for these two N compounds (Fig. 3.33-3.36). Although there was moderate noise in the percent removal data, the Low-N treatment appears to achieve fairly consistent N removal from the 0.5 min $(0.25 \text{ hr})^{-1}$. The High-N treatment appears to have increased N removal during the final two trickling treatments. Except for a large increase in percent N removal during the 0.5 min $(0.25 \text{ hr})^{-1}$, N removal also appears reasonably steady throughout the first three trickling treatments.
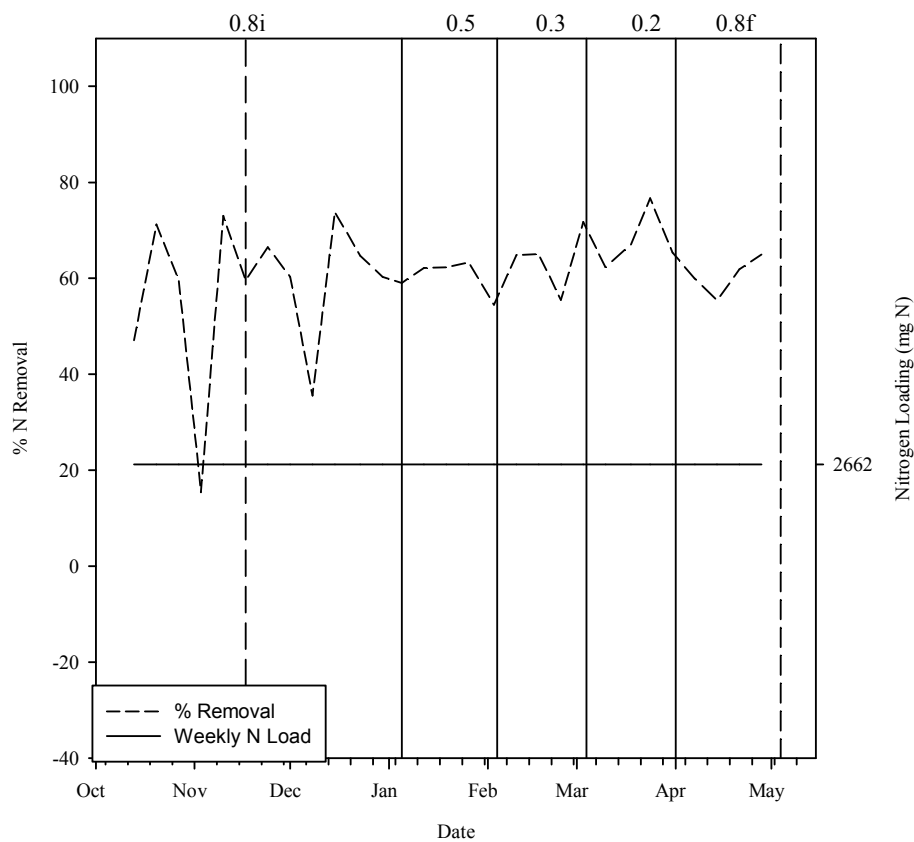
Fig. 3.31 – The percent N removal observed in the Low-N, trickling treatment, based on microbial mediated, and effluent N losses. The dashed vertical lines represent the first and final sampling events. Solid vertical lines depict the end of a trickling regime. Trickling regimes are depicted along the top of the graph and represent the trickling duration that recurs every quarter hour. The letters i and f distinguish the initial and final 0.8 min (0.25 hr)[-1].
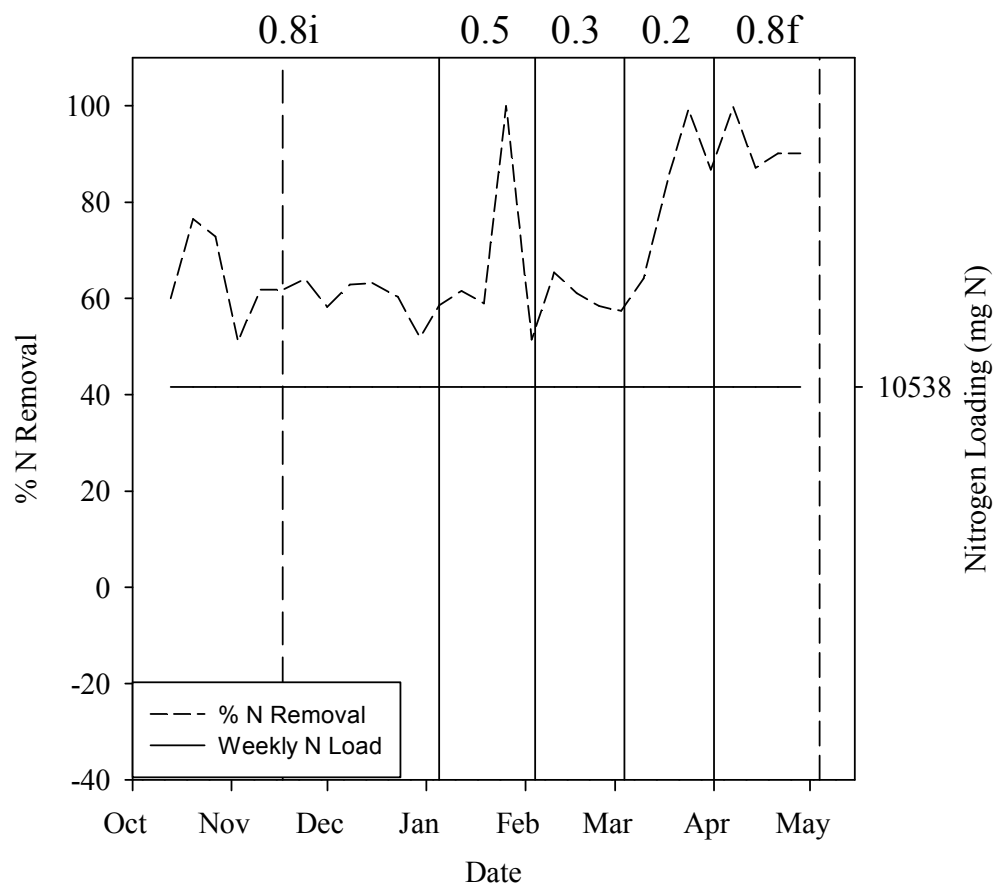
Fig. 3.32 – The percent N removal observed in the High-N, trickling treatment, based on microbial mediated, and effluent N losses. The dashed vertical lines represent the first and final sampling events. Solid vertical lines depict the end of a trickling regime. Trickling regimes are depicted along the top of the graph and represent the trickling duration that recurs every quarter hour. The letters i and f distinguish the initial and final 0.8 min (0.25 hr)$^{-1}$.
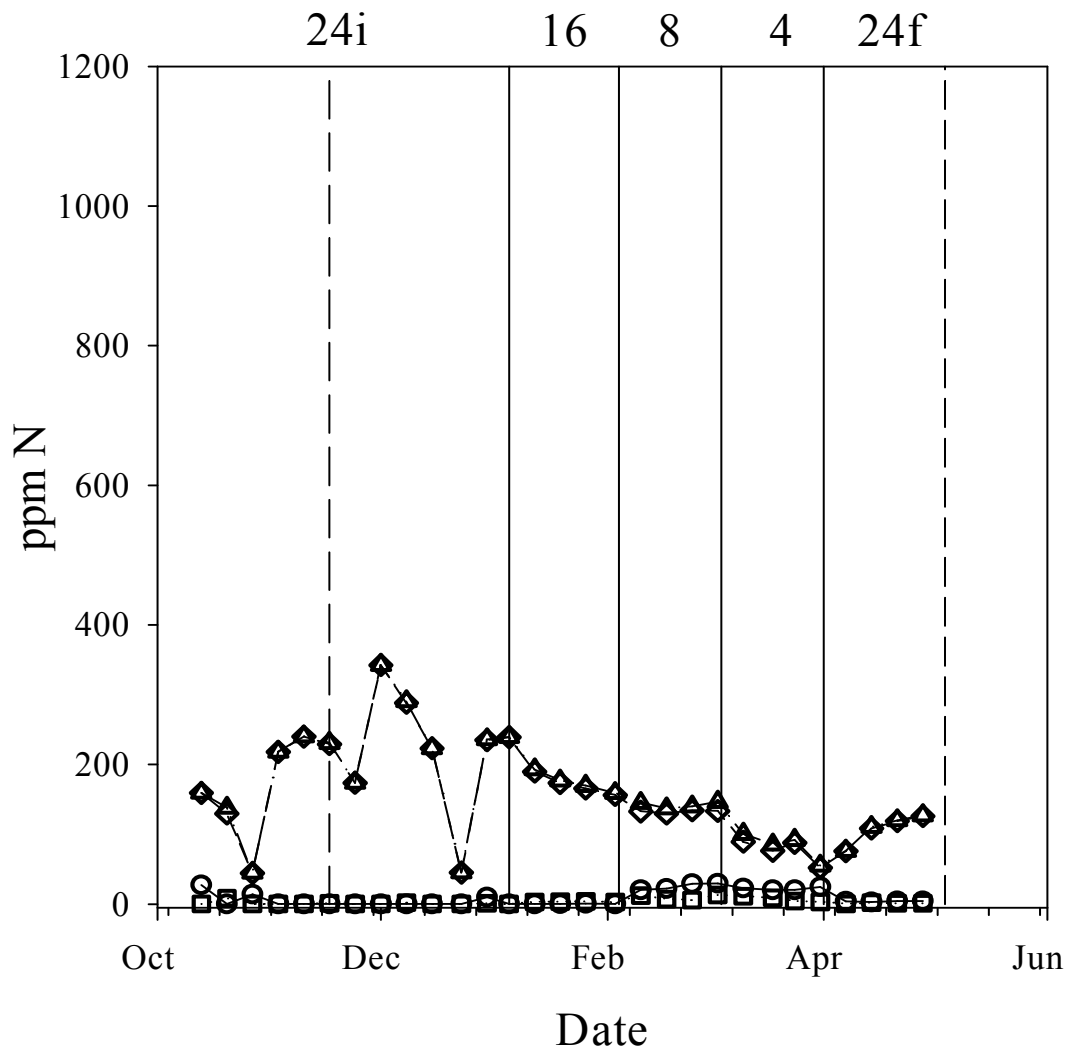
Fig. 3.33 – Concentration data for the Low-N tidal treatment, including summation of NO_2^- and NO_3^- (triangle), NO_3^- (diamond) NO_2^- (square) and NH_4^+ (circle). Tidal cycling frequencies are given along the top of the graph. Solid vertical bars represent a change in hydraulic regime and dashed vertical bars represent the initial and final sampling events. The initial and final 24 cycles day[-1] treatments are distinguished by an i and an f respectively.
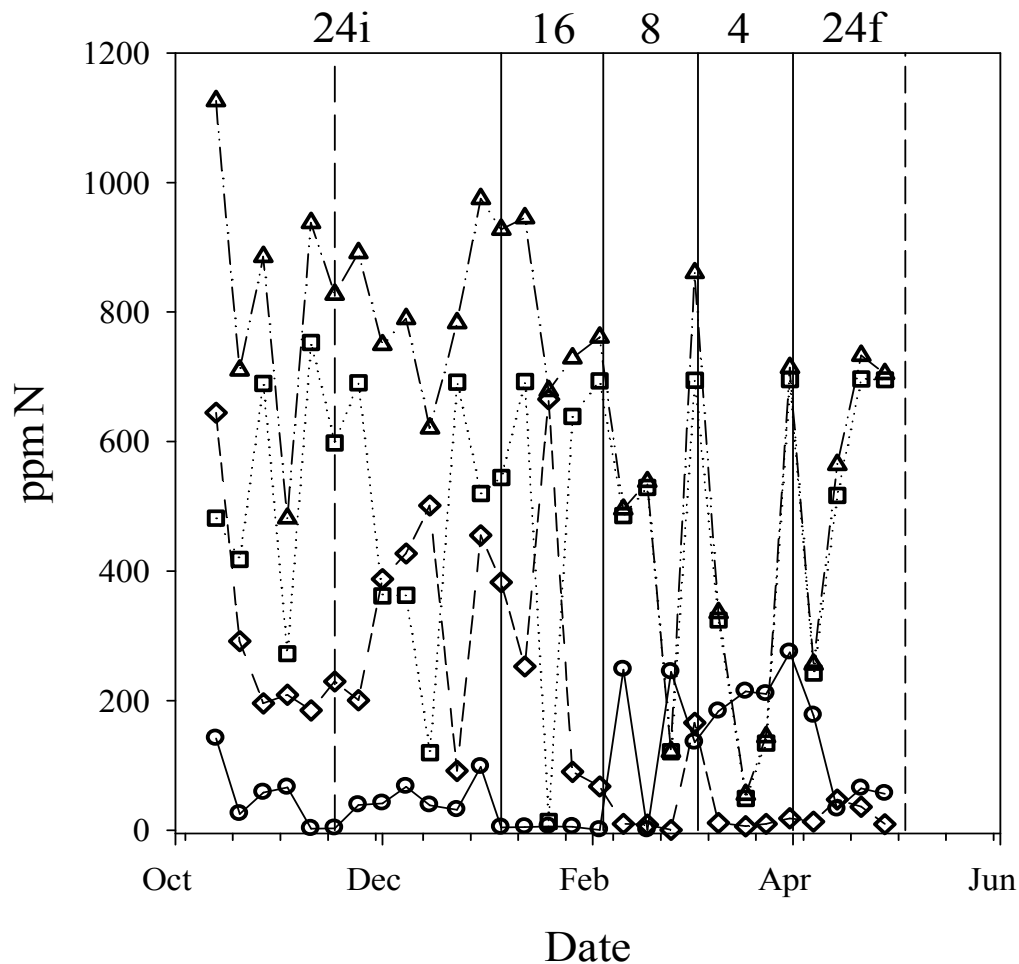
Fig. 3.34 – Concentration data, including summation of NO_2^- and NO_3^- (triangles), NO_3^- (diamonds) NO_2^- (squares) and NH_4^+ (circles) for the High-N tidal treatment. Hydraulic regime is depicted across the top of each graph. Tidal regimes are in units of cycles day^{-1}. Solid vertical bars represent a change in hydraulic regime and dashed vertical bars represent the initial and final sampling events. The initial and final 24 cycles day^{-1} treatments are distinguished by an i and an f respectively.
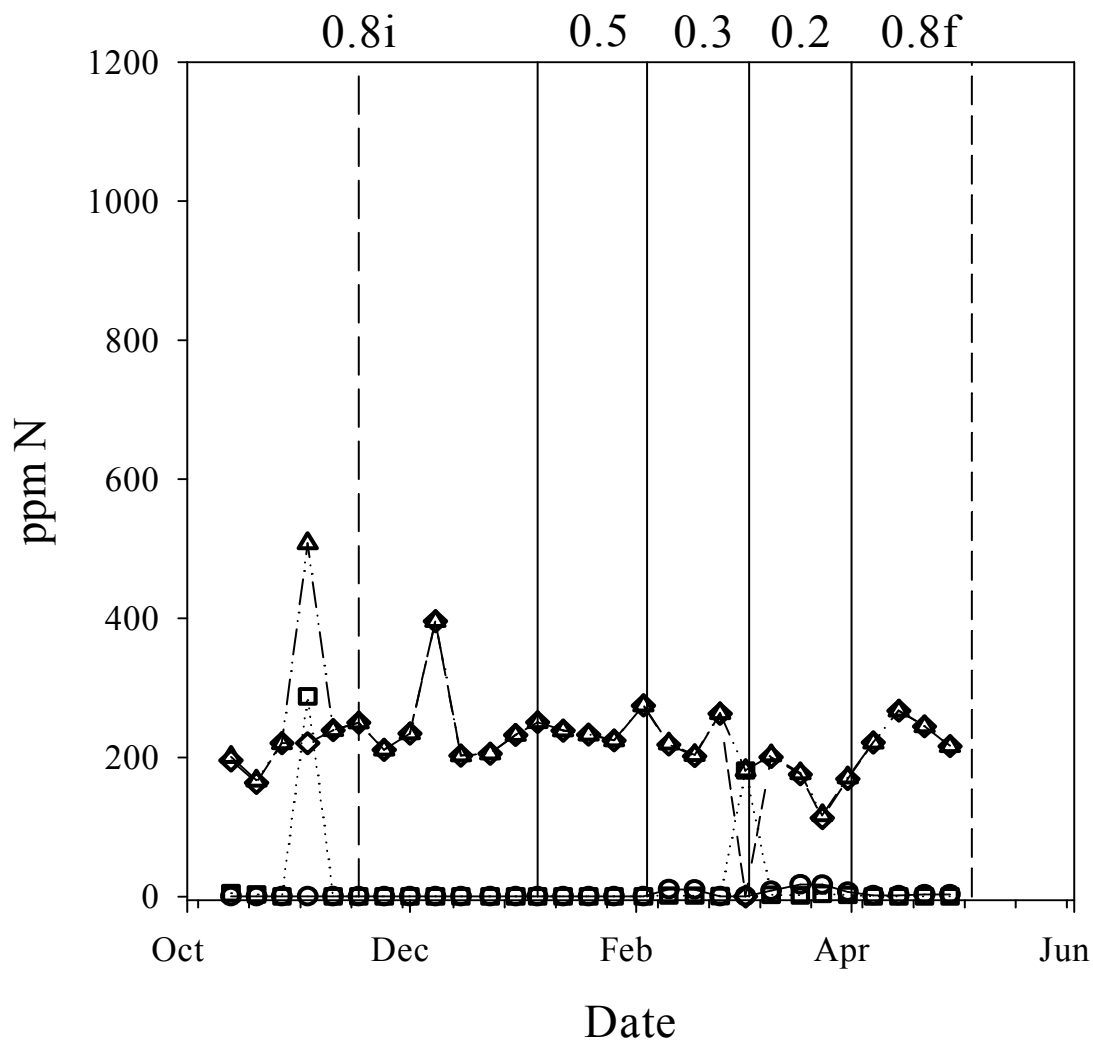
Fig. 3.35 – Concentration data including summation of NO_2^- and NO_3^- (open grey triangle), NO_3^- (red cross) NO_2^- (open green square) and NH_4^+ (open blue circle) for the Low-N trickling treatment. Hydraulic regime is depicted across the top of each graph. Trickling regimes are in units of trickling min $(0.25$ hr$)^{-1}$ and are depicted across the top of the graph. The initial and final 0.8 min $(0.25$ hr$)^{-1}$ treatments are distinguished by an i and an f respectively. Solid vertical bars represent a change in hydraulic regime and dashed vertical bars represent the initial and final sampling events.
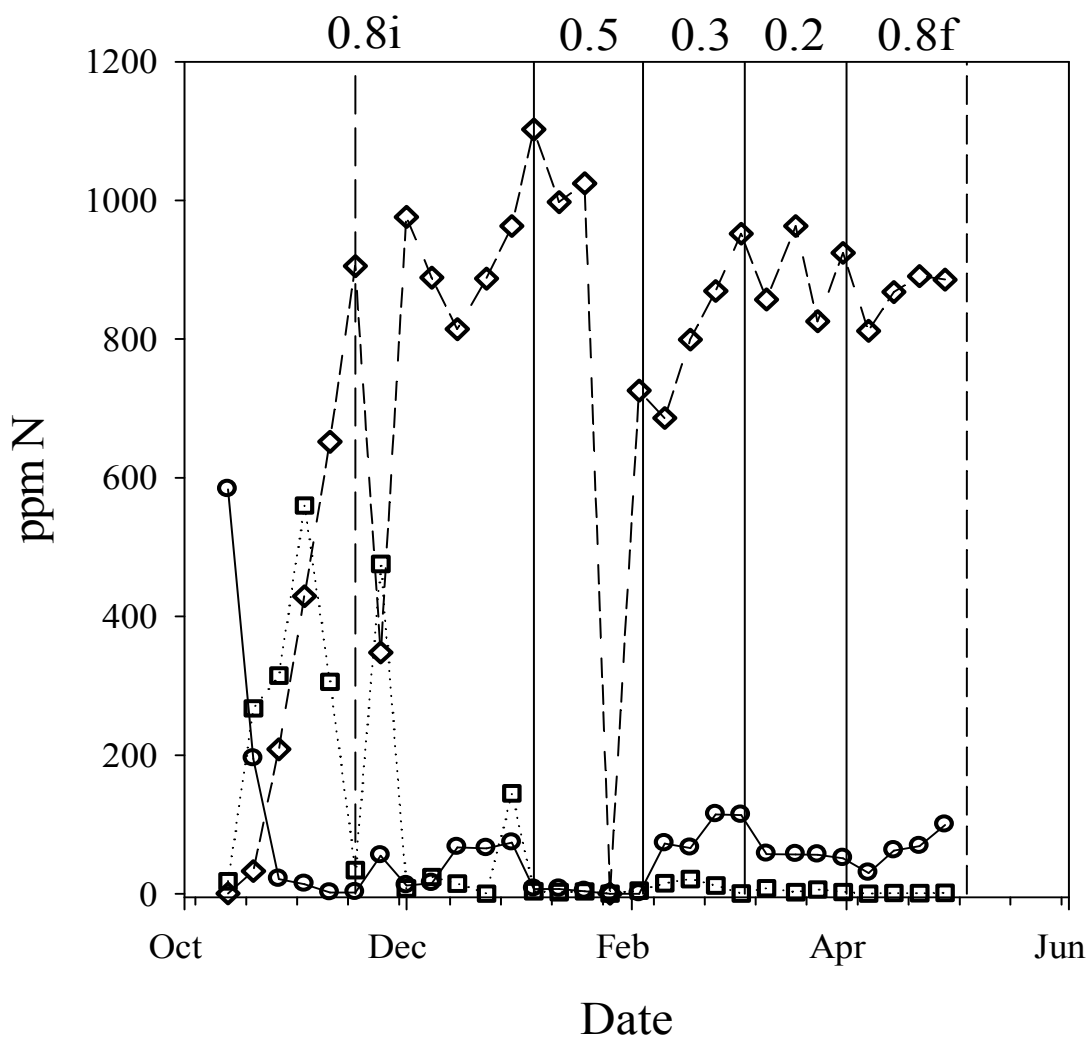
Fig. 3.36 – Concentration data including summation of NO_2^- and NO_3^- (triangle), NO_3^- (diamond) NO_2^- (square) and NH_4^+ (circle) for the High-N trickling treatment. Trickling duration is presented across the top of the graph as min $(0.25 \text{ hr})^{-1}$ and the initial and final 0.8 min $(0.25 \text{ hr})^{-1}$ are distinguished by an i and an f, respectively. A solid vertical bar represents a change in hydraulic regime and dashed vertical bars represent the initial and final sampling events.

3.2   **Denitrifier Abundance Study**

Samples from the Cobb Mill Creek experimental hill slope were analyzed for denitrifier

abundance, denitrifier activity, nitrate concentration, and organic matter. Vertical

profiles of NO_3^- showed a steady decline in NO_3^- –N concentration, from 12.1 ppm NO_3^-

N at 30 cm depth, to 1.0 ppm NO_3^- N at 2 cm depth (Fig. 3.37). Also, organic matter

peaked at 4% 20 cm below the sediment-water interface (Fig. 3.38). Denitrifier (DNF)

abundance values were reasonably constant for the first 30 cm below the sediment water

interface. The average DNF abundance in the first 30 cm was 4.2 x 10^5 cells (g

sediment)$^{-1}$. The abundance of DNF then declined to an average of 1.5 cells (g

sediment)$^{-1}$ (Fig. 3.39). Denitrifier abundances are compared with activity from

Galavotti, (2004), (Fig. 3.40)
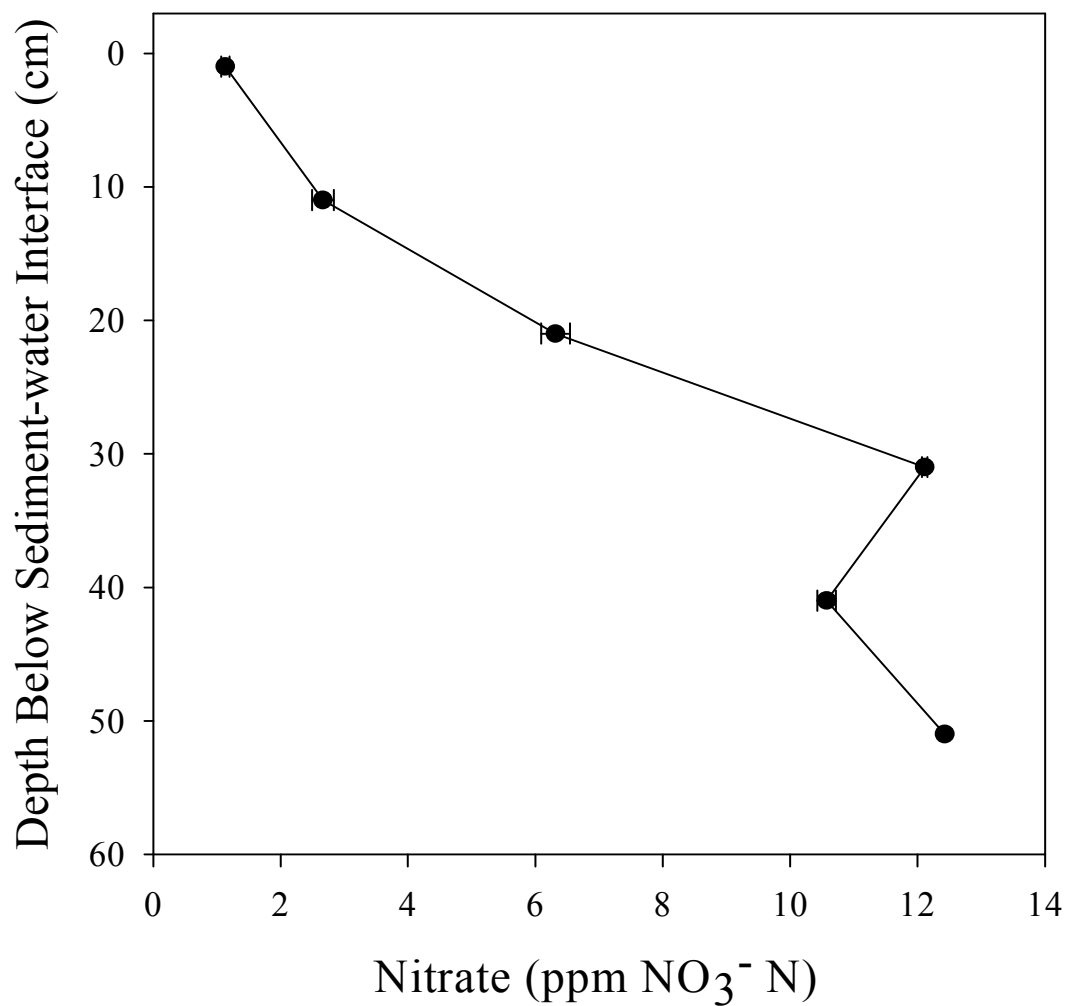
Fig. 3.37 – A vertical profile of the average NO$_3^-$ concentration in Cobb Mill Creek (Galivotti 2004). Error bars represent standard error of 9 pore-water samples collected from sampling portals along 9 replicate cores.
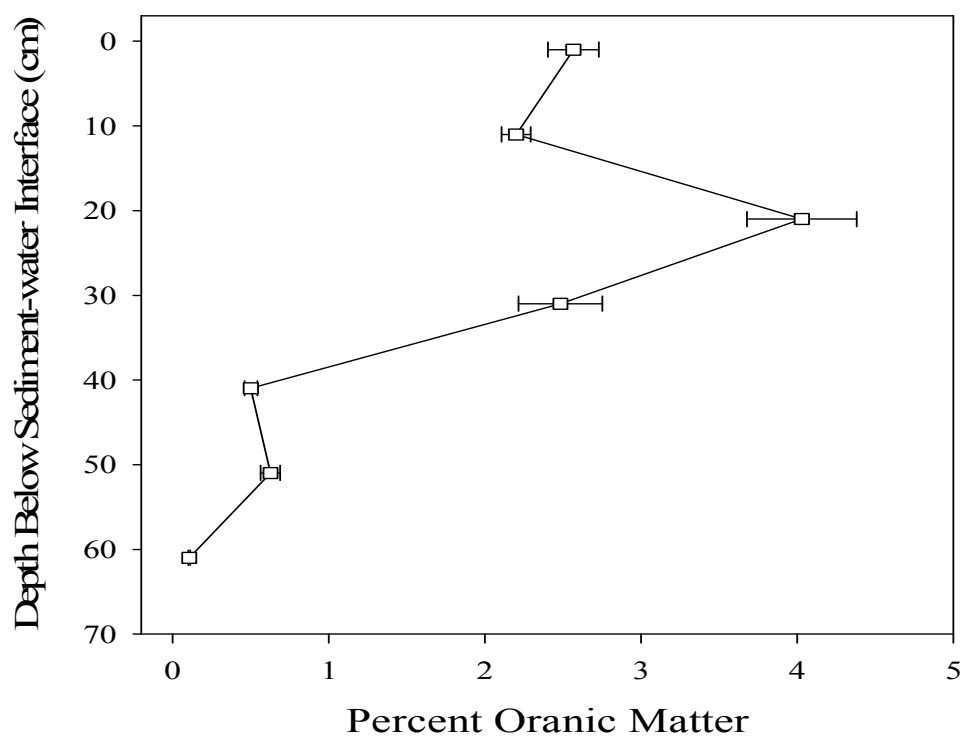
Fig. 3.38 – The average organic matter (OM) content to a depth of 70 cm in Cobb Mill Creek, taken from Galivotti (2004), with error bars representing standard error of the mean (n = 8, for each depth).
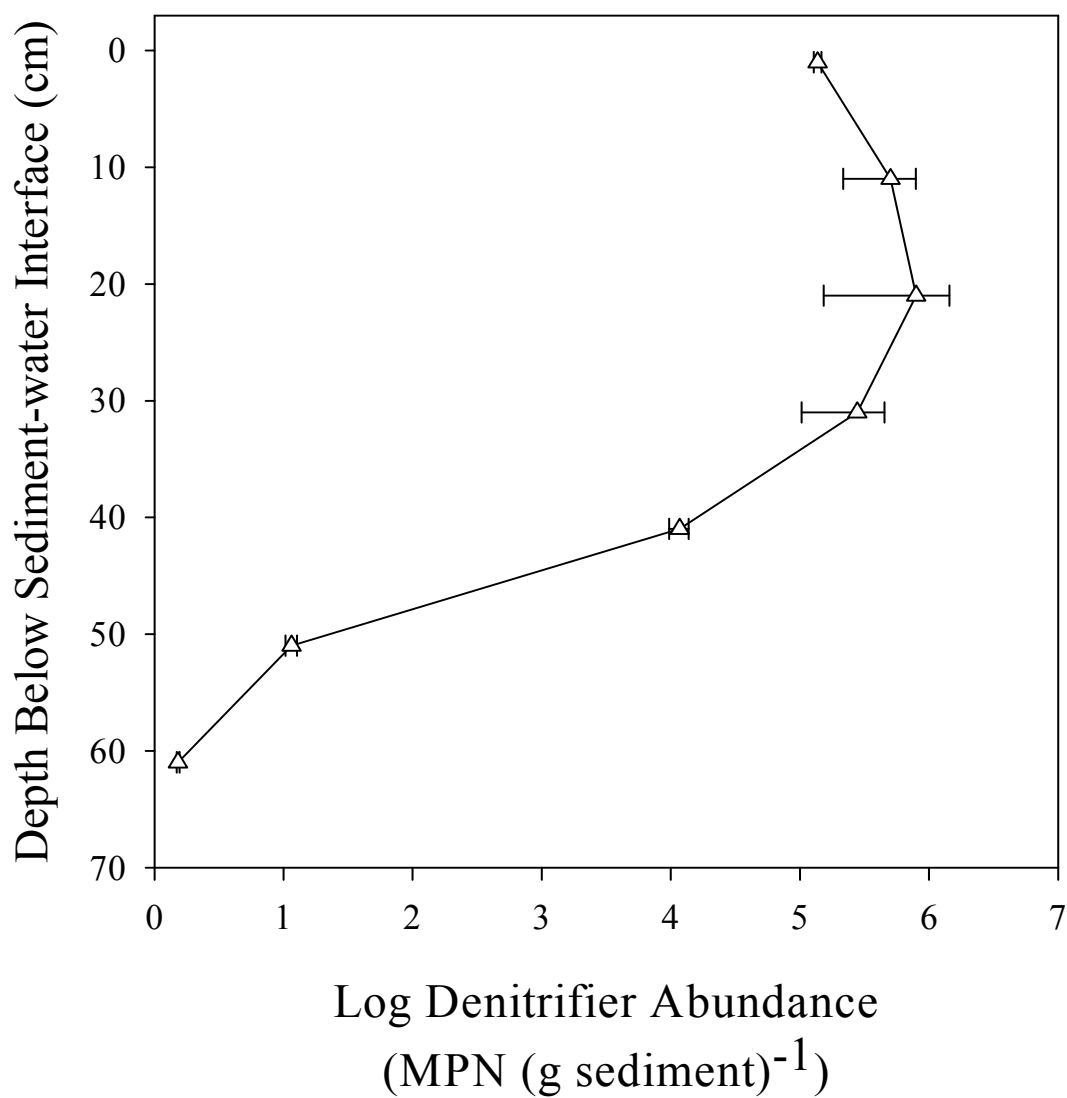
Fig. 3.39 – Denitrifier abundance values for 7 points along a depth gradient, as determined by most probable number (MPN), averaged from 8 sediment cores. Errors bars represent standard error of the mean based on averages of a sample taken from each of the 8 sediment cores.
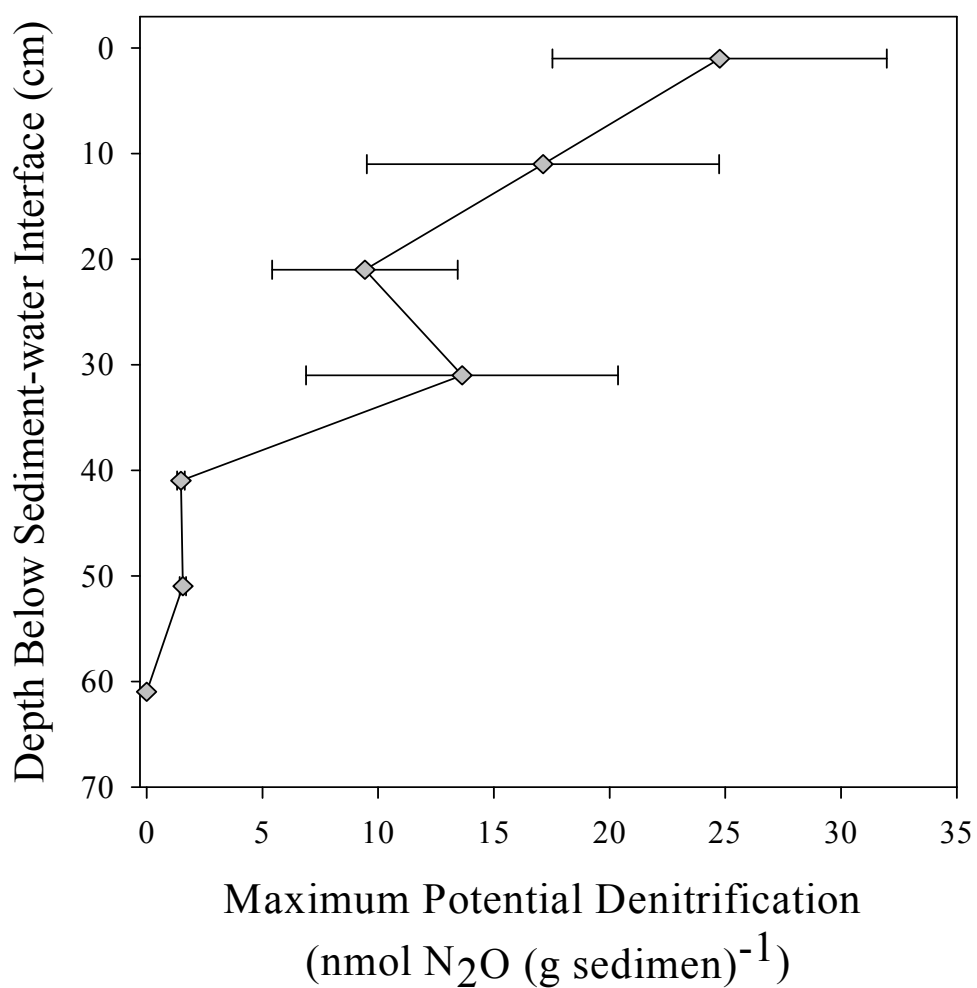
Fig. 3.40 – Maximum potential denitrification values determined for each depth by averaging sub-samples from 8 sediment cores taken from Cobb Mill Creek (Galivotti 2004). Error bars represent standard error of the mean from portals along the 8 sediment cores.

4. **Discussion**

4.1 **Microbial Abundance & Distribution**

Microbial distribution profiles showed variation between Tidal- and Trickling-flow types and appeared responsive to changes in both tidal and trickling regimes. In addition, water chemistry data suggests there are changes in microbial activity associated with changes in hydraulic regime. Integrated abundance values (Fig. 3.11) illustrate abundance changes in each of the four microbial groups in relation to changes in tidal cycling. There is a clear decline in abundance associated with a decline in tidal frequency. The observed decline is likely related to reduced oxygen availability, and therefore a reduction in energy yield, and a subsequent reduction in microbial abundance and activity. Integrated abundances from the Trickling-flow columns show a similar relationship to decreases in trickling duration (Fig. 3.27). In both Trickling and Tidal High-N systems there is a minimum abundance associated with a minimum in water recirculation volume (12 L day^{-1} ≈ 4 cycles day^{-1} ≈ 0.2-min (0.25 hr)$^{-1}$).

Abundance in similar systems (Fig 4.1) shows that systems with excess Nr and O$_2$, combined with low or no organic matter, such as the water waste stream seen on the International Space Station, or in sequencing batch reactors used to enrich for nitrifiers, produce microbial communities primarily composed of nitrifiers (Smith et al. 2008, Ward et al. 2011). For example, the nitrifying sequencing batch reactor (SBR) studied by Hao, et al. (2009), had no organic matter additions, whereas the tidal and trickling systems had a relatively high organic matter load expressed as COD. The COD load in all treatment types was 1.71 g COD d^{-1}, mimicking and influent concentration of 0.24 g COD L^{-1}. The variation in COD load is likely responsible for the difference in nitrifier abundance.
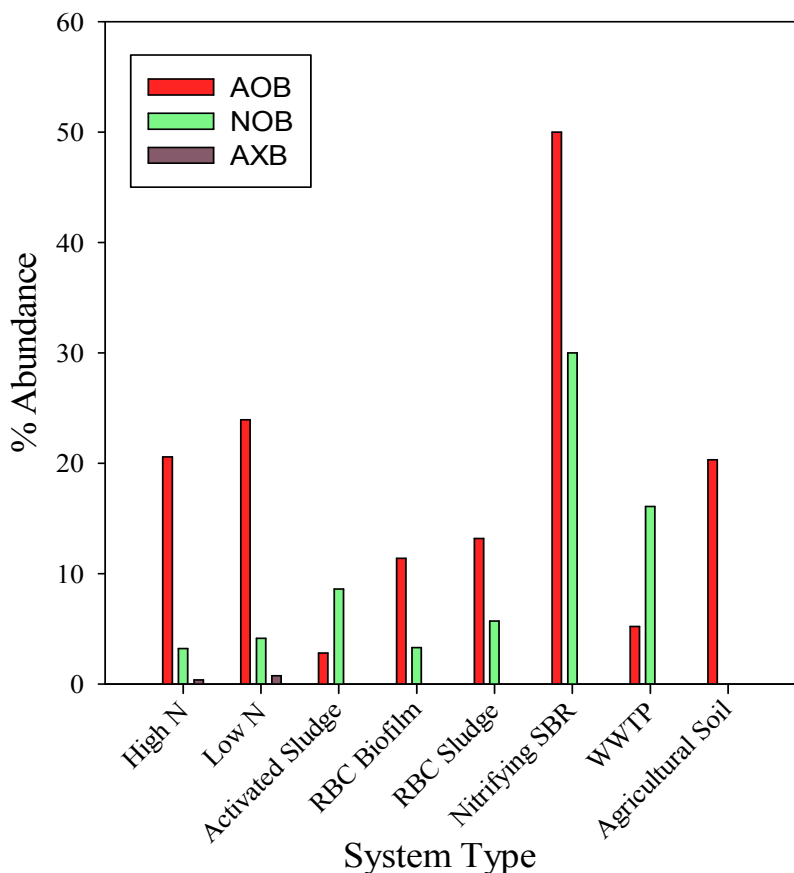
4.1 – Abundances of ammonia oxidizing bacteria (AOB), nitrite oxidizing bacteria (NOB) and anaerobic ammonia oxidizing bacteria (AXB), averaged from all 5 tidal regimes for the High- and Low-N treatments, as well as other microbial systems, expressed as percentages of the total microbial community, for comparison. Activated sludge samples from a partial nitrification reactor were analyzed using an abundance modeling technique (Ye and Zhang 2011). Rotating biological contactor (RBC) sludge and biofilm abundances of AOB were determined by fluorescent *in situ* hybridization (FISH) using the NSO190 probe for AOB, and the NSR1156 for NOB (You et al. 2003). The nitrifying sequencing batch reactor (SBR) was designed to enrich for nitrifiers, that were identified by FISH with probes NSO1225 for AOB and probes NIT3 and NTSPA662 for NOB (Hao et al. 2009). Wastewater treatment plant (WWTP) samples were from single stage reactor and abundances of NOB, total bacteria and AOB were determined by qPCR for the 16s rRNA gene and *amoA* gene (Harms et al. 2003). Agricultural soils were assessed for total abundance and ammonia oxidizing bacterial abundance using qPCR for 16s rRNA gene and *amoA* gene. The NOB abundance was not determined in the agricultural soil (Kong et al. 2010).

While the microbial biomass in the SBR studied by Hao, et al., (2009) was primarily

nitrifiers, the microbial biomass inside the tidal treatment system was approximately 30%

nitrifiers. The COD concentration used in the Tidal- and Trickling-flow study was low

for conventional piggery waste, but average for conventional municipal sewage. The

COD for municipal sewage ranges from 0.19–0.34 mg L^{-1}(Abou-Elela and Hellal 2012).

In comparison, Boursier et al., (2005) found piggery waste stream COD concentrations

ranging from 20–50 g COD L^{-1}. While the treatment systems established by Worrell

Water are low in organic matter compared to fully functional piggeries, they are still high

in organic matter compared to systems commonly used to enrich for nitrifiers or

anammox. Systems that enrich for anammox characteristically have NH_4^+ and NO_2^-

available in a stable anaerobic environment with low organic carbon. In contrast, the

Tidal and Trickling systems had a high organic matter load relative to nitrifying or

anammox enriching reactors, and were continually experiencing perturbation, including

complete saturation with O_2, all of which likely discouraged anammox from proliferating.

The anammox process has also been documented as experiencing a 50% reduction in

activity under NH_3 concentrations of 38 ppm NH_3 –N (Fernandez et al. 2012) while

Waki, et al. (2009), found concentrations as low as 10.7 ppm NH_3-N could be toxic to

AXB. The variation in NH_3 tolerance has been attributed to acclimatization or

differences in other environmental parameters resulting in synergistic inhibition. In both

the Tidal- and Trickling-flow systems there were multiple instances where NH_3

concentrations calculated from total NH_4^+ concentrations and pH, were above the

reported inhibitory concentrations. Further, most CANON or SHARON processors need

tight control of O_2 to ensure the AOB utilize the O_2 completely. Sonde data, collected

from the reactors' reservoirs suggests that heterotrophic activity was not sufficient to remove the O_2. Similarly, the Trickling-flow columns never express complete N removal, suggesting there was too much oxygen, or not enough organic matter, to stimulate denitrification. Denitrifiers are facultative anaerobes and likely present even if denitrification is not occurring (Atlas and Bartha 1998). Similar effects were observed at Cobb Mill Creek (Fig. 3.35 & 3.36) where denitrification potential maximums and denitrifier abundance were greatest between 0 cm below the sediment-water interface, and a depth of approximately 30 cm below the sediment-water interface. Immediately below the sediment-water interface, the sediment is likely fully oxygenated due to turbulent flow. Despite oxygenation, potential denitrification maximums, measured in anaerobic incubations, and DNF abundance measurements, were near their maxima at the sediment-water interface: likely the result of facultative anaerobiosis. In rice paddy soils, Chen et al., (2010) found the average abundance of DNF to be 4.8×10^6 gene copies g^{-1} of untreated soil. Abundance of DNF was increased to 0.85×10^7, 0.996×10^7, and 1.8×10^7 gene copies g^{-1} soil in treatment plots receiving, N; N, phosphorous and potassium (NPK); or organic matter and NPK additions respectively. The rice paddy soils exhibited similar behavior to what was observed in Cobb Mill Creek; sediments or soils with increased organic matter, and available nitrogen had increased DNF abundance. Of particular importance is the agreement in treatment effect. Despite differing techniques for DNF enumeration, the MPN PCR technique amplifying a *nosZ* gene fragment with primers nos661F and nos1771R, as a denitrifier indicator employed at Cobb Mill Creek, and the *nosZ* qPCR using primers nosZ1126qF1 and 1381R, both showed organic matter and available NO_3^- to be controlling factors for denitrifier distribution. Sediments from

20 different Rocky Mountain lakes analyzed for DNF by culture based MPN found an average abundance of 3.8 x 10^4 cells (g sediment dry weight) $^{-1}$(McCrackin and Elser 2012). While this number is low in comparison to the organic matter rich regions of Cobb Mill Creek sediment, which had an average abundance of 4.2 x 10^5 cells (g sediment)$^{-1}$, this is not unexpected as preliminary culture based MPN data from Cobb Mill Creek also produced low denitrifier abundance data. The low abundance values generated from culture based MPN analysis was a partial motivation for the use of molecular genetics techniques to overcome the limitation of culture based techniques. In addition, the lake sediments had a mean organic matter content of 0.14%, while the vertical profiles of Cobb Mill Creek had a mean organic matter content of 1.7%, and there was a peak in average organic matter content of 4% at depth of 21 cm. As organic matter enriches for DNF by facilitating heterotrophic metabolism, and therefore O_2 consumption, to create an anoxic environment for denitrification, the observed difference in abundance was expected. Deeper sediments in Cobb Mill Creek with less organic matter have substantially fewer DNF present (Fig. 3.38). Johnson et al, (2012) used *nosZ* qPCR to enumerate DNF and found denitrifier abundance in Sugar Creek sediments to be 1.2 x 10^7 gene copies (g sediment)$^{-1}$. The increase in abundance was likely due to increased sensitivity of the qPCR technique when compared with the MPN PCR technique. Henderson, et al., (2010) also found DNF on the order of 10^7 gene copies g^{-1} soil using qPCR for the *nosZ* gene. A consistent finding among all studies was the prevalence of DNF in environments with substantial organic matter and available NO_3^-. As the Tidal and Trickling-flow columns provided both organic matter and NO_3^-, we suspected there would be wide spread denitrification, which chemical data (Fig. 3.12–3.16; 3.28–3.35)

confirms by showing the removal of NO_3^-. Abundance data and chemical data do not support the hypothesis that AXB are responsible for a significant portion of NO_3^- removal. Abundance of AXB was less than 1% of the total microbial population in any of the treatments and chemical data and fluctuations suggest the treatment columns were not an environment that would be expected to enrich for AXB.

Microbial distributions in the Tidal- and Trickling-flow columns showed variation in abundance along vertical profiles associated with changes in hydraulic regime; both the shape of the profile, and the overall abundance, appear connected to column hydraulics. For example, in Fig. 3.1 the Low-N, Tidal-flow column exhibited an increase in NOB abundance at the third and fourth sampling portals and an increase in AXB at the second sampling portal at the onset of the experiment, i.e., the 24i-Tidal cycling regime. By the time the Low-N column had been decreased to the 8-cycles day^{-1} Tidal treatment, the distribution of functional groups along the vertical profile exhibited change. There was a decline in NOB abundance at the second sampling portal, the AXB abundance had a less pronounced peak at the second sampling portal, and the AOB abundance was more uniform along the vertical profile (Fig. 3.3). Similar effects were seen in the High-N and Trickling-flow columns. At the onset of the experiment, under the 24i-cycles day^{-1} treatment, the High-N, tidal column had a peak in abundance at the third sampling portal in AOB and NOB and an abundance peak in TAB at the fourth sampling portal (Fig. 3.6), but at the conclusion of the 8-cycles day^{-1} treatment, there was no peak in abundance in AOB, or TAB, while the NOB abundance declined at the second sampling portal (Fig. 3.8). In addition, reduced Tidal-cycling frequencies appeared to result in reduced microbial abundances (Fig. 3.11). The Low-N treatment also appeared

to have reduced microbial abundance compared to the Tidal, High-N treatment, suggesting the Tidal, Low-N column was N limited. In the High-N tidal treatment, the integrated abundance values declined in association with reduced cycling frequency, and there was a slight increase in abundance when the Tidal-cycling frequency was returned to 24-cycles day^{-1} (Fig. 3.11). The declining trend associated with reduced cycling frequency was not as apparent in the Low-N treatment. In the Low-N treatment, there was not a strong variation in the TAB associated with changes in tidal cycling; however, AOB, NOB and AXB vary between tidal-cycling treatments. The absence of an abundance trend associated with tidal-cycling frequency in the Low-N Tidal treatment suggests that the tidal regime was not controlling environmental factors limiting microbial growth. Since the High-N treatment had greater microbial abundance compared to the Low-N treatment, it is possible that the Low-N treatment is N limited. In the Low-N tidal treatment, the NH_4^+, NO_2^-, and NO_3^- concentrations remained consistently low, except for peaks in NO_3^- during the 24i- and 16- cycles day^1 treatments, throughout the duration of the experiment, suggesting that N was being completely, or almost completely, utilized by bacteria (Fig. 3.12–3.14).

In the Trickling-flow columns, the vertical distribution pattern was different than patterns observed in the Tidal-flow columns. Whereas the Tidal-flow columns were likely to show a peak in functional group abundance at one of the sampling portals in the center of the column, or a broad peak across two sampling portals (e.g. AOB in Fig. 3.2 & Fig. 3.5), the profiles of functional group abundances in the Trickling-flow columns were likely to peak at the first sampling portal, at the top of the column, and slowly decline with column depth (e.g. all functional groups in Fig. 3.19). The water chemistry

data for the trickling-flow columns shows reasonably consistent removal of NH_4^+ and

NO_2^-, but poor removal of NO_3^-, which remained elevated throughout the entire

experiment at approximately 900 ppm NO_3^-–N in the High-N treatment, and 200 ppm

NO_3^-–N in the Low-N treatment. The accumulation of NO_3^- was likely due to

perturbation every 14 min resulting in near complete oxygenation of the bulk fluid;

thereby, preventing adequate denitrification from occurring, but encouraging complete

nitrification to NO_3^-. The consistency in net process effect between the different trickling

treatments is likely due to the trickling process occurring every 14 minutes resulting in

complete aeration irrespective of the trickling duration, which ranged from 0.2–0.8 min.

In addition, the trickling columns did not provide a uniform wetting front. When samples

were collected, the extracted LESA was often dry to the touch suggesting that the entire

reactor was not uniformly covered by the trickling fluid; therefore, the trickle reactors

were likely not utilizing all of the space available for microbial activity. The uneven

wetting front could also be responsible for the reduced biomass detected in the trickling-

flow columns. As water is the carrier for C and N compounds, uneven wetting would

result in uneven resource distribution. In addition, the LESA could potentially strip NH_4^+

from the bulk fluid resulting in nitrogen limitation in the bottom of the trickling-flow

columns. There were multiple examples of a decline in abundance along the vertical

profile of the Trickling-flow column (e. g., Fig. 3.19) which could be a response to

reduced N availability.

      The distribution and activity of microorganisms within the tidal and trickling

columns are examples of the Goldilocks Principle, which, in this case, is largely a

restatement of niche theory. The Goldilocks Principle, which leads to a consideration of

Goldilocks Zones, in which conditions are "just right," applies at all scales of life. The

Goldilocks principal states that there is a range within the environment that is most

hospitable to some suite of life forms (Martin 2011). Niche theory, in comparison, states

that an organism best suited to an environment will excel in that environment and

outcompete other organisms for resources (Prosser 2012). In this study the Goldilocks

Zone, or the idealized niche of AOB, NOB and AXB, was studied by examining the

vertical profiles in the different reactor treatments and assessing net system processes by

interpreting the N-compound concentration data. The peaks in abundance represent

locations where conditions were just right to encourage the proliferation of TAB, AOB,

NOB or AXB.

Microorganisms are special in ecosystems with respect to the variety of scales on

which they can be studied. While the organisms themselves are miniscule, the processes

they mediate occur at scales ranging from fractions of mm to km. Thus, microbes can be

studied at the microscale, within biofilms, they can be examined at field scales in an

effort to determine how microbial distribution relates to the distribution of microbially

driven processes across a landscape, or they can even be studied on a planetary scale by

researchers searching for extraterrestrial life on other planets or even outside our galaxy.

On a planetary scale, the habitable range is usually related to a planet's age and

distance from the nearest sun-like star, which are the major factors controlling surface

conditions. For example Gliese 581g is suspected to fall within the habitable zone based

on its distance from the central star, which results in its high percentage of water cover

(von Bloh et al. 2011). The Goldilocks Zone can also be explored on a temporal scale.

Since time of the big bang, the number of planets residing in the Goldilocks Zone has

likely declined due to changes in planetary geochemistry which diminish crystallized CO_2 in the atmosphere. The crystallized CO_2 is necessary for screening ultra-violet light during the initial stages of life (Franck et al. 2007). It is interesting to note that even on a planetary scale, geochemical changes can impact the propensity of a planet to support life, be it microbial or otherwise. Gliese 581g is not only the correct distance from its central star, but also of the correct age to support life, thus it falls in the Goldilocks Zone both temporally and spatially.

In contrast, on a microscale, Zhang et al. (2011) studied the effects of antibiotic stress on microbes colonizing a microarray chip (Fig. 4.1). A microarray chip has 1200 hexagonal wells that are 200 µm on each side. The wells were 10 µm deep and interconnected by slits along each side. A wild-type *Escherichia coli*, with no antibiotic resistance, was used to inoculate the center of the chip. The strain of E. coli would quickly develop antibiotic resistance and the resistant strain would proliferate in regions of the microarray chip where the highest concentration of antibiotic was present. An antibiotic gradient was established inside the microarray by passing nutrient broth with no antibiotic across one end of the chip and a nutrient broth containing an antibiotic across the other end of the chip. In this system, the antibiotic was the environmental stressor to which a strain of *E. coli* was adapting.
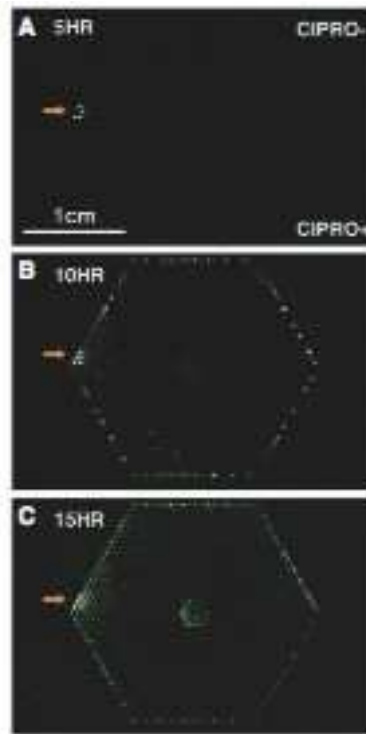
Fig. 4.1 – Taken from Zhang, et al., (2011), a microchip undergoing colonization by *Escherichia coli.* The *E. coli* are developing resistance to ciprofloxin dissolved in the nutrient broth entering the wells of the chip from the bottom edge of the microarray. Bacteria colonizing wells highlighted by a red arrow are rapidly multiplying at the Goldilocks point were bacteria that have recently developed antibiotic resistance are outcompeting wild-type bacteria for nutrients carried in the liquid broth.

The point where resistant cells would begin their colonies was referred to as the "Goldilocks point." Proliferation of antibiotic resistant bacteria is an example of microscale competition by bacteria. It is likely that this kind of competition is occurring within the biological reactors studied in this experiment, only in place of environmental stress induced by antibiotic, the microorganisms are facing competition for dissolved oxygen and other resources such as NO_2^-, or stress induced by high NH_3 concentrations or other environmental factors.

On a microscale, dissolved oxygen still plays a critical role in the distribution and activity of nitrifying bacteria (Aoi et al. 2004). Biofilms developed on small cement balls (0.2-mm diameter) in a fluidized bed reactor showed an increase in AOB near the biofilm surface when dissolved oxygen was increased in the system through aeration of the bulk media. This is both an example of the Goldilocks Zone and an example of how important a role dissolved oxygen plays in defining the Goldilocks Zone for nitrifying bacteria. Dissolved oxygen in the tidal columns can be increased by more frequent tidal cycles which results in increased aeration. As seen in Fig. 3.11, increased tidal cycling frequencies result in greater abundances of nitrifying bacteria, both at the beginning, and end of the experiment. Similarly, Schramm, et al., (2003) found that in a nitrifying biofilm, AOB existed predominantly at the exterior perimeter of a bound biofilm with NOB residing in a subsurface layer. Small numbers of heterotrophic bacteria were interspersed in the deeper layers of the biofilm. Shramm, et al., (2003) also noted that AOB greatly outnumbered NOB. In both these experiments, O_2 availability was limited by diffusion through the biofilm. As ammonia oxidation is the rate limiting step in nitrification, and is more oxygen intensive, it is likely that competition for O_2 is driving

biofilm organization and activity. Microscale distributions found by both Schramm, et al.

(1999), and Aoi, et al. (2004), demonstrated that AOB were better able to compete for O_2

than NOB by the increased abundance of AOB both in the biofilm overall, and in

particular, along the surface layers of the biofilm where O_2 is most abundant. Likewise,

in both the tidal and intermittent trickling treatments, where AOB outnumber NOB in all

treatment types (Fig. 3.11 & 3.27), the AOB are suspected to be the rate limiting step in

nitrification. As the Tidal- and Trickling-flow columns were both frequently aerated it

appears that denitrification was limiting N removal. However, had the system been

allowed to remain at 8-cycles day^{-1} or 4-cycles day^{-1} for a prolonged period of time, it is

likely we would have seen NH_4^+ conversion to NO_2^- become the rate limiting step. The

High-N treatment had considerable variation in NO_2^- concentration over the duration of

the experiment (Fig. 3.13). By following trends in concentrations of NH_4^+ and NO_2^-, it

appears likely that AOB are impacting the NO_2^- concentration, and not the activity of

NOB. In the tidal High-N column, increases in NO_2^- were always accompanied by

decreases in NH_4^+ concentration. If process rates of NOB were changing then

simultaneous changes in NH_4^+ concentration would not be expected. This interpretation

is supported by a long line of research showing that NH_4^+ oxidation is the rate limiting

step in nitrification (Grady et al. 1999, Henze et al. 1987). However, additional research

has shown that NO_2^- oxidation can limit the overall nitrification process when NH_4^+–N

concentration exceeds 62 ppm (Chandran and Smets 2000). While AOB activity is more

likely to be rate limiting, considering the reactors received daily N inputs, but reservoir

grab samples were collected weekly, there is a high likelihood that observed changes in

concentration may not fully reflect the overall activity of the microorganisms. The

temporal conundrum of weekly sampling and daily N additions also affected interpretation of N-concentration data in the Trickling-flow columns in a similar way.

In the case of nitrifiers, dissolved oxygen is often a limiting reagent (Kampschreur et al. 2008a, Ward et al. 2011). Nitrifiers are slow growing organisms often unable to compete with aerobic heterotrophs (Ward et al. 2011). As such, dissolved oxygen and nutrient distribution were most likely responsible for the observed patterns of nitrifier abundance in the tidal columns. In the Trickling-flow columns nutrient distribution probably played a larger role due to the uneven wetting front providing uneven nutrient distribution, and the frequent perturbation providing frequent replenishment of dissolved oxygen.

The Tidal columns were likely controlled by the availability of dissolved oxygen because the tidal columns were uniformly saturated but dissolved oxygen was likely depleted due to diffusion limitation. The differences seen in the microbial abundance profiles in the Tidal-flow columns, as compared to the Trickling-flow columns (Fig. 3.1–3.10, & 3.17–3.26), suggests that different factors control the distribution of microbes in the two treatments. Field-scale studies in waste-water reservoirs have likewise found that dissolved oxygen plays a role in controlling nitrifier abundance and activity. Environments with large amounts of available carbon and nitrogen are hypertrophic and while these environments were found to sustain nitrifiers, they did not yield appreciable nitrification. Concentrations of dissolved O_2 as low as 0.05 mg L^{-1} were capable of supporting nitrification in domestic waste waters (Abeliovich 1987). Low oxygen concentrations that enable the nitrifier population to persist, but not conduct appreciable nitrification may be a problem for both N removal and for the production of N_2O.

Although we know nitrifiers are present throughout the reactor we do not know that they are all conducting nitrification at the same rate.

Frequent tidal cycling will likely increase the availability of oxygen, making aerobic processes, such as nitrification, more favorable, but can prohibit denitrification by preventing extended anaerobic phases. Conversely, extended fill phases would likely encourage denitrification, but would also likely discourage nitrification. A low dissolved oxygen content can stress nitrifying bacteria resulting in diminished nitrification and increased nitrifier-denitrification which often produces N_2O, a potent greenhouse gas (Kampschreur et al. 2008b). Nitrifier-denitrification occurs when an ammonium oxidizing bacteria use NO_2^- in place of oxygen as an electron acceptor for the oxidation of ammonium and the NO_2^- –N is reduced to N_2 using the enzyme pathway of denitrifiers (Poth and Focht 1985). While nitrifier-denitrification is the oxidation of ammonium under anaerobic conditions, it is a completely different biochemical pathway than anammox and is referred to as either nitrifier-denitrification or oxygen-limited autotrophic nitrification-denitrification (OLAND) (Kuai and Verstraete 1998). Given that OLAND occurs under oxidative stress and is more likely to produce N_2O than regular denitrification or nitrification, there is a likelihood of N_2O production in the tidal columns. Considering we see the Goldilocks Principle at play, in that nitrifiers were at a maximum in in selected areas of the column (Fig. 3.1, 3.3–3.10; 3.17, 3.19–3.22, 3.24, & 3.26), not only are peaks in abundance observed where conditions are primed for nitrification, but there are a larger number of bacteria present at suboptimal conditions where OLAND, and therefore N_2O production are likely to occur. For example, in Fig. 3.6 we see 1.1×10^{10} AOB (g LESA)$^{-1}$ at portal 3, which when integrated represents 3.2 x

10^{13} AOB in the third segment of the High-N, Tidal-flow column. However, there are

2.8 x 10^{13} AOB existing in the rest of the column, under what are likely suboptimal

conditions. Given that temporal juxtaposition of anaerobic and microaerophilic phases

with aerobic phases in a single chamber, the potential for nitrifier denitrification is high.

Denitrification is also less likely to reduce N_2O to N_2 gas in the presence of excess nitrate

(Mosier et al. 2002). In all treatments there was consistently excess NO_3^- (Fig. 3.14 &

2.28). Therefore, both denitrifiers and nitrifiers are likely to produce N_2O gas. As N_2O is

a greenhouse gas, and the tidal treatment systems will likely be part of "green

architecture," or part of a Leadership in Energy and Environmental Design (LEEDS, for

more information please see: http://www.usgbc.org/) certification step, it makes sense that

greenhouse gas production (i.e., N_2O) in the system should be assessed.

4.2 Thermodynamic Ecosystem Controls

Microorganisms are often distributed zonally in nature, and the size and location of those zones, especially with respect to other organisms and their processes are controlled by thermodynamic properties of the metabolic reactions carried out by the individual functional groups of microbes. In both the Tidal- and Trickling-flow columns examined in this study, the numbers of the various bacteria examined followed a logical thermodynamic sequence. The total abundance of bacteria (TAB) was always substantially larger than any of the others enumerated. TAB comprised any heterotrophs living in the reactors (including denitrifiers), as well as the N-oxidizing organisms that were also enumerated. The AOB, NOB, and AXB are autotrophic organisms that subsist on lithotrophic metabolism which yields significantly less energy per mole of reducing agent than heterotrophic metabolism, especially aerobic heterotrophy. The AOB were always more abundant than NOB (Fig. 3.11 & 3.27), and this has a clear connection to metabolic energetics. The oxidation of ammonia yields over 3 times more energy than the oxidation of nitrite (-275 kJ mole^{-1} *vs.* -74 kJ mole^{-1}). In addition to this energetic advantage, the NOB require the NO_2^- produced by the oxidation of NH_4^+. As a result, AOB have a greater abundance than NOB. In another study of spatial arrangement of these organisms (AOB and NOB) in biofilms, AOB are found on the surface of the biofilm, in close proximity to the NH_4^+ and O_2 in the bulk liquid, while the NOB inhabit the interior region and use the NO_2^- formed by the AOB and whatever O_2 is not consumed by the ammonia oxidizers (Schramm et al. 2000). The observed profile is likely the result not only of bacterial succession, where AOB are the first to colonize, but also a competitive advantage of AOB resulting from the increased energy yield per mole

of N oxidized allowing the AOB to remain on the surface of the biofilm where O_2 is plentiful.

Such zonal distributions are commonly seen in aquifers and sediments when O_2 is depleted (by aerobic heterotrophs or aerobic autotrophs). Organic matter breakdown continues under anaerobic conditions, albeit more slowly. The bacteria carrying out the decomposition reactions utilize a variety of different electron acceptor as oxidizing agents, and the functional groups often separate spatially into zones that are ordered based on the energy yield of the reaction that employs a specific electron acceptor. The order is often referred to as a "redox cascade," although there is nothing passed from one guild to the next. Rather, each successive guild lives on the organic remnants not decomposed by the previous guild. Each successive guild utilizes a different terminal electron acceptor, and the order of sequence depends almost entirely on the ΔG of the oxidation reaction using the specific electron acceptor. For example, in a landfill leachate plume through an adjacent aquifer the availability of electron acceptor results in zonation of redox processes vertical and horizontal gradients(Lyngkilde and Christensen 1992). Lensing, et al (1994) found similar redox based stratification of microbial processes in a diffusion limited aquifer system. Thus, the typical ordering of anaerobic processes, often in highly discreet zones at increasing depths (distance from the oxic-anoxic interface in sediments or stratified waters) is denitrification, followed by either iron or manganese reduction, or both, followed by sulfate reduction. Often, in the absence of available sulfate, methanogenesis, in which CO_2 or acetate is the terminal electron acceptor, replaces sulfate reduction in the redox cascade (Atlas and Bartha 1998, Madigan et al. 2000). This is often the case in freshwater wetlands, such as those studied by Neubauer,

et al. (Neubauer and Craft 2009, Neubauer et al. 2002, Neubauer et al. 2000).

Methanogenesis is far more prevalent than sulfate reduction in freshwater wetland soils.

However, saline additions to freshwater plots, mimicking sea level rise, result in

increased sulfate reduction as reduction of sulfate is more energetically favorable than

methanogenesis. In both saline and freshwater wetlands Fe oxidation and reduction

reactions are found in the soil substrata. The soil from freshwater wetlands is often used

as inoculum for Winogradsky columns which exhibit highly stratified bacterial functional

groups based on resource distribution, light and available reducing agents (Fig 1.1) (Atlas

and Bartha 1998, Madigan et al. 2000).

Much has been published on zonation of anaerobic reactions that follow the

previously described "redox cascade." Less has been published from a similar viewpoint

with respect to processes that occur under aerobic conditions. Because of the high energy

yields and the abundance of organic compounds, aerobic heterotrophic respiration

invariably dominates metabolism (and oxygen consumption) in the presence of O_2. A

series of autotrophic reactions also compete for O_2, but they tend to be ordered more on

substrate availability than strictly by energetics. Nitrification, iron oxidation, and sulfur

oxidation will all proceed in the presence of sufficient O_2 and substrate. Indeed, they are

often seen occurring simultaneously in many locations. Both sulfate and iron oxidation

can inhibit other processes (including heterotrophy) by extreme acid production as seen

in equations 4.1 and 4.2 (taken from Stumm and Morgan(1996)):

$$4Fe^{2+} + O_2 + 10H_2O \rightleftharpoons 4Fe(OH)_3 + 8H^+ \qquad \text{eq. 4.1}$$

$$H_2S + 2O_2 \rightleftharpoons SO_4^{2-} + 2H^+ \qquad \text{eq. 4.2}$$
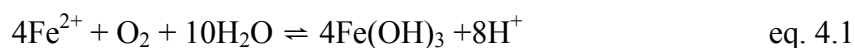
Under conditions appropriate for nitrification, the unique arrangement in which the oxidation of NH_4^+ to NO_3^- occurs in two steps, each mediated by a different functional groups, establishes the potential for a zonation of function. Examination of the abundance profiles did not show any real spatial segregation of AOB and NOB but there were distinct differences in abundance. It is likely that the lack of stratification of conditions within the columns, given the frequent draining and filling in the tidal columns, or the pulses of fluid through the trickled columns never allowed for enough spatial variability in conditions to establish zonation. Given that the sampling procedure used did not maintain any structural integrity in the biofilm, if microscale patterns like those observed by Aoi et al. (2004) or Schramm et al. (2003) were present, they would not have been seen.

The abundance data for the organisms examined did reflect energy yield of the oxidation-reduction reactions they catalyze, at least for the organisms operating aerobically. The relatively large ΔG for the ammonium-oxidation reaction (ca. -275 kJ mole^{-1}) was reflected by the abundance of AOB, which always exceeded that of the NOB. Nitrite oxidation yields only -88 kJ mole^{-1}, such that the nitrite oxidizers must run their portion of the nitrification process 3 times to get the same energy as their ammonia-oxidizing counterparts.

The abundance of AXB was less than either AOB or NOB, but the abundance cannot be interpreted strictly on the basis of energy yield of the reaction. Anammox is an anaerobic process and the AXB are very slow growers. Comparing the abundance of AXB to the AOB and NOB based on energetics is not legitimate, as the AXB will not

function well under aerobic conditions. When the columns were initially flooded (or drained of water), oxygen is present in the system. Ammonia oxidizers can then remove the substrate necessary for the AXB to grow. During anaerobic periods, the AXB might be functioning, but the rate of reaction and growth of the cells is so slow that they never gain the opportunity to increase their abundance much before oxygen is introduced again to the column. Although the flooding mechanics differed for the tidal and the trickling columns, the issue of too much oxygen and insufficient ammonia for proliferation of the AXB would be similar. A further consideration in the abundance relationship of NOB and AXB is their dependence on NO_2^-, a product of aerobic respiration, and competition for the product between NOB and AXB and with denitrifiers, denitrifying nitrifiers, combined with the need for an anaerobic environment. The anammox process does yield more energy than NO_2^- oxidation, but the niche of anammox is particularly complex so under this rational, thermodynamic component to the organization of the microbial community responsible for removing N from waste waters is possible.

The relationship of the chemoautotrophs to the TAB is also not based entirely on energetics, although energetics is a component of the observed relationship. The heterotrophic component of the TAB gain more energy per mole of reactant and are able, therefore, to increase in abundance more readily. The heterotrophs and the autotrophs are not in direct competition for the same reductant; however, the heterotrophs and the aerobic lithoautotrophs do compete for oxygen. In this case, the greater energy yield of the heterotrophic reactions makes those organisms better competitors for the available oxygen and allows more abundant growth. The heterotrophs do not overwhelm autotrophs in the reactors as is often the case in non-engineered environments, for

example, in acidic forest soils, the average AOB abundance was found to be only 0.3% of the microbial community using qPCR for the *amoA* gene. Abundance of AOB ranged from of 0.3–9.3 x 10^7 *amoA* gene copies (g sediment)$^{-1}$ (He et al. 2007). In pristine soils the abundance range of AOB was found to be 0.24–2.2 x 10^7 *amoA* gene copies g^{-1}(Szukics et al. 2010). In contrast, in the engineered systems in this study, across all hydraulic and N treatments, the average nitrifier composition of the microbial community is 25%, suggesting that in the reactors, the autotrophs were at least partially competitive with the heterotrophs. Indeed, as the cycle rates decreased to allow longer and longer periods of anoxia, it is evident that heterotrophic denitrifiers rose in importance as evidenced by the loss of NO_3^- from the system. Given that most denitrifiers are facultative anaerobes (Blum and Mills, 2012), shifting to NO_3^- respiration in the absence of O_2, one might expect to see a lesser importance of AOB and NOB in relationship to TAB; however, aerobic heterotrophy would also decline in the absence of O_2 and the data presented in Fig. 3.11, 3.12 and 3.27 reflect a decline in TAB associated with a decline in AOB and NOB during the treatments of lowest water recirculation.

Additionally, there appears to be a relationship between the organization and behavior of the microbial ecosystem to the tidal frequency or trickling duration in the reactor systems. These pulses in both nutrients and O_2 are essential to encouraging two dependent, but mutually exclusive processes to occur in the same space, but at different times. Abundance profiles of the nitrifiers and total bacteria change in response to each change in cycling regime; however, the degree of change and its relationship to treatment type is not quantifiable. The pulsing paradigm (Odum et al. 1995) suggests that these artificial microbially dominated ecosystems behave similarly to wetland ecosystems; they

have developed a dependence on tidal pulsing which frequently replenishes nutrients and removes waste products. In particular, the draining phase of the tidal columns results in a pulse of oxygen, the terminal electron acceptor needed for nitrification to occur. While too frequent a pulse can be disruptive to N removal, as seen by the lack of denitrification during the 24i- and 24f-cycles day^{-1} treatments, correct pulsing would likely enhance productivity by encouraging nitrification and denitrification to occur simultaneously in the same container. The 8-cycles day^{-1} treatment to be approaching the correct resonance, but was not long enough to achieve steady state where the enhanced nitrification and combined denitrification could be seen chemically through reduced NH_4^+ and NO_3^- concentrations (Fig. 3.12–3.14). However, at 4-cycles per day, nitrification continued to occur at an acceptable rate (although the NH_4^+ concentration increased slightly, but not objectionably so), and denitrification proceeded at a rate adequate to remove all the NO_3^- produced by nitrification of NH_4^+ added to the reservoirs.

4.3   **Mass Balance**

Microbial processes were assumed to be dominated by organisms within the columns, and the systems received daily additions of N and C compounds (added to the reservoirs). However, sampling for chemical analysis occurred on a weekly basis, and then only the concentration of N within the reservoir was monitored. Neither the volume of the effluent generated during reactor feeding nor the concentrations of N species in that effluent water removed during feeding were measured or recorded. While IC sampling for water chemistry on a weekly basis provides information about the processes occurring inside the reactor, the data set is insufficient to construct a mass balance, because there were water losses and N losses that were not accounted for. Further, Worrell Water constructed their mass balance incorrectly by subtracting the concentration of N in the reactors from one sampling from a theoretical concentration of N, based on the dissolution of the N additions added the previous day. This procedure created a data set that was misleading and gave the illusion that a complete mass balance could be constructed: the mass balance constructed by Worrell did not calculate a mass of N, and did not quantify effluent losses. This approach did not consider dilution caused by daily addition of 2 L of water, or residual N from the prior days N additions. A correct mass balance would account for the amount of N added each day and the amount of N leaving the system. To do this, a sample of the effluent would need to be analyzed to determine N loss through the effluent and the effluent volume would need to be recorded. Complete mixing prior to passing through the overflow port would also need to be ensured. There would also need to be a sample taken prior to feeding to assess the amount of N in the reactor prior to water and N additions. Daily measurements would allow for a more

continuous mass balance to be constructed, but the weekly sampling, if done correctly, would at least allow for a weekly assessment of reactor performance. As there were daily additions of N, constant microbial activity and only weekly measurements of N concentrations within the reactor, the meaning of any mass balance calculation using the aforementioned process was obscured. A proper mass balance should have been computed in order to assess net microbial activity and changes in net community response to environmental stressors, although it would not have enabled discernment of individual functional group activity. Future work should include a water balance, and a mass balance to determine the microbial component of Nr removed from the waste stream. Also, in the tidal columns collecting samples from the sampling portals at the time the column filled and immediately prior to column draining might provide valuable information on the activity of microorganisms inside the column during fill phases.

4.4   Denitrification Study at Cobb Mill Creek

Findings from the denitrification study are consistent with other research that has occurred in the Cobb Mill Creek watershed (Flewelling et al. in review, Galavotti 2004, Gu et al. 2007, Mills et al. 2008, Robertson 2009). Gu et al., (2007), found that 70% of NO_3^- was removed from groundwater prior to entering the stream water and that the NO_3^- removal was occurring in organic matter rich regions of the subsurface sediments. Similarly, the potential denitrification maxima, found by Galavotti (2004), showed a strong relationship to organic matter values and show that maximal denitrification rates are found in a depth range from approximately 3–40 cm below the sediment-water interface. In other systems, denitrification has been shown to be highly correlated to the availability of organic matter as it is an energy source for heterotrophic activity that

quickly depletes the available oxygen creating an anoxic environment (Burt et al. 1999). Burt et al. (1999) also observed a 75% NO_3^- removal rate within the riparian buffer zone. The authors note that due to gravel lenses in their study site, subsurface water flow was capable of circumventing the riparian soils and reaching the stream without undergoing denitrification; however sediment cores collected close to the stream where sediments were usually higher in organic matter, inundated, and therefore anaerobic, had higher potential denitrification rates as determined by acetylene block. Microorganisms are capable of rapid growth under idealized conditions. The vertical profiles for denitrifiers show an increase in abundance by over 6 orders of magnitude between two points separated by less than 40 cm (Fig. 3.39). This suggests a Goldilocks Zone is also present in the vertical profile of the creek sediment and has impact not only on abundance but also on activity (Fig. 3.40). The denitrification potential showed a similar decline, going from a value of 24.8 nMol N_2O (g sediment)$^{-1}$ at a depth of 1 cm below the sediment-water interface to below detection limit at a depth of 61 cm (Fig. 3.40). These results are consistent with the findings of Mills, et al., (2008), and Gu, et al. (2007), both of which found that organic matter was a controlling factor for denitrification.

4.5   C, O, and N

Carbon, oxygen and nitrogen are critical in regulating microbial activity. They do not act independently of each other and they play a role in regulating activity at an ecosystem and pilot scale. In Cobb Mill Creek, oxygen depletion is required for denitrification to occur, but organic carbon is required for oxygen depletion to occur. Similarly, in the treatment systems, dissolved oxygen is required for nitrification to occur, however the presence of organic matter often hinders nitrification through heterotrophic O_2

consumption. Relationships between C and O, such as those described in water treatment systems have been noted by Mills, et al. (2008), and by Gu, et al. (2007). The effects of C, O and N are seen as inhibitory and as enhancing microbial growth and activity based on specific functional group and specific niche requirements. Nutrient effects are seen in both engineered and naturally occurring systems. The implications of defining microbial niche parameters for biogeochemical cycling microbes have implications for design of engineered systems, and for land use management. While environmental parameters may play a large role in the distribution and activity of there is likely a high degree of unexplained variation in community structure (Franklin and Mills 2003). Functional redundancy within a functional group leads to an expanded goldilocks zone thus there is a connection between abundance, distribution patterns and environmental gradients and net community activity.

5.   References

Abeliovich, A. (1987) Nitrifying bacteria in waste-water reservoirs. Applied and Environmental Microbiology 53(4), 754-760.

Abou-Elela, S.I. and Hellal, M.S. (2012) Municipal wastewater treatment using vertical flow constructed wetlands planted with canna, phragmites and cyprus. Ecological Engineering 47, 209-213.

Amann, R.I., Binder, B.J., Olson, R.J., Chisholm, S.W., Devereux, R. and Stahl, D.A. (1990) Combination of 16s ribosomal-RNA-targeted oligonucleotide probes with flow-cytometry for analyzing mixed microbial-populations. Applied and Environmental Microbiology 56(6), 1919-1925.

Aoi, Y., Tsuneda, S. and Hirata, A. (2004) Transition of bacterial spatial organization in a biofilm monitored by FISH and subsequent image analysis. Water Science and Technology 49(11-12), 365-370.

Atlas, R., M. and Bartha, R. (1998) Microbial ecology, fundamentals and applications, Addison Wesley Longman, New York.

Austin, D. (2006) Influence of cation exchange capacity (cec) in a Tidal-flow, flood and drain wastewater treatment wetland. Ecological Engineering 28(1), 35-43.

Austin, D. and Nivala, J. (2009) Energy requirements for nitrification and biological nitrogen removal in engineered wetlands. Ecological Engineering 35(2), 184-192.

Benefield (2002) Wastewater quality/strength/content. Washington State, Department of Health Research Report T5, 1-18.

Blum, L.K. and Mills, A.L. (2012) Estuarine microbial ecology, in Estuarine Ecology, 2nd edition. Day, J.W., Crump, B.C., Kemp, W.M. and Yáñez-Arancibia, A. (eds), p. 261, John Wiley & Sons, Inc, Hoboken, NJ.

Boursier, H., Beline, F. and Paul, E. (2005) Piggery wastewater characterisation for biological nitrogen removal process design. Bioresource Technology 96(3), 351-358.

Boyer, D., Cole, J. and Bartholomae, C. (2000) Southwestern Africa: Northern Benguela current region. Marine Pollution Bulletin 41(1-6), 123-140.

Brock, T., D. (1987) Ecology of microbial communities, Cambridge University Press, New York.

Burt, T.P., Matchett, L.S., Goulding, K.W.T., Webster, C.P. and Haycock, N.E. (1999) Denitrification in riparian buffer zones: The role of floodplain hydrology. Hydrological Processes 13(10), 1451-1463.

Canfield, D.E., Jorgensen, B.B., Fossing, H., Glud, R., Gundersen, J., Ramsing, N.B., Thamdrup, B., Hansen, J.W., Nielsen, L.P. and Hall, P.O.J. (1993) Pathways of organic-carbon oxidation in 3 continental-margin sediments. Marine Geology 113(1-2), 27-40.

Carvalho, G., Meyer, R.L., Yuan, Z.G. and Keller, J. (2006) Differential distribution of ammonia- and nitrite-oxidising bacteria in flocs and granules from a nitrifying/denitrifying sequencing batch reactor. Enzyme and Microbial Technology 39(7), 1392-1398.

Chandran, K. and Smets, B.F. (2000) Single-step nitrification models erroneously describe batch ammonia oxidation profiles when nitrite oxidation becomes rate limiting. Biotechnology and Bioengineering 68(4), 396-406.

Chen, Z., Hou, H.J., Zheng, Y., Qin, H.L., Zhu, Y.J., Wu, J.S. and Wei, W.X. (2010) Influence of fertilization regimes on a *nosZ*-containing denitrifying community in a rice paddy soil. Journal of the Science of Food and Agriculture 92(5), 1064-1072.

Cooke, J.G. and White, R.E. (1987) Spatial-distribution of denitrifying activity in a stream draining an agricultural catchment. Freshwater Biology 18(3), 509-519.

Daims, H., Bruhl, A., Amann, R., Schleifer, K.H. and Wagner, M. (1999) The domain-specific probe eub338 is insufficient for the detection of all bacteria: Development and evaluation of a more comprehensive probe set. Systematic and Applied Microbiology 22(3), 434-444.

Daims, H., Purkhold, U., Bjerrum, L., Arnold, E., Wilderer, P.A. and Wagner, M. (2001) Nitrification in sequencing biofilm batch reactors: Lessons from molecular approaches. Water Science and Technology 43(3), 9-18.

Daims, H. and Wagner, M. (2010) Microbial ecology of activated sludge. Seviour, R.J. and Nielsen, P.H. (eds), IWA Publishing, London.

Damste, J.S.S., Strous, M., Rijpstra, W.I.C., Hopmans, E.C., Geenevasen, J.A.J., van Duin, A.C.T., van Niftrik, L.A. and Jetten, M.S.M. (2002) Linearly concatenated cyclobutane lipids form a dense bacterial membrane. Nature 419(6908), 708-712.

Damste, J.S.S., Rijpstra, W.I.C., Geenevasen, J.A.J., Strous, M. and Jetten, M.S.M. (2005) Structural identification of ladderane and other membrane lipids of planctomycetes capable of anaerobic ammonium oxidation (anammox). FEBS Journal 272(16), 4270-4283.

Ehrlich, H.L. and Newman, D.K. (2009) Geomicrobiology, CRC Press, Boca Raton.

Emerson, S., Jahnke, R., Bender, M., Froelich, P., Klinkhammer, G., Bowser, C. and Setlock, G. (1980) Early diagenesis in sediments from the eastern equatorial pacific .1. Pore water nutrient and carbonate results. Earth and Planetary Science Letters 49(1), 57-80.

EPA (2004) Guidelines for water reuse. Environmental Protection Agency, Camp Dresser and McKee, Inc, Washington, D. C.

Fernandez, I., Dosta, J., Fajardo, C., Campos, J.L., Mosquera-Corral, A. and Mendez, R. (2012) Short- and long-term effects of ammonium and nitrite on the anammox process. Journal of Environmental Management 95, S170-S174.

Fierer, N., Schimel, J.P. and Holden, P.A. (2003) Variations in microbial community composition through two soil depth profiles. Soil Biology & Biochemistry 35(1), 167-176.

Fixen, P.E. and West, F.B. (2002) Nitrogen fertilizers: Meeting contemporary challenges. Ambio 31(2), 169-176.

Flewelling, S.A., Herman, J.S., Hornberger, G.M., Mills, A.L. and Robertson, W.M. (in review) Evapotranspiration causes diel patterns in stream nitrate concentrations. Hydrological Processes.

Floyd, A.L. (2007) Effects of inundation regime and plant community on soil bacterial communities in an Eastern Shore, VA salt marsh, University of Virginia, Charlottesville.

Forney, L.J., Zhou, X. and Brown, C.J. (2004) Molecular microbial ecology: Land of the one-eyed king. Current Opinion in Microbiology 7(3), 210-220.

Franck, S., von Bloh, W. and Bounama, C. (2007) Maximum number of habitable planets at the time of earth's origin: New hints for panspermia and the mediocrity principle. International Journal of Astrobiology 6(2), 153-157.

Franklin, R.B. and Mills, A.L. (2003) Multi-scale variation in spatial heterogeneity for microbial community structure in an Eastern Virginia agricultural field. FEMS Microbiology Ecology 44(3), 335-346.

Franklin, R.B. and Mills, A.L. (2007) The spatial distribution of microbes in the environment. Franklin, R.B. and Mills, A.L. (eds), Springer.

Galavotti, H.S. (2004) Spatial profiles of sediment denitrification at the ground water - surface water interface in Cobb Mill Creek on the Eastern Shore of Virginia, University of Virginia, Charlottesville.

Galloway, J.N. and Cowling, E.B. (2002) Reactive nitrogen and the world: 200 years of change. Ambio 31(2), 64-71.

Galloway, J.N., Cowling, E.B., Seitzinger, S.P. and Socolow, R.H. (2002) Reactive nitrogen: Too much of a good thing? Ambio 31(2), 60-63.

Galloway, J.N., Dentener, F.J., Capone, D.G., Boyer, E.W., Howarth, R.W., Seitzinger, S.P., Asner, G.P., Cleveland, C.C., Green, P.A., Holland, E.A., Karl, D.M., Michaels, A.F., Porter, J.H., Townsend, A.R. and Vorosmarty, C.J. (2004) Nitrogen cycles: Past, present, and future. Biogeochemistry 70(2), 153-226.

Gieseke, A., Bjerrum, L., Wagner, M. and Amann, R. (2003) Structure and activity of multiple nitrifying bacterial populations co-existing in a biofilm. Environmental Microbiology 5(5), 355-369.

Gottschalk, G. (1979) Bacterial metabolism, Springer Verlag, New York.

Grady, C., Jr., Daigger, G. and Lim, H.C. (1999) Biological wastewater treatment, Marcel Dekker, New York.

Gu, C.H., Hornberger, G.M., Mills, A.L., Herman, J.S. and Flewelling, S.A. (2007) Nitrate reduction in streambed sediments: Effects of flow and biogeochemical kinetics. Water Resources Research 43(12),W12413.

Gu, C.H., Hornberger, G.M., Herman, J.S. and Mills, A.L. (2008a) Influence of stream-groundwater interactions in the streambed sediments on NO_3^- flux to a low-relief coastal stream. Water Resources Research 44(11), W11432.

Gu, C.H., Hornberger, G.M., Herman, J.S. and Mills, A.L. (2008b) Effect of freshets on the flux of groundwater nitrate through streambed sediments. Water Resources Research 44(5), W05415.

Gutknecht, J.L.M., Goodman, R.M. and Balser, T.C. (2006) Linking soil process and microbial ecology in freshwater wetland ecosystems. Plant and Soil 289(1-2), 17-34.

Haese, R.R. (2006) Marine Geochemistry, Springer, Berlin

Hao, X.D., Wang, Q.L., Zhang, X.P., Cao, Y.L. and Loosdrecht, C.M.V. (2009) Experimental evaluation of decrease in bacterial activity due to cell death and activity decay in activated sludge. Water Research 43(14), 3604-3612.

Harms, G., Layton, A.C., Dionisi, H.M., Gregory, I.R., Garrett, V.M., Hawkins, S.A., Robinson, K.G. and Sayler, G.S. (2003) Real-time PCR quantification of nitrifying bacteria in a municipal wastewater treatment plant. Environmental Science & Technology 37(2), 343-351.

He, J., Shen, J., Zhang, L., Zhu, Y., Zheng, Y., Xu, M., and Di, H. (2007) Quantitative analyses of the abundance and composition of ammonia-oxidizing bacteria and ammonia-oxidizing archaea of a Chinese upland red soil under long-term fertilization practices. Environmental Microbiology 9(12), 3152-3152.

Hedin, L.O., von Fischer, J.C., Ostrom, N.E., Kennedy, B.P., Brown, M.G. and Robertson, G.P. (1998) Thermodynamic constraints on nitrogen transformations and other biogeochemical processes at soil-stream interfaces. Ecology 79(2), 684-703.

Henderson, S.L., Dandie, C.E., Patten, C.L., Zebarth, B.J., Burton, D.L., Trevors, J.T. and Goyer, C. (2010) Changes in denitrifier abundance, denitrification gene mRNA levels, nitrous oxide emissions, and denitrification in anoxic soil microcosms amended with glucose and plant residues. Applied and Environmental Microbiology 76(7), 2155-2164.

Henze, M., Grady, C.P.L., Gujer, W., Marais, G.V.R. and Matsuo, T. (1987) A general-model for single-sludge waste-water treatment systems. Water Research 21(5), 505-515.

Hill, A.R. (1983) Denitrification - its importance in a river draining an intensively cropped watershed. Agriculture Ecosystems & Environment 10(1), 47-62.

Hinrichsen, D., Robey, B. and Upadhyay, U.D. (1998) Solutions for a water-short world. Populations Reports 26(1), 1-32.

Hobbie, J.E., Daly, R.J. and Jasper, S. (1977) Use of nuclepore filters for counting bacteria by fluorescence microscopy. Applied and Environmental Microbiology 33, 1225-1228.

Hu, B.L., Shen, L.D., Xu, X.Y. and Zheng, P. (2011) Anaerobic ammonium oxidation (anammox) in different natural ecosystems. Biochemical Society Transactions 39, 1811-1816.

IPCC (2001) Climate change 2001: The scientific basis, contribution of Working Group I to the third assessment report of the Intergovernmental Panel on Climate Change., Cambridge University Press, Cambridge and New York.

Jaeschke, A., den Camp, H., Harhangi, H., Klimiuk, A., Hopmans, E.C., Jetten, M.S.M., Schouten, S. and Damste, J.S.S. (2009) 16s rRNA gene and lipid biomarker evidence for anaerobic ammonium-oxidizing bacteria (anammox) in California and Nevada hot springs. FEMS Microbiology Ecology 67(3), 343-350.

Jetten, M.S.M., Logemann, S., Muyzer, G., Robertson, L.A., deVries, S., vanLoosdrecht, M.C.M. and Kuenen, J.G. (1997) Novel principles in the microbial conversion of nitrogen compounds. Antonie Van Leeuwenhoek International Journal of General and Molecular Microbiology 71(1-2), 75-93.

Jetten, M.S.M., Strous, M., van de Pas-Schoonen, K.T., Schalk, J., van Dongen, U., van de Graaf, A.A., Logemann, S., Muyzer, G., van Loosdrecht, M.C.M. and Kuenen, J.G. (1998) The anaerobic oxidation of ammonium. FEMS Microbiology Reviews 22(5), 421-437.

Jetten, M.S.M., Wagner, M., Fuerst, J., van Loosdrecht, M., Kuenen, G. and Strous, M. (2001) Microbiology and application of the anaerobic ammonium oxidation ('anammox') process. Current Opinion in Biotechnology 12(3), 283-288.

Johnson, L.T., Royer, T.V., Edgerton, J.M. and Leff, L.G. (2012) Manipulation of the dissolved organic carbon pool in an agricultural stream: Responses in microbial community structure, denitrification, and assimilatory nitrogen uptake. Ecosystems 15(6), 1027-1038.

Jordan, T.E., Correll, D.L. and Weller, D.E. (1993) Nutrient interception by a riparian forest receiving inputs from adjacent cropland. Journal of Environmental Quality 22(3), 467-473.

Kampschreur, M.J., Tan, N.C.G., Kleerebezem, R., Picioreanu, C., Jetten, M.S.M. and Loosdrecht, M.C.M. (2008a) Effect of dynamic process conditions on nitrogen oxides emission from a nitrifying culture. Environmental Science & Technology 42(2), 429-435.

Kampschreur, M.J., van der Star, W.R.L., Wielders, H.A., Mulder, J.W., Jetten, M.S.M. and van Loosdrecht, M.C.M. (2008b) Dynamics of nitric oxide and nitrous oxide emission during full-scale reject water treatment. Water Research 42(3), 812-826.

Kang, S. (2005) Spatial structures of soil microbial communities and their controlling factors, University of Virginia, Charlottesville.

Kepner, R.L. and Pratt, J.R. (1994) Use of fluorochromes for direct enumeration of total bacteria in environmental-samples - past and present. Microbiological Reviews 58(4), 603-615.

Kidd, C., Piantadosi, S.T. and Aslin, R.N. (2012) The goldilocks effect: Human infants allocate attention to visual sequences that are neither too simple nor too complex. Plos One 7(5).

Kong, A.Y.Y., Hristova, K., Scow, K.M. and Six, J. (2010) Impacts of different n management regimes on nitrifier and denitrifier communities and n cycling in soil microenvironments. Soil Biology & Biochemistry 42(9), 1523-1533.

Kuai, L.P. and Verstraete, W. (1998) Ammonium removal by the oxygen-limited autotrophic nitrification-denitrification system. Applied and Environmental Microbiology 64(11), 4500-4506.

Kuypers, M.M.M., Sliekers, A.O., Lavik, G., Schmid, M., Jorgensen, B.B., Kuenen, J.G., Damste, J.S.S., Strous, M. and Jetten, M.S.M. (2003) Anaerobic ammonium oxidation by anammox bacteria in the black sea. Nature 422(6932), 608-611.

Kuypers, M.M.M., Lavik, G., Woebken, D., Schmid, M., Fuchs, B.M., Amann, R., Jorgensen, B.B. and Jetten, M.S.M. (2005) Massive nitrogen loss from the Benguela upwelling system through anaerobic ammonium oxidation. Proceedings of the National Academy of Sciences of the United States of America 102(18), 6478-6483.

Lemke, M.J., McNamara, C.J. and Leff, L.G. (1997) Comparison of methods for the concentration of bacterioplankton for *in situ* hybridization. Journal of Microbiological Methods 29(1), 23-29.

Lensing, H.J., Vogt, M. and Herrling, B. (1994) Modeling of biologically mediated redox processes in the subsurface. Journal of Hydrology 159(1-4), 125-143.

Loy, A., Maixner, F., Wagner, M. and Horn, M. (2007) Probebase - an online resource for rRNA-targeted oligonucleotide probes: New features 2007. Nucleic Acids Research 35, D800-D804.

Lyngkilde, J. and Christensen, T.H. (1992) Redox zones of a landfill leachate pollution plume (vejen, denmark). Journal of Contaminant Hydrology 10(4), 273-289.

Madigan, M.T., Martinko, J.M. and Parker, J. (2000) Brock biology of microorganisms, Prentice Hall, Upper Saddle River.

Martin, S.J. (2011) Oncogene-induced autophagy and the goldilocks principle. Autophagy 7(8), 922-923.

McClain, M.E., Boyer, E.W., Dent, C.L., Gergel, S.E., Grimm, N.B., Groffman, P.M., Hart, S.C., Harvey, J.W., Johnston, C.A., Mayorga, E., McDowell, W.H. and Pinay, G. (2003) Biogeochemical hot spots and hot moments at the interface of terrestrial and aquatic ecosystems. Ecosystems 6(4), 301-312.

McCrackin, M.L. and Elser, J.J. (2012) Denitrification kinetics and denitrifier abundances in sediments of lakes receiving atmospheric nitrogen deposition (Colorado, USA). Biogeochemistry 108(1-3), 39-54.

Mills, A.L. and Bell, P.E. (1986) Microbial autecology: A method for environmental studies. Tate, R.L., III (ed), John Wiley & Sons Inc.

Mills, A.L., Hornberger, G.M. and Herman, J.S. (2008) Sediments in low-relief coastal streams as effective filters of agricultural nitrate, American Water Resources Association, Norfolk, VA.

Mosier, A.R., Doran, J.W. and Freney, J.R. (2002) Managing soil denitrification. Journal of Soil and Water conservation 57(6), 505-512.

Mulder, A., Vandegraaf, A.A., Robertson, L.A. and Kuenen, J.G. (1995) Anaerobic ammonium oxidation discovered in a denitrifying fluidized-bed reactor. FEMS Microbiology Ecology 16(3), 177-183.

Neef, A., Amann, R., Schlesner, H. and Schleifer, K.H. (1998) Monitoring a widespread bacterial group: *In situ* detection of planctomycetes with 16s rRNA-targeted probes. Microbiology-UK 144, 3257-3266.

Neubauer, S.C., Miller, W.D. and Anderson, I.C. (2000) Carbon cycling in a tidal freshwater marsh ecosystem: A carbon gas flux study. Marine Ecology-Progress Series 199, 13-30.

Neubauer, S.C., Emerson, D. and Megonigal, J.P. (2002) Life at the energetic edge: Kinetics of circumneutral iron oxidation by lithotrophic iron-oxidizing bacteria isolated from the wetland-plant rhizosphere. Applied and Environmental Microbiology 68(8), 3988-3995.

Neubauer, S.C. and Craft, C.B. (2009) Tidal freshwater wetlands. Barendregt, A., Whigham, D.F. and Baldwin, A.H. (eds), Backhuys Publishers, Leiden.

Odum, W.E., Odum, E.P. and Odum, H.T. (1995) Nature's pulsing paradigm. Estuaries 18(4), 547-555.

Philips, S., Wyffels, S., Sprengers, R. and Verstraete, W. (2002) Oxygen-limited autotrophic nitrification/denitrification by ammonia oxidizers enables upward motion towards more favourable conditions. Applied Microbiology and Biotechnology 59(4-5), 557-566.

Poth, M. and Focht, D.D. (1985) N-15 kinetic-analysis of n2o production by *Nitrosomonas europaea* - an examination of nitrifier denitrification. Applied and Environmental Microbiology 49(5), 1134-1141.

Prosser, J.I. (1989) Autotrophic nitrification in bacteria. Advances in Microbial Physiology 30, 125-181.

Prosser, J.I. (2012) Ecosystem processes and interactions in a morass of diversity. FEMS Microbiology Ecology 81(3), 507-519.

Rabalais, N.N. (2002) Nitrogen in aquatic ecosystems. Ambio 31(2), 102-112.

Rheinheimer, G. (1991) Aquatic microbiology, John Wiley and Sons, New York, NY.

Ritz, K., Black, H.I.J., Campbell, C.D., Harris, J.A. and Wood, C. (2009) Selecting biological indicators for monitoring soils: A framework for balancing scientific and technical opinion to assist policy development. Ecological Indicators 9(6), 1212-1221.

Robertson, W.M. (2009) Diurnal variations in nitrate concentrations in the Cobb Mill Creek, VA, University of Virginia, Charlottesville.

Scala, D.J. and Kerkhof, L.J. (1998) Nitrous oxide reductase (*nos*Z) gene-specific PCR primers for detection of denitrifiers and three *nos*Z genes from marine sediments. FEMS Microbiology Letters 162(1), 61-68.

Schmid, M., Twachtmann, U., Klein, M., Strous, M., Juretschko, S., Jetten, M., Metzger, J.W., Schleifer, K.H. and Wagner, M. (2000) Molecular evidence for genus level diversity of bacteria capable of catalyzing anaerobic ammonium oxidation. Systematic and Applied Microbiology 23(1), 93-106.

Schmid, M., Walsh, K., Webb, R., Rijpstra, W.I.C., van de Pas-Schoonen, K., Verbruggen, M.J., Hill, T., Moffett, B., Fuerst, J., Schouten, S., Damste, J.S.S., Harris, J., Shaw, P., Jetten, M. and Strous, M. (2003) *Candidatus "Scalindua brodae"*, sp nov., *candidatus "Scalindua wagneri"*, sp nov., two new species of anaerobic ammonium oxidizing bacteria. Systematic and Applied Microbiology 26(4), 529-538.

Schmid, M.C., Maas, B., Dapena, A., de Pas-Schoonen, K.V., de Vossenberg, J.V., Kartal, B., van Niftrik, L., Schmidt, I., Cirpus, I., Kuenen, J.G., Wagner, M., Damste, J.S.S., Kuypers, M., Revsbech, N.P., Mendez, R., Jetten, M.S.M. and Strous, M. (2005) Biomarkers for *in situ* detection of anaerobic ammonium-oxidizing (anammox) bacteria. Applied and Environmental Microbiology 71(4), 1677-1684.

Schmidt, I., Sliekers, O., Schmid, M., Cirpus, I., Strous, M., Bock, E., Kuenen, J.G. and Jetten, M.S.M. (2002) Aerobic and anaerobic ammonia oxidizing bacteria competitors or natural partners? FEMS Microbiology Ecology 39(3), 175-181.

Schmidt, I., Sliekers, O., Schmid, M., Bock, E., Fuerst, J., Kuenen, J.G., Jetten, M.S.M. and Strous, M. (2003) New concepts of microbial treatment processes for the nitrogen removal in wastewater. FEMS Microbiology Reviews 27(4), 481-492.

Schramm, A., de Beer, D., van den Heuvel, J.C., Ottengraf, S. and Amann, R. (1999) Microscale distribution of populations and activities of *Nitrosospira* and *Nitrospira spp.* Along a macroscale gradient in a nitrifying bioreactor: Quantification by *in situ* hybridization and the use of microsensors. Applied and Environmental Microbiology 65(8), 3690-3696.

Schramm, A., De Beer, D., Gieseke, A. and Amann, R. (2000) Microenvironments and distribution of nitrifying bacteria in a membrane-bound biofilm. Environmental Microbiology 2(6), 680-686.

Schramm, A. (2003) *In situ* analysis of structure and activity of the nitrifying community in biofilms, aggregates, and sediments. Geomicrobiology Journal 20(4), 313-333.

Smith, D.P., Rector, T., Reid-Black, K., Hummerick, M., Strayer, R., Birmele, M., Roberts, M.S. and Garland, J.L. (2008) Redox control bioreactor: A unique biological water processor. Biotechnology and Bioengineering 99(4), 830-845.

Smith, E.B. (1993) Basic chemical thermodynamics, Oxford University Press, New York.

Strous, M., Fuerst, J.A., Kramer, E.H.M., Logemann, S., Muyzer, G., van de Pas-Schoonen, K.T., Webb, R., Kuenen, J.G. and Jetten, M.S.M. (1999a) Missing lithotroph identified as new planctomycete. Nature 400(6743), 446-449.

Strous, M., Kuenen, J.G. and Jetten, M.S.M. (1999b) Key physiology of anaerobic ammonium oxidation. Applied and Environmental Microbiology 65(7), 3248-3250.

Stumm, W. and Morgan, J., J. (1996) Aquatic chemistry, Wiley-Interscience, New York.

Szukics, U., Abell, G.C.J., Hoedl, V., Mitter, B., Sessitsch, A., Hackl, E. and Zechmeister-Boltenstern, S. (2010) Nitrifiers and denitrifiers respond rapidly to changed moisture and increasing temperature in a pristine forest soil. FEMS Microbiology Ecology 72(3), 395-406.

Thamdrup, B. and Dalsgaard, T. (2002) Production of N_2 through anaerobic ammonium oxidation coupled to nitrate reduction in marine sediments. Applied and Environmental Microbiology 68(3), 1312-1318.

van Breemen, N., Boyer, E.W., Goodale, C.L., Jaworski, N.A., Paustian, K., Seitzinger, S.P., Lajtha, K., Mayer, B., Van Dam, D., Howarth, R.W., Nadelhoffer, K.J., Eve, M. and Billen, G. (2002) Where did all the nitrogen go? Fate of nitrogen inputs to large watersheds in the northeastern USA. Biogeochemistry 57(1), 267-293.

van de Graaf, A.A., Mulder, A., Debruijn, P., Jetten, M.S.M., Robertson, L.A. and Kuenen, J.G. (1995) Anaerobic oxidation of ammonium is a biologically mediated process. Applied and Environmental Microbiology 61(4), 1246-1251.

Verstraete, W. and Philips, S. (1998) Nitrification-denitrification processes and technologies in new contexts. Environmental Pollution 102, 717-726.

von Bloh, W., Cuntz, M., Franck, S. and Bounama, C. (2011) Habitability of the goldilocks planet Gliese 581g: Results from geodynamic models. Astronomy & Astrophysics 528.

Vrede, K., Heldal, M., Norland, S. and Bratbak, G. (2002) Elemental composition (c, n, p) and cell volume of exponentially growing and nutrient-limited bacterioplankton. Applied and Environmental Microbiology 68(6), 2965-2971.

Waki, M., Yasuda, T., Suzuki, K., Sakai, T., Suzuki, N., Suzuki, R., Matsuba, K., Yokoyama, H., Ogino, A., Tanaka, Y., Ueda, S., Takeuchi, M., Yamagishi, T. and Suwa, Y. (2009) Rate determination and distribution of anammox activity in activated sludge treating swine wastewater. Bioresource Technology 101(8), 2685-2690.

Wallace, S. and Austin, D. (2008) Emerging models for nitrogen removal in treatment wetlands. Journal of Environmental Health 71(4), 10-16.

Ward, B.B., Arp, D.J. and Klotz, M.G. (2011) Nitrification, ASM Press, Washington, D.C.

WHO (2006) Guidelines for the safe use of wastewater, excreta and greywater: Policy and regulatory aspects, WHO Press., Geneva.

Wilms, R., Sass, H., Kopke, B., Koster, H., Cypionka, H. and Engelen, B. (2006) Specific bacterial, archaeal, and eukaryotic communities in tidal-flat sediments along a vertical profile of several meters. Applied and Environmental Microbiology 72(4), 2756-2764.

Wright, S.F. (1994) Serology and conjugation of antibodies, Soil Science Society of America, Inc., Madison.

Ye, L. and Zhang, T. (2011) Estimation of nitrifier abundances in a partial nitrification reactor treating ammonium-rich saline wastewater using DGGE, T-RFLP and mathematical modeling. Applied Microbiology and Biotechnology 88(6), 1403-1412.

You, S.J., Chuang, S.H. and Ouyang, C.F. (2003) Nitrification efficiency and nitrifying bacteria abundance in combined AS-RBC and A2O systems. Water Research 37(10), 2281-2290.

Zart, D. and Bock, E. (1998) High rate of aerobic nitrification and denitrification by nitrosomonas eutropha grown in a fermentor with complete biomass retention in the presence of gaseous NO_2 or NO. Archives of Microbiology 169(4), 282-286.

Zhang, Q.C., Lambert, G., Liao, D., Kim, H., Robin, K., Tung, C.K., Pourmand, N. and Austin, R.H. (2011) Acceleration of emergence of bacterial antibiotic resistance in connected microenvironments. Science 333(6050), 1764-1767.

Zhu, B.L., Sanchez, J., van Alen, T.A., Sanabria, J., Jetten, M.S.M., Ettwig, K.F. and Kartal, B. (2011) Combined anaerobic ammonium and methane oxidation for nitrogen and methane removal. Biochemical Society Transactions 39, 1822-1825.

Zumft, W.G. (1997) Cell biology and molecular basis of denitrification. Microbiology and Molecular Biology Reviews 61(4), 533-616.

A.   Appendix I – Abundance Data

Table A-1. Abundance data from replicate samples taken from each sampling portal for the total abundance of bacteria (TAB), ammonia oxidizing bacteria (AOB), nitrite oxidizing bacteria (NOB), and anaerobic ammonia oxidizing (anammox) bacteria (AXB).

Portal	TAB	AOB	NOB	AXB
Low-N Tidal Column, 24i Cycles day^{-1}				
1	2.49E+09	2.03E+08	3.23E+07	1.85E+07
1	3.95E+09	1.71E+08	4.62E+06	9.24E+06
1	2.28E+09	2.42E+08	4.57E+06	0.00E+00
2	1.98E+09	3.06E+08	4.71E+06	7.54E+07
2	2.29E+09	7.65E+08	1.81E+07	0.00E+00
2	5.60E+09	4.39E+08	1.83E+08	4.57E+06
3	3.18E+09	1.38E+09	6.04E+08	5.03E+07
3	1.61E+09	1.47E+09	1.10E+09	1.39E+07
3	1.40E+09	1.27E+09	4.14E+08	0.00E+00
4	2.39E+09	1.19E+09	2.55E+08	0.00E+00
4	3.92E+09	1.58E+09	3.84E+08	1.37E+07
4	2.53E+09	1.15E+09	6.72E+08	0.00E+00
High-N, Tidal Column, 24i Cycles day^{-1}				
1	1.60E+09	4.67E+08	1.12E+08	4.06E+07
1	2.49E+09	2.24E+08	1.17E+08	5.08E+06
1	2.42E+09	5.13E+07	2.05E+07	5.13E+06
2	9.88E+09	8.54E+08	1.60E+08	8.01E+06
2	2.52E+10	1.16E+09	2.52E+08	2.52E+06
2	1.60E+10	2.36E+09	1.47E+09	7.85E+06
3	1.40E+10	9.84E+09	1.55E+09	7.77E+06
3	2.40E+10	1.84E+10	4.01E+09	2.67E+06
3	9.68E+09	5.23E+09	1.83E+09	1.05E+07
4	2.23E+10	1.71E+10	6.22E+09	1.30E+07
4	4.27E+10	6.22E+09	1.55E+09	0.00E+00
4	3.74E+10	6.02E+09	1.57E+09	1.31E+07
Low-N, Trickling Column, 0.8i min (0.25 hr)$^{-1}$				
1	5.11E+09	6.59E+08	1.88E+08	0.00E+00
1	2.10E+09	1.35E+09	1.60E+08	5.08E+06
1	2.26E+09	5.08E+08	4.62E+07	0.00E+00
2	5.07E+09	2.27E+09	8.89E+07	2.22E+06
2	6.59E+09	1.65E+09	6.59E+08	1.05E+07

Portal	TAB	AOB	NOB	AXB
2	4.71E+09	1.54E+09	3.62E+08	0.00E+00
3	2.49E+09	1.30E+09	3.06E+08	9.42E+06
3	1.37E+09	4.62E+08	1.66E+08	4.62E+06
3	2.45E+09	8.85E+08	3.53E+08	2.36E+07
4	2.98E+09	4.85E+08	9.33E+07	0.00E+00
4	8.30E+08	3.73E+08	1.87E+08	4.66E+06
4	6.04E+08	5.94E+08	1.69E+08	0.00E+00
High-N, Trickling Column, 0.8i min (0.25 hr)$^{-1}$				
1	4.55E+09	2.17E+09	1.88E+08	2.83E+07
1	5.30E+09	1.17E+09	2.29E+07	2.74E+07
1	8.48E+08	2.14E+09	1.65E+08	4.71E+07
2	1.32E+10	4.47E+09	7.61E+08	4.76E+06
2	4.57E+09	1.87E+09	3.26E+08	1.40E+07
2	1.83E+10	3.85E+09	6.18E+08	4.76E+06
3	1.95E+10	1.22E+10	9.42E+08	9.94E+07
3	8.77E+09	9.70E+09	1.62E+09	4.10E+07
3	8.38E+09	9.74E+09	2.26E+08	1.51E+07
4	1.62E+09	2.08E+08	2.34E+01	2.29E+07
4	7.40E+08	3.07E+08	4.49E+07	1.35E+07
4	3.66E+08	5.36E+08	3.73E+07	9.33E+06
Low-N Tidal, Column, 16 Cycles day^{-1}				
1	2.15E+09	2.47E+08	5.60E+07	2.59E+07
1	1.62E+09	1.79E+08	1.41E+07	3.30E+07
1	1.18E+09	1.77E+08	3.17E+07	4.08E+07
2	3.32E+09	3.12E+08	8.39E+07	0.00E+00
2	3.14E+08	4.16E+07	4.62E+06	1.85E+07
2	1.98E+09	2.23E+08	6.37E+07	2.73E+07
3	5.11E+09	2.38E+08	4.66E+07	4.66E+06
3	2.06E+09	8.55E+08	4.60E+06	3.68E+07
3	2.05E+09	3.14E+08	1.39E+07	2.77E+07
4	2.78E+09	3.19E+08	6.93E+07	3.23E+07
4	1.82E+09	2.22E+08	9.24E+06	4.62E+06
4	1.20E+08	1.33E+08	1.78E+07	4.44E+06
High-N, Tidal Column, 16 Cycles day^{-1}				
1	1.66E+09	1.60E+08	4.71E+07	1.41E+07
1	2.33E+09	2.39E+08	2.02E+08	9.37E+06
1	7.38E+09	4.30E+08	1.64E+08	8.19E+06
2	1.75E+10	4.66E+08	1.48E+08	2.31E+07

Portal	TAB	AOB	NOB	AXB
2	1.21E+09	2.58E+08	3.17E+07	7.70E+07
2	1.14E+10	2.12E+09	1.54E+08	5.14E+07
3	1.04E+10	1.58E+09	2.84E+08	1.39E+07
3	4.71E+09	1.33E+09	1.73E+08	1.87E+07
3	1.44E+10	1.82E+09	2.36E+08	5.75E+07
4	3.52E+10	2.41E+09	1.42E+08	1.84E+07
4	7.89E+09	1.99E+09	1.84E+08	0.00E+00
4	2.12E+10	2.35E+09	2.15E+08	1.35E+07
Low-N, Trickling Column, 0.5 min (0.25 hr)$^{-1}$				
1	3.19E+09	4.58E+08	1.13E+08	1.89E+07
1	2.80E+09	2.31E+08	4.36E+07	2.61E+07
1	1.97E+09	3.96E+08	4.40E+07	1.60E+07
2	2.04E+09	3.99E+08	6.78E+07	1.70E+07
2	2.14E+09	4.38E+08	6.26E+07	3.31E+07
2	1.81E+09	2.77E+08	3.12E+07	1.17E+07
3	1.49E+09	2.30E+08	6.77E+07	2.26E+07
3	1.86E+09	2.15E+08	2.80E+07	9.34E+06
3	1.09E+09	3.03E+08	4.49E+07	7.48E+06
4	7.50E+08	4.94E+07	8.98E+06	1.35E+07
4	1.44E+09	2.27E+08	5.44E+07	4.08E+07
4	1.49E+09	4.24E+07	0.00E+00	3.86E+06
High-N, Trickling Column, 0.5 min (0.25 hr)$^{-1}$				
1	1.19E+09	9.41E+08	1.16E+08	2.50E+07
1	2.59E+09	3.55E+08	4.79E+07	7.98E+06
1	1.38E+09	1.52E+08	4.41E+07	2.00E+07
2	1.82E+09	2.02E+08	2.95E+07	4.21E+06
2	1.12E+09	2.68E+08	6.89E+07	1.15E+07
2	2.08E+09	9.33E+07	6.61E+07	3.50E+07
3	2.42E+09	5.87E+08	7.57E+07	2.27E+07
3	1.81E+09	4.48E+08	5.90E+07	2.36E+07
3	1.48E+09	8.94E+07	3.11E+07	1.94E+07
4	1.88E+09	2.92E+08	1.02E+08	1.85E+07
4	3.72E+09	5.00E+07	2.08E+07	1.67E+07
4	1.94E+09	5.67E+08	1.46E+08	1.97E+07
Low-N Tidal Column, 8 Cycles day^{-1}				
1	1.94E+09	8.02E+08	2.56E+08	2.36E+06
1	1.22E+09	7.07E+07	1.41E+07	2.36E+06
1	2.16E+09	8.24E+08	2.76E+08	2.36E+06

Portal	TAB	AOB	NOB	AXB
2	2.25E+09	3.69E+08	4.16E+07	1.39E+07
2	1.64E+09	5.96E+08	5.01E+07	2.36E+06
3	2.06E+09	7.79E+08	1.73E+08	2.36E+06
3	3.62E+09	2.76E+08	1.98E+08	2.36E+06
3	2.64E+09	1.62E+09	1.25E+08	2.36E+06
4	4.86E+09	9.97E+08	6.00E+07	2.36E+06
4	3.70E+09	7.90E+08	5.54E+07	2.36E+06
4	4.09E+09	1.80E+09	3.20E+08	4.44E+06
High-N, Tidal Column, 8 Cycles day^{-1}				
1	2.60E+09	1.23E+09	6.12E+07	9.42E+06
1	2.27E+09	1.65E+09	8.90E+07	2.36E+06
1	3.15E+09	8.40E+08	8.19E+07	2.36E+06
2	2.78E+09	1.43E+09	2.36E+06	2.36E+06
2	6.30E+09	1.89E+09	1.36E+07	9.06E+06
2	7.60E+09	1.76E+09	3.00E+07	2.36E+06
3	2.34E+09	7.30E+08	6.00E+07	2.36E+06
3	6.43E+09	3.43E+09	1.15E+09	2.33E+07
3	7.85E+09	1.68E+08	4.42E+06	2.36E+06
4	6.23E+09	1.63E+09	4.55E+08	2.36E+06
4	3.69E+09	1.16E+09	3.22E+07	2.36E+06
4	6.06E+09	2.27E+09	9.38E+08	4.98E+06
Low-N, Trickling Column, 0.3 min (0.25 hr)$^{-1}$				
1	4.96E+09	8.97E+07	3.78E+07	1.42E+07
1	7.97E+08	2.00E+08	5.66E+07	2.36E+06
1	2.13E+09	5.40E+08	2.00E+07	2.36E+06
2	9.88E+08	1.23E+08	4.24E+06	2.36E+06
2	1.48E+09	2.80E+08	6.63E+07	2.36E+06
2	1.69E+09	2.34E+07	2.36E+06	3.90E+06
3	1.01E+09	1.35E+07	9.02E+06	2.36E+06
3	5.09E+08	5.61E+07	2.80E+07	2.36E+06
3	1.61E+08	5.98E+07	2.36E+06	2.36E+06
4	3.95E+08	8.98E+06	8.98E+06	2.36E+06
4	4.08E+08	5.89E+07	2.36E+06	2.36E+06
4	4.24E+08	1.54E+07	2.36E+06	3.86E+06
High-N, Trickling Column, 0.3 min (0.25 hr)$^{-1}$				
1	1.78E+09	1.63E+08	1.67E+07	4.17E+06
1	6.14E+08	1.08E+08	5.98E+07	2.36E+06
1	9.38E+08	2.73E+08	7.22E+07	2.36E+06

Portal	TAB	AOB	NOB	AXB
2	1.09E+09	6.51E+08	9.57E+07	2.36E+06
2	1.57E+09	2.33E+08	3.89E+06	2.36E+06
3	2.81E+09	3.71E+08	2.27E+07	3.79E+06
3	1.97E+09	1.18E+07	7.87E+06	2.36E+06
3	2.23E+09	1.09E+08	2.72E+07	7.78E+06
4	4.45E+08	2.23E+08	3.25E+07	2.36E+06
4	4.18E+09	3.00E+08	2.50E+07	2.36E+06
4	6.34E+08	3.15E+07	2.36E+06	2.36E+06
Low-N Tidal, Column, 4 Cycles day^{-1}				
1	2.69E+09	9.33E+07	9.33E+06	0.00E+00
1	1.38E+09	3.01E+08	7.54E+07	3.77E+07
1	5.98E+08	2.72E+08	1.81E+07	2.72E+07
2	1.21E+08	1.03E+08	0.00E+00	9.33E+06
2	3.53E+09	4.89E+08	1.85E+07	2.77E+07
2	1.53E+09	3.19E+08	0.00E+00	2.73E+07
3	7.37E+08	3.45E+08	3.73E+07	0.00E+00
3	1.46E+09	2.12E+08	2.77E+07	0.00E+00
4	1.09E+09	1.20E+08	3.69E+07	0.00E+00
4	1.96E+09	7.64E+08	0.00E+00	2.22E+07
High-N, Tidal Column, 4 Cycles day^{-1}				
1	1.37E+09	2.05E+08	6.06E+07	2.33E+07
1	8.37E+08	1.62E+08	3.81E+07	1.90E+07
1	1.57E+09	9.79E+07	5.13E+07	4.66E+06
2	5.68E+08	1.06E+08	2.77E+07	1.85E+07
2	2.00E+09	1.32E+09	4.57E+06	9.15E+06
2	2.46E+09	7.87E+08	3.77E+07	9.42E+06
3	2.73E+09	1.64E+08	2.34E+07	1.41E+07
3	2.81E+09	2.64E+08	1.88E+07	1.41E+07
4	1.82E+09	1.53E+08	2.78E+07	2.78E+07
4	1.24E+08	1.24E+08	4.76E+06	2.38E+07
Low-N, Trickling Column, 0.2 min (0.25 hr)$^{-1}$				
1	1.78E+09	1.18E+08	4.62E+07	1.39E+07
1	1.59E+10	6.28E+09	4.62E+07	9.82E+06
2	4.50E+00	5.54E+07	3.69E+07	1.96E+06
3	5.32E+09	1.98E+09	4.71E+07	1.00E+07
3	8.32E+08	9.15E+07	4.57E+06	3.89E+06
4	5.93E+08	1.18E+08	4.71E+07	2.00E+06
4	1.02E+09	1.96E+08	4.20E+07	0.00E+00

Portal	TAB	AOB	NOB	AXB
High-N, Trickling Column, 0.2 min (0.25 hr)$^{-1}$				
1	1.20E+01	0.00E+00	0.00E+00	3.93E+06
2	6.00E+00	6.09E+08	5.95E+06	0.00E+00
3	4.00E+00	5.03E+07	0.00E+00	0.00E+00
4	3.00E+00	2.29E+08	4.20E+07	4.66E+06
Low-N, Tidal Column, 24f Cycles day^{-1}				
1	1.47E+09	2.47E+08	1.12E+08	9.33E+06
1	1.25E+09	1.39E+08	7.39E+07	1.85E+07
1	1.86E+09	7.97E+07	3.28E+07	7.50E+07
2	2.38E+09	7.96E+08	1.65E+08	5.18E+07
2	1.29E+10	8.86E+07	5.13E+07	3.26E+07
2	3.01E+09	3.28E+08	5.23E+07	2.85E+07
3	3.17E+09	1.74E+09	3.66E+07	2.29E+07
3	2.83E+09	7.59E+08	3.75E+07	3.84E+07
3	1.41E+09	1.25E+09	3.70E+07	9.37E+06
4	2.64E+09	1.78E+09	1.18E+08	2.26E+07
4	1.95E+09	3.12E+08	4.73E+06	4.26E+07
4	2.53E+09	8.64E+08	8.27E+07	2.30E+07
High-N, Tidal Column, 24f Cycles day^{-1}				
1	3.60E+09	3.37E+09	3.61E+08	3.66E+07
1	2.41E+09	6.85E+08	1.52E+08	6.66E+07
1	2.77E+09	4.66E+07	3.78E+08	2.80E+07
2	4.17E+09	1.14E+08	1.83E+07	1.83E+07
2	4.32E+09	1.01E+09	1.03E+08	2.24E+07
2	6.34E+09	2.64E+09	8.48E+07	2.83E+07
3	4.84E+09	1.81E+09	7.32E+07	9.15E+06
3	3.12E+09	8.27E+08	3.69E+07	2.31E+07
3	4.95E+09	7.76E+08	2.31E+07	2.77E+07
4	3.12E+09	1.81E+09	4.62E+07	1.39E+07
4	6.24E+09	1.69E+09	1.73E+08	9.33E+06
4	2.48E+10	9.42E+08	5.13E+07	1.40E+07
Low-N, Trickling Column, 0.8f min (0.25 hr)$^{-1}$				
1	6.15E+09	2.61E+08	2.24E+08	1.26E+08
1	1.06E+09	9.33E+07	5.60E+07	7.00E+07
1	1.40E+09	1.03E+08	4.20E+07	5.13E+07
2	6.42E+08	6.00E+07	6.46E+07	2.77E+07
2	7.80E+08	1.86E+08	8.35E+07	9.28E+06
2	2.68E+09	1.75E+08	1.06E+08	1.84E+07

Portal	TAB	AOB	NOB	AXB
3	1.87E+09	3.14E+08	1.90E+08	4.76E+07
3	2.48E+09	1.62E+08	6.93E+07	4.62E+06
3	1.47E+09	1.42E+08	1.14E+08	4.26E+07
4	9.09E+08	5.16E+07	3.28E+07	4.22E+07
4	1.03E+09	9.79E+07	7.93E+07	9.33E+06
4	9.91E+08	1.51E+08	8.25E+07	1.94E+07
High-N, Trickling Column, 0.8f min (0.25 hr)$^{-1}$				
1	1.44E+09	9.89E+07	4.24E+07	2.83E+07
1	6.55E+08	3.34E+08	1.98E+08	2.36E+07
1	1.32E+09	1.47E+08	1.89E+07	1.89E+07
2	1.23E+09	3.54E+08	4.66E+06	9.33E+06
2	2.39E+09	1.79E+08	1.55E+08	2.36E+07
2	1.65E+09	5.04E+08	7.14E+07	1.90E+07
3	1.66E+09	6.39E+08	4.20E+07	1.87E+07
3	9.56E+08	9.89E+07	2.83E+07	0.00E+00
3	1.40E+09	1.04E+08	4.73E+06	9.47E+06
4	3.29E+10	4.52E+08	4.71E+07	0.00E+00
4	1.26E+09	2.73E+08	1.05E+08	2.36E+07
4	2.35E+09	4.18E+08	6.31E+07	3.88E+07

B.   **Appendix II – IC Data**

Weekly Grab Samples

Table B-1. IC data for the reservoir grab samples from the tidal columns.

Date	Cycles day^{-1}	Low-N, Tidal Column			High-N, Tidal Column		
		NH_4^+	NO_2^-	NO_3^-	NH_4^+	NO_2^-	NO_3^-
		ppm N			ppm N		
10/13/10	24	27.3	0.3	159.2	141.5	481.6	644.7
10/20/10	24	0.4	8.6	129.7	25.4	418.1	291.8
10/27/10	24	14	0.5	44.6	58	689.8	195.9
11/3/10	24	0.4	0.3	218.2	65.9	272.6	209
11/10/10	24	0.4	0.3	240.1	2	753.2	184.8
11/17/10	24i	0.4	1.6	229.3	2.9	598	229.4
11/24/10	24i	0.4	0.3	173.7	38.8	690.8	200.7
12/1/10	24i	0.4	0.3	342.5	41.4	361.9	387.7
12/8/10	24i	0.4	2.3	288.4	67.2	362.7	427.1
12/15/10	24i	0.4	0.3	223.2	38.6	119.5	501.4
12/23/10	24i	0.4	0.3	45.2	31.2	691.8	91.7
12/30/10	24i	10	1.3	234.9	97.8	519.9	455.2
1/5/11	16	0.4	0.3	239.1	4.2	544.5	382.9
1/12/11	16	0.4	3.3	189.8	4.7	692.8	252.8
1/19/11	16	0.7	3.6	173.6	5.6	13.5	665.3
1/26/11	16	0.8	3.9	165.8	5.2	639	90.1
2/3/11	16	0.4	2.9	156.4	0.4	693.8	67.4
2/10/11	8	20.6	12.4	132.9	247.8	486	9.6
2/17/11	8	22.2	7.5	129.7	0.4	529.4	8.5
2/24/11	8	29.4	5.8	134.4	244.2	121.1	0.3
3/3/11	8	29.9	13.3	133.4	135.4	694.8	165.8
3/9/11	4	23	11.5	89.3	183.5	324.4	11.2
3/18/11	4	20.6	9	76.6	214.3	49.2	5.9
3/24/11	4	20.4	4.4	87.8	210.5	134.5	9.6
3/31/11	4	24.8	3.2	52	274.7	695.8	18.4
4/7/11	24f	4	0.5	75.9	177.1	242.9	13.1
4/14/11	24f	3	2	108.5	32.3	516.8	47.4
4/21/11	24f	4.5	1.2	118.9	64.4	696.8	36
4/28/11	24f	4.6	1.3	126.1	56.4	695.6	9.4

Table B-2. IC data for the reservoir grab samples from the trickling columns.

Date	min (0.25 hr)$^{-1}$	Low-N, Trickling Column			High-N, Trickling Column		
		NH_4^+	NO_2^-	NO_3^-	NH_4^+	NO_2^-	NO_3^-
			ppm N			ppm N	
10/13/10	0.8	0.4	5.1	195.7	583.1	17.9	0.6
10/20/10	0.8	0.4	3.2	163.7	195	267.6	32.7
10/27/10	0.8	0.4	0.3	220.4	21.5	314.7	208.5
11/3/10	0.8	0.4	287.7	220.6	14	560.1	429.4
11/10/10	0.8	0.4	0.3	239.3	1.9	305.8	651.9
11/17/10	0.8i	0.4	0.3	250	2.2	34.3	905.3
11/24/10	0.8i	0.4	0.3	210.7	55.1	475.6	348
12/1/10	0.8i	0.4	0.3	234.2	11.9	7.7	976
12/8/10	0.8i	0.4	0.3	395.9	15.3	24.4	888.7
12/15/10	0.8i	0.4	0.3	202.6	67.1	14.6	814.3
12/23/10	0.8i	0.4	0.3	205.4	65.5	0.3	887.2
12/30/10	0.8i	0.4	0.3	232.3	73.7	144.8	963
1/5/11	0.5	0.4	0.3	250.6	7.1	3.8	1102.2
1/12/11	0.5	0.4	0.3	238.5	6.8	2.5	997.3
1/19/11	0.5	0.4	0.3	232.9	4	3.6	1024.6
1/26/11	0.5	0.4	0.3	224.4	0.4	0.3	0.3
2/3/11	0.5	0.4	0.3	274.8	0.4	4.9	725.6
2/10/11	0.3	10.6	1.6	218.4	72.5	15.3	686.2
2/17/11	0.3	10.2	1.5	201.9	66.3	21.5	799.3
2/24/11	0.3	0.4	1	263	114.3	12.1	869.3
3/3/11	0.3	0.4	181.3	0.3	113.5	0.5	952
3/9/11	0.2	8.4	2.6	200.5	57.6	8	857.1
3/18/11	0.2	17.4	1.9	175.6	57	2.5	963.1
3/24/11	0.2	17.2	3.9	113	56.3	6.3	825.6
3/31/11	0.2	6.8	2.4	169.1	51.3	2.6	924.2
4/7/11	0.8f	1.9	0.3	221.5	30.1	0.3	811.7
4/14/11	0.8f	1.9	0.3	267.2	62.3	1.1	867.9
4/21/11	0.8f	2.9	0.3	244.5	68.6	1	890.9
4/28/11	0.8f	3.3	0.3	216.2	99.5	1.5	885.6

Vertical Profile Samples

Table B-3. Vertical profiles of N species from water samples collected at the time of LESA sampling. Sample below detection limit are marked n.d., unavailable samples are marked --.

Portal	NH_4^+	NO_2^-	NO_3^-
Low–N Tidal Column, 24i Cycles Day^{-1}			
1	12.6	9.8	164.2
2	12.1	10.5	181.2
3	12.9	7.7	176.0
4	14.0	10.5	177.3
High-N, Tidal Column, 24i Cycles Day^{-1}			
1	n.d.	531.6	206.4
2	55.6	492.2	176.0
3	61.1	488.5	180.0
4	50.1	466.3	172.0
Low-N, Trickling Column, 0.8i min (0.25 hr)$^{-1}$			
1	--	--	--
2	--	--	--
3	6.0	3.8	194.5
4	7.1	3.6	192.7
High-N, Trickling Column, 0.8i min (0.25 hr)$^{-1}$			
1	--	--	--
2	42.4	35.1	728.6
3	41.1	30.5	726.7
4	39.7	27.9	716.3
Low–N Tidal, Column, 16 Cycles Day^{-1}			
1	n.d.	1.2	1.3
2	6.9	5.9	1.4
3	n.d.	7.2	1.3
4	n.d.	4.5	1.4
High–N, Tidal Column, 16 Cycles day^{-1}			
1	66.9	618.1	0.8
2	71.6	605.9	0.5
3	68.5	557.3	0.5
4	98.2	554.2	0.5
Low-N, Trickling Column, 0.5 min (0.25 hr)$^{-1}$			
1	--	n.d.	1.3
2	--	n.d.	1.3
3	157.3	n.d.	1.4
4	--	n.d.	1.2
High-N, Trickling Column, 0.5 min (0.25 hr)$^{-1}$			
1	--	--	--
2	--	--	--
3	64.6076	1	6.5094

Portal	NH_4^+	NO_2^-	NO_3^-
High-N, Trickling Column, 0.5 min (0.25 hr)$^{-1}$			
4	61.8	1	6.7
Low–N Tidal Column, 8 Cycles Day^{-1}			
1	n.d.	1.2	1.3
2	6.9	5.9	1.4
3	n.d.	7.2	1.3
4	n.d.	4.5	1.4
High–N, Tidal Column, 8 Cycles Day^{-1}			
1	66.9	618.1	0.8
2	71.6	605.9	0.5
3	68.5	557.3	0.5
4	98.2	554.2	0.5
Low-N, Trickling Column, 0.3 min (0.25 hr)$^{-1}$			
1	n.d	n.d.	1.9
2	n.d	n.d	1.9
3	n.d	n.d.	2.0
4	n.d	n.d.	1.8
High-N, Trickling Column, 0.3 min (0.25 hr)$^{-1}$			
1	--	--	--
2	--	--	--
3	64.6	n.d.	6.5
4	61.8	n.d.	6.9
Low–N Tidal, Column, 4 Cycles Day^{-1}			
1	8.0	1.2	130.4
2	11.7	1.4	140.3
3	9.8	8.5	125.1
4	11.6	4.1	126.3
High–N, Tidal Column, 4 Cycles Day^{-1}			
1	153.8	647.9	36.1
2	164.6	670.2	32.4
3	309.3	652.2	42.7
4	268.1	676.7	34.5
Low-N, Trickling Column, 0.2 min (0.25 hr)$^{-1}$			
1	--	--	--
2	--	--	--
3	15.1	1.2	269.2
4	15.5	5.0	225.6

Portal	NH_4^+	NO_2^-	NO_3^-
High-N, Trickling Column, 0.2 min (0.25 hr)$^{-1}$			
1	--	--	--
2	--	--	--
3	31.3	4.2	769.8
4	33.6	4.5	779.7
Low-N, Tidal Column, 24f Cycles Day^{-1}			
1	--	1.2	130.4
2	--	1.4	140.3
3	--	8.5	125.1
4	--	4.1	126.3
High-N, Tidal Column, 24f Cycles Day^{-1}			
1	--	647.9	36.1
2	--	670.2	32.4
3	--	652.2	42.7
4	--	676.7	34.5
Low-N, Trickling Column, 0.8f min (0.25 hr)$^{-1}$			
1	--	--	--
2	--	--	--
3	--	1.2	269.2
4	--	5.0	225.6
High-N, Trickling Column, 0.8f min (0.25 hr)$^{-1}$			
1	--	--	--
2	--	--	--
3	--	4.2	769.8
4	--	4.5	779.7

C. Appendix III – Sonde Data

Table C-1. Data for temperature (Temp.), pH, oxidation-reduction potential (ORP), specific conductivity (S.C.), dissolved oxygen (D.O.), and NH_4^+, collected using the YSI sonde at Worrell Water for the Low-N, tidal column.

Date	Temp (°C)	pH	ORP (mV)	S.C. (µS/cm)	DO (mg/L)	NH_4^+ (mg-N L^{-1})
11/15/10	18.8	7.1	457.0	3.2	4.7	1.9
11/16/10	18.6	6.9	528.0	2.9	4.4	1.8
11/18/10	18.2	6.9	486.0	2.6	5.2	1.6
11/22/10	18.7	6.9	489.0	2.5	5.4	1.8
11/23/10	19.1	7.0	535.0	0.1	4.2	1.2
11/29/10	18.2	7.2	519.0	4.4	3.6	1.7
11/30/10	18.3	6.8	370.0	4.0	3.8	2.4
12/2/10	18.1	6.3	559.0	4.1	3.7	4.4
12/6/10	17.9	6.7	557.0	0.0	5.5	1.4
12/7/10	17.8	6.8	523.0	0.0	4.2	1.2
12/9/10	17.7	6.4	654.0	3.0	4.4	1.2
12/13/10	17.5	6.9	496.0	3.0	4.0	1.2
12/14/10	17.4	6.7	511.0	2.8	3.6	1.4
12/17/10	17.4	6.6	509.0	2.4	3.4	1.2
12/20/10	17.6	6.8	478.0	2.6	4.9	1.3
12/21/10	17.6	6.5	537.0	0.9	5.0	1.4
12/28/10	17.6	6.7	478.0	2.6	6.3	1.4
12/29/10	17.6	6.6	533.0	2.8	4.4	1.6
12/30/10	17.9	6.6	482.0	0.0	4.4	1.4
1/3/11	18.0	6.7	462.0	2.8	5.6	1.5
1/4/11	18.0	6.4	423.0	2.4	4.1	2.1
1/5/11	17.6	6.6	516.0	2.1	3.0	9.2
1/6/11	17.8	6.8	485.0	2.2	3.9	1.5
1/7/11	18.0	6.7	508.0	2.1	2.7	1.9
1/10/11	18.0	7.0	537.0	2.3	3.4	1.5
1/13/11	18.0	6.8	525.0	2.1	2.5	1.6
1/14/11	18.0	6.8	525.0	2.0	2.4	1.6
1/17/11	18.0	6.8	520.0	2.2	3.1	1.6
1/20/11	18.2	6.8	513.0	2.0	2.3	1.7
1/21/11	18.1	6.8	519.0	1.9	2.6	1.7
1/24/11	17.9	7.0	521.0	2.0	3.1	1.6
1/25/11	18.1	7.1	502.0	2.0	2.5	1.8
1/27/11	17.9	7.0	518.0	1.9	2.4	1.6
1/28/11	17.9	6.9	534.0	1.9	2.4	1.6
1/31/11	17.7	7.1	526.0	2.1	3.1	1.4

Date	Temp (°C)	pH	ORP (mV)	S.C. (μS/cm)	DO (mg/L)	NH_4^+ (mg-N L^{-1})
2/1/11	17.8	7.0	505.0	2.1	2.7	1.7
2/2/11	18.1	6.9	488.0	2.0	2.3	2.0
2/4/11	17.4	6.9	504.0	2.0	2.4	1.5
2/7/11	17.5	6.8	511.0	2.1	2.5	1.5
2/8/11	17.4	7.0	516.0	2.1	2.1	4.8
2/9/11	17.5	6.8	499.0	2.1	2.1	6.4
2/11/11	17.4	6.7	499.0	1.9	2.1	4.9
2/14/11	17.8	7.0	507.0	2.1	2.1	1.6
2/15/11	17.6	6.9	502.0	2.0	1.8	4.1
2/16/11	17.5	6.9	646.0	2.0	1.8	13.0
2/18/11	18.2	6.8	509.0	1.9	1.8	5.4
2/21/11	18.1	6.9	523.0	2.0	2.1	1.6
2/23/11	17.4	6.9	520.0	2.0	1.7	6.4
3/3/11	18.0	7.0	527.0	2.2	2.2	7.8
3/4/11	17.5	7.0	581.0	2.1	2.7	6.9
3/7/11	17.8	7.0	542.0	2.1	2.4	3.7
3/9/11	17.6	7.1	549.0	2.0	1.4	17.1
3/11/11	18.2	7.0	549.0	1.9	1.6	14.7
3/14/11	17.6	7.1	548.0	2.1	1.6	5.7
3/16/11	17.7	7.2	572.0	1.9	1.3	14.7
3/18/11	19.6	7.1	344.0	1.8	1.9	20.8
3/21/11	18.7	7.1	526.0	1.9	1.6	7.4
3/23/11	19.8	7.2	527.0	1.8	4.2	15.1
3/25/11	18.5	7.1	532.0	1.7	1.6	25.8
3/28/11	17.5	7.1	538.0	1.8	1.9	6.7
4/1/11	18.3	7.2	520.0	1.7	2.1	17.6
4/4/11	19.2	6.8	460.0	1.9	2.0	10.7
4/6/11	20.6	7.0	508.0	1.7	2.4	6.2
4/8/11	21.3	7.2	491.0	1.6	2.4	2.0
4/12/11	22.7	7.0	496.0	1.8	2.6	2.3
4/13/11	22.0	7.0	525.0	1.7	2.8	2.1
4/15/11	22.0	7.0	505.0	1.6	2.9	2.2
4/18/11	21.1	7.1	493.0	1.9	3.4	2.3
4/20/11	22.6	7.0	502.0	1.8	2.9	2.2
4/22/11	20.6	7.0	497.0	1.7	3.3	1.9
4/26/11	23.3	6.9	524.0	1.9	2.6	2.5
4/27/11	23.1	7.0	543.0	1.9	2.5	2.2
4/29/11	22.5	7.0	512.0	1.8	2.6	2.2
5/3/2011	23.3	7.0	501.0	1.9	2.4	2.7
5/4/2011	22.0	7.0	513.0	1.9	2.5	2.3

Table C-2. Data for temperature (Temp.), pH, oxidation-reduction potential (ORP), specific conductivity (S.C.), dissolved oxygen (D.O.), and NH_4^+, collected using the YSI sonde at Worrell Water for the High-N, tidal column.

Date	Temp (°C)	pH	ORP (mV)	S.C. (µS/cm)	DO (mg/L)	NH_4^+ (mg-N L^{-1})
11/15/10	18.6	7.0	465.0	9.0	4.0	2.2
11/16/10	18.5	6.8	530.0	8.6	2.5	19.7
11/18/10	18.0	6.7	493.0	7.8	2.7	9.5
11/22/10	18.5	6.8	495.0	8.1	3.7	2.3
11/23/10	18.7	7.0	532.0	8.1	2.3	24.0
11/29/10	18.0	7.2	518.0	7.6	3.5	1.4
11/30/10	18.2	6.9	381.0	7.5	2.2	15.2
12/2/10	17.9	6.6	554.0	7.1	2.6	13.1
12/6/10	17.5	6.8	523.0	0.0	3.7	1.9
12/7/10	17.6	6.7	523.0	7.9	2.5	1.2
12/9/10	17.6	6.4	617.0	7.4	2.5	10.2
12/13/10	17.4	6.9	501.0	7.2	3.1	1.4
12/14/10	17.3	6.7	517.0	7.4	2.3	13.8
12/17/10	17.4	8.5	482.0	8.2	1.4	over range
12/20/10	17.4	6.6	488.0	8.7	2.6	19.9
12/21/10	17.4	6.6	546.0	8.6	2.6	29.0
12/28/10	17.4	6.8	486.0	8.8	4.4	2.0
12/29/10	17.6	7.0	528.0	9.9	2.4	65.2
12/30/10	17.8	6.7	490.0	9.5	2.5	39.8
1/3/11	17.9	6.6	472.0	9.6	3.3	3.5
1/4/11	17.9	6.4	449.0	8.3	3.3	24.6
1/5/11	17.8	7.1	528.0	7.4	3.0	54.6
1/6/11	17.7	6.6	498.0	7.7	2.4	25.8
1/7/11	17.7	6.7	517.0	7.5	1.8	42.2
1/10/11	17.7	6.6	552.0	8.1	2.4	7.8
1/13/11	17.8	6.8	535.0	7.2	2.1	47.7
1/14/11	17.8	6.8	534.0	7.1	2.0	50.6
1/17/11	17.9	6.6	533.0	7.8	2.1	8.6
1/20/11	17.9	6.9	523.0	7.4	2.0	51.8
1/21/11	18.1	6.8	528.0	7.2	2.0	47.0
1/24/11	17.8	6.7	534.0	7.7	259.0	6.9
1/25/11	18.0	7.0	512.0	7.5	2.0	33.9
1/27/11	17.7	6.9	529.0	7.1	2.2	45.1
1/28/11	17.6	6.9	546.0	7.1	2.4	46.2
1/31/11	17.4	6.8	541.0	7.8	2.2	26.9
2/1/11	17.7	7.0	514.0	7.6	2.6	40.3
2/2/11	18.0	6.9	496.0	7.3	2.0	42.3

Date	Temp (°C)	pH	ORP (mV)	S.C. (µS/cm)	DO (mg/L)	NH_4^+ (mg-N L^{-1})
2/4/11	17.1	7.1	512.0	7.1	2.7	55.0
2/7/11	17.4	6.9	522.0	7.5	2.3	19.0
2/8/11	17.4	7.7	516.0	8.4	1.7	95.7
2/9/11	17.4	7.6	500.0	8.3	1.7	over range
2/11/11	17.3	7.5	501.0	7.7	1.6	over range
2/14/11	17.7	7.2	516.0	7.8	1.9	54.2
2/15/11	17.5	7.4	505.0	7.5	1.7	71.1
2/16/11	17.3	7.6	631.0	7.5	1.6	99.6
2/18/11	18.1	7.4	516.0	6.5	2.0	83.7
2/21/11	17.2	8.7	501.0	7.7	1.8	over range
2/23/11	16.9	8.9	420.0	6.1	0.4	over range
3/3/11	16.7	7.2	530.0	4.5	4.1	42.6
3/4/11	17.0	7.3	579.0	5.5	3.0	64.5
3/7/11	17.9	7.6	536.0	6.5	2.5	over range
3/9/11	17.6	7.9	533.0	6.4	1.3	over range
3/11/11	17.7	8.1	522.0	6.3	0.5	over range
3/14/11	17.5	8.9	492.0	7.2	1.5	over range
3/16/11	17.5	9.0	483.0	6.6	0.4	over range
3/18/11	19.4	9.0	442.0	7.7	1.1	over range
3/21/11	18.4	9.1	449.0	8.7	0.9	over range
3/23/11	20.2	8.7	481.0	7.4	1.8	over range
3/25/11	18.8	8.5	502.0	7.3	1.9	over range
3/28/11	17.7	8.3	509.0	8.4	2.8	over range
4/1/11	18.0	8.5	487.0	7.4	1.1	over range
4/4/11	18.9	8.3	403.0	8.5	1.5	over range
4/6/11	19.3	8.5	410.0	7.4	0.4	over range
4/8/11	21.3	7.2	499.0	5.5	2.6	95.5
4/12/11	22.5	6.9	508.0	5.5	2.9	19.9
4/13/11	22.0	6.9	536.0	4.7	3.8	4.2
4/15/11	21.8	6.8	519.0	5.1	4.1	16.6
4/18/11	21.2	6.8	506.0	5.9	5.2	3.5
4/20/11	22.4	6.6	517.0	5.6	3.0	44.1
4/22/11	20.6	6.7	509.0	5.6	3.2	35.8
4/26/11	23.4	6.7	537.0	6.4	2.8	34.2
4/27/11	23.2	6.8	552.0	6.4	2.7	46.6
4/29/11	22.5	6.8	525.0	6.5	2.9	24.8
5/3/11	23.4	6.9	512.0	6.8	2.8	18.3

Table C-3. Data for temperature (Temp.), pH, oxidation-reduction potential (ORP), specific conductivity (S.C.), dissolved oxygen (D.O.), and NH_4^+, collected using the YSI sonde at Worrell Water for the Low-N, trickling column.

Date	Temp (°C)	pH	ORP (mV)	S.C. (μS/cm)	DO (mg/L)	NH_4^+ (mg-N L^{-1})
11/15/10	19.3	7.3	454.0	3.2	6.7	1.7
11/16/10	18.9	7.1	520.0	3.0	6.2	2.6
11/18/10	18.5	7.2	483.0	2.9	7.1	1.8
11/22/10	19.2	7.2	485.0	2.7	7.0	1.7
11/23/10	19.3	7.2	521.0	2.6	6.2	2.5
11/29/10	18.5	7.4	510.0	3.0	6.8	1.3
11/30/10	18.6	7.2	395.0	2.8	6.2	2.0
12/2/10	18.4	6.9	545.0	2.5	7.2	2.1
12/6/10	18.2	7.0	543.0	2.8	7.2	1.4
12/7/10	18.2	7.0	514.0	2.7	6.4	2.0
12/9/10	18.2	6.8	608.0	2.5	6.4	1.6
12/13/10	18.1	7.0	494.0	2.6	6.4	1.3
12/14/10	18.0	6.2	510.0	2.5	5.9	2.2
12/17/10	18.1	7.5	485.0	2.4	4.8	24.4
12/20/10	17.6	6.8	477.0	2.5	2.1	2.0
12/21/10	17.6	7.8	523.0	2.4	1.4	34.9
12/28/10	18.1	7.2	475.0	2.6	9.8	1.5
12/29/10	18.2	7.3	516.0	2.8	5.3	2.5
12/30/10	18.2	7.1	480.0	2.7	5.5	2.4
1/3/11	18.3	6.9	463.0	2.9	5.2	1.7
1/4/11	18.3	6.6	432.0	2.4	5.7	2.4
1/5/11	18.3	6.8	515.0	2.3	4.7	10.1
1/6/11	18.2	6.7	487.0	2.3	6.0	2.3
1/7/11	18.3	6.8	506.0	2.2	4.9	2.5
1/10/11	18.3	6.7	540.0	2.5	5.3	1.9
1/13/11	18.3	6.8	525.0	2.2	5.1	2.1
1/14/11	18.3	6.7	525.0	2.2	5.3	1.9
1/17/11	18.3	6.6	523.0	2.5	5.4	2.0
1/20/11	18.5	6.8	513.0	2.2	5.2	2.0
1/21/11	18.5	6.9	519.0	2.1	5.2	2.3
1/24/11	18.3	6.8	525.0	2.4	6.0	1.9
1/25/11	18.5	6.9	504.0	2.3	5.5	2.4
1/27/11	18.3	7.0	519.0	2.1	5.6	2.0
1/28/11	18.2	7.0	536.0	2.1	5.2	2.0
1/31/11	18.1	6.9	530.0	2.4	5.7	2.2
2/1/11	18.2	6.9	504.0	2.3	5.9	2.4
2/2/11	18.7	6.9	486.0	2.2	5.2	2.5

Date	Temp (°C)	pH	ORP (mV)	S.C. (µS/cm)	DO (mg/L)	NH_4^+ (mg-N L^{-1})
2/4/11	17.9	6.8	504.0	2.1	5.1	2.0
2/7/11	18.0	6.9	512.0	2.3	4.8	2.2
2/8/11	17.9	7.1	507.0	2.2	4.1	3.2
2/9/11	17.8	7.3	491.0	2.2	3.9	3.9
2/11/11	17.8	7.3	494.0	2.1	3.6	2.8
2/14/11	18.2	7.0	506.0	2.3	4.0	2.9
2/15/11	18.2	7.2	498.0	2.2	3.5	3.0
2/16/11	18.0	7.3	619.0	2.2	3.2	5.4
2/18/11	18.8	6.9	510.0	2.9	3.6	5.2
2/21/11	18.4	7.8	505.0	3.0	3.7	4.7
2/23/11	17.9	7.9	443.0	2.6	2.9	7.6
3/3/11	18.3	6.9	526.0	2.8	3.4	3.0
3/4/11	18.0	7.1	575.0	2.6	3.1	5.4
3/7/11	18.2	7.3	533.0	3.7	3.7	6.9
3/9/11	18.0	7.3	5.3	2.3	2.5	11.5
3/11/11	18.3	7.9	524.0	2.2	2.0	7.8
3/14/11	18.2	7.8	513.0	2.3	2.9	6.5
3/16/11	18.3	7.9	521.0	2.2	2.0	14.5
3/18/11	19.9	7.7	482.0	1.9	2.7	24.4
3/21/11	19.6	8.1	465.0	2.2	3.0	32.9
3/23/11	20.5	7.7	492.0	2.0	2.5	25.0
3/25/11	19.2	7.9	504.0	1.9	2.3	35.2
3/28/11	18.1	7.7	504.0	2.1	3.3	11.3
4/1/11	18.5	7.7	495.0	3.0	3.2	50.0
4/4/11	19.9	7.8	410.0	2.8	3.0	8.7
4/6/11	20.8	7.5	440.0	2.4	4.5	4.8
4/8/11	21.8	7.2	490.0	2.2	4.9	4.3
4/12/11	23.2	7.0	497.0	2.3	4.8	4.5
4/13/11	22.7	6.9	529.0	2.8	4.2	3.4
4/15/11	22.6	7.0	506.0	2.5	5.1	4.0
4/18/11	21.7	6.8	497.0	2.8	5.5	2.8
4/20/11	23.2	6.7	507.0	2.5	4.3	5.6
4/22/11	21.1	6.7	498.0	2.3	4.8	3.0
4/26/11	24.0	6.7	528.0	2.4	4.5	9.6
4/27/11	23.7	6.7	544.0	2.3	4.4	5.9
4/29/11	23.0	6.7	519.0	2.9	4.5	5.4
5/3/11	23.9	6.8	504.0	2.8	4.3	8.0
5/4/11	22.7	6.6	517.0	2.7	5.2	7.6
5/6/11	21.0	6.5	509.0	2.6	5.8	3.9

Table C-4. Data for temperature (Temp.), pH, oxidation-reduction potential (ORP), specific conductivity (S.C.), dissolved oxygen (D.O.), NH$_4^+$ and total dissolved solids (TDS), collected using the YSI sonde at Worrell Water for the Low-N, trickling column.

Date	Temp (°C)	pH	ORP (mV)	S.C. (μS/cm)	DO (mg/L)	NH$_4^+$ (mg-N L^{-1})
11/16/10	18.8	6.6	533.0	8.8	6.3	7.3
11/18/10	18.4	7.4	487.0	7.9	4.1	39.1
11/22/10	18.9	8.5	456.0	10.1	2.3	over range
11/23/10	19.2	8.6	480.0	9.8	1.9	over range
11/29/10	18.5	6.7	525.0	9.3	6.8	13.3
11/30/10	18.6	6.5	413.0	9.0	5.7	22.4
12/2/10	18.3	6.2	537.0	7.6	7.1	17.4
12/6/10	17.9	6.4	556.0	8.5	7.0	19.1
12/7/10	18.1	6.4	527.0	8.6	5.9	29.3
12/9/10	18.1	6.1	618.0	8.4	6.6	32.6
12/13/10	18.0	6.2	509.0	8.6	6.5	30.8
12/14/10	17.9	6.2	525.0	8.4	5.5	36.2
12/17/10	18.0	6.8	499.0	8.0	4.4	42.1
12/20/10	17.9	6.1	492.0	8.7	6.0	30.5
12/21/10	17.9	6.8	539.0	8.4	6.2	39.4
12/28/10	18.0	6.3	491.0	9.6	8.1	33.3
12/29/10	18.3	6.8	525.0	10.3	4.4	37.7
12/30/10	18.2	6.4	494.0	9.9	5.3	42.8
1/3/11	18.3	6.1	478.0	10.6	5.4	49.5
1/4/11	18.3	5.8	459.0	8.9	5.8	40.3
1/5/11	18.3	6.9	526.0	7.6	4.2	30.8
1/6/11	18.1	6.0	501.0	8.2	6.2	30.1
1/7/11	18.2	6.1	521.0	8.0	4.3	28.3
1/10/11	18.2	5.8	553.0	9.1	5.2	30.9
1/13/11	18.3	5.6	538.0	8.0	4.7	33.1
1/14/11	18.3	5.9	538.0	7.8	4.5	31.6
1/17/11	18.3	5.7	536.0	9.1	5.5	36.7
1/20/11	18.5	5.7	527.0	8.2	5.1	32.5
1/21/11	18.1	7.3	526.0	7.9	1.0	53.3
1/24/11	18.0	8.8	479.0	8.9	2.0	over range
1/25/11	18.2	8.9	457.0	8.6	1.0	over range
1/28/11	18.1	6.9	539.0	3.7	3.7	38.7
1/31/11	18.0	6.1	542.0	5.9	6.0	21.1
2/1/11	18.2	6.0	518.0	6.1	5.9	30.2
2/2/11	18.6	6.1	500.0	6.2	5.2	33.7
2/4/11	17.7	5.7	516.0	6.2	5.2	28.7

Date	Temp (°C)	pH	ORP (mV)	S.C. (µS/cm)	DO (mg/L)	NH_4^+ (mg-N L^{-1})
2/7/11	17.9	6.2	524.0	6.8	5.2	7.0
2/8/11	17.8	6.4	518.0	5.6	5.3	6.8
2/9/11	17.8	6.5	505.0	5.8	3.8	19.7
2/11/11	17.7	6.5	506.0	6.2	3.6	21.8
2/14/11	18.1	6.1	518.0	7.2	4.0	4.1
2/15/11	18.2	6.5	513.0	7.2	2.4	9.5
2/16/11	18.0	6.1	623.0	7.1	4.0	19.5
2/18/11	18.8	6.3	521.0	6.9	3.5	17.8
2/21/11	18.3	6.7	519.0	8.2	3.8	19.9
2/23/11	17.9	6.4	479.0	7.6	2.4	35.4
3/3/11	18.3	6.4	542.0	9.4	2.7	46.8
3/4/11	17.9	6.6	597.0	8.7	2.3	44.4
3/7/11	18.1	6.5	552.0	9.5	3.4	41.6
3/9/11	18.0	6.8	549.0	7.9	2.0	46.4
3/11/11	18.3	6.8	546.0	7.3	2.1	36.8
3/14/11	18.3	6.7	539.0	8.4	3.3	30.0
3/16/11	18.4	7.1	547.0	7.7	2.1	41.3
3/18/11	20.0	7.0	508.0	7.5	3.7	54.2
3/21/11	19.6	6.6	497.0	8.5	4.7	55.7
3/23/11	20.5	7.1	513.0	7.6	3.1	44.0
3/25/11	19.2	7.1	530.0	7.1	2.5	42.1
3/28/11	18.2	6.4	528.0	8.1	5.3	27.7
4/1/11	18.3	6.9	511.0	6.4	4.9	33.4
4/4/11	20.0	6.8	438.0	7.2	3.1	24.1
4/6/11	21.2	6.7	437.0	6.8	5.2	37.2
4/8/11	21.7	6.4	501.0	6.8	5.4	24.2
4/12/11	23.2	6.3	511.0	7.9	4.5	44.3
4/13/11	22.6	6.5	540.0	7.6	5.4	36.3
4/15/11	22.6	5.5	532.0	7.4	6.6	29.9
4/18/11	22.0	5.1	537.0	8.5	7.4	23.3
4/20/11	23.5	6.4	519.0	7.9	4.4	51.1
4/22/11	21.2	5.3	527.0	7.6	5.9	28.7
4/26/11	24.2	7.5	509.0	8.8	3.7	over range
4/27/11	23.9	7.0	538.0	8.4	2.8	over range
4/29/11	23.2	5.5	550.0	6.9	5.9	2.6
5/3/11	24.1	6.9	508.0	7.8	4.2	68.4
5/4/11	22.8	6.8	520.0	7.6	4.4	56.6
5/6/11	21.1	6.4	519.0	7.3	5.2	31.7
5/9/11	22.7	5.3	538.0	8.5	5.6	46.1
5/11/11	23.5	5.2	558.0	7.9	5.4	43.3

D. Appendix IV – Microscopy Count Data

Table D-1. Abundance counts from each field of view for each replicate sample. AOB = Ammonia oxidizing bacteria, TAB = Total Abundance of Bacteria, NOB = Nitrite oxidizing bacteria, AXB = anaerobic ammonia oxidizing (anammox) bacteria. – indicates a field was not counted. // indicates the sample was flawed.

Tidal, Low-N, 24i Cycles Day^{-1}

Portal Replicate	Functional Group	1	2	3	4	5	6	7	8	9	10	Average Cells Field^{-1}
1a	TAB	64	19	62	37	45	96	–	–	–	–	53.83
	AOB	7	3	2	2	0	2	5	16	0	7	4.40
	NOB	0	0	7	0	0	0	0	0	0	0	0.70
	AXB	1	3	0	0	0	0	0	0	0	0	0.40
1b	TAB	41	64	82	143	98	–	–	–	–	–	85.60
	AOB	7	8	1	9	9	0	0	0	3	0	3.70
	NOB	1	0	0	0	0	0	0	0	0	0	0.10
	AXB	1	1	0	0	0	0	0	0	0	0	0.20
1c	TAB	34	32	13	92	73	53	52	–	–	–	49.86
	AOB	6	3	4	0	5	4	6	18	3	4	5.30
	NOB	1	0	0	0	0	0	0	0	0	0	0.10
	AXB	0	0	0	0	0	0	0	0	0	0	0.00
2a	TAB	44	68	49	42	7	–	–	–	–	–	42.00
	AOB	8	1	0	30	1	4	0	0	0	21	6.50
	NOB	1	0	0	0	0	0	0	0	0	0	0.10
	AXB	1	2	7	3	1	2	0	0	0	0	1.60
2b	TAB	37	42	88	62	24	–	–	–	–	–	50.60
	AOB	7	36	9	8	2	1	6	6	0	94	16.90
	NOB	0	3	0	0	0	1	0	0	0	0	0.40
	AXB	0	0	0	0	0	0	0	0	0	0	0.00
2c	TAB	162	161	72	70	147	–	–	–	–	–	122.40
	AOB	5	5	9	11	25	26	6	1	8	0	9.60
	NOB	15	0	0	4	1	17	0	2	1	0	4.00
	AXB	1	0	0	0	0	0	0	0	0	0	0.10
3a	TAB	54	47	51	63	133	–	–	–	–	–	69.60
	AOB	0	0	17	67	46	25	29	45	40	32	30.10
	NOB	0	1	0	49	14	2	15	25	16	10	13.20
	AXB	1	2	6	2	0	0	0	0	0	0	1.10
3b	TAB	47	47	41	24	15	–	–	–	–	–	34.80
	AOB	34	63	3	54	23	8	40	6	59	28	31.80
	NOB	14	83	10	63	11	3	25	1	21	7	23.80
	AXB	0	0	0	0	3	0	0	0	0	0	0.30
3c	TAB	30	12	42	17	21	26	26	20	71	30	29.50
	AOB	26	39	17	34	25	46	11	9	34	–	26.78
	NOB	6	0	4	0	0	3	22	0	52	0	8.70
	AXB	0	1	0	0	0	0	0	0	0	0	0.00

Tidal, Low-N, 24i Cycles Day⁻¹

Portal Replicate	Functional Group	Microscope Field										Average Cells Field⁻¹
		1	*2*	*3*	*4*	*5*	*6*	*7*	*8*	*9*	*10*	
4a	TAB	67	7	51	95	29	–	–	–	–	–	49.80
	AOB	38	10	1	29	6	0	41	72	42	8	24.70
	NOB	0	0	0	1	1	0	34	6	5	6	5.30
	AXB	0	0	0	0	0	0	0	0	0	0	0
4b	TAB	87	78	69	11	184	–	–	–	–	–	85.80
	AOB	87	17	113	3	22	2	0	5	48	48	34.50
	NOB	7	9	4	4	11	0	0	4	26	19	8.40
	AXB	3	0	0	0	0	0	0	0	0	0	0.30
4c	TAB	72	40	36	51	72	–	–	–	–	–	54.20
	AOB	40	36	20	22	26	0	27	24	23	29	24.70
	NOB	9	18	11	38	15	0	13	9	10	21	14.40
	AXB	0	0	0	0	0	0	0	0	0	0	0.00

Tidal, High-N, 24i Cycles Day⁻¹

Portal Replicate	Functional Group	Microscope Field									Average Cells Field⁻¹
		1	*2*	*3*	*4*	*5*	*6*	*7*	*8*	*9*	
1a	TAB	17	34	24	52	52	17	52	22	44	34.89
	AOB	10	3	9	1	7	2	22	23	15	10.22
	NOB	5	5	0	0	3	1	3	0	5	2.44
	AXB	8	2	6	0	0	0	0	0	0	1.78
1b	TAB	20	21	84	53	67	73	76	14	82	54.44
	AOB	0	6	0	11	1	8	6	5	7	4.89
	NOB	0	1	0	6	5	3	2	0	6	2.56
	AXB	0	0	0	0	0	0	0	0	0	0.00
1c	TAB	60	51	44	52	55	–	–	–	–	52.40
	AOB	0	2	2	4	0	0	0	0	2	1.11
	NOB	0	2	0	2	0	0	0	0	0	0.44
	AXB	2	0	0	0	0	0	0	0	0	0.22
2a	TAB	24	6	5	15	17	46	30	4	38	20.56
	AOB	12	0	0	0	3	1	0	0	0	1.78
	NOB	0	0	1	0	2	0	0	0	0	0.33
	AXB	3	0	0	0	0	0	0	0	0	0.33
2b	TAB	49	64	57	119	44	24	32	34	78	55.67
	AOB	4	0	6	0	7	0	2	1	3	2.56
	NOB	1	0	1	0	2	0	1	0	0	0.56
	AXB	1	0	0	0	0	0	0	0	0	0.11
2c	TAB	21	32	24	21	9	71	42	59	27	34.00
	AOB	5	2	8	4	1	3	0	15	7	5.00
	NOB	2	3	6	4	3	3	0	4	3	3.11
	AXB	1	1	1	0	0	0	0	0	0	0.33
3a	TAB	0	16	4	0	9	15	7	0	3	6.00
	AOB	8	3	3	11	6	2	2	0	3	4.22
	NOB	0	0	0	3	1	1	0	0	1	0.67
	AXB	3	0	0	0	0	0	0	0	0	0.33

Tidal, High-N, 24i Cycles Day^{-1}

Portal Replicate	Functional Group	Microscope Field									Average Cells Field^{-1}
		1	2	3	4	5	6	7	8	9	
3b	TAB	2	14	0	9	24	8	1	0	32	10.00
	AOB	1	3	0	14	5	0	4	6	36	7.67
	NOB	0	0	0	0	0	0	5	0	10	1.67
	AXB	1	0	0	0	0	0	0	0	0	0.11
3c	TAB	1	2	16	4	0	7	3	4	0	4.11
	AOB	6	12	0	0	0	0	0	2	0	2.22
	NOB	5	1	0	0	0	0	0	1	0	0.78
	AXB	2	2	0	0	0	0	0	0	0	0.44
4a	TAB	12	6	6	0	5	13	15	14	15	9.56
	AOB	1	2	10	17	6	9	2	13	6	7.33
	NOB	0	1	4	5	5	1	0	7	1	2.67
	AXB	1	0	4	0	0	0	0	0	0	0.56
4b	TAB	1	17	45	6	4	6	29	44	13	18.33
	AOB	0	3	7	1	4	4	0	5	0	2.67
	NOB	0	0	2	0	1	0	0	3	0	0.67
	AXB	0	0	0	0	0	0	0	0	0	0.00
4c	TAB	6	4	30	25	10	28	7	3	30	15.89
	AOB	4	0	7	3	0	0	4	1	4	2.56
	NOB	0	0	0	2	0	0	1	3	0	0.67
	AXB	1	4	0	0	0	0	0	0	0	0.56

Trickling, Low-N, 0.8i min (0.25 hr)$^{-1}$

Portal Replicate	Functional Group	Microscope Field										Average Cells Field^{-1}
		1	2	3	4	5	6	7	8	9	10	
1a	TAB	14	38	15	16	19	11	12	75	5	12	21.70
	AOB	4	0	4	0	0	1	2	4	5	8	2.80
	NOB	4	0	0	0	0	0	0	2	1	1	0.80
	AXB	0	0	0	0	0	0	0	0	0	0	0
1b	TAB	5	2	21	11	13	3	6	11	9	11	9.20
	AOB	0	2	0	4	0	11	34	2	5	1	5.90
	NOB	0	0	0	2	0	1	3	0	1	0	0.70
	AXB	0	1	1	0	0	0	0	0	0	0	0.22
1c	TAB	3	4	3	13	1	6	10	34	22	2	9.80
	AOB	1	2	2	0	3	4	0	4	0	6	2.20
	NOB	0	0	0	0	0	0	0	1	0	1	0.20
	AXB	9	0	0	0	0	0	0	0	0	0	0.90
2a	TAB	10	20	28	13	11	12	7	1	9	3	11.40
	AOB	0	1	3	4	5	1	2	0	35	0	5.10
	NOB	0	0	1	1	0	0	0	0	0	0	0.20
	AXB	1	0	0	0	0	0	0	0	0	0	0.10
2b	TAB	3	25	17	23	13	11	7	8	16	17	14.00
	AOB	4	4	0	0	14	3	1	0	5	4	3.50
	NOB	1	0	0	0	5	3	1	0	0	4	1.40
	AXB	0	1	3	0	0	0	0	0	0	0	0.44

Trickling, Low-N, 0.8i min (0.25 hr)$^{-1}$

Portal Replicate	Functional Group	1	2	3	4	5	6	7	8	9	10	Average Cells Field^{-1}
						Microscope Field						
2c	TAB	3	1	6	11	4	2	49	2	19	7	10.40
	AOB	3	1	1	1	2	8	10	3	5	0	3.40
	NOB	0	0	1	0	0	1	4	0	2	0	0.80
	AXB	1	1	6	0	0	0	0	0	0	0	0.80
3a	TAB	12	25	92	87	48	–	–	–	–	–	52.80
	AOB	11	81	32	32	46	30	21	9	6	9	27.70
	NOB	3	20	8	16	0	9	0	4	0	5	6.50
	AXB	2	1	1	0	0	0	0	0	0	0	0.40
3b	TAB	14	3	16	8	1	58	26	2	31	137	29.60
	AOB	0	22	10	23	7	6	5	13	6	8	10.00
	NOB	0	0	4	2	4	4	4	7	6	5	3.60
	AXB	2	0	0	0	0	0	0	0	0	0	0.20
3c	TAB	23	37	14	35	32	54	6	129	107	84	52.10
	AOB	28	11	28	19	9	20	16	20	15	22	18.80
	NOB	6	7	11	8	6	7	3	14	6	7	7.50
	AXB	1	5	4	0	0	0	0	0	0	0	1.00
4a	TAB	19	192	72	28	43	116	57	46	31	34	63.80
	AOB	2	17	2	4	21	19	6	7	7	19	10.40
	NOB	2	0	3	1	3	3	1	2	3	2	2.00
	AXB	0	0	0	0	0	0	0	0	0	0	0.00
4b	TAB	8	14	15	18	19	20	29	16	16	23	17.80
	AOB	7	9	12	11	6	4	14	5	4	8	8.00
	NOB	4	4	5	4	2	1	2	4	2	12	4.00
	AXB	2	0	0	0	0	0	0	0	0	0	0.20
4c	TAB	11	5	17	56	1	5	14	14	3	6	13.20
	AOB	3	3	1	5	2	16	23	54	10	13	13.00
	NOB	1	3	0	0	7	0	2	15	7	2	3.70
	AXB	1	0	0	0	0	0	0	0	0	0	0.00

Trickling, High-N, 0.8i min (0.25 hr)$^{-1}$

Portal Replicate	Functional Group	1	2	3	4	5	6	7	8	9	10	Average Cells Field^{-1}
						Microscope Field						
1a	TAB	47	37	1	27	5	0	10	4	8	54	19.30
	AOB	0	8	5	3	27	13	2	5	14	15	9.20
	NOB	0	1	0	1	5	1	0	0	0	0	0.80
	AXB	3	3	0	0	0	0	0	0	0	0	0.60
1b	TAB	31	9	31	4	27	21	69	13	11	16	23.20
	AOB	0	4	15	12	2	2	7	0	5	4	5.10
	NOB	0	0	0	0	0	1	0	0	0	0	0.10
	AXB	1	1	1	1	2	0	0	0	0	0	0.60
1c	TAB	10	8	1	0	2	0	5	3	5	2	3.60
	AOB	4	12	8	15	14	6	6	8	6	12	9.10
	NOB	0	2	0	0	0	0	1	0	2	2	0.70
	AXB	0	0	0	0	0	0	0	0	0	0	1.00

Trickling, High-N, 0.8i min (0.25 hr)$^{-1}$

Portal Replicate	Functional Group	Microscope Field										Average Cells Field^{-1}
		1	*2*	*3*	*4*	*5*	*6*	*7*	*8*	*9*	*10*	
2a	TAB	14	20	9	88	11	12	40	26	37	21	27.80
	AOB	7	6	17	8	7	18	4	10	12	5	9.40
	NOB	2	0	3	0	1	2	1	6	1	0	1.60
	AXB	0	1	0	0	0	0	0	0	0	0	0.10
2b	TAB	1	6	8	4	3	5	4	4	46	17	9.80
	AOB	8	0	1	2	4	0	8	6	8	3	4.00
	NOB	0	0	0	1	2	0	2	0	2	0	0.70
	AXB	1	2	0	0	0	0	0	0	0	0	0.30
2c	TAB	18	24	7	91	63	22	70	57	21	11	38.40
	AOB	21	12	8	6	5	12	0	5	7	5	8.10
	NOB	2	3	2	2	1	2	0	1	0	0	1.30
	AXB	0	0	1	0	0	0	0	0	0	0	0.10
3a	TAB	7	0	6	10	10	30	4	14	1	1	8.30
	AOB	2	4	3	0	0	1	26	2	9	5	5.20
	NOB	0	1	0	0	0	0	0	0	3	0	0.40
	AXB		16	3	0	0	0	0	0	0	0	2.11
3b	TAB	2	12	0	0	1	0	3	14	3	3	3.80
	AOB	6	0	13	10	0	4	0	5	0	4	4.20
	NOB	1	0	1	4	0	0	0	0	1	0	0.70
	AXB	0	6	2	0	0	0	0	0	0	0	0.89
3c	TAB	0	3	1	0	3	4	4	7	12	3	3.70
	AOB	0	6	7	7	0	0	7	2	12	2	4.30
	NOB	0	0	1	0	0	0	0	0	0	0	0.10
	AXB	0	1	1	1	0		0	0	0	0	0.33
4a	TAB	85	37	77	32	43	98	73	66	105	93	70.90
	AOB	4	12	8	15	14	6	6	8	6	12	9.10
	NOB	0	2	2	3	2	0	3	1	0	2	1.50
	AXB	0	5	0	0	0	0	0	0	0	0	0.50
4b	TAB	13	95	35	80	12	22	7	5	15	46	33.00
	AOB	13	18	12	18	5	16	25	4	11	15	13.70
	NOB	3	0	3	3	2	0	2	1	3	3	2.00
	AXB	2	1	0	0	0	0	0	0	0	0	0.30
4c	TAB	16	13	21	15	37	21	7	6	8	13	15.70
	AOB	24	28	25	17	18	21	15	27	29	26	23.00
	NOB	0	2	0	0	0	2	0	2	6	4	1.60
	AXB	1	1	0	0	0	0	0	0	0	0	0.20

Tidal, Low-N, 16-cycles Day^{-1}

Portal Replicate	Functional Group	Microscope Field										Average Cells Field^{-1}
		1	*2*	*3*	*4*	*5*	*6*	*7*	*8*	*9*	*10*	
1a	TAB	37	11	51	20	112	–	–	–	–	–	46.20
	AOB	9	12	8	0	0	5	0	2	9	8	5.30
	NOB	1	2	0	1	2	0	1	1	1	3	1.20
	AXB	3	1	1	0	0	0	0	0	0	0	0.50

Tidal, Low-N, 16-cycles Day^{-1}

Portal Replicate	Functional Group	Microscope Field										Average Cells Field^{-1}
		1	*2*	*3*	*4*	*5*	*6*	*7*	*8*	*9*	*10*	
1b	TAB	48	29	7	23	75	24	–	–	–	–	34.33
	AOB	4	11	6	3	0	5	0	2	3	4	3.80
	NOB	0	2	0	0	0	0	0	0	1	0	0.30
	AXB	1	3	2	1	0	0	0	0	0	0	0.70
1c	TAB	13	24	15	43	22	40	32	20	0	0	26.13
	AOB	4	1	6	2	10	3	5	3	0	5	3.90
	NOB	0	1	0	0	2	2	1	1	0	0	0.70
	AXB	2	3	1	2	1	0	0	0	0	0	0.90
2a	TAB	68	65	56	96	71	–	–	–	–	–	71.20
	AOB	17	3	10	3	12	6	3	5	1	7	6.70
	NOB	6	1	3	1	2	1	0	1	2	1	1.80
	AXB	0	0	0	0	0	0	0	0	0	0	0.00
2b	TAB	13	17	9	3	0	3	16	5	0	2	6.80
	AOB	1	0	2	0	0	2	0	0	0	4	0.90
	NOB	1	0	0	0	0	0	0	0	0	0	0.10
	AXB	1	2	1	0	0	0	0	0	0	0	0.40
2c	TAB	33	47	47	55	36	–	–	–	–	–	43.60
	AOB	7	5	0	2	0	2	5	8	8	12	4.90
	NOB	3	4	0	0	0	0	0	2	1	4	1.40
	AXB	1	1	0	1	0	1	0	0	0	2	0.60
3a	TAB	153	126	189	12	68	–	–	–	–	–	109.60
	AOB	3	6	8	2	4	1	4	4	8	11	5.10
	NOB	1	1	1	1	2	1	2	1	0	0	1.00
	AXB	1	0	0	0	0	0	0	0	0	0	0.10
3b	TAB	46	40	48	65	25	–	–	–	–	–	44.80
	AOB	9	25	6	33	8	25	19	27	16	18	18.60
	NOB	1	0	0	0	0	0	0	0	0	0	0.10
	AXB	3	2	0	1	0	0	0	1	1	0	0.80
3c	TAB	18	95	6	59	44	–	–	–	–	–	44.40
	AOB	10	12	7	6	3	1	6	0	20	3	6.80
	NOB	1	2	0	0	0	0	0	0	0	0	0.30
	AXB	2	1	2	0	0	0	1	0	0	0	0.60
4a	TAB	47	69	29	83	73	–	–	–	–	–	60.20
	AOB	5	11	8	3	15	8	1	7	0	11	6.90
	NOB	1	2	0	3	3	2	1	1	2	0	1.50
	AXB	0	2	1	0	0	0	2	2	0	0	0.70
4b	TAB	30	17	63	54	33	–	–	–	–	–	39.40
	AOB	10	4	3	1	6	7	5	6	5	3	4.80
	NOB	1	1	0	0	0	0	0	0	0	0	0.20
	AXB	1	0	0	0	0	0	0	0	0	0	0.10
4c	TAB	4	7	5	2	2	1	6	0	0	0	2.70
	AOB	3	5	6	3	5	4	2	0	0	2	3.00
	NOB	0	0	0	1	1	1	1	0	0	0	0.40
	AXB	1	0	0	0	0	0	0	0	0	0	0.10

Tidal, High-N, 16-cycles Day^{-1}

Portal Replicate	Functional Group	Microscope Field										Average Cells Field^{-1}
		1	2	3	4	5	6	7	8	9	10	
1a	TAB	16	35	47	30	48	36	−	−	−	−	35.33
	AOB	6	2	2	8	2	4	3	6	1	0	3.40
	NOB	2	1	1	3	0	3	0	0	0	0	1.00
	AXB	0	0	0	2	0	0	1	0	0	0	0.30
1b	TAB	44	56	67	50	32	−	−	−	−	−	49.80
	AOB	9	6	2	3	12	2	2	2	6	7	5.10
	NOB	2	1	0	4	18	4	3	8	0	3	4.30
	AXB	1	1	0	0	0	0	0	0	0	0	0.20
1c	TAB	17	720	77	44	43	−	−	−	−	−	180.20
	AOB	7	12	6	25	12	10	13	11	1	8	10.50
	NOB	1	2	7	6	4	2	7	6	5	0	4.00
	AXB	1	1	0	0	0	0	0	0	0	0	0.20
2a	TAB	710	239	330	108	510	−	−	−	−	−	379.40
	AOB	5	18	5	8	11	9	23	4	8	10	10.10
	NOB	1	2	2	8	3	4	4	2	3	3	3.20
	AXB	0	0	0	2	1	1	0	1	0	0	0.50
2b	TAB	25	29	23	15	20	47	9	22	51	−	26.78
	AOB	20	14	0	9	1	0	3	8	1	1	5.70
	NOB	6	1	0	0	0	0	0	0	0	0	0.70
	AXB	4	1	0	0	1	0	2	3	6	0	1.70
2c	TAB	810	216	64	138	104	−	−	−	−	−	266.40
	AOB	40	69	5	69	64	−	−	−	−	−	49.40
	NOB	2	4	11	0	1	−	−	−	−	−	3.60
	AXB	1	0	2	1	0	0	0	2	2	4	1.20
3a	TAB	116	102	75	700	129	−	−	−	−	−	224.40
	AOB	7	13	13	73	11	11	38	107	−	−	34.13
	NOB	4	4	1	4	8	7	15	-	−	−	6.14
	AXB	1	0	0	1	0	0	1	0	0	0	0.30
3b	TAB	104	111	78	84	128	−	−	−	−	−	101.00
	AOB	2	39	69	6	32	25	26	−	−	−	28.43
	NOB	4	7	3	3	5	4	0	−	−	−	3.71
	AXB	0	2	0	0	1	0	1	0	0	0	0.40
3c	TAB	120	710	166	600	33	−	−	−	−	−	325.80
	AOB	4	48	17	11	85	82	−	−	−	−	41.17
	NOB	3	7	8	5	7	2	−	−	−	−	5.33
	AXB	1	1	1	2	7	1	0	0	0	0	1.30
4a	TAB	1130	790	560	720	630	−	−	−	−	−	766.00
	AOB	49	2	97	11	103	−	−	−	−	−	52.40
	NOB	2	2	8	0	8	1	0	0	2	8	3.10
	AXB	0	2	0	0	0	−	−	−	−	−	0.40
4b	TAB	207	164	172	190	126	−	−	−	−	−	171.80
	AOB	13	53	67	8	75	−	−	−	−	−	43.20
	NOB	4	0	6	6	4	−	−	−	−	−	4.00
	AXB	0	0	0	0	0	0	0	0	0	0	0.00

		Tidal, High-N, 16-cycles Day^{-1}	

Tidal, High-N, 16-cycles Day^{-1}

Portal Replicate	Functional Group	1	2	3	4	5	6	7	8	9	10	Average Cells Field^{-1}
4c	TAB	166	192	1100	730	179	−	−	−	−	−	473.40
	AOB	69	28	37	47	81	−	−	−	−	−	52.40
	NOB	4	2	7	11	0	−	−	−	−	−	4.80
	AXB	0	0	0	0	1	0	0	1	1	0	0.30

Trickling, Low-N, 0.5 min (0.25 hr)$^{-1}$

Portal Replicate	Functional Group	1	2	3	4	5	6	7	8	9	10	Average Cells Field^{-1}
1a	TAB	73	76	85	90	14	−	−	−	−	−	67.60
	AOB	6	6	7	6	20	37	1	4	1	9	9.70
	NOB	2	0	3	0	4	7	0	2	4	2	2.40
	AXB	1	0	0	1	1	0	0	0	1	0	0.40
1b	TAB	44	126	85	36	30	−	−	−	−	−	64.20
	AOB	0	16	13	3	4	2	6	1	6	2	5.30
	NOB	0	1	1	1	1	0	2	1	0	3	1.00
	AXB	0	0	1	0	2	0	0	1	2	0	0.60
1c	TAB	9	61	87	24	65	−	−	−	−	−	49.20
	AOB	2	11	13	27	4	3	4	11	14	10	9.90
	NOB	2	4	1	0	0	2	0	1	1	0	1.10
	AXB	1	0	0	1	0	0	0	0	1	1	0.40
2a	TAB	32	30	86	48	45	−	−	−	−	−	48.20
	AOB	8	0	20	0	4	29	9	18	0	6	9.40
	NOB	5	0	2	1	0	1	3	1	0	3	1.60
	AXB	2	0	0	1	1	0	0	0	0	0	0.40
2b	TAB	37	87	50	73	43	−	−	−	−	−	58.00
	AOB	28	2	6	5	5	33	0	1	8	31	11.90
	NOB	2	1	1	2	3	2	0	2	4	0	1.70
	AXB	2	0	1	0	2	0	2	0	0	2	0.90
2c	TAB	56	73	92	0	11	−	−	−	−	−	46.40
	AOB	26	11	16	0	0	8	10	0	0	0	7.10
	NOB	4	0	1	0	0	1	2	0	0	0	0.80
	AXB	0	0	0	1	0	0	1	0	1	0	0.30
3a	TAB	13	36	48	24	17	42	51	−	−	−	33.00
	AOB	3	4	7	8	6	4	2	8	5	4	5.10
	NOB	1	0	0	2	0	5	0	5	0	2	1.50
	AXB	0	0	0	2	2	0	0	0	1	0	0.50
3b	TAB	12	38	51	71	34	33	−	−	−	−	39.83
	AOB	7	16	8	0	5	3	2	1	0	4	4.60
	NOB	1	1	0	0	3	1	0	0	0	0	0.60
	AXB	0	1	0	1	0	0	0	0	0	0	0.20
3c	TAB	54	7	59	14	22	25	23	−	−	−	29.14
	AOB	5	20	6	3	8	8	8	7	3	13	8.10
	NOB	1	3	2	1	0	0	3	1	0	1	1.20
	AXB	0	0	0	0	0	0	1	1	0	0	0.20

Trickling, Low-N, 0.5 min (0.25 hr)

Trickling, Low-N, 0.5 min (0.25 hr)$^{-1}$

Portal Replicate	Functional Group	1	2	3	4	5	6	7	8	9	10	Average Cells Field^{-1}
	TAB	5	25	11	12	6	5	20	72	3	8	16.70
4a	AOB	3	1	1	0	0	1	0	1	2	2	1.10
	NOB	1	0	0	0	0	1	0	0	0	0	0.20
	AXB	2	1	0	0	0	0	0	0	0	0	0.30
	TAB	18	31	48	26	36	40	35	–	–	–	31.80
4b	AOB	10	5	5	2	3	12	7	3	5	11	5.00
	NOB	4	0	0	2	0	1	0	4	1	0	1.20
	AXB	0	1	1	1	0	0	0	1	2	3	0.90
	TAB	28	13	28	47	48	68	–	–	–	–	38.67
4c	AOB	0	3	0	0	1	1	2	2	2	0	1.10
	NOB	0	0	0	0	0	0	0	0	0	0	0.00
	AXB	1	0	0	0	0	0	0	0	0	0	0.10

Trickling, High-N, 0.5 min (0.25 hr)$^{-1}$

Portal Replicate	Functional Group	1	2	3	4	5	6	7	8	9	10	Average Cells Field^{-1}
	TAB	21	63	8	10	12	24	61	29	–	–	28.50
1a	AOB	2	38	25	12	6	65	10	37	8	–	22.56
	NOB	0	0	0	5	4	1	3	5	7	–	2.78
	AXB	1	0	1	0	1	0	2	1	0	0	0.60
	TAB	94	68	70	34	58	–	–	–	–	–	64.80
1b	AOB	3	16	4	9	19	12	4	0	13	9	8.90
	NOB	5	2	0	1	0	0	0	0	4	0	1.20
	AXB	0	0	0	0	0	0	1	0	0	1	0.20
	TAB	23	12	61	36	29	37	18	59	–	–	34.38
1c	AOB	4	3	0	3	3	10	0	2	12	1	3.80
	NOB	2	2	1	0	0	2	2	0	2	0	1.10
	AXB	0	0	2	0	0	0	2	0	1	0	0.50
	TAB	75	46	5	27	34	72	–	–	–	–	43.17
2a	AOB	2	2	6	3	0	2	0	7	18	8	4.80
	NOB	0	0	2	0	0	1	0	0	3	1	0.70
	AXB	0	0	0	0	1	0	0	0	0	0	0.10
	TAB	39	37	28	23	25	59	7	16	–	–	29.25
2b	AOB	10	6	3	4	0	4	3	23	6	11	7.00
	NOB	3	5	0	6	0	0	0	0	0	4	1.80
	AXB	0	0	0	1	0	0	1	1	0	0	0.30
	TAB	53	55	43	48	69	–	–	–	–	–	53.60
2c	AOB	10	3	0	0	7	0	1	0	3	0	2.40
	NOB	4	2	0	0	3	8	0	0	0	0	1.70
	AXB	1	3	0	1	0	2	0	0	2	0	0.90
	TAB	91	47	66	41	75	–	–	–	–	–	64.00
3a	AOB	22	21	3	13	1	17	15	0	22	41	15.50
	NOB	1	3	0	2	1	1	3	6	1	2	2.00
	AXB	0	1	0	0	0	1	1	0	2	1	0.60

Trickling, High-N, 0.5 min (0.25 hr)$^{-1}$

Portal Replicate	Functional Group	Microscope Field										Average Cells Field^{-1}
		1	2	3	4	5	6	7	8	9	10	
3b	TAB	49	23	44	74	40	–	–	–	–	–	46.00
	AOB	5	12	14	0	8	1	4	2	2	66	11.40
	NOB	0	2	2	0	0	2	2	1	1	5	1.50
	AXB	2	0	1	0	1	1	0	1	0	0	0.60
3c	TAB	24	53	16	47	56	33	–	–	–	–	38.17
	AOB	1	0	1	3	8	0	0	3	5	2	2.30
	NOB	0	0	0	1	1	0	1	1	2	2	0.80
	AXB	1	1	0	2	1	0	0	0	0	0	0.50
4a	TAB	29	46	23	42	63	–	–	–	–	–	40.60
	AOB	1	4	5	5	1	3	11	12	0	21	6.30
	NOB	0	1	3	4	0	1	2	8	0	3	2.20
	AXB	0	0	1	0	0	0	1	2	0	0	0.40
4b	TAB	214	26	81	52	73	–	–	–	–	–	89.20
	AOB	4	3	5	0	0	0	0	0	0	0	1.20
	NOB	4	1	0	0	0	0	0	0	0	0	0.50
	AXB	0	1	0	0	1	0	0	2	0	0	0.40
4c	TAB	27	43	67	68	41	–	–	–	–	–	49.20
	AOB	1	4	3	43	78	4	3	2	0	6	14.40
	NOB	4	3	2	6	12	2	1	4	1	2	3.70
	AXB	1	1	2	0	0	1	0	0	0	0	0.50

Tidal, Low-N, 8-cycles Day^{-1}

Portal Replicate	Functional Group	Microscope Field										Average Cells Field^{-1}
		1	2	3	4	5	6	7	8	9	10	
1a	TAB	19	62	58	27	42	–	–	–	–	–	41.6
	AOB	10	95	14	4	3	0	0	28	8	10	17.2
	NOB	1	18	11	0	0	0	0	23	2	0	5.5
	AXB	0	0	0	0	0	0	0	0	0	0	0
1b	TAB	33	25	10	0	45	74	23	10	15	24	25.9
	AOB	2	0	1	0	0	1	2	8	0	1	1.5
	NOB	0	0	0	0	0	2	1	0	0	0	0.3
	AXB	0	0	0	0	0	0	0	0	0	0	0
1c	TAB	28	88	10	63	50	–	–	–	–	–	47.8
	AOB	19	16	36	48	21	10	0	0	4	28	18.2
	NOB	6	1	0	37	5	2	7	2	0	1	6.1
	AXB	0	0	0	0	0	0	0	0	0	0	0
2a	TAB	76	27	47	125	40	–	–	–	–	–	63
	AOB	5	6	0	5	0	0	4	4	0	0	2.4
	NOB	0	0	2	0	1	0	0	3	0	0	0.6
	AXB	0	0	0	0	0	0	0	0	0	0	0
2b	TAB	6	29	61	77	71	–	–	–	–	–	48.8
	AOB	0	2	0	2	1	0	75	0	0	0	8
	NOB	0	2	0	6	0	0	0	0	0	1	0.9
	AXB	1	1	1	0	0	0	0	0	0	0	0.3

Tidal, Low-N, 8-cycles Day^{-1}

Portal Replicate	Functional Group	Microscope Field										Average Cells Field^{-1}
		1	*2*	*3*	*4*	*5*	*6*	*7*	*8*	*9*	*10*	
2c	TAB	12	90	34	40	4	–	–	–	–	–	36
	AOB	28	5	0	8	6	8	0	21	55	0	13.1
	NOB	5	0	0	3	0	3	0	0	0	0	1.1
	AXB	0	0	0	0	0	0	0	0	0	0	0
3a	TAB	55	11	16	46	93	–	–	–	–	–	44.2
	AOB	0	2	48	0	4	2	63	3	5	40	16.7
	NOB	0	0	1	0	1	1	22	5	3	4	3.7
	AXB	0	0	0	0	0	0	0	0	0	0	0
3b	TAB	9	174	60	128	23	–	–	–	–	–	78.8
	AOB	4	4	0	0	9	10	3	0	2	28	6
	NOB	0	6	0	0	0	5	2	0	4	26	4.3
	AXB	0	0	0	0	0	0	0	0	0	0	0
3c	TAB	46	108	27	7	98	–	–	–	–	–	57.2
	AOB	24	0	33	1	8	33	51	64	117	20	35.1
	NOB	15	2	6	1	0	0	1	0	2	0	2.7
	AXB	0	0	0	0	0	0	0	0	0	0	0
4a	TAB	10	302	85	68	61	–	–	–	–	–	105.2
	AOB	2	0	26	2	35	111	0	1	0	39	21.6
	NOB	0	0	2	4	2	5	0	0	0	0	1.3
	AXB	0	0	0	0	0	0	0	0	0	0	0
4b	TAB	16	20	120	223	22	–	–	–	–	–	80.2
	AOB	7	3	7	2	13	5	134	0	0	0	17.1
	NOB	2	2	1	0	7	0	0	0	0	0	1.2
	AXB	0	0	0	0	0	0	0	0	0	0	0
4c	TAB	51	137	88	172	12	–	–	–	–	–	92
	AOB	48	38	30	5	0	26	107	12	40	98	40.4
	NOB	11	5	3	0	0	0	18	3	25	7	7.2
	AXB	1	0	0	0	0	0	0	0	0	0	0.1

Tidal, High-N, 8-cycles Day^{-1}

Portal Replicate	Functional Group	Microscope Field										Average Cells Field^{-1}
		1	*2*	*3*	*4*	*5*	*6*	*7*	*8*	*9*	*10*	
1a	TAB	59	85	41	50	41	–	–	–	–	–	55.2
	AOB	21	11	3	4	0	8	43	143	21	7	26.1
	NOB	0	4	0	0	0	2	5	0	2	0	1.3
	AXB	1	1	0	0	0	0	0	0	0	0	0.2
1b	TAB	57	43	75	41	16	109	34	17	69	23	48.4
	AOB	111	52	7	63	6	88	10	8	3	5	35.3
	NOB	4	6	4	0	2	0	0	2	1	0	1.9
	AXB	0	0	0	0	0	0	0	0	0	0	0
1c	TAB	96	116	57	43	73	–	–	–	–	–	77
	AOB	1	10	15	0	5	25	0	100	41	8	20.5
	NOB	0	0	2	0	3	5	0	4	2	4	2
	AXB	0	0	0	0	0	0	0	0	0	0	0

Tidal, High-N, 8-cycles Day^{-1}

Portal Replicate	Functional Group	Microscope Field										Average Cells Field^{-1}
		1	*2*	*3*	*4*	*5*	*6*	*7*	*8*	*9*	*10*	
2a	TAB	120	17	74	46	44	–	–	–	–	–	60.2
	AOB	19	61	29	53	32	10	41	54	8	3	31
	NOB	0	0	0	0	0	0	0	0	0	0	0
	AXB	0	0	0	0	0	0	0	0	0	0	0
2b	TAB	34	66	440	47	109	–	–	–	–	–	139.2
	AOB	57	152	2	13	66	39	1	7	34	47	41.8
	NOB	2	1	0	0	0	0	0	0	0	0	0.3
	AXB	1	1	0	0	0	0	0	0	0	0	0.2
2c	TAB	107	155	77	138	410	–	–	–	–	–	177.4
	AOB	97	74	30	13	40	25	5	10	116	0	41
	NOB	2	0	4	0	0	0	0	0	0	1	0.7
	AXB	0	0	0	0	0	0	0	0	0	0	0
3a	TAB	47	61	23	33	89	–	–	–	–	–	50.6
	AOB	0	63	1	23	1	3	20	1	46	0	15.8
	NOB	0	8	2	0	0	2	1	0	0	0	1.3
	AXB	0	0	0	0	0	0	0	0	0	0	0
3b	TAB	141	113	135	110	190	–	–	–	–	–	137.8
	AOB	13	164	0	73	46	35	0	116	80	208	73.5
	NOB	3	42	0	4	13	11	0	80	8	85	24.6
	AXB	1	2	1	1	0	0	0	0	0	0	0.5
3c	TAB	175	175	175	254	109	–	–	–	–	–	177.6
	AOB	6	1	0	0	12	0	1	4	11	3	3.8
	NOB	0	1	0	0	0	0	0	0	0	0	0.1
	AXB	0	0	0	0	0	0	0	0	0	0	0
4a	TAB	165	86	101	268	58	–	–	–	–	–	135.6
	AOB	0	10	2	1	16	8	15	169	35	98	35.4
	NOB	1	5	2	2	42	15	32	0	0	0	9.9
	AXB	0	0	0	0	0	0	0	0	0	0	0
4b	TAB	68	63	95	106	70	–	–	–	–	–	80.4
	AOB	5	2	33	81	21	15	0	88	2	5	25.2
	NOB	1	0	1	0	0	0	0	3	0	2	0.7
	AXB	0	0	0	0	0	0	0	0	0	0	0
4c	TAB		264	123	59	66	163	–	–	–	–	135
	AOB	55	75	78	5	0	31	91	41	40	91	50.7
	NOB	34	56	50	0	0	20	8	30	11	0	20.9
	AXB		1	0	0	0	0	0	0	0	0	0.11

Trickling, Low-N, 0.5 min (0.25 hr)$^{-1}$

Portal Replicate	Functional Group	Microscope Field										Average Cells Field^{-1}
		1	*2*	*3*	*4*	*5*	*6*	*7*	*8*	*9*	*10*	
1a	TAB	15	7	640	18	17	8	9	96	200	40	105
	AOB	3	0	2	1	0	0	12	0	0	1	1.9
	NOB	2	2	1	3	0	0	0	0	0	0	0.8
	AXB	1	1	1	0	0	0	0	0	0	0	0.3

Trickling, Low-N, 0.5 min (0.25 hr)$^{-1}$

Portal Replicate	Functional Group	Microscope Field										Average Cells Field^{-1}
		1	*2*	*3*	*4*	*5*	*6*	*7*	*8*	*9*	*10*	
1b	TAB	34	47	35	11	5	4	3	22	13	9	18.3
	AOB	23	2	2	3	0	2	1	3	0	10	4.6
	NOB	5	0	1	5	0	0	0	2	0	0	1.3
	AXB	0	0	0	0	0	0	0	0	0	0	0
1c	TAB	12	6	46	116	87	–	–	–	–	–	53.4
	AOB	46	47	2	16	24	0	0	0	0	0	13.5
	NOB	1	4	0	0	0	0	0	0	0	0	0.5
	AXB	0	0	0	0	0	0	0	0	0	0	0
2a	TAB	12	5	2	102	10	15	20	2	19	46	23.3
	AOB	8	15	1	1	1	3	0	0	0	0	2.9
	NOB	1	0	0	0	0	0	0	0	0	0	0.1
	AXB	0	0	0	0	0	0	0	0	0	0	0
2b	TAB	3	99	28	12	90	58	21	14	20	56	40.1
	AOB	2	47	10	0	2	0	7	4	0	4	7.6
	NOB	4	3	0	0	2	0	2	5	0	2	1.8
	AXB	0	0	0	0	0	0	0	0	0	0	0
2c	TAB	16	2	18	18	7	155	2	192	12	12	43.4
	AOB	5	1	0	0	0	0	0	0	0	0	0.6
	NOB	0	0	0	0	0	0	0	0	0	0	0
	AXB	0	0	0	0	0	0	0	0	0	1	0.1
3a	TAB	5	62	50	12	9	11	10	53	8	3	22.3
	AOB	1	1	1	0	0	0	0	0	0	0	0.3
	NOB	2	0	0	0	0	0	0	0	0	0	0.2
	AXB	0	0	0	0	0	0	0	0	0	0	0
3b	TAB	2	8	9	6	4	13	3	16	31	17	10.9
	AOB	2	7	2	1	0	0	0	0	0	0	1.2
	NOB	3	1	2	0	0	0	0	0	0	0	0.6
	AXB	0	0	0	0	0	0	0	0	0	0	0
3c	TAB	11	0	18	4	0	3	0	0	2	5	4.3
	AOB	1	15	0	0	0	0	0	0	0	0	1.6
	NOB	0	0	0	0	0	0	0	0	0	0	0
	AXB	0	0	0	0	0	0	0	0	0	0	0
4a	TAB	7	21	4	10	12	6	15	4	0	9	8.8
	AOB	0	2	0	0	0	0	0	0	0	0	0.2
	NOB	2	0	0	0	0	0	0	0	0	0	0.2
	AXB	0	0	0	0	0	0	0	0	0	0	0
4b	TAB	0	12	4	25	9	3	6	11	11	9	9
	AOB	3	9	0	0	1	0	0	0	0	0	1.3
	NOB	0	0	0	0	0	0	0	0	0	0	0
	AXB	0	0	0	0	0	0	0	0	0	0	0
4c	TAB	0	35	0	16	2	2	28	20	5	2	11
	AOB	4	0	0	0	0	0	0	0	0	0	0.4
	NOB	0	0	0	0	0	0	0	0	0	0	0
	AXB	1	0	0	0	0	0	0	0	0	0	0.1

Trickling, High-N, 0.5 min (0.25 hr)$^{-1}$

Portal Replicate	Functional Group	Microscope Field										Average Cells Field^{-1}
		1	*2*	*3*	*4*	*5*	*6*	*7*	*8*	*9*	*10*	
1a	TAB	3	3	63	8	16	179	0	103	12	40	42.7
	AOB	1	1	20	9	2	4	2	0	0	0	3.9
	NOB	1	1	2	0	0	0	0	0	0	0	0.4
	AXB	1	0	0	0	0	0	0	0	0	0	0.1
1b	TAB	54	12	21	2	17	11	19	12	3	3	15.4
	AOB	3	4	12	6	0	0	0	1	0	1	2.7
	NOB	1	2	2	8	0	1	0	0	0	1	1.5
	AXB	0	0	0	0	0	0	0	0	0	0	0
1c	TAB	18	10	55	2	21	9	15	78	6	20	23.4
	AOB	26	3	4	30	4	1	0	0	0	0	6.8
	NOB	1	1	1	13	1	1	0	0	0	0	1.8
	AXB	0	0	0	0	0	0	0	0	0	0	0
2a	TAB	3	8	3	13	30	4	3	18	7	23	11.2
	AOB	0	5	40	0	30	70	15	14	14	0	18.8
	NOB	0	2	4	0	6	0	1	0	0	0	1.3
	AXB	0	0	0	0	0	0	0	0	0	0	0
2b	TAB	13	3	15	13	121	34	18	21	14	32	28.4
	AOB	13	2	1	13	0	64	60	3	0	14	17
	NOB	2	2	0	3	0	5	9	0	0	4	2.5
	AXB	0	0	0	0	0	0	0	0	0	0	0
2c	TAB	5	93	17	18	69	–	–	–	–	–	40.4
	AOB	0	13	0	6	0	11	0	30	0	0	6
	NOB	1	0	0	0	0	0	0	0	0	0	0.1
	AXB	0	0	0	0	0	0	0	0	0	0	0
3a	TAB	54	85	141	1	90	–	–	–	–	–	74.2
	AOB	0	0	0	37	0	10	2	1	0	48	9.8
	NOB	0	0	0	3	0	3	0	0	0	0	0.6
	AXB	1	0	0	0	0	0	0	0	0	0	0.1
3b	TAB	88	4	83	1	5	8	162	–	–	–	50.14
	AOB	0	0	1	0	0	0	1	0	0	1	0.3
	NOB	2	0	0	0	0	0	0	0	0	0	0.2
	AXB	0	0	0	0	0	0	0	0	0	0	0
3c	TAB	6	0	4	394	130	3	13	5	17	1	57.3
	AOB	1	6	3	4	14	0	0	0	0	0	2.8
	NOB	3	2	2	0	0	0	0	0	0	0	0.7
	AXB	1	1	0	0	0	0	0	0	0	0	0.2
4a	TAB	21	15	4	1	8	4	5	7	17	14	9.6
	AOB	2	1	2	8	3	32	0	0	0	0	4.8
	NOB	5	1	1	0	0	0	0	0	0	0	0.7
	AXB	0	0	0	0	0	0	0	0	0	0	0
4b	TAB	7	114	200	54	127	–	–	–	–	–	100.4
	AOB	1	30	4	35	0	0	0	0	2	0	7.2
	NOB	0	3	1	1	0	0	1	0	0	0	0.6
	AXB	0	0	0	0	0	0	0	0	0	0	0

Trickling, High-N, 0.5 min (0.25 hr)$^{-1}$

Portal Replicate	Functional Group	Microscope Field										Average Cells Field^{-1}
		1	3	3	4	5	6	7	8	9	10	
4c	TAB	1	15	6	12	11	34	6	30	31	15	16.1
	AOB	1	1	4	2	0	0	0	0	0	0	0.8
	NOB	0	0	0	0	0	0	0	0	0	0	0
	AXB	0	0	0	0	0	0	0	0	0	0	0

Tidal Low-N, 4 Cycles Day^{-1}

Portal Replicate	Functional Group	Microscope Field										Average Cells Field^{-1}
		1	2	3	4	5	6	7	8	9	10	
1a	TAB	76	114	50	12	36	–	–	–	–	–	57.6
	AOB	3	3	2	2	0	0	0	0	0	0	2
	NOB	0	0	0	0	1	0	0	0	0	0	0.2
	AXB	0	0	0	0	0	0	0	0	0	0	0
1b	TAB	19	47	32	41	8	47	27	–	–	–	29.4
	AOB	8	11	10	2	1	4	6	0	6	2	6.4
	NOB	3	1	1	1	2	0	0	0	0	0	1.6
	AXB	1	1	2	0	0	0	0	0	0	0	0.8
1c	TAB	0	17	13	21	15	11	11	3	3	16	13.2
	AOB	4	7	4	6	9	5	0	0	0	6	6
	NOB	1	1	0	0	0	0	0	0	0	0	0.4
	AXB	1	1	1	0	0	0	0	0	0	0	0.6
2a	TAB	8	4	1	0	0	1	0	3	2	8	2.6
	AOB	2	0	0	9	0	15	22	16	6	5	2.2
	NOB	0	0	0	0	0	0	0	0	0	0	0
	AXB	0	1	0	0	0	0	0	0	0	0	0.2
2b	TAB	119	6	55	12	190	–	–	–	–	–	76.4
	AOB	11	1	13	5	23	0	44	24	2	12	10.6
	NOB	1	1	0	0	0	2	0	0	2	0	0.4
	AXB	0	1	0	2	0	0	0	0	0	0	0.6
2c	TAB	62	31	30	14	31	81	–	–	–	–	33.6
	AOB	7	10	8	6	4	8	10	0	3	12	7
	NOB	0	0	0	0	0	1	1	0	2	0	0
	AXB	0	2	1	0	0	0	0	0	0	0	0.6
3a	TAB	15	11	28	9	16	13	27	6	18	8	15.8
	AOB	2	2	0	0	33	35	7	0	2	4	7.4
	NOB	0	1	0	0	3	9	0	0	1	13	0.8
	AXB	0	0	0	0	0	0	0	0	0	0	0
3b	TAB	//	//	//	//	//	//	//	//	//	//	//
	AOB	//	//	//	//	//	//	//	//	//	//	//
	NOB	//	//	//	//	//	//	//	//	//	//	//
	AXB	//	//	//	//	//	//	//	//	//	//	//
3c	TAB	19	27	5	66	41	11	49	–	–	–	31.6
	AOB	3	1	16	0	3	1	0	0	4	0	4.6
	NOB	1	0	2	0	0	0	0	0	0	0	0.6
	AXB	0	0	0	0	0	0	0	0	0	0	0

Tidal Low-N, 4 Cycles Day^{-1}

Portal Replicate	Functional Group	1	2	3	4	5	6	7	8	9	10	Average Cells Field^{-1}
4a	TAB	46	10	19	32	11	49	135	–	–	–	23.6
	AOB	4	7	0	0	2	15	1	0	4	5	2.6
	NOB	1	1	1	1	0	0	0	0	0	0	0.8
	AXB	0	0	0	0	0	0	0	0	0	0	0
4b	TAB	//	//	//	//	//	//	//	//	//	//	//
	AOB	//	//	//	//	//	//	//	//	//	//	//
	NOB	//	//	//	//	//	//	//	//	//	//	//
	AXB	//	//	//	//	//	//	//	//	//	//	//
4c	TAB	20	14	95	36	55	13	–	–	–	–	44
	AOB	20	53	13	0	0	0	0	10	2	0	17.2
	NOB	0	0	0	0	0	0	0	0	0	0	0
	AXB		1	1	0	0	0	0	0	0	0	0.5

Tidal High-N, 4 Cycles Day^{-1}

Portal Replicate	Functional Group	1	2	3	4	5	6	7	8	9	10	Average Cells Field^{-1}
1a	TAB	26	86	14	27	29	33	3	0	46	29	29.30
	AOB	6	3	1	3	0	2	29	0	0	0	4.40
	NOB	0	0	1	3	6	0	3	0	0	0	1.30
	AXB	1	1	1	2	0	0	0	0	0	0	0.50
1b	TAB	4	5	0	2	53	2	25	9	41	35	17.60
	AOB	1	1	0	15	0	1	12	1	3	0	3.40
	NOB	0	2	0	2	4	0	0	0	0	0	0.80
	AXB	1	1	1	1	0	0	0	0	0	0	0.40
1c	TAB	48	55	16	30	36	19	66	20	18	28	33.60
	AOB	12	1	2	1	5	0	0	0	0	0	2.10
	NOB	2	0	4	0	1	2	0	0	2	0	1.10
	AXB	1	0	0	0	0	0	0	0	0	0	0.10
2a	TAB	12	11	4	28	10	49	5	2	2	0	12.30
	AOB	6	1	7	1	3	1	4	0	0	0	2.30
	NOB	6	0	0	0	0	0	0	0	0	0	0.60
	AXB	1	1	2	0	0	0	0	0	0	0	0.40
2b	TAB	42	32	61	67	17	–	–	–	–	–	43.80
	AOB	14	0	107	0	1	24	47	36	29	31	28.90
	NOB	1	0	0	0	0	0	0	0	0	0	0.10
	AXB	1	1	0	0	0	0	0	0	0	0	0.20
2c	TAB	33	55	42	68	63	–	–	–	–	–	52.20
	AOB	14	25	12	26	19	22	33	0	9	7	16.70
	NOB	2	1	1	0	1	1	0	0	0	2	0.80
	AXB	1	1	0	0	0	0	0	0	0	0	0.20
3a	TAB	42	86	57	60	46	–	–	–	–	–	58.20
	AOB	3	9	3	4	1	3	2	2	6	2	3.50
	NOB	1	0	0	0	1	0	2	0	0	1	0.50
	AXB	2	1	0	0	0	0	0	0	0	0	0.30

Tidal High-N, 4 Cycles Day^{-1}

Portal Replicate	Functional Group	Microscope Field										Average Cells Field^{-1}
		1	*2*	*3*	*4*	*5*	*6*	*7*	*8*	*9*	*10*	
3b	TAB	//	//	//	//	//	//	//	//	//	//	//
	AOB	//	//	//	//	//	//	//	//	//	//	//
	NOB	//	//	//	//	//	//	//	//	//	//	//
	AXB	//	//	//	//	//	//	//	//	//	//	//
3c	TAB	57	59	93	51	38	–	–	–	–	–	59.60
	AOB	6	2	9	3	2	1	18	4	4	7	5.60
	NOB	1	2	1	0	0	0	0	0	0	0	0.40
	AXB	1	1	1	0	0	0	0	0	0	0	0.30
4a	TAB	20	47	27	22	73	46	–	–	–	–	39.17
	AOB	0	0	3	6	2	5	10	6	0	1	3.30
	NOB	0	1	0	1	0	0	0	0	4	0	0.60
	AXB	1	1	1	1	2	0	0	0	0	0	0.60
4b	TAB	//	//	//	//	//	//	//	//	//	//	//
	AOB	//	//	//	//	//	//	//	//	//	//	//
	NOB	//	//	//	//	//	//	//	//	//	//	//
	AXB	//	//	//	//	//	//	//	//	//	//	//
4c	TAB	12	2	0	2	0	3	1	0	5	1	2.60
	AOB	1	0	0	3	7	1	13	1	0	0	2.60
	NOB	1	0	0	0	0	0	0	0	0	0	0.10
	AXB	1	1	1	2	0	0	0	0	0	0	0.50

Trickling Low-N, 0.2 min (0.25 hr)$^{-1}$

Portal Replicate	Functional Group	Microscope Field										Average Cells Field^{-1}
		1	*2*	*3*	*4*	*5*	*6*	*7*	*8*	*9*	*10*	
1a	TAB	33	15	51	39	26	73	47	14	22	66	38.60
	AOB	10	1		2	3	3	2	2	0	0	2.56
	NOB	5	2	1	2	0	0	0	0	0	0	1.00
	AXB	0	1	0	0	1	1	0	0	0	0	0.30
1b	TAB	46	35	29	37	20	23	26	24	30	25	29.50
	AOB	53	15	68	10	29	25	15	43	31	19	30.80
	NOB	1	0	0	0	0	0	0	0	0	0	0.10
	AXB	0	1	0	0	0	0	1	1	0	0	0.30
1c	TAB	4	12	23	40	22	30	110	–	–	–	34.43
	AOB	25	30	35	5	10	7	1	7	11	5	13.60
	NOB	1	0	0	0	0	0	0	0	0	0	0.10
	AXB	0	0	0	2	2	0	0	1	0	0	0.50
2a	TAB	10	11	10	5	10	15	21	35	40	22	17.90
	AOB	28	45	17	47	18	30	20	18	32	18	27.30
	NOB	1	2	0	0	0	0	0	0	0	0	0.30
	AXB	1	0	2	0	0	1	0	0	0	0	0.40
2b	TAB	10	20	41	5	19	15	4	29	16	44	20.30
	AOB	10	12	32	17	19	28	23	31	16	20	20.80
	NOB	0	0	2	0	0	0	0	0	0	0	0.20
	AXB	0	0	0	0	0	1	0	0	0	2	0.30

Trickling Low-N, 0.2 min (0.25 hr)$^{-1}$

Portal Replicate	Functional Group	Microscope Field										Average Cells Field^{-1}
		1	*2*	*3*	*4*	*5*	*6*	*7*	*8*	*9*	*10*	
2c	TAB	20	26	22	61	18	47	26	22	–	–	30.25
	AOB	4	3	1	3	1	0	0	0	0	0	1.20
	NOB	2	6	0	0	0	0	0	0	0	0	0.80
	AXB	0	0	0	0	1	0	0	0	0	0	0.10
3a	TAB	21	9	10	19	5	30	0	4	15	0	11.30
	AOB	11	8	10	5	0	0	7	1	0	0	4.20
	NOB	1	0	0	0	0	0	0	0	0	0	0.10
	AXB	0	0	1	2	0	0	1	1	0	0	0.50
3b	TAB	//	//	//	//	//	//	//	//	//	//	//
	AOB	//	//	//	//	//	//	//	//	//	//	//
	NOB	//	//	//	//	//	//	//	//	//	//	//
	AXB	//	//	//	//	//	//	//	//	//	//	//
3c	TAB	8	29	8	10	26	11	20	24	19	27	18.20
	AOB	5	1	12	2	0	0	0	0	0	0	2.00
	NOB	0	0	0	0	1	0	0	0	0	0	0.10
	AXB	2	0	0	0	0	0	0	0	0	0	0.20
4a	TAB	6	13	6	17	10	13	9	35	3	14	12.60
	AOB	6	2	3	2	4	6	0	0	2	0	2.50
	NOB	1	0	0	3	3	3	0	0	0	0	1.00
	AXB	1	0	0	0	0	0	0	0	0	0	0.10
4b	TAB	//	//	//	//	//	//	//	//	//	//	//
	AOB	//	//	//	//	//	//	//	//	//	//	//
	NOB	//	//	//	//	//	//	//	//	//	//	//
	AXB	//	//	//	//	//	//	//	//	//	//	//
4c	TAB	8	15	10	11	6	70	61	11	12	14	21.80
	AOB	0	0	23	1	3	3	7	2	1	2	4.20
	NOB	0	0	2	1	0	1	3	0	0	2	0.90
	AXB	0	0	0	0	0	0	0	0	0	0	0.00

Trickling High-N, 0.2 min (0.25 hr)$^{-1}$

Portal Replicate	Functional Group	Microscope Field										Average Cells Field^{-1}
		1	*2*	*3*	*4*	*5*	*6*	*7*	*8*	*9*	*10*	
1a	TAB	22	2	0	1	0	0	0	0	0	0	2.50
	AOB	0	0	0	0	0	0	0	0	0	0	0.00
	NOB	0	0	0	0	0	0	0	0	0	0	0.00
	AXB	2	0	0	0	0	0	0	0	0	0	0.20
1b	TAB	3	1	0	0	0	0	0	0	0	0	0.40
	AOB	30	15	10	23	21	15	25	15	33	10	19.70
	NOB	2	8	2	1	1	0	1	3	2	0	2.00
	AXB	1	0	0	0	0	0	0	0	0	0	0.10
1c	TAB	10	13	25	22	9	17	8	13	11	14	14.20
	AOB	22	14	13	14	23	18	5	12	15	4	14.00
	NOB	0	2	0	15	0	0	0	0	0	15	3.20
	AXB	0	0	0	0	0	0	0	0	0	0	0.00

Trickling High-N, 0.2 min (0.25 hr)$^{-1}$

Portal Replicate	Functional Group	Microscope Field										Average Cells Field^{-1}
		1	*2*	*3*	*4*	*5*	*6*	*7*	*8*	*9*	*10*	
2a	TAB	51	34	28	43	24	44	–	–	–	–	37.33
	AOB	39	16	16	21	18	61	32	22	63	19	30.70
	NOB	0	0	1	0	2	0	0	0	0	0	0.30
	AXB	0	0	0	0	0	0	0	0	0	0	0.00
2b	TAB	2	0	0	0	0	0	0	0	0	0	0.20
	AOB	2	3	3	2	0	0	0	0	0	0	1.00
	NOB	2	1	0	0	0	0	0	0	0	0	0.30
	AXB	0	0	0	0	0	0	0	0	0	0	0.00
2c	TAB	//	//	//	//	//	//	//	//	//	//	//
	AOB	//	//	//	//	//	//	//	//	//	//	//
	NOB	//	//	//	//	//	//	//	//	//	//	//
	AXB	2	0	0	0	0	0	0	0	0	0	0.20
3a	TAB	0	0	0	0	0	0	0	0	0	0	0.00
	AOB	0	0	0	0	0	0	0	0	0	0	0.00
	NOB	0	0	0	0	0	0	0	0	0	0	0.00
	AXB	0	0	0	0	0	0	0	0	0	0	0.00
3b	TAB	//	//	//	//	//	//	//	//	//	//	//
	AOB	//	//	//	//	//	//	//	//	//	//	//
	NOB	//	//	//	//	//	//	//	//	//	//	//
	AXB	//	//	//	//	//	//	//	//	//	//	//
3c	TAB	12	21	14	14	11	70	20	11	16	8	19.70
	AOB	0	4	1	2	0	2	1	1	0	0	1.10
	NOB	0	0	0	0	0	0	0	0	0	0	0.00
	AXB	0	0	0	0	0	0	0	0	0	0	0.00
4a	TAB	//	//	//	//	//	//	//	//	//	//	//
	AOB	//	//	//	//	//	//	//	//	//	//	//
	NOB	//	//	//	//	//	//	//	//	//	//	//
	AXB	//	//	//	//	//	//	//	//	//	//	//
4b	TAB	//	//	//	//	//	//	//	//	//	//	//
	AOB	//	//	//	//	//	//	//	//	//	//	//
	NOB	//	//	//	//	//	//	//	//	//	//	//
	AXB	//	//	//	//	//	//	//	//	//	//	//
4c	TAB	18	14	33	25	31	12	18	16	21	5	19.30
	AOB	8	10	2	20	4	0	0	1	3	1	4.90
	NOB	2	2	1	3	1	0	0	0	0	0	0.90
	AXB	1	0	0	0	0	0	0	0	0	0	0.10

Tidal Low-N, 24f Cycles Day^{-1}

Portal Replicate	Functional Group	Microscope Field										Average Cells Field^{-1}
		1	*2*	*3*	*4*	*5*	*6*	*7*	*8*	*9*	*10*	
1a	TAB	47	21	25	31	20	36	107	10	10	9	31.60
	AOB	12	15	3	10	2	1	10	0	0	0	5.30
	NOB	7	6	0	6	2	0	3	0	0	0	2.40
	AXB	1	0	0	0	0	0	0	0	0	1	0.20

Tidal Low-N, 24f Cycles Day^{-1}

Portal Replicate	Functional Group	Microscope Field										Average Cells Field^{-1}
		1	*2*	*3*	*4*	*5*	*6*	*7*	*8*	*9*	*10*	
1b	TAB	21	6	71	1	45	18	49	15	32	12	27.00
	AOB	0	4	0	18	1	1	0	0	0	6	3.00
	NOB	4	4	0	4	2	0	0	0	2	0	1.60
	AXB	0	3	0	0	0	0	1	0	0	0	0.40
1c	TAB	37	44	32	23	19	30	64	4	105	–	39.78
	AOB	1	2	8	0	3	2	1	0	0	0	1.70
	NOB	0	3	2	0	0	2	0	0	0	0	0.70
	AXB	5	4	1	2	0	0	2	2	0	0	1.60
2a	TAB	23	21	69	56	84	–	–	–	–	–	50.60
	AOB	38	3	12	8	1	15	40	10	39	3	16.90
	NOB	5	3	0	5	0	4	3	1	14	0	3.50
	AXB	1	0	0	0	3	1	0	3	2	1	1.10
2b	TAB	56	37	116	19	1154	–	–	–	–	–	276.40
	AOB	0	0	1	10	2	0	2	0	2	2	1.90
	NOB	0	7	0	0	2	0	2	0	0	0	1.10
	AXB	0	2	1	1	3	0	0	0	0	0	0.70
2c	TAB	83	100	53	33	47	–	–	–	–	–	63.20
	AOB	9	20	0	0	9	11	9	0	7	4	6.90
	NOB	2	4	0	0	1	1	0	0	2	1	1.10
	AXB	1	0	4	1	0	0	0	0	0	0	0.60
3a	TAB	44	97	20	132	54	–	–	–	–	–	69.40
	AOB	79	64	16	36	0	20	85	20	43	18	38.10
	NOB	1	0	4	1	0	1	1	0	0	0	0.80
	AXB	0	0	1	0	1	1	1	0	1	0	0.50
3b	TAB	80	58	65	29	62	–	–	–	–	–	58.80
	AOB	//	//	//	//	//	//	//	//	//	//	//
	NOB	//	//	//	//	//	//	//	//	//	//	//
	AXB	0	2	0	2	2	0	0	1	1	0	0.80
3c	TAB	16	29	24	9	33	21	12	58	64	34	30.00
	AOB	33	0	0	1	0	9	19	9	71	20	16.20
	NOB	3	5	0	0	0	0	0	0	0	0	0.80
	AXB	0	1	0	0	1	0	0	0	0	0	0.20
4a	TAB	17	122	86	54	13	–	–	–	–	–	58.40
	AOB	129	10	57	97	2	2	34	4	47	11	39.30
	NOB	5	3	2	4	1	1	3	0	7	0	2.60
	AXB	1	0	0	0	1	0	1	0	1	1	0.50
4b	TAB	47	37	13	29	99	38	49	33	41	25	41.10
	AOB	1	0	0	0	0	18	2	0	0	45	6.60
	NOB	0	0	0	0	0	1	0	0	0	0	0.10
	AXB	1	1	1	5	1	0	0	0	0	0	0.90
4c	TAB	21	56	95	56	47	–	–	–	–	–	55.00
	AOB	24	56	9	7	9	11	51	16	2	3	18.80
	NOB	0	4	6	2	0	3	1	1	0	1	1.80
	AXB	0	0	1	2	0	1	0	0	0	1	0.50

Tidal High-N, 24f Cycles Day^{-1}

Portal Replicate	Functional Group	Microscope Field 1	2	3	4	5	6	7	8	9	10	Average Cells Field^{-1}
1a	TAB	102	99	44	69	80						78.8
	AOB	250	81	92	36	29	127	53	22	6	42	73.8
	NOB	13	13	3	8	9	0	12	7	0	14	7.9
	AXB	0	0	1	3	1	1	0	1	0	1	0.8
1b	TAB	50	78	6	30	89						50.6
	AOB	0	21	4	2	66	2	5	1	0	43	14.4
	NOB	1	2	0	9	6	3	2	3	0	6	3.2
	AXB	0	4	2	3	0	0	1	0	3	1	1.4
1c	TAB	71	6	68	93	59						59.4
	AOB	0	0	0	5	0	2	3	0	0	0	1
	NOB	3	0	20	18	0	6	7	8	9	10	8.1
	AXB	0	0	0	0	3	1	0	1	0	1	0.6
2a	TAB	54	128	98	97	79						91.2
	AOB	0	0	2	0	4	8	2	0	0	9	2.5
	NOB	0	0	0	0	1	0	1	0	0	2	0.4
	AXB	0	1	0	0	2	0	1	0	0	0	0.4
2b	TAB	68	105	118	70	121						96.4
	AOB	39	12	60	0	4	74	3	13	10	11	22.6
	NOB	5	2	1	1	2	4	5	0	3	0	2.3
	AXB	0	0	1	2	0	0	1	0	0	1	0.5
2c	TAB	165	93	131	168	116						134.6
	AOB	144	119	13	28	8	67	106	1	8	67	56.1
	NOB	0	0	2	2	6	0	1	4	0	3	1.8
	AXB	0	0	1	2	0	1	0	0	1	1	0.6
3a	TAB	106	90	131	117	85						105.8
	AOB	6	16	31	21	87	112	36	15	70	1	39.5
	NOB	3	1	1	2	2	0	2	3	1	1	1.6
	AXB	0	0	0	1	0	0	0	0	0	1	0.2
3b	TAB	100	84	18	48	88						67.6
	AOB	22	30	18	11	28	14	1	0	10	45	17.9
	NOB	1	0	1	0	0	1	3	2	0	0	0.8
	AXB	0	1	1	0	0	1	0	1	1	0	0.5
3c	TAB	79	148	119	83	107						107.2
	AOB	1	39	48	4	10	4	27	0	33	2	16.8
	NOB	1	0	0	2	1	0	1	0	0	0	0.5
	AXB	0	0	1	1	0	0	0	3	0	1	0.6
4a	TAB	64	32	93	86	63						67.6
	AOB	121	26	0	50	25	21	60	0	22	67	39.2
	NOB	4	0	0	0	1	0	1	0	2	2	1
	AXB	0	0	0	1	0	2	0	0	0	0	0.3
4b	TAB	276	103	118	95	77						133.8
	AOB	3	16	23	109	79	30	20	13	64	6	36.3
	NOB	1	4	1	15	6	5	2	2	1	0	3.7
	AXB	0	0	0	1	0	0	0	0	0	1	0.2

Tidal High-N, 24f Cycles Day^{-1}

Portal Replicate	Functional Group	Microscope Field										Average Cells Field^{-1}
		1	*2*	*3*	*4*	*5*	*6*	*7*	*8*	*9*	*10*	
4c	TAB	223	660	640	780	360						532.6
	AOB	7	6	15	41	45	18	14	0	5	51	20.2
	NOB	0	2	3	0	1	2	0	1	0	2	1.1
	AXB	0	0	0	0	0	0	1	1	0	1	0.3

Trickling Low-N, 0.8f min (0.25 hr)$^{-1}$

Portal Replicate	Functional Group	Microscope Field										Average Cells Field^{-1}
		1	*2*	*3*	*4*	*5*	*6*	*7*	*8*	*9*	*10*	
1a	TAB	23	106	301	129	100						131.80
	AOB	11	6	2	15	2	9	6	1	1	3	5.60
	NOB	8	3	6	21	0	0	6	0	4	0	4.80
	AXB	5	4	4	2	1	0	1	3	3	4	2.70
1b	TAB	23	4	8	17	35	25	28	52	26	9	22.70
	AOB	3	0	1	1	2	7	0	2	3	1	2.00
	NOB	0	3	0	2	0	6	0	0	0	1	1.20
	AXB	3	1	0	1	0	6	2	1	0	1	1.50
1c	TAB	17	6	15	42	46	58	19	29	21	48	30.10
	AOB	3	0	0	4	0	2	0	9	0	4	2.20
	NOB	3	0	3	0	0	0	0	0	0	3	0.90
	AXB	0	0	1	0	3	2	0	0	2	3	1.10
2a	TAB	5	20	3	2	10	11	32	17	34	5	13.90
	AOB	5	0	0	1	4	0	3	0	0	0	1.30
	NOB	0	0	0	4	3	0	7	0	0	0	1.40
	AXB	0	0	0	0	1	1	0	1	0	3	0.60
2b	TAB	1	6	23	9	34	3	11	32	32	17	16.80
	AOB	0	2	8	1	0	1	2	26	0	0	4.00
	NOB	0	2	9	0	0	1	6	0	0	0	1.80
	AXB	0	0	0	0	0	0	0	0	1	1	0.20
2c	TAB	7	38	46	126	75						58.40
	AOB	3	8	6	3	1	2	4	3	6	2	3.80
	NOB	2	2	0	5	0	0	3	0	5	6	2.30
	AXB	1	0	2	0	0	0	0	0	0	1	0.40
3a	TAB	41	19	20	65	49	42					39.33
	AOB	4	9	20	4	0	5	0	2	13	9	6.60
	NOB	5	8	5	2	0	6	5	7	0	2	4.00
	AXB	0	1	0	1	0	2	2	2	2	0	1.00
3b	TAB	23	103	5	113	25						53.80
	AOB	4	6	0	8	3	2	1	2	6	3	3.50
	NOB	1	3	1	1	2	5	1	1	0	0	1.50
	AXB	0	0	1	0	0	0	0	0	0	0	0.10
3c	TAB	13	20	33	3	41	5	103				31.14
	AOB	10	1	7	4	0	1	2	1	0	4	3.00
	NOB	7	2	2	7	2	0	2	2	0	0	2.40
	AXB	0	3	1	1	2	0	0	0	2	0	0.90

Trickling Low-N, 0.8f min (0.25 hr)$^{-1}$

Portal Replicate	Functional Group	Microscope Field										Average Cells Field^{-1}
		1	*2*	*3*	*4*	*5*	*6*	*7*	*8*	*9*	*10*	
4a	TAB	13	38	18	49	5	9	24	6	14	18	19.40
	AOB	2	5	0	0	0	3	0	0	0	1	1.10
	NOB	2	0	0	1	2	1	1	0	0	0	0.70
	AXB	0	3	0	0	0	3	1	0	0	2	0.90
4b	TAB	57	21	13	20	15	41	13	19	14	7	22.00
	AOB	0	5	1	5	0	1	2	1	3	3	2.10
	NOB	3	0	2	4	0	2	0	0	5	1	1.70
	AXB	2	0	0	0	0	0	0	0	0	0	0.20
4c	TAB	4	27	27	9	5	30	19	24	39	20	20.40
	AOB	2	1	4	3	1	0	1	7	3	9	3.10
	NOB	0	0	0	1	0	1	0	0	0	15	1.70
	AXB	1	0	1	0	0	0	1	1	0	0	0.40

Trickling High-N, 0.8f min (0.25 hr)$^{-1}$

Portal Replicate	Functional Group	Microscope Field										Average Cells Field^{-1}
		1	*2*	*3*	*4*	*5*	*6*	*7*	*8*	*9*	*10*	
1a	TAB	20	48	15	48	35	29	44	16	15	35	30.50
	AOB	2	0	0	3	9	0	0	7	0	0	2.10
	NOB	0	0	0	1	4	0	1	3	0	0	0.90
	AXB	0	0	0	0	0	2	1	0	3	0	0.60
1b	TAB	7	9	20	9	2	19	18	7	24	24	13.90
	AOB	3	47	1	1	1	11	3	2	0	2	7.10
	NOB	0	22	0	1	3	9	3	2	0	2	4.20
	AXB	0	1	1	0	0	2	1	0	0	0	0.50
1c	TAB	33	21	22	23	6	29	25	65	31	24	27.90
	AOB	0	3	0	6	4	13	1	1	0	3	3.10
	NOB	0	1	0	0	0	1	1	1	0	0	0.40
	AXB	0	0	3	0	1	0	0	0	0	0	0.40
2a	TAB	39	46	14	57	17	23	7	20	28	12	26.30
	AOB	1	1	1	0	24	0	36	9	3	1	7.60
	NOB	0	0	0	0	1	0	0	0	0	0	0.10
	AXB	0	0	1	0	0	0	0	0	1	0	0.20
2b	TAB	74	26	25	73	56						50.80
	AOB	4	3	7	10	4	2	2	3	2	1	3.80
	NOB	4	2	5	20	0	1	0	0	1	0	3.30
	AXB	2	0	0	0	1	1	0	0	0	1	0.50
2c	TAB	7	43	55	29	52	22					34.67
	AOB	2	5	3	37	0	3	0	40	2	14	10.60
	NOB	3	1	3	2	6	0	0	0	0	0	1.50
	AXB	1	1	1	1	0	0	0	0	0	0	0.40
3a	TAB	19	40	64	9	33	48					35.50
	AOB	31	49	5	2	1	2	17	22	2	6	13.70
	NOB	5	1	0	0	0	1	1	0	0	1	0.90
	AXB	0	0	0	0	0	1	2	1	0	0	0.40

Trickling High-N, 0.8f min (0.25 hr)$^{-1}$

Portal Replicate	Functional Group	Microscope Field										Average Cells Fields^{-1}
		1	2	3	4	5	6	7	8	9	10	
3b	TAB	1	39	29	25	15	23	19	12	26	14	20.30
	AOB	1	3	4	2	0	0	0	3	0	8	2.10
	NOB	0	1	0	0	2	3	0	0	0	0	0.60
	AXB	0	0	0	0	0	0	0	0	0	0	0.00
3c	TAB	37	27	21	21	27	26	27	39	51	20	29.60
	AOB	3	0	0	0	2	4	2	1	4	6	2.20
	NOB	1	0	0	0	0	0	0	0	0	0	0.10
	AXB	0	1	0	0	0	0	0	0	0	1	0.20
4a	TAB	25	46	4015	16	43	48					698.83
	AOB	6	0	0	25	53	3	0	1	5	3	9.60
	NOB	4	0	1	0	2	0	0	0	2	1	1.00
	AXB	0	0	0	0	0	0	0	0	0	0	0.00
4b	TAB	29	22	17	17	41	6	42	38	29	26	26.70
	AOB	1	6	8	6	5	13	4	8	3	4	5.80
	NOB	0	0	6	2	2	4	1	4	1		2.22
	AXB	2	0	0	0	0	2	1	0	0	0	0.50
4c	TAB	104	10	34	24	20	171	100	1	2	17	48.30
	AOB	1	2	12	15	0	11	3	36	1	5	8.60
	NOB	1	0	3	5	1	2	0	1	0	0	1.30
	AXB	4	0	0	0	0	2	1	0	1	0	0.80